CELL AUTONOMOUS EFFECTS OF FOXF2 IN ENDOTHELIAL CELLS AND PERICYTES

Judit González Gallego

Graduate School of
Systemic Neurosciences

LMU Munich

Dissertation der
Graduate School of Systemic Neurosciences der
Ludwig-Maximilians-Universität München

May, 2023

Supervisors
Prof. Dr. Martin Dichgans
Institute for Stroke and Dementia Research (ISD), University Hospital, Ludwig-Maximilians-Universität München & German Centre for Cardiovascular Research (DZHK, Munich), Munich, Germany

Prof. Dr. Dominik Paquet
Institute for Stroke and Dementia Research (ISD), University Hospital, Ludwig-Maximilians-Universität München

First Reviewer: Prof. Dr. Martin Dichgans
Second Reviewer: Dr. Sabina Tahirovic
External Reviewer Dr. Nicolas Renier

Date of Submission: 17.05.2023
Date of Defense : 6.10.2023

Table of contents

Abbreviations

2D	2-dimensional
3D	3-dimensional
AJ	Adherens junctions
BBB	Blood-brain-barrier
BEC	Brain endothelial cells
CBF	Cerebral blood flow
CNS	Central nervous system
cSVD	Cerebral small vessel disease
CT	Computed tomography scan
DSB	Double strand break
EC	Endothelial cells
ECM	Extracellular matrix
eQTL	Expression quantitative trait loci
fMCAo	Filament-mediated middle cerebral artery occlusion
hBMECs	Human brain microvascular endothelial cells
HDR	Homology-directed repair
HUVECs	Umbilical vein endothelial cells
iAS	iPSC-derived astrocytes
iEC	iPSC-derived endothelial cells
iPE	iPSC-derived pericytes
iPSC	induced pluripotent stem cells
iSMC	iPSC-derived smooth muscle cells
LNPs	Lipid nanoparticles
MRI	Magnetic resonance imaging
NHEJ	Non-homologous end joining
NPCs	Neural precursor cell
NPs	nanoparticles
NVU	Neurovascular unit
pAS	Human primary mid brain astrocytes
PCA	Principal component analysis
pEC	Human primary capillary endothelial cells
pPE	Human primary vascular pericytes
pSMC	Human primary vascular smooth muscle cells
qPCR	Quantiative polymerase chain reaction
RMT	Receptor-mediated transcytosis
ROS	Reactive oxygen species
sgRNA	Single guide RNA
TEER	Transendothelial electrical resistance
TJ	Tight junctions
vSMCs	Vascular smooth muscle cells

1. Introduction

1.1 The neurovascular unit (NVU) and the blood-brain-barrier (BBB)

The human brain consumes approximately 20% of the body´s glucose and oxygen. This consumption is on demand, as the central nervous system (CNS) lacks a storage mechanism and therefore needs vascularization. Although the human brain represents only 2% of the body mass, it is a highly vascularized organ, containing approximately 644km of blood vessels, which supply oxygen and nutrients to brain cells and remove waste products from the brain parenchyma (M. D. Sweeney et al. 2019).

Endothelial cells forming blood vessels differ in their properties depending on the tissue in which they are located. This allows vascular networks to adapt to specific oxygen and nutrient demands. Within the CNS, brain endothelial cells (BEC) form the blood-brain-barrier (BBB), which allows a controlled chemical and metabolic environment for the proper functioning of the brain. The BBB generates a selective barrier between the CNS and the circulating blood. The BBB not only prevents blood cells and neurotoxic plasma pathogens from entering the brain (Daneman 2012; M. D. Sweeney et al. 2019) but also controls the delivery of oxygen, nutrients and removal of carbon dioxide and other toxic metabolites from the brain (Zlokovic 2011).

Although some of the properties of the BBB are due to BEC specifications, BBB formation and maintenance depends on critical interactions between all the components of the neurovascular unit (NVU): vascular cells (endothelial cells, pericytes and vascular smooth muscle cells), glial cells (astrocytes, microglia and oligodendrocytes), neurons and immune cells (Zlokovic 2011; Daneman and Prat 2015).

1.1.1 Cellular composition

The cellular composition and function differs along the vascular tree (**Figure 1).** At the level of the penetrating arteries, several endothelial cells (or endothelium) generate the inner layer of the vessel wall, which is covered by a thin extracellular membrane. The endothelial cells are surrounded by one to three smooth muscle cells and at the same time enclosed by the pia. The cerebrospinal fluid is located between the pia and the astrocytic endfeet. At the arteriole level in contrast with the penetrating artery, the endothelium is only surrounded by one smooth muscle cell, which is in direct contact with the astrocytic endfeet.

At the capillary level, most of the endothelium is formed by only one endothelial cell surrounded by one pericyte, both sharing a common basement membrane. Those pericytes extend their processes along the capillaries, making several contacts with the endothelial cells, which receive the name of "peg-socket". Here, similarly to the arteriole level, the astrocytic endfeet make direct contact with the endothelial cells and pericytes. In the NVU, the contractile cells are the mural cells (smooth muscle cells or pericytes), which control the vessel diameter and therefore, blood flow (Kisler et al. 2017).

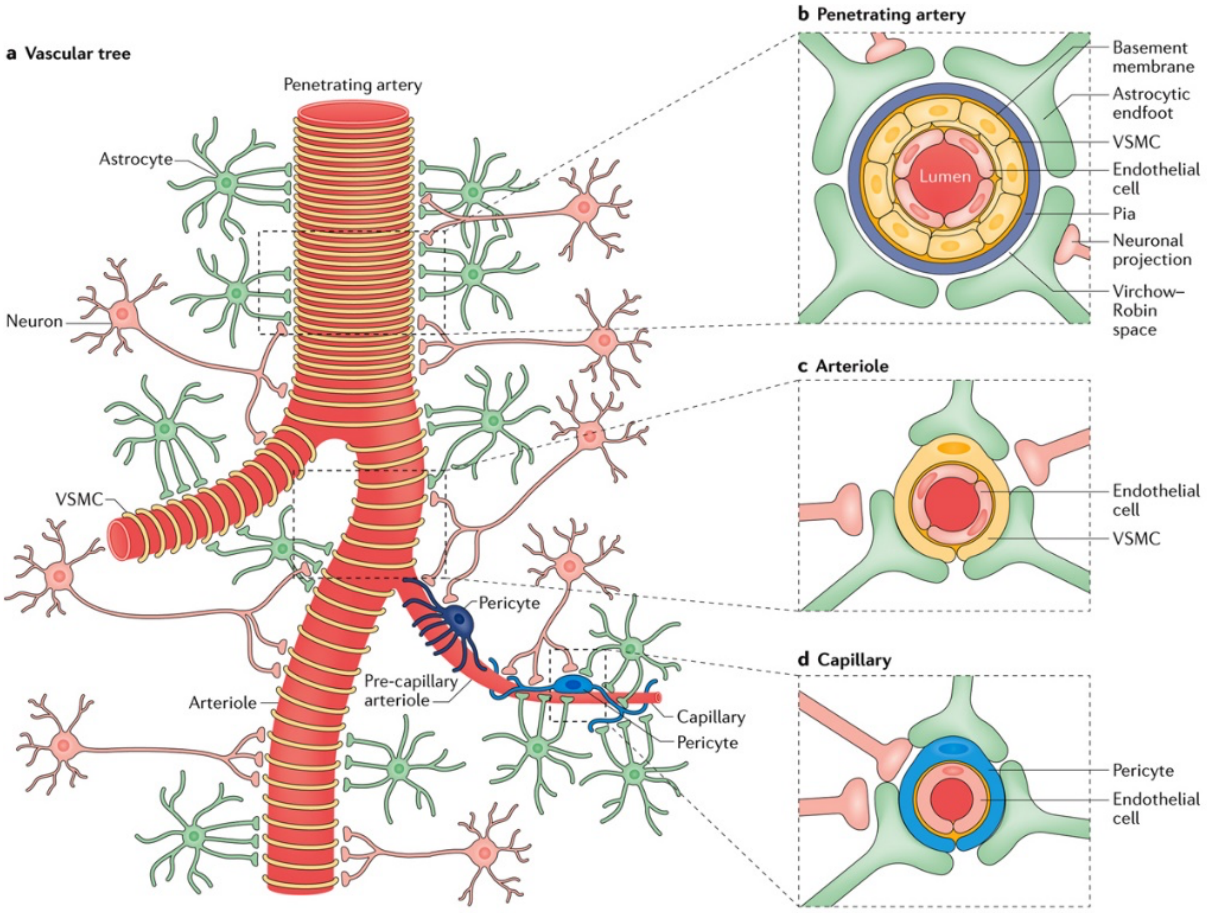

Figure 1| Schematic representation of the neurovascular unit (NVU). A) The neurovascular unit is composed of endothelial cells (red), smooth muscle cells (yellow), pericytes (blue), astrocytes (green) and neurons (pink). The cell distribution and composition differ along the vascular tree. **B**) The penetrating arteriole is composed of several endothelial cells covered by a thin extracellular basement membrane (light yellow) and surrounded by several smooth muscle cells. Everything is surrounded by the pia (dark blue). The astrocytic endfeet are separated from the pia and the vascular cell types by the Virchow-Robin space. **C)** At the arteriole level, the endothelial cells are only surrounded by one smooth muscle cell and the astrocytic endfeet contact the vascular cells directly. **D)** At the capillary level, the main difference is the mural cell composition, the endothelial cells are wrapped by one pericyte, which extend their processes along the endothelium. From Kisler et al., 2017. Copyright permission given in chapter 7

1.1.1.1 Brain endothelial cells (BECs)

Endothelial cells (ECs) are derived from the mesoderm and form the walls of blood vessels. The CNS vasculature is formed during embryonic development from endothelial sprouts, which invade the neuroectoderm in response to a vascular endothelial growth factor (VEGF) gradient derived from neuronal progenitors (McCarty 2009) (**Figure 1**). BECs have unique characteristics when compared to peripheral ECs, which contribute to the formation of the BBB as a selective physical barrier. BECs present with high abundance of mitochondria, low transcytosis rates and pronounced tight junctions between adjacent cells, which results in a non-fenestrated cell layer (Abbott, Rönnbäck, and Hansson 2006). Moreover, they also present common EC features such as the expression of integrin receptors, glycoprotein or adhesion molecules (Nag 2011).

One of the main functions of the BBB is restricting the trafficking between the blood and the CNS through four different cellular properties of BECs (**Figure 2**): (1) Specialized tight junctions limit the paracellular trafficking between two adjacent endothelial cells, generating a physical barrier. (2) BEC also suppress transcytosis and (3) express specialized transporters for carrying important molecules to the brain by endocytosis-dependent and independent methods, which allows selective transport. Furthermore, (4) BEC express only low levels of luminal adhesion molecules, which reduce leukocyte adhesion and therefore immunosurveillance of the CNS (Kaplan, Chow, and Gu 2020).

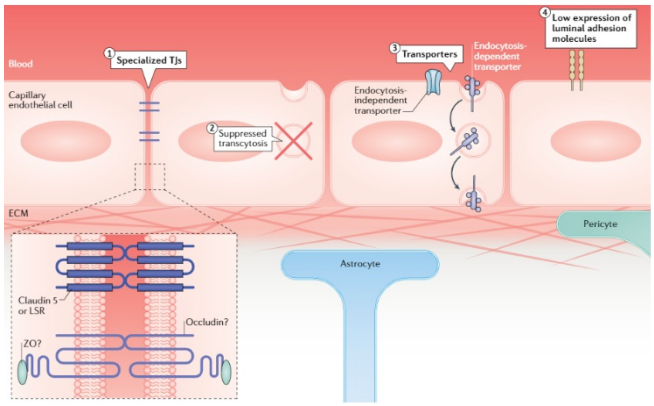

Figure 2| Endothelial cell properties at the BBB. Endothelial cells are represented in red. The main functions for the BBB formation are (1) specialized tight junctions, (2) suppressed transcytosis, (3) expression of specific transporters and (4) low expression of luminal adhesion molecules. From Kaplan et al., 2020. Copyright permission given in chapter 7.

Adjacent BECs express tight (TJ) and adherens junctions (AJ), which restrict transport between ECs (Keaney and Campbell 2015). There have also been some observations of expression of gap junctions, but their role in the BBB function remains unclear (Nagasawa et al. 2006). The main tight junctions in BECs are claudins (CLDN-3,5 and 12), occludin, zona occludens (ZO-1,2 and 3), junctional adhesion molecules (JAMS, JAM-A, B and C) and endothelial selective adhesion molecule (ESAM). The main AJ are vascular endothelial cadherin (VE-cadherin, CD144) and platelet-endothelial cell adhesion molecule (PECAM, CD31). Those AJ are responsible for stabilizing cell-cell interactions at the junctional site (Abbott, Rönnbäck, and Hansson 2006) (**Figure 2**).

Different TJ are present at the cellular membrane and in the cytoplasm, allowing the connection of two cell membranes and the linkage of those to their corresponding cytoskeleton. In freeze-fracture imaging, TJ appear like intramembrane fibrils or networks that completely seal the cell-cell contact (Tsukita, Furuse, and Itoh 2001).

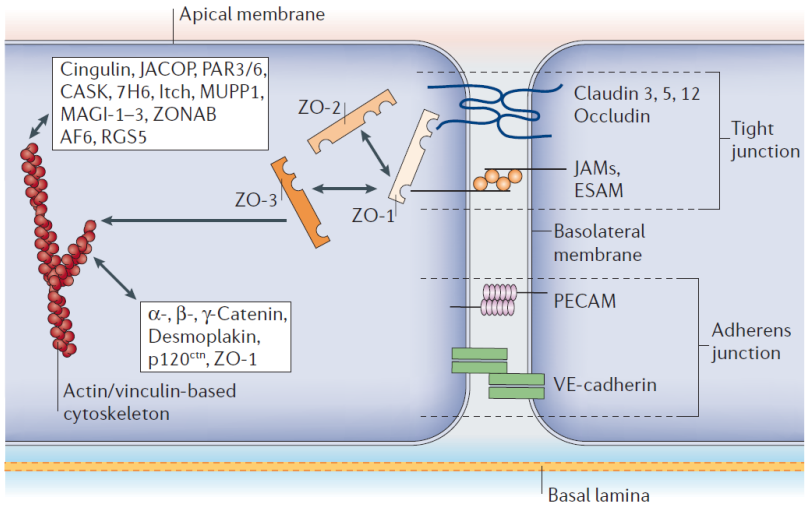

Figure 3| Molecular composition of endothelial tight and adherens junctions. Two endothelial cells are represented in blue. The main transmembrane tight junctions are claudins, occludin, JAMs and ESAM. Within the cytoplasm, the main tight junctions are zona occludens 1,2 and 3, which allow the intramembrane proteins to bind with the actin cytoskeleton. The main adheren junctions are PECAM and VE-cadherin. From Abbott et.al, 2006. Copyright permission given in chapter 7.

Claudins, occludin, JAMs and ESAM are located at the cell membrane. Claudins are involved in connecting two consecutive cells and in the formation of transendothelial electrical resistance (TEER), which restrict even the movement of small ions such as sodium (Na+) and chloride (Cl-) (Abbott, Rönnbäck, and Hansson 2006). Claudin-5-deficient mice show BBB leakage of tracers smaller than 800 Daltons despite presenting normal tight junctions visualized by electron microscopy (Nitta et al. 2003). Occludin can bind zona occludens protein 1 (ZO-1), located in the cytoplasm, and its main function is believed to be the regulation of tight junctions. The specific contribution of occludin and ZO to the BEC barrier remains difficult to determine since knockout mice lack BBB dysfunction phenotypes (Saitou et al. 2000; Umeda et al. 2006). Although peripheral endothelial cells also express tight junctions, it is believed that the transcriptomic expression in BECs is higher, especially for occludin (Vanlandewijck et al. 2018; Munji et al. 2019). Lastly, JAMS are necessary for the formation and maintenance of the tight junctions. These transmembrane proteins are connected to the cytoplasmic side via the cytoplasmic plaques, composed by large protein complexes such as ZO-1,2 and 3. This specific protein location not only restricts the paracellular trafficking but also generates a polarization of the cell by having an apical and basal side (Abbott, Rönnbäck, and Hansson 2006).

1.1.1.2 Mural cells

The mural cells include vascular smooth muscle cells (vSMCs) and pericytes. Both cell types surround ECs but at different parts of the vascular tree (**Figure 1**).

vSMCs surround most of the large vessels, such as arteries, arterioles, venules and veins. They express contractile proteins such as αSMA, myosin, vimentin and desmin, which allow them to regulate the blood flow (Smyth et al. 2018b). Pericytes have been difficult to study for a lack of specific markers expressed uniquely in this cell type. The most accepted characterization of this cell type is the co-expression of PDGFR-ß and NG2. Other markers also expressed in other cell types such as ANPEP, ABCC9, ZIC1, DLK, RGS5 and KCNJ8 have also been used for their study (Armulik, Genové, and Betsholtz 2011a).

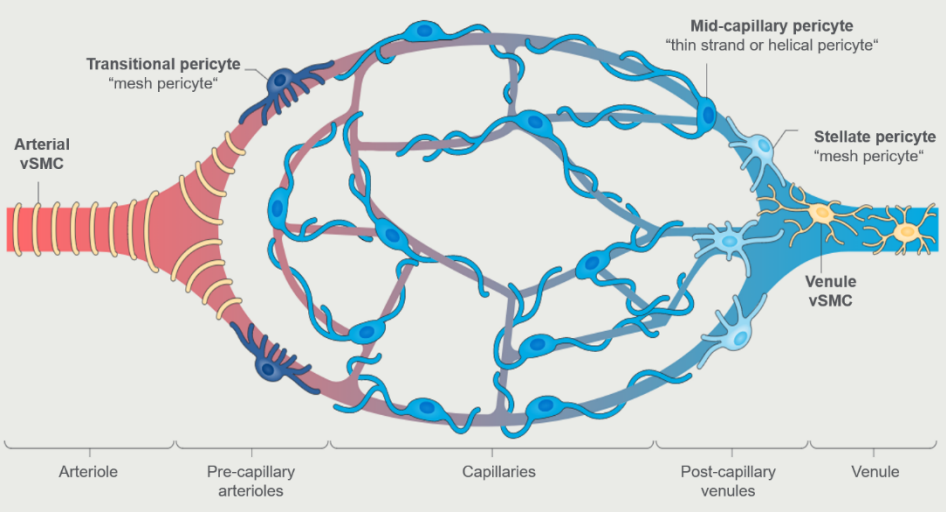

Figure 4| Mural cell diversity organization in the vasculature. vSMCs are represented in yellow and different types of pericytes in different blue tonalities. vSMC are located in the arterioles and venules. Transitional pericytes are located in the pre-capillary arterioles. Mid-Capillary pericytes are located in the capillaries and stellate pericytes are located in the post-capillary venules. Adapted from Kisler et al., 2017. Copyright permission given in Chapter 7.

Studies using different Cre-driver lines for key pericyte markers such as PDGFR-ß and NG2 reveal a heterogeneous pericyte population that differs in cellular marker expression, morphology, function and location along the vascular tree. There are three main pericyte subtypes: transitional pericytes, mid-capillary pericytes and stellate pericytes (**Figure 4**). Transitional pericytes are located in the pre-capillary arterioles and are very close to vSMCs, which are completely wrapping the arterioles in concentering rings. These pericytes present with different primary and secondary processes with a mesh-like structure that completely surrounds the entire vessel. Mid-capillary pericytes are located at the capillary bed, which represents most of the microvasculature, and have thin helical processes that cover the microvasculature in single strands. Stellate pericytes are on the post-capillary venules that do not display a vSMC ring, and present also with a mesh-like structure (Hartmann et al. 2015; Kisler et al. 2017).

Whether each pericyte subtype has different marker expression and functions still remains unclear. One of the most debated functions is whether pericytes are contractile cells or not and if they can regulate CBF. While the expression of αSMA still remains unclear, a recent study in mice using single-cell RNA sequencing showed that pericyte express transcripts for vimentin, desmin, calponin, skeletal muscle actin and αSMA (Zeisel et al. 2015). Moreover, studies in rats have also shown that mid-capillary pericytes express vimentin and contractile myosins (Bandopadhyay et al. 2001). Despite the expression of key contractile proteins, several studies have shown opposite results in pericyte contractibility *in vivo,* leaving this question unanswered (Kisler et al. 2017; Hall et al. 2014).

Pericyte cell bodies are separated from the endothelial cells by the basement membrane and they can extend their processes over several EC bodies. When the pericyte processes are in touch directly with the endothelium, they form the peg-and-socket junctions, mainly mediated by N-Cadherin (Gerhardt, Wolburg, and Redies 2000). At the BBB, pericytes contribute to several functions such as vascular stability, BBB formation and permeability, angiogenesis, CNS clearance, extracellular matrix deposition and cerebral blood flow control (M. D. Sweeney, Ayyadurai, and Zlokovic 2016; Armulik, Genové, and Betsholtz 2011a).

1.1.1.3 Astrocytes

Astrocytes are the main glial cell type expressed in the brain and their processes serve as a link between the vasculature and the neurons. Astrocytes extend their processes, known as astrocytic endfeet, to the endothelium and the neurons, thus being able to regulate the cerebral blood flow depending on neuronal activity (Daneman and Prat 2015). The astrocytic endfeet present with specialized features such as a high density of orthogonal array of particles (OAPs), allowing ion and volume regulation. Those OAPs are mainly composed by the water channel aquaporin 4 (AQP4) and the Kir4.1 K+ channel (Abbott, Rönnbäck, and Hansson 2006).

The full role of astrocytes in the formation and maintenance of the BBB remains unclear and has been debated over time. Currently, it is believed that astrocytes are not necessary for the BBB formation but rather for its maintenance and modulation (Daneman and Prat 2015). Despite that, regional ablation of astrocytes has no impact in BBB permeability (Tsai et al. 2012) and some other studies have shown that astrocyte progenitors modulate VEGF and Ang-1 expression, regulating angiogenesis and tight junction formation (S. W. Lee et al. 2003). However, *in vitro* studies have demonstrated that astrocytes upregulate key BBB features such as tighter tight junctions (Dehouck et al. 1990; Rubin et al. 1991), expression of specific transporters such as Glut1 or Pgp (Mcallister et al. 2001) and induction of greater endothelial barrier (Lippmann et al. 2012).

1.1.2 Cellular interactions

The NVU is a heterogeneous cellular complex that for proper functioning needs direct and indirect cell-cell communication, which leads to a bidirectional communication between vascular cell types (BEC, vSMCs and pericytes) glial cells (astrocytes and microglia) and neurons. This communication and signaling pathways are essential to maintaining homeostasis at the NVU (**Figure 5**) (Kugler, Greenwood, and MacDonald 2021).

BECs form a specialized single layer of tubular vessels (Kaplan, Chow, and Gu 2020). The mural cells, vSMCs and pericytes, are embedded in a shared basement membrane with BECs and provide not only vascular stability (Armulik, Genové, and Betsholtz 2011a; Winkler, Bell, and Zlokovic 2011) and blood vessel support but also control vasodilation and constriction (Hall et al. 2014; Tong et al. 2020). Furthermore, they support the phagocytosis of toxic metabolites (Sagare et al. 2013a). Glial cells, and especially astrocytes, extend their endfeet towards the endothelium, creating a glia limitans (Kutuzov, Flyvbjerg, and Lauritzen 2018). Moreover, they connect the vasculature with the neurons, which allows them to modulate neurotransmission (Falk and Götz 2017). Furthermore, *in vitro* studies have shown that both, astrocytes and endothelial cells express receptors for most neurotransmitters (Abbott 2002). This expression could help modulate the tightening or loosening of the BBB depending on the circumstances, for example a release of histamine could modulate tight junctions allowing the passage of growth factors and antibodies from the circulation (Abbott 2002). On the other hand, during hypoxia or stress conditions, intracellular cyclic AMP (cAMP) increases, which could lead to a higher TEER and Pgp activity (Âla Kis et al., n.d.). Microglia and macrophages take care of the CNS immunosurveillance and phagocytosis as an immunoinflammatory response (Kugler, Greenwood, and MacDonald 2021). Lastly, neurons also communicate with the NVU components to control cerebral blood flow via nitric oxide (NO), arachnoid acid or potassium (Attwell et al. 2010). Furthermore, neuronal activity also modulates vessel density and branching (Lacoste et al. 2014; Whiteus, Freitas, and Grutzendler 2013).

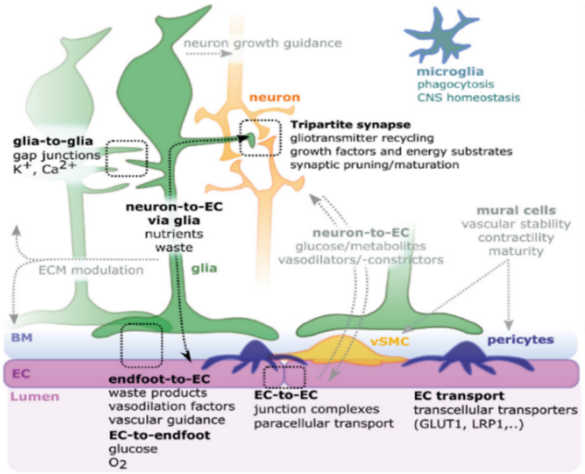

Figure 5|NVU cellular communication in health. Cellular composition of the NVU: in purple endothelial cells, blue pericytes, yellow vSMCs, green astrocytes, orange neurons and blue microglia. Cell-Cell communication at the NVU during homeostasis. From Kugler et al., 2021.

1.1.3 Transport across the BBB

The BBB forms a selective physical barrier which separates the brain from the circulating blood. The high abundance of TJs between adjacent cells limits most of the paracellular transport through junctions and forces a transcellular pathway to cross the BBB. Gasses (like oxygen and carbon dioxide) and small molecules (smaller than 400Da) are an exception since they can diffuse freely across the brain endothelium. Therefore, endothelial expression of specific transporters in the abluminal side regulates most of the molecular exchange and generates a selective transport barrier between the CNS and the blood (M. D. Sweeney, Ayyadurai, and Zlokovic 2016; Abbott, Rönnbäck, and Hansson 2006).

There are several pathways involved in the transport of a molecule between the blood and the brain parenchyma, which are necessary to keep brain homeostasis. The main pathways across the BBB are the paracellular diffusion pathway, transcellular diffusion, transporter protein pathway, receptor-mediated transcytosis, adsorptive transcytosis and cell-mediated pathway (Alahmari 2021) (**Figure 6**).

Small molecules that are water-soluble can cross freely through two adjacent cells or paracellular area by using a negative concentration gradient. At the BBB this type of transport is limited by the presence of TJs, which also limits the crossing of polar drugs. Lipid-soluble substances can dissolve in lipidic rafts of cellular membranes and thus cross the BBB passively (Chen and Liu 2012). This transport, known as transcellular diffusion, presents an opportunity for potentially harmful substances to cross to the CNS. To avoid this, BECs also express efflux pumps, which limit the entrance of lipid-soluble particles by pumping them towards the blood stream again (Alahmari 2021; Abbott, Rönnbäck, and Hansson 2006).

For proper brain function, nutrients, and larger molecules such as glucose or amino acids must cross the BBB. BECs express specific transport proteins or solute carriers, allowing an active transport of them into the brain, known as the transporter or carrier protein pathway. Some of these carriers act as efflux transporters since they are energy-dependent, like the P-glycoprotein. Another important transport route through the endothelium is receptor-mediated transcytosis (RMT), which allows the entrance of substances like insulin or transferrin. In this case, BEC express specific receptors for substances, and once they are bound, they get invaginated in vesicles and carried to different locations (Alahmari 2021).

Charged molecules and macromolecules take advantage of electrostatic differences between the positively charged transporters and the negatively charged microdomains on the membrane. Cationic molecules interact with the negatively charged glycocalyx, which triggers the formation of transcytotic vesicles, that move to the abluminal membrane of the cells, fuse and get released into the brain (Terstappen et al. 2021). This type of transport is called adsorptive-mediated endocytosis and transcytosis. Albumin and other native plasma proteins are following this transport method and cationization of those molecules can increase their uptake by endothelial cells (Alahmari 2021; Abbott, Rönnbäck, and Hansson 2006).

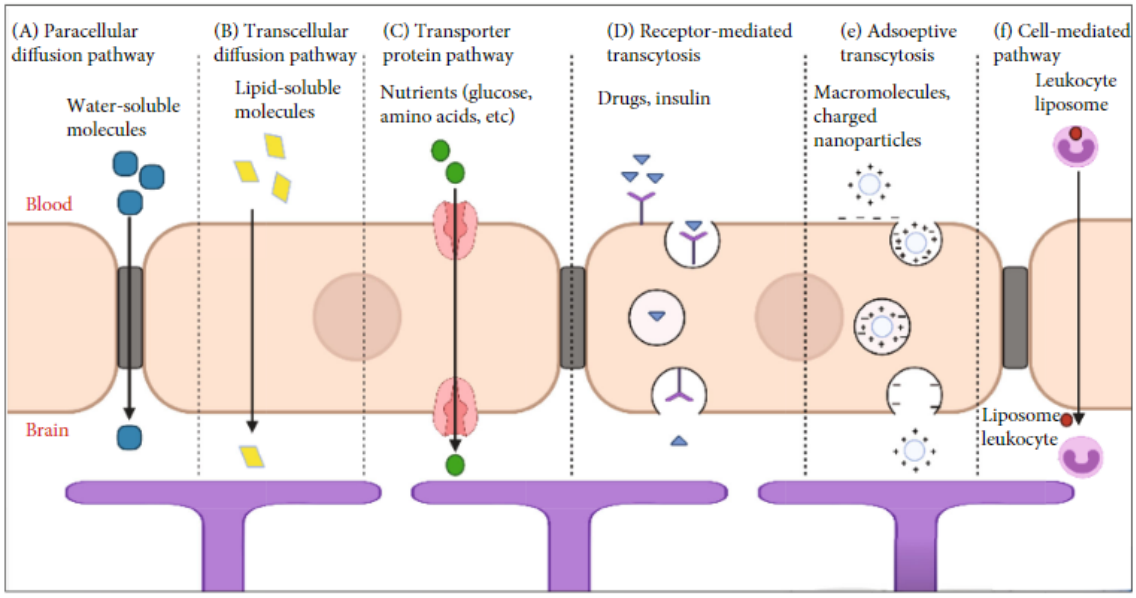

Figure 6|Pathways across the BBB mediated by endothelial cells processes. Endothelial cells are represented in orange and astrocyte end feet are represented in purple. There are several pathways to cross the BBB: (A) Paracellular diffusion pathway, (B) transcellular diffusion pathway, (C) transporter protein pathway, (D) receptor-mediated endocytosis or, (E) Adsorptive-mediated endocytosis and transcytosis and (F) cell-mediated pathway. From Alahmari et al., 2021

The last transport route across the BBB is the cell-mediated pathway or transcytosis. This is the main pathway followed by mononuclear cells, which interact with the endothelium and cross using the cytoplasm rather than disturbing the cell junctions. This receives the name of diapedesis and is the main pathway that leukocytes follow in in both healthy and diseased conditions (Abbott et al. 2010).

This tightly controlled transport across the BBB protects the CNS from harmful substances but also poses a challenge for CNS drug delivery. In the recent years, there has been an increasing interest in developing new brain delivery technologies and several of the transport pathways across the BBB have been tested. Most of the studies have been focusing on using carrier protein pathway, adsorptive-mediated transcytosis, cell-mediated transcytosis, and receptor mediated transcytosis for delivering drugs into the CNS (Terstappen et al. 2021).

Therapeutics can use the carrier protein pathway to enter the brain if they are modified to be recognized by the transporter protein expressed in the cell membrane, which might be difficult or impossible depending on the case (Ding et al. 2020). Recently, some studies have used the delivery of nanoparticles (NPs) into the brain by coating them with polysorbate 80 (P80), so they are recognized by the cells and undergo transcytosis (Blasi et al. 2007). Adsorptive mediated transcytosis can also be used for drugs to enter the CNS by adding charges to them. Despite these modifications being relatively easy, the uptake pathway is not specific and can result in drug build up in different organs, which may have undesired clinical consequences (Alahmari 2021). Another method tested for drug delivery has been cell-mediated transcytosis. In this case, the drugs can be sheathed into liposomes that will be later absorbed by leukocytes and transported into the CNS (Ding et al. 2020). Lastly, therapeutics can also be delivered by using RMT, one of the most studied methods for drug delivery. The drug is coupled to a ligand that can bind to a specific receptor expressed in the cell surface of brain endothelial cells. Ligand and receptor are taken up by the cells through clathrin-dependent or clathrin-independent vesicles, which fuse with the abluminal membrane and deliver them into the CNS (Terstappen et al. 2021). Transferrin receptor have been one of the most studied, tested and validated for drug delivery in the last years (Johnsen et al. 2019).

1.1.4 Neurovascular coupling

Neuronal stimuli cause an increase in cerebral blood flow (CBF), which allows cerebral arteries, arterioles and capillaries to supply the CNS with the necessary metabolites for proper functioning (M. D. Sweeney et al. 2019). The brain controls the CBF in a regional matter, increasing the rate of CBF in activated brain regions, mechanisms known as neurovascular coupling or functional hyperemia (Cox, Woolsey, and Rovainen 2016; Chaigneau et al. 2003; Kisler et al. 2017). In the brain, there is a direct link between neural activity and CBF, which leads to a regional modification of CBF depending on the neuronal energy demands. Therefore, brain function can be measured by changes in the blood flow using functional brain imaging (Raichle and Mintun 2006; Iadecola 2017). Altered functional connectivity and neurovascular uncoupling resulting from a mismatch between CBF, O2 supply and neuronal activity are seen in different neurological disorders (Zlokovic 2011; Kisler et al. 2017).

Oxygen and glucose are needed upon neuronal activity increase. Although neurons can directly signal to the vasculature, most often they use astrocytes as intermediaries to send signals to mural cells and make changes in the vascular tone (Attwell et al. 2010). Neuronal activity releases glutamate, which activates the neuronal N-methyl-D aspartate (NMDA) receptor resulting in an activation of neuronal nitric oxide synthase (Nos1) and the release of nitric oxide, which dilates blood vessels (Busija et al. 2007). Glutamate can also bind to astrocytes leading to an intracellular calcium increase and the release of vasoactive mediators such as nitric oxide (NO), prostaglandins (PG), arachidonic acid (AA),

potassium or epoxyeicosatrienoic acids (EETs) that act on the mural cells to promote constriction or dilation (Gordon et al. 2008; Zonta et al. 2002; Mcconnell et al. 2016). Furthermore, neuronal activity can lead to astrocytic potassium (K+) causing vSMC relaxation (Filosa et al. 2006; Girouard et al. 2010).

In a vascular network, coordinated dilation of downstream and upstream vessels must occur to increase regionally CBF while avoiding changes in interconnected vasculature. Moreover, neuronal activity signals must be conveyed from deep vasculature areas to upstream arterioles in order to increase the CBF efficiently (Ngai et al. 1988; Segal 2015). In peripheral blood vessels, conducted vasomotor responses have two components: a fast component by propagation of electrical signals between cells mediated by calcium (Ca^{2+}) and potassium (K_{Ca}) channels, and a slow component mediated by the release of NO and prostanoids created by calcium waves (Tallini et al. 2007; Segal 2015). At the capillary level, endothelial cells express specific potassium channels (K_{IR}), which are highly sensitive to potassium release during neuronal activity. Moreover, KIR channel inhibition leads to reduced vasodilatation propagation, demonstrating that they are key mediators of the hyperpolarization conduction (Longden et al. 2017). Ionic currents traveling through endothelial cell gap junctions or through myoendothelial junctions (between endothelial cells and mural cells) might be the mechanism for a rapid propagation of the signal (Tallini et al. 2007; Segal 2015; Iadecola 2017).

Signals generated by neurons, astrocytes or endothelial cells end up in the mural cells regulating vasomotor responses and CBF. While the implication of vSMCs in flow regulation is clear (Cipolla 2009), the involvement of pericytes is still under debate (Mishra et al. 2016; Hall et al. 2014; Cudmore, Dougherty, and Linden 2017; Wei et al. 2016). Changes between the membrane potential and intracellular calcium control the assembly of the contractile proteins, allowing vSMCs to contract or relax, changing the CBF (Cipolla 2009; Longden, Hill-Eubanks, and Nelson 2016).

1.1.4 NVU pathology

Proper neuronal activity, such as neuronal synapses and connectivity, depends on maintaining the integrity of the BBB. Several diseases and pathologies can lead to an abnormal pericyte-endothelial and or astrocyte-endothelial communication, which results in BBB breakdown and is associated with reduced CBF and increased vascular permeability (Z. Zhao et al. 2015). BBB breakdown enables the entry of toxic molecules, immune cells and plasma components into the brain, which is associated with inflammatory and immune responses. Blood-derived proteins like fibrinogen or plasmin not only lead to microglia activation, but also degrade neuronal extracellular matrix (ECM), leading to a neuronal detachment and cell death (Bell et al. 2010; Davalos et al. 2012; Z. Zhao et al. 2015). Moreover, fibrinogen also alters neuronal myelination state, promoting at the same time demyelination and preventing myelination by oligodendrocytes progenitor cells (J. K. Ryu et al. 2015). Furthermore, albumin contributes to vascular edema, reduces CBF and increases hypoxia. Lastly, extravasated red

blood cell (RBC)-derived hemoglobin and iron cause an increase in the production of reactive oxygen species (ROS) that generates and oxidative stress in neurons and microglia, leading to cell death and activation respectively (Z. Zhao et al. 2015). Collectively, loss of BBB integrity can initiate multiple neurodegeneration pathways, compromising proper brain functioning (M. Sweeney and Foldes 2018).

Analysis of postmortem brain samples and functional imaging of human patients has identified BBB dysfunction and breakdown in different neurological disorders such as stroke, Alzheimer´s disease (AD), Parkinson´s disease (PD), multiple sclerosis (MS), epilepsy and brain trauma (Daneman and Prat 2015). Recent evidence has clearly suggested that vascular dysfunction is linked to neurodegeneration and neuronal dysfunction. One clear example is cerebral autosomal dominant arteriopathy with subcortical infarcts (CADASIL), a small vessel disease that causes ischemic lesions, neurodegeneration and, later, dementia. Moreover, some evidence also points to a BBB dysfunction and CBF reduction before amyloid-ß deposition in sporadic cases of AD (Zlokovic 2011).

1.2 Pericyte – Endothelial cell signaling at the NVU

At the NVU, pericytes are embedded in the same basement membrane as endothelial cells and have a central position between the endothelium, astrocytes and neurons. Pericytes extend their processes along the endothelium, generating specialized cell-cell connections called peg-socket contacts, containing N-cadherin and connexin 43 (Armulik, Genové, and Betsholtz 2011a). During BBB homoeostasis pericyte-endothelial crosstalk via several signaling transduction pathways regulates BBB integrity, angiogenesis, phagocytosis, CBF and capillary diameter, neuroinflammation response, multipotent stem cell activity and extracellular matrix protein secretion (**Figure 7**) (M. D. Sweeney, Ayyadurai, and Zlokovic 2016; Winkler, Bell, and Zlokovic 2011).

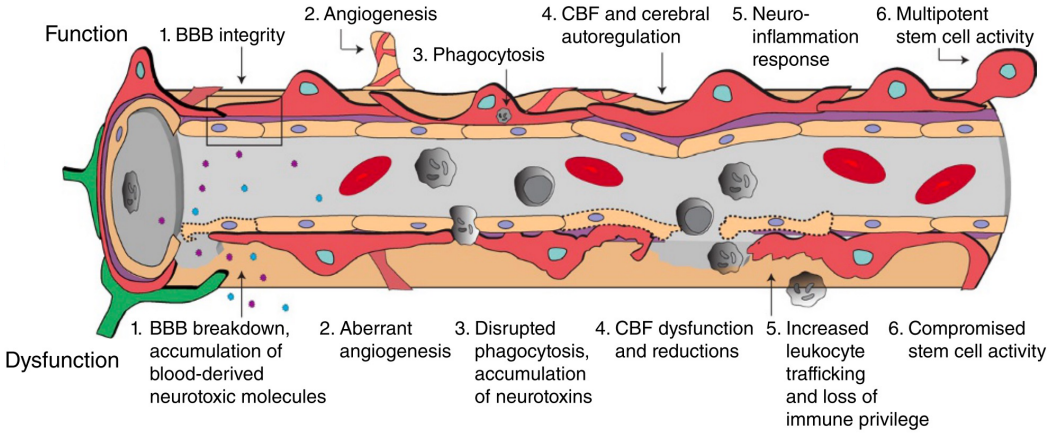

Figure 7|BBB functions controlled by pericyte-endothelial crosstalk. Endothelial cells are represented in orange and pericyte in green. The functions are (1) Regulation of vascular stability, architecture and BBB integrity, (2) angiogenesis, (3) phagocytosis, (4) CBF and capillary diameter, (5) neuroinflammation response, (6) multipotent stem cell activity and (7) extracellular matrix protein secretion. From Sweeney et al., 2016. Copyright permission given in Chapter 7.

1.2.1 Signaling pathways involved in BBB integrity

Recent studies have demonstrated that pericytes play an important role in the formation and maintenance of the BBB. During development, deficient platelet-derived growth factor receptor beta (Pdgfrß) signaling leads to poor pericyte recruitment and coverage, which alters the formation of tight junctions and reduction of transcytosis in the endothelial cells, leading to BBB disruption. Moreover, pericyte-deficient mice don´t downregulate Angiopoietin-2 (Angpt2) or plasmalemma vesicle associated protein (Plvap) proteins, associated with increased vascular permeability (Daneman et al. 2010). Similarly, during adulthood, disrupted Pdgfrß signaling leads to a reduction of tight junction protein expression and an increase in transendothelial transport. Furthermore, adult pericyte loss has been linked to the leakage of neurotoxic and vasculotoxic molecules which increase ROS, cause neuronal injury and lead to neurodegeneration (Bell et al. 2010).

Several studies have shown that pericyte transduction signaling is involved in stabilizing BBB permeability. Pericytes release vesicles containing angiopoietin-1 (Angpt1), which bind to Angiopoietin-1 receptor (also known as Tek or Tie2), activating downstream signaling mediated by phosphatidylinositol 3-kinase (Pi3k)/Akt, leading to an increase of junction proteins like occludin and VE-cadherin and therefore stabilizing endothelial cells (Sharma et al. 2022). Moreover, some studies have shown that during hypoxic conditions, pericyte-derived vesicles increase the expression of tight junctions like ZO1 and claudin-5 in endothelial cells (Yuan et al. 2019). Furthermore, the pericyte release of miR-27b targets semaphoring 6A/D in ECs, leading to an increased endothelial barrier (Demolli et al. 2017).

1.2.2 Signaling pathways involved in Angiogenesis and vascular stability

Pericyte-endothelial crosstalk is involved in angiogenesis and it is believed that pericytes might have opposing roles in angiogenesis depending on the state and point in development. Therefore, during early development, pericytes might be implicated in promoting endothelial cell survival and migration and, later, inducing quiescence and reducing proliferation (Winkler, Bell, and Zlokovic 2011).

During early stages of development, pericytes release connective tissue growth factor (ctgf), which activates the extracellular signal-regulated kinase 1 and 2 (Erk1/2)- signal transducer and activator of transcription 3 (Stat3) axis in the endothelial cells, promoting angiogenesis (Sharma et al. 2022; Zhou et al. 2021). In adulthood and healthy aging, deficiency in Pdgfb or Pdgfrb leads to capillary density reduction and vascular regression (Armulik et al. 2010; Bell et al. 2010). Moreover, pericytes express several matrix metalloproteinases like MMP2, MMP3 and MMP9, which degrade the extracellular matrix, removing mechanical obstacles and therefore promoting endothelial cell migration and proliferation during early development (Winkler, Bell, and Zlokovic 2011).

1.2.3 Signaling pathways involved in phagocytosis and neuroinflammation

Recent *in vitro* studies suggested that pericytes might play a role in an immunological response since they react to different inflammatory cytokines. Upon stimulation, pericytes upregulate MHC II and increase phagocytosis (Pieper et al. 2014). Moreover, pericytes have also been linked with Aß-clearance in AD disease models *in vivo* (Sagare et al. 2013b).

Pericytes might also contribute to and influence neuroinflammation. Studies in pericyte-deficient mice have demonstrated their regulatory effect on leukocyte adhesion in endothelial cells. Moreover, capillaries without pericyte coverage show higher leukocyte trafficking thorough the endothelium (M. D. Sweeney, Ayyadurai, and Zlokovic 2016).

1.2.4 Signaling pathways involved in CBF and vessel diameter

Whether pericytes are contractile cells or not and if they regulate capillary diameter and blood flow in response to neuronal activity has been highly debated in the recent years. However, some studies have shown that pericytes express contractile proteins and receptors for vasoactive molecules (Winkler, Bell, and Zlokovic 2011). Moreover, pericyte dilation and constriction after neurotransmitter stimulation has been shown in organotypic slices (Peppiatt et al. 2006). Furthermore, pericyte-deficient mice show a reduction of CBF, suggesting a role of the pericytes in the regulation of functional hyperemia (Bell et al. 2010).

1.3 Cerebral small vessel disease (cSVD)

Cerebral small vessel disease (cSVD) affects the integrity of small vessels of the brain, including small perforating arterioles, arteries and capillaries. This results in brain damage of the white and deep grey matter, which can be observed by brain imaging using magnetic resonance imaging (MRI) or computed tomography scan (CT) (Wardlaw, Smith, and Dichgans 2019). Imaging analysis revealed that cSVD causes white and grey matter changes like white matter hyperintensities (WMHs), cerebral microbleeds (CMBs), subcortical infarcts, lacunes and atrophy (Wardlaw et al. 2013). These lesions are often associated with dementia, cognitive impairment, depression, increased risk for and a worse outcome from stroke (Debette et al. 2019; Georgakis et al. 2019). cSVD is 6 to 10 times more common than stroke, contributing to approximately 20% of them and to 45% of the dementia cases, resulting in a large healthcare cost. Silent cerebral infarcts are the most frequently identified incidental finding on brain scans, especially in the elderly population (Chojdak-Łukasiewicz et al. 2021).

cSVD is highly diverse and includes rare familial and common sporadic forms, all with different subtypes. However, most of the cSVD cases are sporadic and the most common risk factors are hypertension and diabetes mellitus (van Norden et al. 2011). In the young population, cSVD is mainly caused by genetic factors, where several single genes present different mutations. The most common

genetic form of cSVD is cerebral autosomal dominant arteriopathy with stroke and ischemic leukoencephalopathy (CADASIL) generated by an autosomal dominant mutation in the NOTCH gene. Similarly, HTRA1 mutations generate the recessive form or autosomal recessive arteriopathy with subcortical infarcts and leukoencephalopaty (CARASIL). Mutations in the genes responsible for the synthesis of collagen type IV (COL4A1 and COL4A2), key component of the extracellular matrix, also generate cSVD associated with microangiopathies (Chojdak-Łukasiewicz et al. 2021).

1.4 Forkhead Box F2 (FOXF2)

The FOX genes encode for the forkhead box (FOX) transcription factor family, composed of 19 different transcription factor subfamilies. All transcription factors are characterized by a conserved wingled helix DNA-binding domain, and they all act as key transcription factors in different organs at different points in development (Wu, Li, and You 2021). The FOXF subfamily is composed of two different genes, FOXF1 and FOXF2, which are both key transcription factors for embryonic development (Aitola et al. 2000).

FOXF2, located on chromosome 6 in humans and on chromosome 13 in mice, is a 444 amino acid protein implicated in cell growth, differentiation and metastasis regulation by DNA-binding through its forkhead domain, which is 100 amino acids long (Myatt and Lam 2007). Aberrant FOXF2 expression dysregulates cell proliferation, differentiation and metastasis, since downstream genes are associated with Wnt/ß-catenin and TGFß/SMAD signaling pathways (Higashimori et al. 2018).

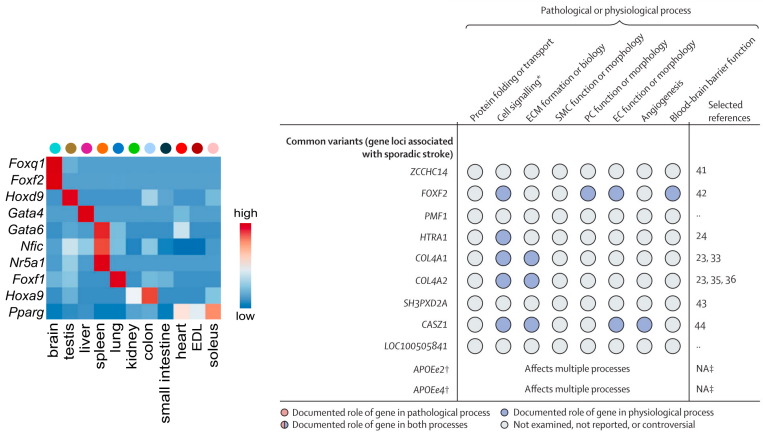

Figure 8|Foxf2 is highly enriched in the brain and FOXF2 is associated with physiological and pathological processes related with cSVD and stroke. Left panel shows Foxf2 enrichment in brain endothelial cells compared to other organs (from Kalucka et al., 2020). Right panel shows FOXF2 relation with key processes such as cell signaling, pericyte (PC) and endothelial (EC) function or morphology and BBB function (adapted from Dichgans, 2019). Copyright permission given in chapter 7.

In the CNS, single-cell sequencing studies have shown that FOXF2 is mainly expressed in endothelial cells and mural cells in both, human and mouse (Vanlandewijck et al. 2018; Kalucka et al. 2020; A. C. Yang et al. 2022). Moreover, FOXF2 has been recently identified as a brain-endothelial specific transcription factor associated with BBB maturation (Hupe et al. 2017) (**Figure 8**). Furthermore, FOXF2 induces the expression of BBB markers such as ABCB1 and SCLOB1 in human brain microvascular

endothelial cells, promoting blood vessel development (Hupe et al. 2017; He et al. 2020). Other studies have shown that FOXF2 is responsible for endothelial cell – pericyte regulation as well as the production of extracellular matrix in the basement membrane of blood vessels (Wu, Li, and You 2021). Along the same lines, Foxf2 inactivation during development has shown that the Pdgfb/Pdgfrß-Tgfß pathway, critical for endothelial – pericyte communication, is affected (Reyahi et al. 2015). *In vitro* studies have also identified FOXF2 as a key transcription upregulating some EC tight junctions and increasing endothelial cell barrier resistance (Roudnicky et al. 2020).

Common genetic variants of FOXF2 are associated with stroke, cSVD and an increase in white matter hyperintensities (Chauhan et al. 2016b; Malik et al. 2018). FOXF2 variant rs12204590 increases small arterial occlusion stroke risk in the European population (Chauhan et al. 2016b) whereas rs1711972 variant increases large-artery atherosclerotic ischemic stroke in the Han Chinese population (Shi et al. 2017). The genetic region containing the variant rs12204590 includes two protein-coding genes FOXF2 and FOXFQ1, and the microRNA MIR6720. 1Mb expansion around the variant also includes two other protein-coding genes FOXC1 and GMS and a non-coding RNA (LINC01622) (**Figure 9**). Expression quantitative trait loci (eQTL) for the protein-coding genes were not available. However, different histone modifications were associated with FOXF2 and FOXQ1, suggesting that cSVD phenotypes are likely due to one or both of those genes (Chauhan et al. 2016b).

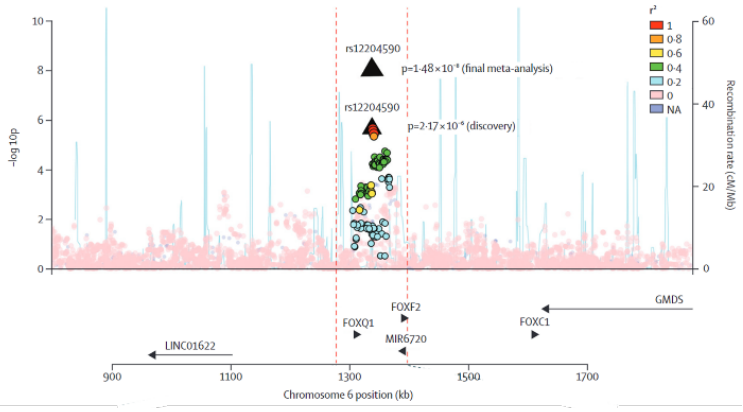

Figure 9|Regional association of variant rs12204590. Plot showing all genes around variant rs1220450. Color code stands for linkage disequilibrium between SNPs (r2). Blue lines represent estimated recombination rates. From From Chauhan et al., 2016. Copyright permission given in chapter 7.

Despite FOXQ1 being expressed in the vasculature (Vanlandewijck et al. 2018; A. C. Yang et al. 2022), mutant mice present with hair differentiation and gastric mucin secretion alterations but no cerebrovascular phenotypes (Hong et al. 2001; Verzi et al. 2008). On the other hand, it is known that FOXC1, located 225kb downstream of FOXF2, is implicated in vessel morphogenesis, proteoglycan expression (Siegenthaler et al. 2013) and arteriovenous specification (Fish and Wythe 2015). Moreover, patients with FOXC1 mutations present with Axenfelder-Rieger syndrome, which generates poor development of the ocular anterior segment and increases MRI affections related with cSVD (French et al. 2014). Despite FOXC1 being implicated in vascular affections, patients with segmental deletions encompassing FOXF2 and FOXC1 presented with ten-times higher white matter hyperintensities typical MRI alteration of cSVD (Chauhan et al. 2016b). Furthermore, recent studies

have shown that these genetic variants decrease the activity of a FOXF2 enhancer, thus decreasing the levels of FOXF2 in the vascular wall over the lifespan of patients, contributing to a higher risk of stroke (J. R. Ryu et al. 2022).

Recent studies in mice have shown that global Foxf2 inactivation during development recapitulates some of the cSVD phenotypes such as intracerebral hemorrhage and perivascular edema (Chauhan et al. 2016b; Reyahi et al. 2015). Moreover, inactivation leads to increased proliferative pericytes, reduction of Smad2/3 and increase of phosphorylated Smad1/5, pathways involved in the differentiation and proliferation of endothelial cells and pericytes. Furthermore, Pdgfb/Pdgfrß and Tgfß pathways involved in pericyte-endothelial communication and related with BBB maintenance are altered, suggesting that Foxf2 mutants' BBB breakdown (**Figure 10**) might be due to a reduction in Pdgfrß signaling, whereas hemorrhage and vascular instability is due to a decrease in the Tgfß pathway. Lastly, global Foxf2 inactivation also leads to endothelial thickening and increased vesicular transport, demonstrating the importance of Foxf2 for the vasculature maintenance (Reyahi et al. 2015).

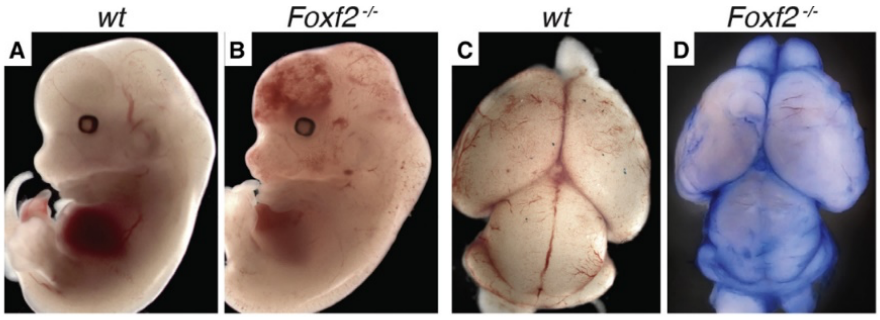

Figure 10|Foxf2 deletion leads to leaky BBB. A-B show ICH from E13.4 embryos and C-D Evans blue leakage in E18.5 embryos. From Reyahi et al., 2015. Copyright permission given in Chapter 7.

1.5 Human induced pluripotent stem cells (iPSCs)

Recent advances in the discovery and generation of induced pluripotent stem cells (iPSCs) from mouse (Takahashi and Yamanaka 2006) and human (Takahashi et al. 2007) have provided new tools for the generation of *in vitro* models. iPSCs can be generated from any somatic cell like skin fibroblast or blood cells by the overexpression of four defined transcription factors: Oct-4, Sox2, c-Myc and Klf4 (Takahashi and Yamanaka 2006). Due to their high proliferation capacity, iPSCs provide an alternative for large-scale cell production for *in vitro* studies without invasive patient sampling or animals usage (Delsing et al. 2020). iPSCs can be generated from several patients carrying different mutations to generate patient-specific cell lines, which allows better disease modelling as well as study human-specific disease mechanisms (C. Liu et al. 2018). Despite the advances they provided in the *in vitro* field, epigenetic memory is lost during reprogramming, complicating studies on diseases influenced by environmental factors (Tapia and Schöler 2016).

Most of the developed iPSC differentiation protocols have been based on mimicking signaling processes that occur during embryogenesis. iPSC-somatic differentiation has allowed the *in vitro* study of many cell types that are very hard to isolate and culture, like endothelial or neural cells (Delsing et al. 2020).

1.5.1 iPSC-derived endothelial cells

There are different methods for the generation of endothelial cells from iPSCs: co-culture with neural or stroma cells, embryoid body formation, 2D monoculture or transdifferentiation (Williams and Wu 2019). Despite the initial belief that feeder cells were needed for endothelial cell differentiation, mesoderm induction via BMP4 is sufficient (S. W. Park et al. 2010).

Since BEC have different characteristics from peripheral endothelial cells, specific differentiation protocols are needed for proper *in vitro* BBB study. One of the most used protocols in recent years for BEC differentiation is based on the spontaneous co-differentiation of endothelial and neural cells followed by an endothelial purification by seeding onto specific matrix coating (Lippmann et al. 2012). Several changes in the protocol have improved the yield of the differentiation, such as the addition of retinoic acid (Lippmann et al. 2014), seeding density optimization (Wilson et al. 2015) or differentiation during hypoxia (T.-E. Park et al. 2019). Endothelial cells generated by the described protocol not only express typical markers like Glut1, Claudin-5, Occludin or Pecam-1 but also display high transendothelial electrical resistance (TEER) and low permeability values (Lippmann et al. 2014; Canfield et al. 2017). Despite being used in a lot of *in vitro* BBB modelling, recent studies have shown that the generated cells resemble epithelial cells more than brain endothelial cells (Lu et al. 2021), illustrating the difficulty of BEC differentiation.

Other protocols with more defined media have been developed in recent years, such as the combination of BMP4 and CHIR99021 (inhibitor of GSK-3 enzyme) for mesoderm induction followed by Forksholin and VEGF-A for endothelial cell specification (Patsch et al. 2015). Moreover, those methods have been combined with endothelial cell selection via MACS sorting to improve purity and differentiation yield (Orlova, Drabsch, et al. 2014; Praça et al. 2019; Gastfriend et al. 2021). Lastly, some other studies have used the overexpression of key endothelial transcription factors like ETV2 for the generation of endothelial cells (K. Wang et al. 2020; H. Zhang et al. 2022).

1.5.2 iPSC-derived mural cells

Pericyte differentiation protocols have been difficult to establish due to the lack of a well-defined cell type, as pericyte origin, marker proteins and functional characteristics have been highly debated in the past years (Delsing et al. 2020). The most commonly used protocols have been based on mesoderm induction combined with endothelial cell differentiation (Orlova, Van Den Hil, et al. 2014; Kumar et al. 2017). Despite the fact that the main brain-pericyte differentiation protocol is neural crest based (Stebbins et al. 2019), mesoderm- and neural crest-derived pericytes have shown similar results (Faal et al. 2019). Recent single cell-RNA studies have shown the expression of specific markers and special functions for pericytes (Vanlandewijck et al. 2018; A. C. Yang et al. 2022), opening new opportunities for the development of optimized protocols.

During development, vSMCs are derived from different lineages: neuroectoderm, lateral-plate mesoderm and paraxial mesoderm. Once they are established in the vasculature, they switch between two different phenotypes, contractile and synthetic (Trillhaase et al. 2015). Some differentiation protocols focus on generating lineage specification (Cheung et al. 2014) while others have facilitated phenotype-specification (L. Yang et al. 2016). Moreover, some other protocols have focused on the generation of vSMCs in combination with endothelial cells (Kumar et al. 2017). Most of the protocols have the mesoderm induction followed by SMC fate through culturing with TGFß and PDGF-BB in common (Trillhaase et al. 2015).

1.5.3 iPSC-derived astrocytes

In vivo astrocyte differentiation spans from embryonic development until after birth, therefore, mimicking embryogenesis signaling processes is time consuming and most of the available protocols take several months until astrocytes are fully mature (Delsing et al. 2020). Despite some protocols attempting to shorten the differentiation process by remodeling the chromatin structure (Majumder et al. 2013) or by the overexpression of different transcription factors (Li et al. 2018) most of the alternatives are still quite laborious and take more than a month. Astrocytes can also be differentiated through the generation of neural precursor cells (NPCs) by inhibition of TGFß/BMP signaling (Chambers et al. 2009). Culturing with epidermal growth factor (EGF) and leukemia inhibitory factor (LIF) promotes a glia lineage, that can be pushed into astrocytes through culturing with ciliary neurotropic factor (CNTF) (Bonni et al., n.d.; TCW et al. 2017). While most of the protocols use serum for the final maturation steps, a recent protocol has shown that avoiding serum exposure not only allows astrocyte differentiation but also generates non-reactive cells (Perriot et al. 2018).

iPSC-derived astrocytes express typical markers such as GFAP, S100B, CD44 and EAAT1 and are functional as seen by glutamate uptake and inflammatory response (Delsing et al. 2020).

1.6 *In vitro* models of the BBB and NVU

1.6.1 Cell precedence for BBB *in vitro* modelling

The NVU is a multicellular structure with several cell-cell and cell-matrix interactions, therefore, proper *in vitro* modelling needs to include different cellular components and appropriate extracellular matrix (Potjewyd, Kellett, and Hooper 2021). BBB *in vitro* models are important and necessary tools to investigate drug development and delivery into the CNS. Most of promising drug candidates identified in animal models fail in clinical trials (Perrin 2014), demonstrating the need of human pre-clinical models also for drug development. *In vitro* modelling will not only provide higher human transferability, but also reduce the use of animals for research (Delsing et al. 2020).

In the last years, several BBB *in vitro* models using human and animal (mainly mouse and rat) primary cells have been described. Despite primary animal cells proving to be a good tool for studying barrier integrity due to their low permeability (Abbott 2004; Garberg et al. 2005), they have high variability since isolation protocols are difficult and laborious, and they also do not further reduce the number of animals in research. Moreover, it has been shown that BBB efflux transporters like Pgp are differentially expressed between mouse and human (Syvänen et al. 2009; Uchida et al. 2011), demonstrating the importance of species-specific modelling.

Immortalized human and mouse cells provide an alternative to primary isolated cells. However, most mouse lines, such as b.End3, do not form a tight barrier and, therefore, do not provide a good source for BBB modelling (Omidi et al. 2003). Despite immortalized human lines, like hMEC/D3, providing important insights in barrier properties, drug uptake and transport, they do not fully form a stable barrier, and co-culturing with other cell types does not increase the BBB properties (Weksler, Romero, and Couraud 2013; Eigenmann et al. 2013).

iPSC-derived models provide an alternative for overcoming most of the limitations, including species differences and the generation of all cell types. Furthermore, such systems provide the opportunity for isogenic models where all the cell types are derived from the same individual. Nevertheless, iPSC models require from several differentiation protocols which can be challenging due to variabilities in protocols and handling. Furthermore, achieving high reproducibility may be difficult due to different parental iPSC lines. Therefore, model standardization, characterization and validation are needed (Delsing et al. 2020). Several iPSC-derived BBB models have been developed recently and used for permeability studies (Appelt-Menzel et al. 2017; Delsing et al. 2018; Lippmann et al. 2012), BBB disruption (Page, Raut, and Al-Ahmad 2019) and disease modelling (Faal et al. 2019; Katt et al. 2019; Orlova et al. 2022), validating the applicability of the iPSC-derived cells.

1.6.2 Model systems to study the BBB *in vitro*

1.6.2.1 Transwell models

Transwell systems are one of the simplest methods where the BBB is mimicked by a semipermeable membrane, which separates a luminal and abluminal side, allowing cell seeding on both sides (Naik and Cucullo 2012). Most commonly, endothelial cells are placed in a monolayer on top of the porous membrane, or luminal side, and mural cells or astrocytes are placed on the bottom, or abluminal, side (Wolff et al. 2015). Although this system ignores key features of the endothelium, like vessel formation or sheer stress, it also reduces the number of variables, generating less variability and easier characterization. This model has been widely used for permeability screening assays, since molecules can be added into the apical or luminal side and the accumulation can be measured in the basal or abluminal side (Zidarič, Gradišnik, and Velnar 2022). Furthermore, it allows a barrier quantification by measuring trans endothelial electrical resistance (TEER) without destroying the cells (Gastfriend, Palecek, and Shusta 2018).

The most commonly used configurations of the transwells models are monoculture, co-culture or tricultures. In all cases, endothelial cells are placed on the surface of the semipermeable membrane, and the supporting cells, like astrocytes or pericytes, are seeded on the bottom. In the triculture, the most common configuration is endothelial cells on top of the porous membrane, mural cells on the bottom part of the membrane and astrocytes on the bottom of the well (Katt and Shusta 2020; Gastfriend, Palecek, and Shusta 2018; Zidarič, Gradišnik, and Velnar 2022; Helms et al. 2016). It has been shown that co-culture and tri-culture induce more BBB-like characteristics, like higher TEER values (Hatherell et al. 2011a; Lippmann et al. 2012).

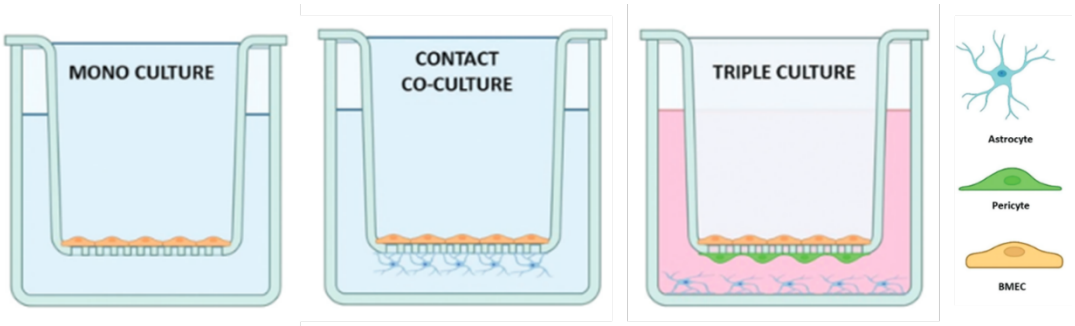

Figure 11|Common configurations of transwell studies. Endothelial cells are represented in orange, pericytes in green and astrocytes in blue. Three types of transwell systems for modelling the BBB: monoculture, co-culture and tri-culture. From Zidarič et al., 2022.

One of the main limitations of the transwell models is that they do not allow for cell-cell contact, which is essential in the formation and maintenance of the NVU (Gastfriend, Palecek, and Shusta 2018). Nevertheless, the transwell system allows the culturing of cell types on both sides of a membrane and the exchange of soluble factors between them (Helms et al. 2016; Gastfriend, Palecek, and Shusta 2018).

1.6.2.2 Organoids

Advances in iPSC technology include the generation of organoids, “mini-organ-like” tissues or self-organized cell aggregates, that recapitulate some of the physiological conditions of a developing brain (Lancaster et al. 2013; Pacitti, Privolizzi, and Bax 2019). Compared to transwell assays, they allow the cell-cell interaction in a 3D environment, which is crucial for NVU functioning. Nevertheless, they have some limitations including variable morphology and size, absence of specific cells and limited oxygen and nutrient diffusion, which lead to a necrotic core most of the time (Chiaradia and Lancaster 2020).

One of the main challenges of organoids is the generation of a well-defined vascularization that allows BBB integrity measurement (Vargas-Valderrama et al. 2020). Some studies have shown that incorporation of endothelial cells leads to tubular-like structure formation and vascularization upon implantation in mice (Cakir et al. 2019; Mansour et al. 2018; Pham et al. 2018). Although this vascularization overcomes the oxygen and nutrient diffusion, reducing the necrotic core, it also limits the human-specific species, since it´s mostly murine (Caffrey, Button, and Robert 2021). Other studies have tried the co-differentiation of endothelial cells with neural cell types. VEGF and Wnt7a treatment increase the expression of CD31 and Claudin-5 tubular-like structures surrounded by pericyte-like cells (Ham et al. 2020). Furthermore, overexpression of ETV2 also leads to the formation of a vascular network expressing Claudin-5, occludin and ZO1 in cerebral organoids (Cakir et al. 2019). Lastly, other studies have tried to approach the vascularization problem by the co-culture of endothelial and cerebral spheroids. The combination of neural progenitor cells with endothelial spheroids and iPSC mesenchymal stem cells led to greater ECM formation and higher expression of CD31 and GLUT1 in ECs (Song et al. 2019).

Other studies have focused more on the generation of BBB organoids or Spheroids. iPSC-derived organoids containing endothelial cells and pericytes generate capillary networks that are fully perfused after transplantation into mice (Wimmer et al. 2019). Furthermore, others have reported BBB organoids expressing tight junctions, transporters and drug efflux pump activity (Cho et al. 2017; Bergmann et al. 2018).

1.6.2.3 Microfluidic models

Advances in microfluidic systems have provided an alternative for improved NVU modelling since they can better approximate the 3D conformation, shear stress and cell-cell interactions (Aday et al. 2016; Oddo et al. 2019). There are two main categories for the generation of 3D models: organoid-like microfluidics, which relay in *in vitro* angiogenesis and therefore self-assembly of the cells, and mold assembly microfluidics, where cells adhere to a specific biomaterial, making a more reproducible and robust model when compared to a self-assembly situation (Fernandes, Reis, and Oliveira 2021; Zidarič, Gradišnik, and Velnar 2022). Most of microfluidic systems mimic the 3D morphology, allow the cell-

cell interaction and are subject to shear stress, recapitulating better *in vivo* conditions (Delsing et al. 2020).

Culturing human brain microvascular endothelial cells (hBMECs) in a channel under shear stress separated from a porous membrane from human pericytes and astrocytes results in less reactive astrocytes and is more similar to physiological conditions, demonstrating the importance of the 3D conformation for *in vitro* modelling (Ahn et al. 2020). Moreover, seeding of hBMEC with pericytes on the surface of a gel containing astrocytes and a chemotactic angiogenesis gradient, resulted in a more *in vivo* 3D morphology and better cellular interactions (S. Lee et al. 2020). Other studies have also shown that co-culturing endothelial cells, pericytes and astrocytes leads to self-organization into a vascular network via vasculogenesis, forming a mature BBB (Campisi et al. 2018), and displaying mural cell disruption in disease (Orlova et al. 2022). However, most of these models use a combination of primary and iPSC-derived human cells, and few fully iPSC-derived models have been reported: one using endothelial cells and pericytes (Jamieson et al. 2019) and one using endothelial cells and neural cells (Vatine et al. 2019a).

The main disadvantage of microfluidic devices is that relay in angiogenesis, and therefore vascular network geometry and flow is difficult to recapitulate and highly variable between experiments (Zidarič, Gradišnik, and Velnar 2022; Caffrey, Button, and Robert 2021).

1.7 CRISPR/Cas9 genome editing

1.7.1 CRISPR/Cas9 as a tool for precise genome editing

The CRISPR/Cas9 system was discovered in bacteria where it acts as an adaptative immune system response. CRISPRs (Clustered Regularly Interspaced Short Palindromic Repeats) are small non-coding RNAs that, together with the Cas proteins, protect bacteria from future viral infections. When bacteria are infected by bacteriophages, they have the ability to cleave the viral DNA and integrate short sequences from it into repetitive genetic elements or CRISPR arrays, which are expressed and destroy the pathogen's DNA in a future infection (Barrangou 2007; Richter, Chang, and Fineran 2012; Hille et al. 2018).

Further developments of the system have adapted it into a precise and efficient tool for genome editing in mammalian cells (Cong et al. 2013; Mali et al. 2013). The Cas9 nuclease, which facilitates RNA-guided DNA cleavage in bacteria (Garneau et al. 2010), can be combined with a single guide RNA (sgRNA) for specific DNA locus targeting, where it will introduce a double strand break (DSB) (Mojica et al. 2009; Sander and Joung 2014). The CRISPR/Cas9 system can be delivered by plasmid (Mali et al. 2013) or by RNPs (Zuris et al. 2014) into the cells for precise genome editing. The cell has two main mechanisms for DSB repair: non-homologous end joining (NHEJ) and homology-directed repair (HDR)

(Scully et al. 2019), and both can be used for modifying the genome. In the NHEJ pathway, the two DNA strand ends are fuse together, a process which is highly prone to error, generating insertion or deletions (InDels) of various lengths around the cut site. These InDels usually produce frameshift, which disrupt the translational reading frame and leads often to premature stop codons, which is useful for the generation of knock-out protein (Mali et al. 2013; Sander and Joung 2014). The HDR pathway uses a donor template to repair the DSB, and therefore, is more precise. This can be used to introduce specific mutations or knock-ins in a target locus by delivering a repair template together with Cas9 and gRNA (**Figure 12**) (Mali et al. 2013; Paquet et al. 2016).

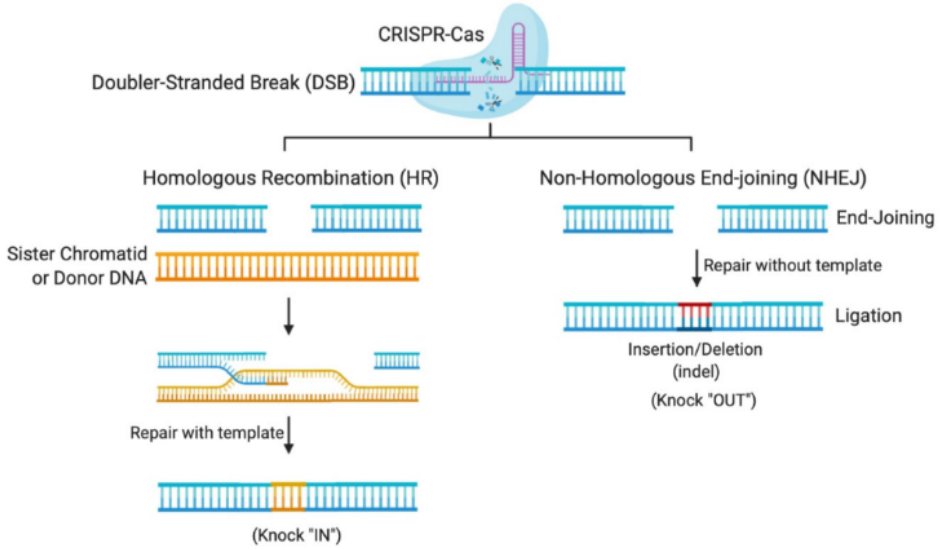

Figure 12|Repair pathways after a DSB introduced by CRISPR/Cas9 system. After the Cas9 nuclease generates a DSB there are two main repair pathways: HR (also HDR) and NHEJ. The HDR pathway uses a template for the repair and can be used for the generation of knock-in edits. The NHEJ pathway repairs the DSB without a template, being prone to error, resulting in insertion or deletion of bases, which can be use for the generation of knock-out edits. From Shalaby et al., 2020.

1.7.2 CRISPR/Cas9 for disease modelling *in vitro* using iPSCs

The combination of iPSC technology and CRISPR/Cas9 genome editing offers new tools for studying and modeling human disorders *in vitro*. One of the main advantages of the combination of technologies is that genetic mutations can be studied in the disease-relevant cell types in different human genetic backgrounds, which is important for complex diseases. Moreover, it allows the analysis of hard-to-access patient cell types, like neurons or oligodendrocytes (Heidenreich and Zhang 2015).

Genome editing can be used to study different mutations that arise from genome-wide association studies (GWASs) by using human iPSCs. There are mainly two approaches for the iPSC source: from patients with specific mutations or disorders, or healthy donors. In both cases, isogenic cell lines can be generated by genome editing, allowing a direct comparison between normal and disease genotypes (**Figure 13**). In the case of iPSCs with specific mutations, genome editing can be used for correcting the mutation, whereas healthy iPSCs can be used to introduce specific mutations or risk variants (Heidenreich and Zhang 2015; Sen and Thummer 2022). Several studies have already used the combination of genome editing and iPSC technology for the study of different neurological disorders like Huntington's disease (Jeon et al. 2012; Linville et al. 2022), Alzheimer's disease (Yagi et al. 2011), Parkinson's disease (Ambasudhan et al. 2013; Soldner et al. 2011) and vascular diseases (Orlova et al. 2022).

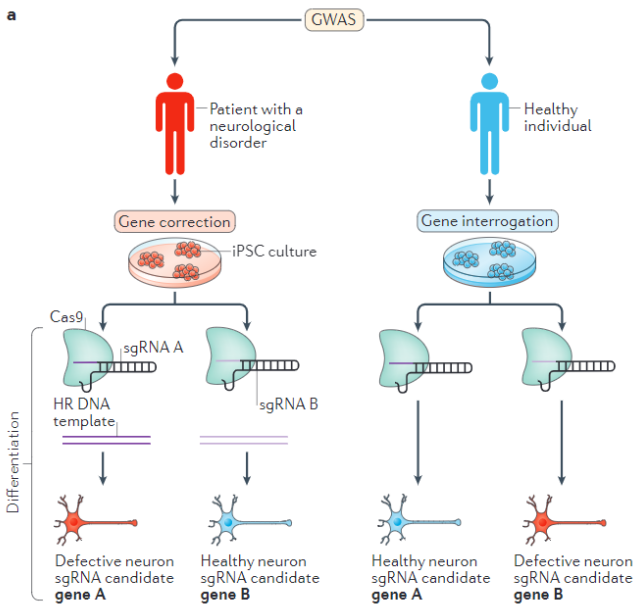

Figure 13|Combination of iPSC and CRISPR/Cas9 genome editing technologies for *in vitro* disease modelling. iPSC-derived disease modelling can be done from patients with mutations (shown in red) and correcting the cells without mutations and from healthy donors (shown in blue) and introducing mutations for disease study. From Heidenreich et al., 2015. Copyright permission given in Chapter 7

2. Aims of this study

FOXF2 encodes a transcription factor that is mainly expressed in endothelial cells and pericytes in the CNS vasculature. Recent genetic studies in humans have shown that genetic variants at FOXF2 associate with stroke, cSVD and chronic white matter lesions in humans. While global Fxf2 inactivation in mice results in BBB impairment and partially recapitulates cSVD phenotypes, the function and mechanisms by which Foxf2 impairs the BBB are poorly understood. Moreover, how Foxf2 specifically regulates endothelial cell and pericyte functions are still elusive. Understanding the molecular mechanism implicating FOXF2 in physiological cell function and disease will not only help to understand BBB impairment in neurovascular diseases but may also provide new targets for therapeutic intervention

Since FOXF2 emerged from a human genetic study during my work on this thesis I aim to develop both a human *in vitro* model providing better transferability of the results to patients and a platform for therapeutic discovery, and a mouse *in vivo* model allowing to study Foxf2 deficiency on a whole organism level.

The first goal of this thesis is to generate a human iPSC 3D model that can fully recapitulate central aspects of the BBB and allows investigating disease phenotypes. For that, we would need first to optimize and adapt protocols for the differentiation of endothelial cells, pericytes, smooth muscle cells and astrocytes. Once the differentiations are established, we will characterize the identity of these cells and subsequently co-culture them in a 3D environment using microfluicid chips.

The second goal is to generate two different models which will allow us to study the consequences of FOXF2 deletion in endothelial cells and pericytes. The first model will be a mouse model, where Foxf2 will be deleted only from endothelial cells or pericytes and which will allow us to study the effects of Foxf2 deletion *in vivo*. The second model will be a human *in vitro* model where we knock out FOXF2 by CRISPR/Cas9 in human iPSCs. These iPSCs will be further differentiated into endothelial cells and pericytes.

The third goal is to better understand the cell-autonomous mechanisms of Foxf2 in endothelial cells and pericytes. For that we will perform proteomic analysis from mouse endothelial cells and human endothelial cells and pericytes.

3. Research articles

3.1. A human iPSC-derived 3D blood-brain-barrier in vitro model recapitulates mouse cerebrovascular phenotypes induced by FOXF2 deficiency

Authors:

Judit González-Gallego*, Katalin Todorov-Völgyi*, Stephan A Müller, Martina Schifferer, Isabel Weisheit, Mihail Ivilinov Todorov, Barbara Lindner[1], Dennis Crusius, Joseph Kroeger, Mark Nelson, Tom R. Webb, Ali Ertürk, Mika Simons, Stefan Lichtenthaler, Martin Dichgans*, Dominik Paquet*

A human iPSC-derived 3D blood-brain-barrier *in vitro* model recapitulates mouse cerebrovascular phenotypes induced by FOXF2 deficiency

Judit González-Gallego[1,2*], Katalin Todorov-Völgyi[1*], Stephan A Müller[3], Martina Schifferer[3,4], Isabel Weisheit[1,2], Mihail Ivilinov Todorov[1,5], Barbara Lindner[1], Dennis Crusius[1], Joseph Kroeger[1,2], Ali Ertürk[1,4,5], Mikael Simons[3,4], Stefan Lichtenthaler[3,4], Martin Dichgans[1,2,4,6*], Dominik Paquet[1,2,4*]

1) Institute for Stroke and Dementia Research (ISD), University Hospital, LMU Munich, Munich, Germany
2) Graduate School of Systemic Neuroscience (GSN), University Hospital, LMU Munich, Munich, Germany
3) German Center for Neurodegenerative Diseases (DZNE) Munich, Munich, Germany
4) Munich Cluster for Systems Neurology (SyNergy), Munich, Germany.
5) Institute for Tissue Engineering and Regenerative Medicine (iTERM), Helmholtz Zentrum München, Neuherberg, Germany
6) German Centre for Cardiovascular Research (DZHK, Munich), Munich, Germany

* Contributed equally.

Electronic address:
Martin.Dichgans@med.uni-muenchen.de
Dominik.paquet@med.uni-muenchen.de

Abstract

Malfunction of the blood-brain-barrier (BBB) takes center stage in neurovascular disorders including cerebral small vessel disease (SVD), a common cause of stroke and vascular dementia. FOXF2 has recently been identified as a major risk gene for stroke and SVD. Yet, the molecular and cellular mechanisms linking FOXF2 deficiency to neurovascular dysfunction remain elusive. So far, SVD has mostly been studied in mouse and non-physiological in vitro models, which display some disease features, but lack complex phenotypes, have limited translatability to humans, and are not well suited for drug discovery. To better understand the role of FOXF2 in SVD, we developed a fully human iPSC-derived 3D model of the BBB by co-culture and microfluidic 3D tissue engineering of key BBB cell types: endothelial cells, mural cells and astrocytes. Our model expresses typical cell fate markers, forms vessel-like tubes and enables controlled perfusion, including with human blood.

FOXF2 knockout cultures display key features of impaired BBB function, including compromised cell junction integrity, decreased transendothelial electrical resistance (TEER) and increased caveolae formation. Proteomics analysis of endothelial cells and pericytes revealed an impairment of pathways related to pericyte-endothelial cell crosstalk, suggesting a role of FOXF2 in vascular signaling. The observed disease features phenocopy those seen in an endothelial cell-specific model of Foxf2 deficiency developed in parallel, validating the importance of iPSC-derived in vitro models. Moreover, treatment of FOXF2 knockout cultures with lipid-nanoparticle-mediated delivery of FOXF2 mRNA restored the levels of cell junction and caveolin-1 proteins, demonstrating the applicability of the model for screening therapeutics.

Introduction

The central nervous system (CNS) requires a tightly controlled chemical and metabolic environment for proper functioning of the brain (Sweeney et al. 2019), which is maintained and regulated by the neurovascular unit (NVU). One of the main role of the NVU is the coupling between neural activity and blood flow astrocytes (Iadecola 2017). In within the NVU, the blood-brain-barrier (BBB) is composed of brain endothelial cells (BECs), pericytes or smooth muscle cells, and astrocytes (Zlokovic 2011; Zhao et al. 2015; Iadecola 2017). BECs are responsible for restricting and controlling the entry of nutrients, oxygen, circulating cells and pathogens into the brain parenchyma (Winkler, Bell, and Zlokovic 2011; Zhao et al. 2015). BECs have unique characteristics that contribute to the formation of the BBB's physical barrier and differ from endothelial cells present in other organs. BECs exhibit low transcytosis rates, high mitochondria abundance and pronounced tight/adherens junction formation between cells, which results in a non-fenestrated cell layer (Abbott, Rönnbäck, and Hansson 2006; Zlokovic 2008). Malfunction of the NVU plays a central role in neurovascular disorders which may lead to neuronal degeneration via NVU disruption and the accumulation of neurotoxic molecules in the brain (Zlokovic 2011).

Recently, Foxf2 has been identified as an important transcription factor in BECs associated with BBB maturation (Hupe et al. 2017). FOXF2 encodes a transcription factor which regulates cell growth, signal transduction and differentiation by direct binding of its forkhead domain to targets on nuclear DNA (Myatt and Lam 2007; Wu, Li, and You 2021). It plays a crucial role during blood vessel development by inducing the expression of BBB markers such as ABCB1 and SCLCOB1 in human brain microvascular endothelial cells (Hupe et al. 2017; He et al. 2020). Single-cell RNA studies have shown that FOXF2 is mainly expressed in endothelial cells, pericytes and smooth muscle cells in the brain (Vanlandewijck et al. 2018; Kalucka et al. 2020; Yang et al. 2021), key components of the NVU. Furthermore, FOXF2 is responsible for regulating the interaction between pericytes and endothelial cells as well as the production of extracellular matrix (ECM) in the basement membrane of blood vessels (Wu, Li, and You 2021). Common genetic variants of FOXF2 are associated with cerebral small vessel disease (SVD) and increased white matter hyperintensities (Chauhan et al. 2016; Malik et al. 2018; Duperron et al. 2023). SVD is responsible for the majority of ischemic and hemorrhagic strokes and contributes to half of dementia cases worldwide (Wardlaw, Smith, and Dichgans 2019). Despite its important role in health, SVD mechanisms are poorly understood. Recent studies have shown that global Foxf2 inactivation during development in mice recapitulates some SVD phenotypes, such as BBB deficits and intracerebral hemorrhage (Reyahi et al. 2015), establishing FOXF2 as a central player in NVU integrity.

So far, animal models have formed the backbone of research for studying the NVU in health and disease as well as investigating drug delivery approaches. While animal models have

provided important insights into physiology and functioning of the NVU, genetic and molecular differences limit translation of animal findings to humans (Hajal et al. 2021).These drawbacks are also reflected by the fact that promising drug candidates identified in mouse models have failed in clinical trials (Perrin 2014). As such, there is an urgent need for the development of human models that recapitulate central aspects of the BBB/NVU and its malfunction in disease.

Recent advances in the generation of induced pluripotent stem cells (iPSCs) (Takahashi and Yamanaka 2006) and differentiation protocols for endothelial cells (ECs), smooth muscle cells, pericytes and astrocytes (Aday et al. 2016) have provided new tools for the generation of human *in vitro* models. Most current BBB models are transwell based co-cultures of different NVU cell types, where endothelial cells and astrocytes/mural cells are cultured on different sides of a semipermeable membrane. Although these models have shown phenotypes closer to the *in vivo* condition than monocultures, such as direct endothelial cell-astrocyte contacts and induction of greater endothelial cell barrier function (Lippmann et al. 2012), they still represent a simplification of the *in vivo* BBB. Moreover, ECs respond to dimensionality by changing gene expression and activating different signaling pathways, indicating the importance of developing more physiological 3D models (Potjewyd et al. 2018; Caffrey, Button, and Robert 2021).

Microfluidic systems have provided a better alternative for approximating the BBB as has been shown in recent studies combining primary and iPSC-derived cells (Aday et al. 2016; Campisi et al. 2018; van Dijk et al. 2020; Orlova et al. 2022). However, despite these recent advancements of iPSC-derived systems, well-characterized fully iPSC derived models recapitulating relevant aspects of human neurovascular diseases have so far not been described.

Here we developed a fully human microfluidic iPSC-derived multicellular model of the BBB. We first established and optimized simple differentiation protocols to produce well-characterized endothelial cells (EC), smooth muscle cells (SMC), pericytes (PE) and astrocytes (AS) with high purity and yield. We then compared them at transcriptome and proteome level to their primary human counterparts and deposited this data in a publicly available comprehensive database, which also reveals correlations between RNA and protein abundance levels of human iPSC-derived cells. Based on these iPSC-derived cell types we engineered a 3D model recapitulating key features of the BBB. To better understand the mechanisms of SVD in the context of FOXF2 loss, we deleted FOXF2 in iPSCs and differentiated them into BBB components to establish an isogenic BBB model of FOXF2 deficiency. FOXF2 knockout cultures display key features of impaired NVU function, including compromised cell junction integrity, decreased transendothelial electrical resistance (TEER) and increased caveolae density. Furthermore, proteomic analysis of KO cells revealed an impairment of pathways involved in pericyte-endothelial crosstalk, suggesting a key role of

FOXF2 in vascular signaling. The observed disease features phenocopy those seen in endothelial (EC-cKO)- and pericyte (PE-cKO)-specific Foxf2 deficient mice developed in parallel, validating the importance of iPSC-derived in vitro models to study NVU biology or malfunction. Lastly, to demonstrate the applicability of the 3D model for therapeutic screening, we treated FOXF2 knockout cultures with lipid-nanoparticle-mediated (LNPs) delivery of FOXF2 mRNA as a rescue paradigm.

Results

Somatic cell differentiation and characterization of iPSCs into neurovascular cell types (endothelial cells, pericytes, smooth muscle cells and astrocytes)

To generate a fully iPSC derived 3D model of the neurovascular unit (NVU) we first established and characterized somatic cell differentiation of iPSC into the NVU components (**Fig. 1A**). iPSC-derived endothelial cells (iEC) were differentiated by mesoderm induction and vascular specification. On day in vitro 5 (DIV5), iECs were selected by CDH5 (CD144) labelling and magnetic activated cell sorting (MACS) and further cultured in endothelial cell medium up to 5 passages (**Supp Fig. 1A**). Before purification, iECs already show an upregulation of the early endothelium-specific transcription factor ETV2 and of FOXF2 (**Supp Fig. 1B**), After CDH5 selection and propagation, iEC downregulate the pluripotency markers OCT4 and NANOG and show an enrichment of key endothelial transcripts such as PECAM1, CDH5, CLDN5 and TJP1, and of ECM transcripts such as COLIV (**Supp Fig. 1C**). At the end of the differentiation, iEC express markers of adherent junctions, such as PECAM 1 and CHD5 (**Fig. 1**). iPSC-derived pericytes (iPE) were differentiated together with iEC up to DIV5. The CDH5 negative MACS fraction was further used to differentiate pericytes as previously described with some modifications (**Supp Fig. 1D**) (Orlova et al. 2014). iPE pericytes downregulate pluripotency markers and upregulate key markers such as PDGFBB, SM22 and CNN1 (**Supp Fig. 1E**). Terminally differentiated iPE express PDGFRß and NG2 (**Fig. 1B**). iPSC-derived smooth muscle cells (iSMC) were differentiated by mesoderm induction and further specification by culturing them into smooth muscle cell medium (**Supp Fig. 1F**). During differentiation, iSMCs downregulate pluripotency markers and upregulate cell-specific markers such as ACTA2, SM22 and CNN1 (**Supp Fig. 1G**). At the stage used for the 3D NVU model, iSMCs expressed SMA and CNN1 (**Fig. 1B**). iPSC-derived astrocytes (iAS) were differentiated under serum-free conditions as previously described with some modifications (**Supp Fig. 1H**) (Perriot et al. 2018). iAS downregulate the pluripotency markers and upregulate key astrocytic transcripts such as GFAP, AQ4, GLAST, GLT1, VIM and S100 (**Supp Fig. 1I**). Furthermore, fully differentiated iAS express GFAP and TUJ1 (**Fig. 1B**).

To characterize and validate our somatic cell differentiation protocols we compared our iPSC-derived cells with commercially available human primary cells: brain microvascular endothelial cells (pEC), human umbilical vein endothelial cells (HUVECs), brain vascular pericytes (pPE), brain vascular smooth muscle cells (pSMC) and midbrain astrocytes (pAS). All cell types were cultured separately, and proteomic analysis was performed in parallel to determine their identity (**Fig. 1C**). Principal-component analysis (PCA) revealed that iPSC formed a distinct population separated from of somatic cells, clearly discriminating the undifferentiated population. In general, the iPSC-differentiated cells displayed small variability between technical replicates, confirming the reproducibility of the differentiation protocol. iECs clustered

closer to human primary capillary endothelial cells (pEC) than to HUVECs, indicating a more brain-like identity and suggesting potential to study cerebrovascular disorders with such cells. Similarly, iAS clustered close to primary astrocytes (pAS) and far from the endothelial cells, discriminating this cell type from the mesoderm derived cells. However, mural cells (iPE and iSMC) clustered together based more on their origin (iPSC-derived vs primary isolated) rather than cell type, which may indicate that differences between young and old mural cells are more pronounced than those between types of mural cells (see also Discussion). Parsing the proteomics profiles for specific markers we found that pluripotency markers are either no longer detected in the differentiated cells, such as NANOG and POU5F1, or at very low levels, like PODXL and SOX2 (**Fig. 1D**). Endothelial cells upregulate key endothelial markers like PECAM1, CDH5, CLDN5, SOX18, KDR, NOS3, TEK, ESAM and VWF. In contrast, they do not express epithelial markers such as EPCAM, CDH1, EMP3, CLDN6, FREM2, ESPR1, ERBB3 or KRT7, which has been described for other protocols aiming for EC differentiation (Lu, 2021). After comparing iPSC vs. iEC by PCA, enrichment analysis of the top 250 negative genes defined by PC1 yielded biological processes associated with angiogenesis, endothelial cell proliferation, nitric oxide biosynthesis and cell adhesion (**Fig. 1D, Supp. Fig. 2A**). Pericytes and smooth muscle cells also upregulate typical mural cell markers such as ANPEP, PDGFRB, CSPG4, VIM, DESM, NES, CNN1 and SMTN. Analysis of top 250 negative genes defined by PC1 yielded biological processes associated with cell-matrix adhesion, basement membrane organization and collagen fibril organization (**Fig. 1D, Supp. Fig. 2B and 2C**). Finally, astrocytes upregulate astrocytic markers such as S100B, ALDH1L1, ALDH1A1, ALDOC, GLUL, GJA1 and NDRG2. Analysis of top 250 PC1 negative genes revealed biological processes associated with nervous system development, glycogen metabolic processes and axon guidance (**Fig. 1D, Supp. Fig. 2D**). To provide the field with an overview of the cell identity and marker expression we detected in the different NVU cell types, we integrated the proteomics results from both, iPSC-derived and primary cells, in a publicly available database which will be made available in parallel to acceptance of the final manuscript.

In conclusion, our iPSC-derived cells express key cell-specific markers of the BBB components, which are absent in iPSCs at protein level (**Fig. 1D**).

Generation and characterization of 3D BBB model by coculturing iPSC-derived cells into a microfluidic chip

To generate a fully iPSC-derived 3D in vitro model of the BBB, we adapted a previously described protocol for co-culturing cells in 3D microfluidic chips (Campisi et al. 2018). Fully differentiated iEC, iAS and iSMC or iPE were combined in a fibrin hydrogel at defined ratios and injected onto the middle channel of the microfluidic chip (**Fig. 1A, Supp. Fig. 3A**). Cultures were fed every 24h by gravity-driven flow, adding different volumes of VASC-media in the left and right port, to promote endothelial microvasculature network formation. One day after

seeding, iECs self-organized into premature vascular networks and continued their sprouting until day 3-10, where branched vessels were observed (**Supp Fig. 3B**). Cultures were analyzed on day 7-10.

Co-culture of endothelial cells with astrocytes and mural cells resulted not only in endothelial cell vessel-like structures and branched vessel formation shown by PECAM1 expression, but also the arrangement of cells to form a vessel lumen (**Fig. 1E, Supp Fig. 3C**). iECs in culture expressed tight junction markers such as ZO1 and CLDN5 (**Fig. 1F**) and presented highly dense contact areas shown by electron microscopy (**Fig. 1G**). The lumenized vascular networks were perfusable with 10- and 40-KDa Dextran (**Fig. 1H**) and human blood (**Fig. 1I, Supp Video 1**) under gravity-driven flow without leaking, showing the functionality of endothelial cells in forming a functional barrier between the cells. After 7 days a rich ECM composed by collagen (COLIV) and Laminin (LAM) was observed. Endothelial cells showed organized polarity with the secretion of Podocalyxin (PODXL) towards the lumen or apical side and of collagen towards abluminal or basal side (**Fig. 1J**). Astrocytes remained star-shaped, expressing GFAP and extending their processes towards the endothelium (**Fig. 1K**). Mural cells were positioned in between endothelial branching points and expressed contractile markers such as SMA (**Fig. 1L**). To examine the functionality of endothelial cells in the 3D environment, we, in a last step, applied calcium to the media and saw slow calcium transient waves in a coordinated manner among all the cells, suggesting a typical EC physiology (**Fig. 1M**).

Taken together, after optimized differentiation and deep characterization of iPSC-derived BBB cell types, we engineered a 3D BBB model recapitulating key features of the BBB such as vessel-like tube conformation, ECM generation, barrier formation and representation of typical cell-cell interactions.

Generation of endothelial- and pericyte-specific Foxf2 deletion in adult mice and human iPSC FOXF2 deficient cell line

To better understand the role of FOXF2 in neurovascular dysfunction, identify cell-autonomous effects on endothelial cells and pericytes, and cross-validate our findings in two independent systems, we generated mouse lines with conditional endothelial (Cdh5-CreERT2; Foxf2fl/fl or EC-cKO) or pericyte (Pdgfrb-CreERT2; Foxf2fl/fl or PE-cKO)-specific inactivation of Foxf2 (**Fig. 2A**), and human FOXF2 KO iPSCs (**Fig. 2B**). Downregulation of Foxf2 in EC-cKO and PE-cKO mice was confirmed by qPCR, compared to age-matched wild-type mice (Foxf2fl/fl or WT) (**Fig. 2C**). For the generation of FOXF2-KO in iPSCs we targeted the DNA binding region in exon 1, following our previously described CRISPR genome editing pipeline (Weisheit et al. 2021). Genome editing led to a +1/-5 bp insertion on each corresponding allele, exposing a premature stop codon resulting in a nonfunctional protein (**Fig. 2D, Supp Fig. 4A**). FOXF2-

KO iPSC were characterized for pluripotency, absence of off-targets and chromosomal integrity (**Supp. Fig. 4B, 4C and 4D and Supp. Fig. 5**). Since FOXF2 is mainly expressed in endothelial cells and pericytes (Vanlandewijck et al. 2018; Yang et al. 2021) we further differentiated the iPSCs into iEC and iPE to study FOXF2 deletion. As expected, FOXF2-KO iEC and iPE showed an almost complete downregulation of FOXF2 RNA levels (**Fig. 2D**). We then studied the KO phenotypes in our human *in vitro* model using the mouse models for validation.

Endothelial FOXF2 deletion causes enhanced caveolae-dependent endocytosis in human and mouse

Recent studies have shown that global Foxf2 deletion leads to endothelial thickening, increased vesicular transport and longer tight junction surfaces in the capillary ECs (Reyahi et al. 2015). However, it remained unclear if these EC phenotypes were cell-autonomous or induced by mural cells. We therefore examined if we could detect similar phenotypes in our newly developed endothelial-specific Foxf2 deficient mice model and our FOXF2-deficient in vitro BBB model.

We found that endothelial Foxf2 deletion led to an upregulation of Cav1 in isolated brain vessels. Similarly, correlative ultrastructure analysis revealed an endothelial thickening and vesicle enrichment (**Fig. 2E**). Immunogold labeling further revealed that most of these vesicles are Cav1-positive, suggesting an upregulation of caveolae-dependent endocytosis (**Supp. Fig. 6A**). To assess the potential of the 3D BBB model for recapitulating in vivo phenotypes, we quantified the density of caveolae in endothelial cells by immunocytochemistry and found CAV1 to be upregulated in FOXF2 deficient iECs compared to WT iECs. The enrichment of caveolae was confirmed by correlative transmission electron microscopy (TEM) analysis, which showed caveolae to be enriched at the surface of endothelial cells, and in addition demonstrated a fusion deficit indicated by connections of multiple vesicles. (**Fig. 2F**). To explore the consequences of FOXF2 deficiency on endothelial transport, we treated KO and WT human endothelial cells FM1-43FX. FOXF2 deficient iECs exhibited a higher density of FM1-43FX positive vesicles compared to WT iECs, suggesting an increased level of endocytic uptake upon FOXF2 deletion (**Fig. 2G**).

Endothelial FOXF2 deletion leads to tight junction deficits and leaky BBB

Endothelial Foxf2 inactivation led to downregulation of Tjp1 in isolated mouse brain microvessels in vivo. Moreover, TEM analysis revealed deficits along the junction area with elongated junctional protrusions or transient openings between the junctional membrane surfaces (**Fig. 2H**). These results are in line with the downregulation of Tjp1, Cldn5 and Ocln at protein level in isolated brain endothelial cells (BEC) (**Supp. Fig. 6B**) (Todorov-Völgy & González-Gallego, *in preparation*). mRNA expression in full tissue further showed a trend of

decreased Tjp1 and Cldn5, and a significant downregulation of Ocln (**Supp. Fig. 6C**). Interestingly, we found similar downregulation of these genes at mRNA level during healthy aging (**Supp Fig. 6D**). To assess whether the downregulation of tight junction protein abundance correlates with BBB leakage, we stained for albumin extravasation in the brain parenchyma and found significant upregulation of albumin positive regions in Foxf2 deficient compared to age-matched WT mice (**Fig. 3G**). Correlative light and electron microscopy (CLEM) examination of brain regions with focal albumin leakage revealed an extravasation of red blood cells in albumin-positive regions suggestive of micro-hemorrhages (Todorov-Völgy & González-Gallego*, in preparation*).

When looking at the human iPSC model, similar phenocopy was seen: TJP1 was downregulated after FOXF2 deletion, and correlative TEM showed similar deficits in junction formation (**Fig. 2I**). At mRNA level, FOXF2-deficient iECs showed a trend of decreased TJP1 and a significant downregulation of CLDN5 and OCLN junction proteins, suggesting an effect on cell junction proteins at the transcriptional level (**Fig. 3H**). To explore whether the structural deficits also resulted in functional abnormalities in vitro, we measured transendothelial electrical resistance (TEER) of seeded endothelial cells and found that FOXF2 deficient iECs showed a significant decrease in TEER compared to WT cells (**Fig. 2J**).

Taken together, disease features caused by endothelial FOXF2 deficiency in the 3D BBB in vitro model phenocopy those seen in vivo in EC-specific Foxf2 deficient mice. These findings validate the relevance of our iPSC-derived in vitro model to study disease-associated phenotypes and BBB biology. They further suggest a cell-autonomous effect of FOXF2 in human and mouse endothelial cells and identify the gene as a key player in the maintenance of brain endothelial function.

Endothelial and pericyte FOXF2 deficiency dysregulate endocytosis and cell junction pathways and increase vascular leakage

To explore the cell specific molecular pathways mediated by FOXF2 we applied LC-MS/MS-based proteomics on human endothelial cells and pericytes differentiated from iPSCs (**Fig. 3A**). Proteomic analysis of endothelial cells captured a total of 8085 proteins identified with ≥ 2 unique peptides. Among them, 7796 proteins were quantified in ≥ 2 samples and 1010 were significantly altered between iEC WT and FOXF2-KO. Out of these, 611 and 399 were up- and downregulated, respectively (t-test, p-value <0,05). (**Fig. 3B**) Enrichment analysis of significantly altered proteins revealed endocytosis, focal adhesion, and tight junction to be among the most affected biological processes and subcellular localizations (**Fig. 3D**). Proteomic analysis of pericytes captured a total of 7059 proteins identified with ≥ 2 unique peptides. Out of those, 6298 proteins were quantified in ≥ 2 samples and 1476 were significantly dysregulated between WT and FOXF2-KO pericytes. From the altered proteins,

1108 and 370 proteins were up- and downregulated, respectively (t-test, p-value <0,05) (**Fig. 3C**). As for endothelial cells, endocytosis, focal adhesion, and tight junction were among the most affected GO terms, suggesting the importance of pericytes in the regulation of these pathways (**Fig. 3E**). Endocytosis and cell adhesion are highly regulated biological processes in both endothelial cells and pericytes and involved in the establishment and maintenance of BBB integrity. Focusing on endocytosis and cell adhesion proteins, we found ITGA4, LDL, VLDR, CLTCL and CAV1 to be among the top30 upregulated endocytosis proteins while ITGA8, STAB2, LAMB2, CLDN5 and ITGA1 were among the top30 downregulated cell adhesion proteins in human FOXF2 deficient ECs (**Fig. 3F**). Complementing these data, we further found CLDN5, ZO1, and OCLN to be downregulated at mRNA level (**Fig. 3G**). In FOXF2 deficient human pericytes we found the matrix metalloproteinase MMP15 and the adhesion molecule ICAM1 to be upregulated at both protein and mRNA level (**Fig. 3G**). To investigate whether cell specific FOXF2 deficiency affects BBB integrity in vivo we analysed endothelial-specific conditional Foxf2 deficient mice (**Fig. 2A**). Using intraperitoneal Evans blue injection and confocal microscopy we found a significantly higher number of brain regions with focal albumin leakage (**Fig. 3H**).

Endothelial and pericyte FOXF2 deficiency compromise vascular remodeling

To further explore the effect of cell-specific Foxf2 deficiency on vessel morphology, we next obtained detailed metrics on the entire brain vasculature in mice using light-sheet microscopy and a recently developed Vessel Segmentation and Analysis Pipeline (VesSAP) (Todorov et al. 2020).We found 20 anatomical regions with significantly reduced microvessel density in EC-KO mice vs. WT, suggesting a role of Foxf2 in brain vessel remodeling in adulthood (**Fig. 3I**). In contrast, pericyte-specific Foxf2 deficient mice showed no significant alterations in vascular metrics (*data not shown*).

Next, we used comparative proteomic analysis of FOXF2 deficient human ECs and PCs, as well as isolated mouse brain microvessels with EC or PC-specific Foxf2 deficiency. Focusing on biological processes related to vessel remodeling we found a significant overrepresentation of cell motility, cell migration, cell division and angiogenesis among the significantly downregulated processes, suggesting a compromise of these pathways upon endothelial or pericyte specific Foxf2 deficiency (**Fig. 3J**). We therefore examined the consequences of FOXF2 deficiency on cell proliferation and indeed found FOXF2 deficiency to reduce the proliferation rate of human iPSC-derived ECs (**Fig 3K**). Accordingly, mRNA expression levels of SRC and NRLP1/2 proliferation markers were downregulated (**Fig. 3L**). Focusing on the top 30 downregulated proteins related to cell migration biological processes we further found LAMB, NOS3, SRC, KDR, ADAM17 to be dysregulated (**Fig. 3O**). In pericytes we found an upregulation of the proliferation rate upon FOXF2 deletion (**Fig. 3M**). Accordingly, mRNA expression levels of key pericyte proliferative markers PDGFRB, BMP4 and MAPK1 were

upregulated (**Fig. 3N**). Focusing on the top 30 upregulated proteins related to cell proliferation biological processes we found PDGFRB, MAPK1 and COPS2 to be dysregulated in FOXF2 deficient pericytes (**Fig. 3O**).

Taken together, FOXF2 deficiency in endothelial cells and pericytes dysregulates proteins involved in tight junction formation, endocytosis regulation and matrix degradation, which could lead to vascular leakage. Endothelial FOXF2 deficiency compromises vessel remodeling and dysregulates proteins involved in cell migration and proliferation. Furthermore, FOXF2 deletion in pericytes induces pathways involved in pericyte proliferation, which could add to the loss of vessel stability and integrity (**Fig. 3P**).

Delivery of FOXF2 mRNA via LNP restores barrier function in the 3D BBB model

As BECs are a major player of NVU function under physiological conditions and malfunction in disease, there is great interest in establishing and optimizing access to BECs for the delivery of therapeutics. Lipid nanoparticles (LNPs) carrying mRNA have recently emerged as a therapeutic agent to treat infectious disease and cancer (Hou et al. 2021). Since ECs form the innermost layer of the vasculature, they may be accessible for LNP-based therapeutic modulation. Recent work has demonstrated LNP modifications with optimized selectivity for ECs (Paunovska et al. 2018; Liu et al. 2023). To assess the applicability of our human BBB model for therapeutic modulation we treated the FOXF2 deficient BBB model with LNPs containing mouse Foxf2 mRNA. We reasoned that following LNP uptake via endocytosis and endosomal escape, therapeutically delivered mRNA would be translated into protein and restore FOXF2 expression (**Fig. 4A**). We found that WT and FOXF2 deficient endothelial cells upregulate mRNA levels of mouse Foxf2 upon LNP treatment, demonstrating that Foxf2 can be successfully delivered into these cells (**Fig. 4B**). LNP-treated FOXF2 deficient cells downregulated CAV1 and upregulated TJP1 protein levels, similar to the WT condition (**Fig. 4C**). Also, FOXF2 overexpression via LNPs reduced the endocytic uptake of the FM1-43FX compound, in WT and KO cultures, rescuing the phenotype observed with FOXF2 deficiency (**Fig. 4D**). Interestingly, mRNA levels of CAV1 were upregulated in FOXF2-KO cells and restored upon mFoxf2 LNP delivery (**Fig. 4E**). An opposite pattern was seen for TJP1 and CLDN5 again confirming that LNP-mediated delivery of Foxf2 rescues the phenotype induced by FOXF2 deficiency (**Fig. 4F**).

Taken together, this demonstrates the applicability of the 3D BBB model to test interventions of therapeutic agents modulating the endothelium.

Discussion

In this study we developed a novel fully human iPSC derived *in vitro* BBB model composed of endothelial cells, mural cells and astrocytes that can be used for studying neurovascular disorders in an isogenic manner. One of the novelties of our study is the usage of only iPSC-derived cells which have been thoroughly characterized by relative RNA expression and proteomics. During the past years several iPSC differentiation protocols for the generation of NVU cell types have been developed but improvements in protocol standardization and validation are still required to better define the cell identity of the generated cells (Delsing et al. 2020). Difficulties in generating and characterizing ECs phenocopying brain microvascular endothelial cell characteristics have led to the usage of misidentified epithelial cells for BBB modelling (Lippmann et al. 2012; Lu et al. 2021). To avoid these issues, we characterized our iPSC-derived iEC, iPE, iSMC and iAS proteomics. Unsupervised PCA analysis revealed distinct population of undifferentiated iPSCs and somatic cells. Furthermore, iEC clustered in closer proximity to primary brain ECs rather than to HUVECs and did not express any of the most common epithelial markers, suggesting that their identity resembles brain endothelium more than other endothelia or epithelia. Additionally, when comparing iPSCs to iEC we could see an upregulation of key brain endothelial processes such as angiogenesis, endothelial cell migration, receptor-mediated endocytosis or cell adhesion. Similarly, iAS also clustered closer to primary astrocytes and were distinct from mesoderm derived cells, indicating their neuroectodermal origin and glial identity. Interestingly, mural cells clustered more by iPSC vs. brain origin than cell identity. Defining mural cell identities and distinguishing between pericytes and smooth muscle cells has been difficult because of their heterogeneous distribution along the vascular tree (Hartmann et al. 2015; Kisler et al. 2017) and the lack of specific markers defining the different mural cell types (Armulik, Genové, and Betsholtz 2011; Obermeier, Daneman, and Ransohoff 2013). Furthermore, their developmental origin is also still poorly understood. While early studies suggested that mural cells are derived from the mesoderm (Drake, Hungerford, and Little 1998) recent studies using lineage-tracing and quail-chick chimeras revealed that mural cells in the forebrain are, at least to some degree, derived from the ectodermal neural crest (Etchevers et al. 2001; Korn, Christ, and Kurz 2002; Armulik, Genové, and Betsholtz 2011). Moreover, a recent study have shown that some hematopoietic lineages can give raise to brain pericytes (Yamazaki et al. 2017), illustrating the heterogeneity in the cell type origin and opening the possibility to two types of populations: neural crest and mesoderm derived pericytes. During our PCA analysis pPE are closer in proximity to pAS than pSMC, possibly indicating neural crest origin of the primary pericytes we used for comparison. Nevertheless, both iSMC and iPE do not cluster well with their primary counterparts, which could be due to a high overlap on expression markers early during development that becomes more specific during adulthood since pPE and pSMC generate two distinct populations.

Despite the lack of mural cell-specific markers, usually pericytes have been defined as a combination of PDGFRb, ANPEP, MCAM and CSPG4 while smooth muscle cells as a combination of PDGFRb, MCAM, DES, ACTA2, ANPEP and CSPG4. Smooth muscle cells express higher levels of MCAM, CSPG4 and ACTA2 and pericytes express low levels of DES and ACTA2, helping the distinction of both cell types (Armulik, Genové, and Betsholtz 2011; Smyth et al. 2018). When checking for those specific markers in our iPE and iSMC we could not only that they were all express but that MCAM, CSPG4 and ACTA2 are upregulated in iSMC while DES is downregulated in iPE, suggesting successful differentiation of distinct pericyte and smooth muscle cell populations. With our proteomics characterization of iEC, iPE, iSMC and iAS we not only provide insights into efficiency of differentiation protocols and cell lineage but also illustrate the importance of proper cell type characterization before generating *in vitro* disease models. To make these data accessible as a resource for the field, we are currently establishing a publicly available and searchable database of protein expression in iPSC-derived cells and primary cells, which provides marker expression patterns of all BBB cell types and can help to identify cell-specific markers for future studies. The database will be available in a few weeks.

We further established a fully human *in vitro* 3D BBB model by co-culturing iPSC-derived endothelial cells, mural cells, and astrocytes in microfluidic chips. Previous reports indicated that such 3D cultures based on a fibrin gel promote self-assembly of endothelial cells into microvascular networks without the addition of a complex ECM (Campisi et al. 2018; Belair et al. 2015; Vila Cuenca et al. 2021). Indeed, our iEC self-organized into vessel-like structures with perfusable lumens and secreted ECM proteins. Furthermore, they recapitulate key BBB features such as typical vessel topology, cell-cell interactions and coordinated calcium waves. Most previous models were generated by combining human iPSC-derived cells with primary cells (Campisi et al. 2018; Orlova et al. 2022), which complicates study of neurovascular disorders as the non-isogenic cells have different genetic backgrounds. The few available fully iPSC-derived models only include subsets of NVU cells like endothelial cells and pericytes (Jamieson et al. 2019) or endothelial cells and neural cells (Vatine et al. 2019). To our knowledge, our model is the first fully human iPSC-derived 3D *in vitro* model of the BBB, which allows studying genetic neurovascular disorders in an isogenic manner. Modelling of the BBB in 3D is essential to better recapitulate *in vivo* conditions, including 3D conformation, cell-cell interactions and shear stress (Aday et al. 2016; Oddo et al. 2019; Delsing et al. 2020). But even though our model recapitulates 3D conformation and cell-cell interaction, media still flows by gravity instead of using a fully controlled circular flow, which generates smaller shear stress. While this needs to be further improved in future studies, it already provides a better alternative than 2D models and allows the maintenance of the vascular network.

To demonstrate that our model can be used to study neurovascular disorders we investigated loss of FOXF2, a known risk gene for SVD (Chauhan et al. 2016; Malik et al. 2018). FOXF2 is mainly expressed in endothelial cells and pericytes in mouse and human brain (Vanlandewijck et al. 2018; Kalucka et al. 2020; Yang et al. 2021) and is an essential brain-endothelial cell specific transcription factor (Hupe et al. 2017) which promotes vessel development (He et al. 2020). To explore the cell-autonomous effect of FOXF2 on BBB cell types we generated FOXF2 deficient human iECs and iPEs differentiated from genome edited iPSCs. To validate the phenotypes of our newly developed FOXF2-KO human *in vitro* models, we also established endothelial or pericyte specific Foxf2 deficient mouse lines and performed correlative *in vitro* – *in vivo* experiments. Similar to the previously published global Foxf2-KO mice, endothelial cell specific Foxf2 deficiency induced endothelial thickening, increased caveolae density and elongated tight junction protrusions in the brain capillaries of the adult mice, suggesting the importance of endothelial Foxf2 in the maintenance of BBB integrity. Moreover, our newly developed *in vitro* model phenocopied most central phenotypes found in mouse, including caveolae upregulation, downregulation of TJP1 and malformation of tight junctions upon loss of FOXF2. Additionally, our *in vitro* model allowed us to perform several functional assays difficult to assess *in vivo*, such as endocytic uptake or TEER. In line with our previous results, FOXF2-KO EC cultures presented with an increased endocytic uptake and decreased TEER, suggesting an involvement of endothelial FOXF2 in regulating vesicle mediated transport and cell junction integrity. Collectively, these findings provide not only proof that *in vitro* models can be used to study relevant disease phenotypes but also show a clear alignment between mouse and human FOXF2 deficiency.

To further understand the cell-autonomous effect of FOXF2 in endothelial cells and pericytes we applied proteomics to our differentiated FOXF2 deficient human cells and isolated mouse brain microvessels. Enrichment analysis of significantly dysregulated proteins revealed endocytosis, cell adhesion, matrix degradation and proliferation among the most affected biological processes in FOXF2 deficient vasculature. To tightly control the CNS environment, BECs present with an extremely low rates of transcytosis and high expression of tight junction proteins between adjacent cells. (Abbott, Rönnbäck, and Hansson 2006; Zlokovic 2008). Among the endocytosis proteins upregulated in FOXF2 deficient human ECs we found several involved in caveolae formation, such as CAV1 and EHD2. This is in line with other genetic models, where increased caveolin-mediated transport has been linked to BBB leakage (Andreone et al. 2017). Moreover, several members of the clathrin-coated vesicles such as CLTCL1, STON1, HIP1R, HEATR5B, TNK2 were likewise upregulated in our FOXF2 deficient ECs. In addition, proteins known to be involved in the intracellular protein transport, specifically in the Golgi vesicle transport system, like COG1, COG2, COG3, COG7, WDR11 and RAB43 were upregulated. This general upregulation of proteins related with endocytosis may

contribute to the upregulation in endocytic uptake that FOXF2-KO cultures exhibit in comparison to WT. In addition, several proteins involved in cell adhesion were also downregulated. Proteins involved in formation of tight junction complexes such as TJP1, CLDN5, RAP2B and F11R were downregulated. These results are in line with previously published data in hypoxia induced brain injury, which has shown to develop leaky BBB with decreased expression and reorganization of the main tight junctions, including CLDN5, TJP1 and OCCLN (Abdullahi, Tripathi, and Ronaldson 2018). Moreover, several neurological disorders presenting with BBB breakdown have been associated with reduced levels of TJP1 levels (Zlokovic 2011). Furthermore, in our FOXF2-KO endothelial cells we found a downregulation of several proteins involved in cell-cell junction such as STAB1, FLRT1, FLOT2, NRP1, TM9SF4, EPHB4, PTPRD, PPP1CA, ADAM17, CEACAM1, ARHGEF6 and TLN1. Interestingly, proteins involved in the cell-matrix adhesion like ITGA1, ITGA8, ITGA9, LAMB2, LRP5, CD63 CORO1A and LYVE1 as well as proteins involved in the cytoskeleton reorganization like MYH10, CORO1A, CORO2B, SDCBP, CARMIL1, F11R and TLN1 were also downregulated, suggesting a cell structure reorganization upon FOXF2 deletion. Altogether, dysregulation of proteins involved in endocytosis, cell adhesion and cytoskeleton reorganization *in vitro* are in line with the reduced TEER in FOXF2 deficient human ECs and with the *in vivo* vascular leakage phenotype in endothelial-cell specific Foxf2 deficient mice. In addition, several proteins involved in the regulation of angiogenesis and cell migration such as NRP2, ADGFRA2, STAB2, STAB1, CARMIL1, ADAM17 and CECAM1 as well as proteins involved in vessel sprouting like NOS3, KDR, PP1CA, NRP1 and EPHB4 were also downregulated in the FOXF2 deficient iECs. These data are consistent with the reduced microvessel density in endothelial Foxf2 deficient mice, suggesting an involvement of Foxf2 in brain vessel remodeling during adult phase. FOXF2 deficiency further induced a reduction in human endothelial cell proliferation, suggesting the involvement of FOXF2 in endothelial cell sprouting. In contrast with endothelial cells, FOXF2 deficient pericytes had increased proliferation rates and no change in microvessel density in adult mice. This could be explained by the increase of proteins related to cell proliferation such as PDGFRB, CXADR, KANK1, LIG4, PDGFRB, CPS2, IL9, GPC3 and PHB2 or cell division like CCND1, NBM, MTA3, RUNX2 and MAPK1. Furthermore, these data are in line with previously published data, where global inactivation of Foxf2 induced increased number of pericytes and proliferation rate during embryonic development (Reyahi et al. 2015). It is known that PDGFRB in pericytes promotes BBB formation and stabilization (Daneman et al. 2010; Armulik et al. 2010). Moreover, PDGFRB signaling increases pericyte vessel coverage, vessel stability and promotes proliferation and migration (Xiang et al. 2019; Smyth et al. 2018). Therefore, the increased PDGFRB expression in our FOXF2 deficient iPEs might contribute to the increases proliferation rate, causing vascular destabilization and leakage.

Lastly, to further explore the applicability of the BBB model for therapeutics screening we developed a rescue paradigm using LNPs. In the past years, LNPs have been used to treat cancer and infectious diseases (Hou et al. 2021) and recently optimized for specific endothelial selectivity (Paunovska et al. 2018; Liu et al. 2023). In order to see if we can target our endothelial cells, we treated FOXF2-KO cultures with LNPs containing mouse Foxf2 mRNA. Upon LNP uptake, Foxf2 overexpression restored the levels of CAV1 and TJP1, which were significantly up- and downregulated respectively, not only at protein but also RNA level. Moreover, Foxf2 overexpression also reduced RNA levels of CLDN5, which is consistent with other studies (Roudnicky et al. 2020). Furthermore, LNP treatment also reduced the endocytic uptake of FOXF2-KO cultures and WT cultures, suggesting a direct involvement of FOXF2 in an endocytic uptake increase. These data demonstrates that a 3D BBB model can be used for testing interventions targeting the endothelium and screening therapeutics.

As a limitation, our 3D BBB model could be improved by adding physiological flow which would induce shear stress in the vessels. It is known that shear stress has an impact on endothelial BBB phenotype since it reduces apoptotic pathways (Dimmeler et al. 1996), increases membrane transporters and tight junctions such as TJP1 and OCLN and further reduces permeability (Chistiakov, Orekhov, and Bobryshev 2017; Cucullo et al. 2011). Second, the usage of microfluidic chips does not allow the measurement of TEER and therefore, BBB permeability must be measured by more sophisticated methods such as tracer imaging in the future. Third, due to the small size of the commercially available microfluidic devices proteomics and transcriptomics studies are limited by the cellular material present in the small devices. Scaling up device size and culture numbers would be possible, but would require custom-made generation following previously published protocols (Hajal et al. 2022). Finally, further incorporation of other cell types such as microglia, neurons and monocytes could be important to study the complexity of the whole NVU and inflammatory responses.

In summary, we developed a human *in vitro* BBB model enabling the study of genetic vascular diseases, as we exemplified by the phenocopy of FOXF2 deficiency induced phenotypes between mice and our human *in vitro* system. Furthermore, we provide insights into the regulatory role of FOXF2 in different vasculature cell types and how it might be implicated in the regulation of vessel integrity and remodeling. Our findings further imply a cell autonomous role of FOXF2 in human endothelial cells and pericytes which is crucial for BBB maintenance.

Materials and methods

iPSC culture

All iPSCs experiments were performed according to all relevant local guidelines and regulations. All work was done with the commercially available female iPSC line A18944 (ThermoFisher, Cat# A18945). iPSCs were maintained on vitronectin-coated (ThermoFisher Cat#A14700) culture plates and Essential 8 Flex Medium (E8F) (ThermoFisher Cat#A2858501) at 37ºC with 5% CO_2 until reached 80% confluency. Cells were routinely passaged using PBS with 500nM EDTA (ThermoFisher, Cat# 15575020) for 5min and plated again in E8F.

CRISPR/Cas9 gene editing

CRISPR/Cas9 editing was performed as described previously (Paquet et al. 2016; Kwart et al. 2017), with modifications for RNP-based DNA cleavage (Skarnes, Pellegrino, and McDonough 2019). Briefly, cells were dissociated in preparation for electroporation using Accutase (ThermoFisher, Cat# A1110501), plated in Geltrex-coated (ThermoFisher Cat# A1413302) culture plates in StemFlex (ThermoFisher Cat# A3349401) with 10μM ROCK inhibitor (Selleckchem Cat# S1049) at a density of 150k cells/cm^2 and cultured for 2 days. To prepare the RNP complex, 60pmol sgRNA targeting FOXF2 (ttcttccgcggcgcctaccaggg, ordered from Synthego) was mixed with 30pmol of high-fidelity Cas9 mutant (IDT, Cat#1081060) and incubated at room temperature (RT) for 10-20min. After Accutase dissociation, 200k cells were resuspended in 20μL of P3 Primary Cell Nucleofector Solution (Lonza, Cat# V4XP-3032) and gently mixed with the incubated RNP complex. The mixture was transferred into one well of a nucleocuvette strip (Lonza, Cat# V4XP-3032) and cells were electroporated in a 4DNucleofactor X Unit (Lonza, Cat# AAF-1002X) using program CA137. After electroporation, cells were plated in one 12w Geltrex-coated culture plate with StemFlex supplemented with 1X RevitaCell (ThermoFisher, Cat# A2644501) and grown for 2-4 days. Cells were then plated at low density and single-cell clone colonies were picked, analyzed by restriction fragment length polymorphism (RFLP) using the enzyme BstNI (NEB, Cat#R0168S) and sanger sequencing as previously described (Kwart et al. 2017). The knockout was confirmed on RNA level using real time qPCR analysis. For quality controls, pluripotency was confirmed via immunocytochemistry using OCT4, NANOG, SSEA4 and TRA16 and chromosomal integrity was validated by molecular karyotyping (LIFE & BRAIN GmbH). Off-target analysis was performed by Sanger sequencing the top five most likely loci based on MIT and CFD scores predicted from CRISPOR (http://crispor.tefor.net/) design tool (Concordet and Haeussler 2018). On-target effects such as loss-of-heterozygosity was also performed using nearby SNP sequencing as previously described (Weisheit et al. 2020).

iPSC somatic cell differentiation

Endothelial cells (EC)

iPSCs were seeded onto Geltrex-coated culture plates at a density of 200k cells/cm^2 in Stem Flex (SF) medium with 10μM ROCK inhibitor for 24h. Medium was replenished every 24h for the following 5 days. On day 1-2 cells were feed with Mesoderm Induction Media (StemCell, Cat# 05220) followed by APEL2 media (StemCell, Cat# 05270) with 200ng/mL VEGF (Peprotech, Cat# 100-20) and 2 μM Forskolin (Peprotech, Cat# 6652995) on days 3-4. On day 5, endothelial cells were selected by CDH5 Magnetic Activated Cell Sorting (MACS). After Accutase dissociation, cells were incubated with CDH5 Microbeads (Milteny Biotec, Cat# 130-097-867) for 15min at 4ºC. CDH5+ fraction was obtained via MACS following manufacturer's instructions and plated onto Collagen IV-coated (Sigma Aldrich, Cat# C5533-5MG) culture plates at a density of 200k cells/cm^2 in endothelial cell medium (PromoCell, Cat# C-22011) supplemented with 50ng/mL VEGF (Peprotech, Cat# 100-20). Endothelial cells were grown until reaching 80-90% confluency and passaged with Trypsin-EDTA (ThermoFisher, Cat# 25200056) in a ratio of 1:2-1:6 up to 5 passages.

Smooth muscle cells (SMCs)

iPSCs were seeded at a density of 200k cells/cm^2 onto Geltrex-coated culture plates with StemFlex medium with 10μM ROCK inhibitor. Differentiation was started 24h after seeding by switching medium to Mesoderm Induction Media. Medium was replenished every 24h for 3 consecutive days. On day 4, medium was switched to APEL2 medium supplemented with 50ng/mL VEGF and 25ng/mL BMP4 (Peprotech, Cat# AF 120-05ET) and replenish every second day. On day8, cells were split in a ratio 1:4-1:6 onto Collagen IV-coated culture plates with smooth muscle cell Medium (Promocell, Cat#C-22062) with 10ng/mL PDGFBB (Peprotech, Cat#100-14B) and 2ng/mL TGFB1 (Peprotech, Cat# AF-100-21C). Cells were passaged upon confluency using Trypsin-EDTA in a ratio of 1:2-1:8 up to 5 passages.

Pericytes

iPSC-derived pericytes were generated as previously described (Orlova et al. 2014) with some modifications. Days 1 to 5 of the differentiation are identical to the endothelial cell protocol above. After the CDH5 cell selection via MACS the negative fraction, CHD5-, was plated onto Gelatin-coated (Merck Millipore, Cat# ES-006-B) culture plates with endothelial cell medium at a density of 200k cells/cm^2. At 90% confluency, cells were split onto Gelatin-coated culture plates with DMEM/Glutamax (ThermoFisher, Cat# 10566016) supplemented with 10% FBS (Biowest, Cat#S1860), 2ng/mL TGFB3 (Peprotech, Cat# 100-36E) and 4ng/mL PDGFBB (Peprotech, Cat#100-14B) in a ratio 1:1-1:2 using TrypLE (ThermoFisher, Cat# 12604013). Media was changed after 3 days to DMEM-10%FBS without growth factors.

Astrocytes

iPSC-derived astrocytes were generated as previously described (Perriot et al. 2018) with some modifications. iPSCs were split into single cells using accutase and seeded onto geltrex-coated plates at a density of 0,3M cells/cm2 in neural induction media (NI) with 10□M ROCK

inhibitor (RI). NI is composed by neural maintenance media (NM) supplemented with 10mM SB-431543 (Selleckchem, Cat#S1067) and 2,5mM LDN-193189 (Selleckchem, Cat#S2617). NM is composed by 0,5X Neurobasal media (ThermoFisher, Cat#211003-049), 0,5X DMEM/F12 (ThermoFisher, Cat#11320-074) supplemented with 100U/mL Penicillin-streptomycin (ThermoFisher, Cat#12140-122), 0,5X B27 supplement with vitamin A (ThermoFisher, Cat#17504044), 2mM GlutaMAX (ThermoFisher, Cat#35050), 1X NEAA (ThermoFisher, Cat#11140-050), 0,5X N-2 supplement (ThermoFisher, Cat#17502048), 1,5 g/mL Insulin (Sigma-Aldrich, Cat#10515) and 0,05 mM 2-Mercapto-ethanol (ThermoFisher, Cat#21985-023). NI media was replenishing every 24h until DIV7. On DIV7, cells were split onto pOL-coated plates. pOL-coated plates were generated by coating first with poly-L-ornithine (Sigma-Aldrich, Cat#P4957, diluted 1:100 in ddH2O) for 4h followed by laminin (ThermoFisher, Cat#23017015, diluted 1:100 in PBS) overnight at RT. Before cell dissociated, laminin coated solution was aspirated and plates were dry in a laminar flow hood for at least 30min. Cells were dissociated with accutase and resuspended with NI+RI at a density of 30M cells/mL. From the cell suspension, 250µL were slowly added onto the pOL coated plate slowly to form a spot. Spots were incubated 1h at RT to let the cells attach and then feed with NI+RI. Cells were feed regularly with NI until DIV10, where media was changed to NM supplemented with 20ng/mL bFGF (StemCell technologies, Cat#78003.2) for until DIV12. Cells were further cultured with NM until first neural rosettes formed, around DIV14-15. On DIV15, media was changed to glial precursor expansion media (GEM), composed by DMEM/F12 supplemented with 1x GlutaMAX, 1x N-2 supplement, 1X B27 supplement, 10ng/mL FGF-2 and 10g/mL EGF (Peprotech, Cat#100-15-100). Media was exchanged every day until DIV17. Rosettes were split using Neural Rosette Selection agent (NRSR, StemCell technologies, Cat#5831). Cells were incubated with NRSR for 60-90min at 37ºC and rosettes from the center of the spot were manually isolated. After brief centrifugation, cells were resuspended in GEM and plated onto pOL-coated plates. When cells reached confluency, they were further split using accutase at a density of 1M cells/mL onto GT-coated plates with GEM. Media was replenish every day and wells were further split using accutase and GEM when confluent. On DIV24 media was changed to astrocyte induction media (AIM), composed by DMEM/F12 supplemented with 1x Penicillin-streptomycin, 1x GlutaMAX, 1x N-supplement, 1x B27 supplement without vitamin A, 10ng/mL EGF and 10ng/mL LIF (Peprotech, Cat#300-05-26). When cells were confluent, they were subsequently split using accutase and plated at a density of 0,5M cells/mL onto GT-coated plates. On DIV38, media was changed to astrocyte media (AM) with 50µg/mL CNTF. AM contains DMEM/F12 supplemented with 1x Penicillin-streptomycin, 1x B27 supplement, 1x GlutaMax and 50µg/mL CNTF (Peprotech, Cat#450-13-20). Cells were feed with AM+CNTF for 28more days, then media on DIV66 media was changed to AM.

Transendothelial electrical resistance (TEER) assay

Transendothelial electrical resistance (TEER) was measured with a Nanoanalytics CellZscope system. For coculture, mural cells and astrocytes were split onto the basal side of Collagen IV-coated transwells (Corning, Cat#353095) on day 1and incubated at 37ºC, 5% CO_2 overnight. On day 2, endothelial cells were split onto the apical side of collagen IV-coated transwells and the cultures were mounted in the CellZcope system placed at 37ºC and 5% CO_2. For monoculture, endothelial cells were split directly onto the apical side of the transwells. Cells were cultured with endothelial cell serum free medium supplemented with 50ng/mL of VEGF. Once cells became confluent VEGF was removed. TEER was measured for 3-4 days after VEGF removal.

Generation of microfluidic 3D *in vitro* BBB model

iPSC derived endothelial cells, pericytes, smooth muscle cells and astrocytes were used between passages 1 and 4. The 3D BBB model was generated using microfluidic chips (AIM Biotech, Cat# DAX-1) following principles described by (Campisi et al. 2018). Cells were detached following their respective protocols and resuspended in endothelial cell medium containing 9U/mL thrombin (Sigma Aldrich, Cat# F8630). The following cell ratios were used: 1.2M/mL endothelial cells, 0.5M/mL astrocytes and 0.1M/mL pericytes or smooth muscle cells. Cell suspension was mixed in a 1:1 ratio with a 6mg/mL fibrinogen solution in PBS (Sigma Aldrich, Cat# F8630) and immediately injected into the gel filling ports. Microfluidic devices were placed in a humidified chamber and polymerized at room temperature for 15min. After gel polymerization, cultures were feed with VASC-media composed by 2/3 endothelial cell medium (PromoCell, Cat# C-22011), 1/3 AM media supplemented with 50ng/mL VEGF (Peprotech, Cat# 100-20) for the first four days, then VEGF was removed. On day 2, media channels were coated with an endothelial cell monolayer by seeding the cells at a concentration of 1.5M/mL. Gravity-driven flow was induced by feeding 70µL onto the right media port and 50µL onto the left port. Cultures were feed daily, incubated at 37ºC, 5% CO_2 and used between day 3 and 6.

Dextran assay in 3D model

To assess endothelial cell junction formation and 3D BBB model permeability, a mixture of 10-KDa (Inivtrogen, Cat# D1976) and 40-kDa dextran (Invitrogen, Cat# D1845) as fluorescent tracers was diluted in endothelial cell medium (PromoCell, Cat# C-22011) and filled into the media ports under a confocal microscope as previously described (Campisi et al. 2018). In brief, after 5 days of culture, microfluidic devices were placed into an environmental conditioning chamber set to 37ºC, 5% CO_2 mounted on a confocal microscope. Culture medium was carefully aspirated only from one media port, imaging was started, and dextran solution was injected into the media port. Confocal images were acquired every 3 min for 27 times to create and entire 3D maximum projection of the microfluidic device.

Calcium imaging in 3D model

Cells were treated with Fluo-4 (ThermoFisher, Cat# F14201) for 30min at 37ºC. After calcium addition into the media, calcium transients were measured in a fluorescent microscope.

FM1-43FX treatment in 3D model

Cells were incubated with 5□g/mL with FM1-43FX (ThermoFisher, Cat#F35355) diluted in ddH20 for 15min at 37ºC. After incubation cells were washed with PBS and fixed with 4% PFA for further analysis.

LNP treatment *in vitro*

Lipid Nanoparticles (LNPs) were obtained from ISAR Bioscience GmbH. LNPs were diluted in endothelial cell medium (PromoCell, Cat# C-22011) 1:1000 and added onto the cells. Cells were fixed after 24-48h with 4% PFA for further analysis.

Proliferation assay in 2D

Cells were seeded at a density of 30k/w in a 12-well plate with cultured media: endothelial cell media or pericyte media and measured in Incucyte from Sartorius for up to 48h.

Animal work

Brain specimens were obtained from Foxf2fl/fl; CAGG-Cre (cKO), Foxf2fl/fl;Cdh5-Cre (EC-cKO), Foxf2fl/fl; Pdgfrb-Cre (PE-cKO) and Foxf2wt/wt;-Cre (WT) mice at 6 months of age. All tissues from the same study were harvested in parallel and during the same daytime. All studies were conducted in a mix-gender mice group. Animal experiments were performed in accordance with the German Animal Welfare Law and approved by the Government of Upper Bavaria (Vet_02-18-21).

Induction of Foxf2 deletion in adult mice

To induce Foxf2 deletion, recombination of LoxP sites was induced by 100µL intraperitoneal injections of 0,25mg/kg of tamoxifen (Sigma, Cat# T5648-5G) in mygliol (Caesar&Loretz, Cat# 1115805) on 3 alternate days. Control mice received the equivalent volume of mygliol.

Tissue harvesting

For all molecular studies mice were first deeply anesthetized using Ketamine (100mg/kg, i.p) -xylazine (10mg/kg i.p). For BEC and vessel isolation, mice were transcardialy perfused with ice-cold 20 mL 1X Hank's Balanced Salt Solution (HBSS) and dissected. Following perfusion, the brain was surgically removed from the skull and kept in HBSS at 4ºC for BEC isolation and immediately frozen on dry ice and stored at -80ºC for vessel isolation. For immunohistochemical analysis, anesthetized mice were transcardialy perfused with 1X HBBS and fixed with 4% paraformaldehyde (PFA). The dissected brain samples were incubated overnight in 4% PFA followed by vibratome sectioning. For electron microscopy, mice were transcardially perfused in fixative (4% PFA and 2.5% glutaraldehyde in 0.1 M sodium cacodylate buffer, pH 7.4; Science Services). Following dissection, brains were post-fixed for 24h by immersion and immediately vibratome coronally sectioned. Brain slides were incubated

overnight in the same fixative and then stored in PBS at 4ºC until the start of the post-embedding.

Brain endothelial cell isolation (BECs)

Brain endothelial cells were isolated from whole brain as previously described (Todorov-Völgyi & González-Gallego, *in revision*). In brief, the full brain was enzymatically and mechanically digested using a modified version of the Adult Brain Dissociation Kit (Miltenyi Biotec, Cat# 130-107-677) followed by myelin removal using a 30% Percoll (GE Healthcare Cat# 17-5445-02) gradient. BECs were enriched using CD31 magnetic beads (Miltenyi Biotec, Cat# 130-097-418) via magnetic activated cell sorting (MACS). Residual MACS buffer was washed twice with PBS and samples were subsequently precipitated for protein extraction.

Vessel isolation

Brain vessels were isolated from half forebrain as previously described (Monet-Leprêtre et al. 2013; Zellner et al. 2018). In brief, tissue was homogenized using a glass tissue grinder (Wheaton) in 15mL of cold Minimum Essential Medium (ThermoFisher, Cat# 11095080) followed by myelin removal using a 15% Ficoll (Sigma-Aldrich, Cat# F4375-250G) gradient. Isolated vessels were then pelleted and resuspended in PBS with 1% BSA (BSA Fraction V, Sigma-Aldrich, Cat#10735096001), transferred onto a 40µm cell strainer (Corning, Cat#431750) and extensively washed with 250mL cold PBS. Isolated vessels were collected by inverting the cell strainer and washing with cold PBS into a falcon followed by centrifugation at 3000g for 5min.

Protein extraction

Isolated vessels

For proteomics analysis, isolated vessels were homogenized with a dounce tissue grinder (Wehaton) followed by heating for 3min at 95ºC in a buffer containing 100mM Tris-Hcl pH 7.6 (Roth, Cat# 9090.3), 4% SDS (Serva, Cat# 20765.03) and 100mM DTT (Sigma, Cat# 3483-12-3). Samples were then sonicated (30s, amplitude 100%, duty cycle 50%) with a VialTweeter sonicator (Hielscher) 5 times with intermediate cooling. Protein was obtained from supernatants after centrifugation at 16000g for 15min at 4ºC and kept at -20ºC for further analysis.

Isolated BECs

For proteomics analysis, protein was extracted from isolated BECs using RIPA buffer containing 150 mM NaCl (Roth, Cat# 3957.1), 1 M Tris-HCl pH 7.5 (Roth, Cat# 9090.3), 1 % NP40 (Sigma Alrich Cat# 74385), 0.5 % Deoxycholate (Roth, Cat# 3484.3), and 0.1 % SDS (Serva, Cat# 20765.03) and protein inhibitors cocktail (Roche, Cat# 4693159001) as previously described (Todorov-Völgyi & González-Gallego, *in revision*). In brief, cell pellets were resuspended in 50µL RIPA buffer, and after incubation on ice and centrifugation at 18000g, 30min at 4ºC, cell supernatants were kept at -80ºC for further analysis.

iPSCs and iPSC-derived somatic cells

For Western blot analysis, protein was extracted from iPSC-derived cells using RIPA buffer containing 150mM NaCl (Roth, Cat# 3957.1), 1M Tris-HCl pH 7.5 (Roth, Cat# 9090.3), 1% NP40(Sigma Alrich Cat# 74385), 0.5 Deoxycholate (Roth, Cat# 3484.3), 0.1% SDS (Serva, Cat# 20765.03) and protein inhibitor cocktail (Roche, Cat# 4693159001). Cell pellets were resuspended in 100µL RIPA buffer and incubated on ice for 30min. Protein suspension was obtained from the supernatant after centrifugation at 18000g, 30min at 4ºC and kept at -20ºC for further analysis. For proteomics analysis, protein was lysed in a buffer containing 100 mM Tris-Hcl pH 7.6 (Roth, Cat# 9090.3), 4 % SDS (Serva, Cat# 20765.03) and 100 mM DTT (Sigma, Cat# 3483-12-3) by homogenization with a dounce tissue grinder (Wheaton) and heating for 3min at 95°C. Samples were further sonicated (30sec, amplitude 100%, duty cycle 50%) 5 times with intermediate cooling using VialTweeter sonicator (Hielscher). Protein lysates were centrifuged at 16.000g for 15min at 4°C for removing of undissolved material. Supernatant was transferred to a new tube and stored at -20°C until further analysis.

Immunohistochemistry

IDs of primary and secondary antibodies and dilutions used during all experiments are specified in **Table 1**.

Brain slices

Brain samples fixed by perfusion were embedded in 3% agarose for 100 µm coronal vibratome sectioning. After sectioning, samples were kept in PBS until the staining was started. Coronal free-floating sections were first permeabilized and blocked with 3% BSA-Triton X100 solution for 1h at room temperature (RT). Primary antibodies were diluted in the same blocking buffer and incubated overnight at 4ºC whereas secondary antibodies were diluted in PBS and incubated at RT for 2h. After washing, DNA was stained using DAPI (Invitrogen Cat# D1306) in a 1:2000 PBS solution for 5min at RT. Brain slices were mounted using Fluoromount medium (Sigma-Aldrich, Cat# F4680-25ML).

Isolated vessels

After isolation, vessels were transferred immediately onto a microscope slide and dried at room temperature (RT). Slices were kept at 4ºC until staining started. Vessels were fixed using ice-cold 100% acetone for 10min at -20ºC. Prior to antibody incubation, vessels were blocked for 1h at RT using 1% BSA solution in PBS. Primary antibodies were diluted in the same blocking buffer and incubated overnight at 4ºC. Secondary antibodies were diluted in PBS and incubated 1h at RT. After washing, DNA was stained using DAPI 1:2000 solution in PBS for 5min at RT. Isolated vessels were mounted using Fluoromount media.

iPSCs and iPSC-derived somatic cells

Prior to staining, iPSCs and iPSC-derived cells were seeded into coated coverslips (Marienfeld, Cat#0107052) using their corresponding coating. When cells reached confluency,

they were fixed using 4% PFA for 15min at room temperature (RT). Cells were blocked using 1% BSA solution in PBS for 1h at RT prior to antibody incubation. Primary antibody was diluted in the same blocking buffer and incubated at 4ºC overnight. Secondary antibody was diluted in PBS and incubated 2h at RT. After washing, DNA was stained using DAPI 1:2000 solution in PBS for 5min at RT. Isolated vessels were mounted using Fluoromount media.

3D in vitro BBB model

Cells in the 3D microfluidic were fixed using 4% PFA for 15min at room temperature (RT) as described for the feeding. Cells were permeabilized using 0,1% Triton X-100 (Company, Cat# xx) in MiliQ H2O for 5min at RT. Next, cells were blocked using 1% BSA solution in PBS for 30min at RT prior to antibody incubation. Primary antibody was diluted in blocking buffer whereas secondary antibody was diluted in PBS. Both antibodies were incubated overnight at 4°C. DNA was stained using DAPI 1:2000 solution in PBS for 5min at RT. Microfluidic chambers were imaged immediately.

Microscopy analysis

Confocal microscopy and image analysis

Fluorescent images were acquired with either with a Zeiss confocal microscope LSM880 or LSM980 using 10X, 40X, 64X objectives on ZEN black software. Images were further processes and analyzed using ImageJ software.

Electron microscopy

Transmission electron microscopy (TEM) of human cell culture

For the ultrastructural analysis of human cells in culture we positioned freshly plasma-coated ACLAR® (plastic) films (Science Services) into the cell culture dish before seeding. 5% glutaraldehyde (EM-grade, Science Services) in 0.2M cacodylate buffer pH 7.4 (Science Services) prewarmed to 37°C was added 1:1 to cell culture medium and replaced by 2.5% glutaraldehyde in 0.1M cacodylate buffer after 5 min. Dishes were incubated for further 25 min on ice. Cells were washed 3x 5 min with 0.1 M cacodylate buffer on ice and stored in buffer at 4°C until postfixation in reduced osmium (1% osmium tetroxide (Science Services), 0.8% potassium ferrocyanide (Sigma Aldrich) in 0.1 M sodium cacodylate buffer). After contrasting in aqueous 0.5% uranylacetate (Science Services), the cell monolayer was dehydrated in an ascending ethanol series, infiltrated in epon (Serva) and cured for 48h at 60 °C. Blocks were trimmed (TRIM2, Leica), 50-80 nm thick ultrathin sections generated on an ultramicrotome (UC7, Leica) and deposited onto formvar-coated copper grids (Plano) without postcontrasting. Transmission Electron Microscopy micrographs were acquired on a JEM 1400plus (JEOL) equipped with a XF416 camera (TVIPS) and the EM-Menu software (TVIPS). Images analysis was performed using Fiji (Schindelin et al. 2012).

Ultrastructural analysis of human 3D cultures

Fixation and heavy metal staining of cells in microfluidic chambers was performed by the application of a drop of reagent on a channel opening and removal at the opposite side. Reagent exchange was performed for 5 min and then in regular intervals for the incubation times mentioned in following protocol. Cultures in microfluidic chambers were fixed in in 2.5% glutaraldehyde in 0.1 M cacodylate for 15 min at 37°C and 45 min on ice. Heavy metal staining was accomplished by 1 h incubation in reduced (2.5% potassium ferricyanide) osmium tetroxide in 0.1 M sodium cacodylate on ice. Washes in buffer and water were followed by 1% uranyl acetate in water at 4°C overnight and at at 40°C for 2 h before washes in buffer. All dehydration steps in an ethanol series (at 10% intervals) were performed on ice, followed by room temperature treatments with 100% ethanol and 100% acetone. Infiltration was performed at 25 and 50% LX112 resin (LADD) in acetone.The plastic from the bottom of the microfluidic chamber was removed for further resin infiltration at 75% and three times 100% LX112 for 20 min. Fresh resin was added to the opened chamber overnight and for further 2 h before polymerization at 60°C for 2 days. Resin bearing cells were removed from the chamber and mounted onto empty resin blocks. The blocks were trimmed, sectioned and imaged by SEM as described for mouse tissue. Adjacent sections were collected onto copper grids for TEM investigation as described for 2D cell cultures. This allowed overview imaging of regions of interest by SEM and consecutive high resolution acquisition at the TEM.

Scanning electron microscopy of mouse tissue

For ultrastructural analysis of vessel crossections, mice were perfusion with % PFA, 2 mM calcium chloride in 1xPBS, pH 7.4 (Science Services). Only one hemisphere was used for ultrastructural analysis and therefore was further fixed by immersion in4% PFA, 2.5% glutaraldehyde, 2 mM calcium chloride in 0.1 M cacodylate buffer for 24h. Fix brains were sectioned using vibratome and further incubated with the same fixative for 24h and stored it 0.1 M cacodylate buffer at 4°C until the start of the postembedding.

We applied a rOTO en bloc staining protocol including postfixation in 2% osmium tetroxide (EMS), 1.5% potassium ferricyanide (Sigma) in 0.1 M sodium cacodylate (Science Services) buffer (pH 7.4) (Kislinger et al. 2020). The staining was further enhaced by incubation with 1% thiocarbohydrazide (Sigma) for 45 min at 40°C. After washing with water, the tissue was incubated in 2% aqueous osmium tetroxide, washed and further contrasted by overnight incubation in 1% aqueous uranyl acetate at 4°C and 2h at 50°C. Dehyadaration using ascending ethanol series and infiltiration with LX112 (LADD) was further done to the samples. Final blocks were cured and trimmed (TRIM2, Leica).

For ultrastructure analysis, using a 35° ultra-diamon knife (Diatome) on a ultramicrotome (UC7, Leica) 100 nm thick sections were taken and collected onto 1x0.5 cm carbon nanotube tape

strips (Science Services) or onto TEM grids as described. Samples when then attached to adhesive carbon tape (Science Services) on 4-inch silicon wafers (Siegert Wafer) and grounded by adhesive carbon tape strips (Science Services). EM micrographs were acquired using a Crossbeam Gemini 340 SEM (Zeiss) with a four-quadrant backscatter detector at 8 kV using ATLAS5 Array Tomography (Fibics). Medium lateral resolution images (40-100 nm) allowed the identification of blood vessels that were in turn reimaged at 4 nm resolution. Higher resolution imaging of sections on grids was performed using a JEM 1400plus (JEOL) as described. (Schindelin et al. 2012).

Western blot and western blot quantification

Protein of cell protein lysates was quantified using standard BCA analysis following manufacturer's instructions (ThermoFisher, Cat# 23227) and the same amount of protein was always loaded on a sodium dodecyl sulfate–polyacrylamide gel electrophoresis (SDS-PAGE). SDS-PAGE gels were transferred onto 0.2 nitrocellulose membrane using the Mini-Protean and Trans-Blot system. After transfer, membranes were blocked in 4% Milk in T-BST buffer or I-Block (Invitrogen, Cat# T2015) in PBS for 1h at room temperature (RT). Primary antibodies were diluted in the same blocking buffer and incubated at 4ºC overnight. Horseradish peroxidase-conjugated secondary antibodies were incubated for 1h at RT. Protein detection was performed by chemiluminescence development (Immobilon ECL detection reagent, Merck Millipore, Cat# WBULS0100) using Fusion FX7 (Vilber Lourmat) imager. Protein expression levels were quantified using ImageJ Gel Analyzer function and statistical significance was analyzed by two-tailed Student's t-test.

Whole vasculature analysis

Whole mouse vasculature was analyzed following a previous published protocol (Todorov et al. 2020).

RNA analysis

RNA extraction

RNA was extracted from cell pellets or half cerebellum using Trizol (Qiagen, Cat# 79306) and purified using the RNeasy mini kit (Qiagen, Cat# 74106) following manufacturer's instructions. Total RNA concentration was determined using a NanoDrop spectrophotometer. RNA was stored at-80ºC.

cDNA synthesis

cDNA synthesis was performed immediately after RNA isolation to avoid freezing and thawing cycles. cDNA was synthetized from 250ng - 1µg of RNA using the Omniscript RT kit (Qiagen, Cat# 205113) following manufacturer's instructions. cDNA was stored at -20ºC until use.

Quantitative real time qPCR (RT-qPCR)

Real time qPCR was performed using SYBR Green Master Mix (Qiagen, Cat# 208056) and reactions were set according to manufacturer's instructions. Detection was done using a Roche thermocycler. Primer sequences used for the study are listed in **Table 2**.

Mass spectrometry and data analysis

Sample preparation

Samples in SDT buffer (15-20 µg protein) were diluted with water to 50 µL and sonicated with a M-220 focused-ultrasonicater (Covaris, US) to disrupt DNA/RNA. Afterwards, samples were subjected to proteolytical digestion using a slightly modified single-pot solid-phase enhanced sample preparation (SP3) method (Faal et al. 2019). Briefly, proteins were bound to 200 µg of a 1:1 mixture of hydrophilic and hydrophobic magnetic Sera-Mag SpeedBeads (GE Healthcare, US) using a final concentration of 70% (v/v) acetonitrile at 1200 rpm on a thermomixer (Eppendorf, Germany) for 30 min at room temperature. Beads were retained on a Dynamag-2 (Thermofisher Scientific, US) magnet and the solvent was removed. Cysteine residues were alkylated by addition of 40 mM iodoacetamide (Sigma Aldrich, US) in 50 mM ammonium bicarbonate for 30 min at room temperature in the dark. Afterwards, the reaction was quenched by adding dithiothreitol to a final concentration of 40 mM. Then, proteins were bound again to the beads adding acetonitrile to a final concentration of 70% (v/v) for 30 min while shaking. Beads were washed four times with 200 µL 80% (v/v) ethanol. For proteolytic digestion, LysC (Promega, Germany) was added in 20 µL 50 mM ammonium bicarbonate with a protease to protein ratio of 1:80 was added to the beads. Samples were incubated on a Thermomixer (Eppendorf, Germany) for 30 min at 1000 rpm and 37°C. Afterwards, trypsin (Promega, Germany) was added in 20 µL 50 mM ammonium bicarbonate with a protease to protein ratio of 1:80 followed by an incubation for 16 h at room temperature. Beads were retained with a magnetic rack and the supernatants were collected. Next, 20 µL 0.1% formic acid were added to the magnetic beads followed by sonication for 30 s in a sonication bath (Hielscher Ultrasonics GmbH, Germany). The supernatants of each sample were combined, filtered with 0.22 µm spin filters (Costar Spin-x, Corning, USA) to remove remaining beads, and dried by vacuum centrifugation. Dried peptides were dissolved in 20 µL 0.1% formic. The peptide concentration after proteolytic digestion was estimated using the Qubit protein assay (Thermo Fisher Scientific, US).

Mass spectrometry

Samples were analyzed on a NanoElute nano-HPLC coupled online with a captive spray ion source to a TimsTOF pro mass spectrometer (Bruker, Germany). An amount of 350 ng of peptides were separated on a on an in-house packed C18 analytical column (15 cm × 75 µm ID, ReproSil-Pur 120 C18-AQ, 1.9 µm, Dr. Maisch GmbH) using a binary gradient of water and acetonitrile (B) containing 0.1% formic acid at flow rate of 250 nL/min (0 min, 2% B; 2 min, 5% B; 70 min, 24% B; 85 min, 35% B; 90 min, 60% B) and a column temperature of 50°C. A

standard Data Independent Acquisition Parallel Accumulation–Serial Fragmentation (DIA-PASEF) method with a cycle time of 1.8 s was used for spectrum acquisition. Briefly, ion accumulation and separation using Trapped Ion Mobility Spectrometry (TIMS) was set to a ramp time of 100 ms. The DIA PASEF windows covered the m/z range from 350 to 1200 m/z with 50 windows of 26 m/z with an overlap of 1 m/z. One scan cycle included one TIMS full MS scan and 17 DIA PASEF peptide fragmentation scans. Each DIA PASEF included 2 m/z windows resulting in a cyle time of 1.8 s.

Data Analysis

The raw data was analyzed by the software DIA-NN version 1.8.1 (Demichev et al. 2019). The MS data was searched against a one protein per gene canonical fasta databases of Homo Sapiens (download: January 18th 2022, 20600 entries) from UniProt and a fasta database with 246 common potential contaminations from Maxquant using a library free search. Trypsin was defined as protease. Two missed cleavages were allowed and peptide charge states were set to 2-4. Carbamidomethylation of cysteine was defined as static modification. Acetylation of the protein N-term as well as oxidation of methionine were set as variable modifications. The false discovery rate for both peptides and proteins was adjusted to less than 1%.

Enrichment analysis

Enrichment analysis of biological processes (GOTERM_BP_DIRECT) and pathways (KEGG_PATHWAY) were performed with DAVID (Database for Annotation, Visualization and Integrated Discovery), version 6.8, software (Huang, Sherman, and Lempicki 2009; Sherman et al. 2022) (https://david.ncifcrf.gov/home.jsp) (using Homo Sapiens or Mus musculus standard background dataset.

Principal component of proteomics samples

Proteomic data of primary and induced human cells was decomposed into four components using the python package sklearn (v 1.1.2) after standardization (removing the mean and scaling to unit variance) with the StandardScaler function of the same package.

Statistical analysis

Data collection and analysis were not performed with blinding of the experimental groups. Proteomic, transcriptomic, and morphological datasets showed normal distribution (tested with GraphPad Prism9, data not shown). Data were analyzed using two-sample t-test or ANOVA (indicated in each experiment). All data values are given as mean ± s.d unless stated otherwise.

Acknowledgements

We thank Tom Webb for technical advice for the endothelial cells and smooth muscle cell differentiation protocols. Mark nelson for the analysis of calcium transients. Peter Carlsson and Azadeh Reyahi for the Foxf2fl/fl mouse line, and Anna Berghofer, Melanie Schneider, Lea Peischer and Alessia Nottebrock for the technical assistance. Georg Kislinger for the 3D

embedding procedure for EM development. This study was supported by DFG under Germany's Excellence Strategy within the framework of the Munich Cluster for Systems Neurology (EXC 2145 SyNergy, ID 390857198), Vascular Dementia Research Foundation and Foundation Leducq. Graphics were created with Biorender.com

Author contributions

J.G.G., K.T.V., M.D and D.P. designed the project; J.G.G. performed cell culture experiments and established *in vitro* model; I.W. helped establish differentiation protocols; D.C and J.K. differentiated astrocytes; J.G.G and J.K. performed TEER and calcium experiments; S.A.M performed mass spectrometry; J.G.G. and K.T.V. analyzed proteomics experiments; M.I.T performed PCA analysis and light-sheet microscopy; K.T.V performed experiments on isolated mouse brain vasculature and BBB permeability; J.G.G. and K.T.V performed and analyzed biochemical and immunocytochemistry experiments; M.S. performed electron microscopy; and A.E, M.S., S.L., M.D. and D.P. supervised the experiments; J.G.G., K.T.V., M.D. and D.P wrote the manuscript; all the authors read and revised the manuscript.

Competing interests

The authors declare no competing interests.

References

Abbott, N. Joan, Lars Rönnbäck, and Elisabeth Hansson. 2006. “Astrocyte-Endothelial Interactions at the Blood-Brain Barrier.” *Nature Reviews Neuroscience* 7 (1): 41–53. https://doi.org/10.1038/nrn1824.

Abdullahi, Wazir, Dinesh Tripathi, and Patrick T. Ronaldson. 2018. “Blood-Brain Barrier Dysfunction in Ischemic Stroke: Targeting Tight Junctions and Transporters for Vascular Protection.” *American Journal of Physiology - Cell Physiology* 315 (3): C343–56. https://doi.org/10.1152/ajpcell.00095.2018.

Aday, S., R. Cecchelli, D. Hallier-Vanuxeem, M. P. Dehouck, and L. Ferreira. 2016. “Stem Cell-Based Human Blood-Brain Barrier Models for Drug Discovery and Delivery.” *Trends in Biotechnology* 34 (5): 382–93. https://doi.org/10.1016/j.tibtech.2016.01.001.

Andreone, Benjamin J., Brian Wai Chow, Aleksandra Tata, Baptiste Lacoste, Ayal Ben-Zvi, Kevin Bullock, Amy A. Deik, David D. Ginty, Clary B. Clish, and Chenghua Gu. 2017. “Blood-Brain Barrier Permeability Is Regulated by Lipid Transport-Dependent Suppression of Caveolae-Mediated Transcytosis.” *Neuron* 94 (3): 581-594.e5. https://doi.org/10.1016/j.neuron.2017.03.043.

Armulik, Annika, Guillem Genové, and Christer Betsholtz. 2011. “Pericytes: Developmental, Physiological, and Pathological Perspectives, Problems, and Promises.” *Developmental Cell*. https://doi.org/10.1016/j.devcel.2011.07.001.

Armulik, Annika, Guillem Genové, Maarja Mäe, Maya H. Nisancioglu, Elisabet Wallgard, Colin Niaudet, Liqun He, et al. 2010. “Pericytes Regulate the Blood-Brain Barrier.” *Nature* 468 (7323): 557–61. https://doi.org/10.1038/nature09522.

Belair, David G., Jordan A. Whisler, Jorge Valdez, Jeremy Velazquez, James A. Molenda, Vernella Vickerman, Rachel Lewis, et al. 2015. “Human Vascular Tissue Models Formed from Human Induced Pluripotent Stem Cell Derived Endothelial Cells.” *Stem Cell Reviews and Reports* 11 (3): 511–25. https://doi.org/10.1007/S12015-014-9549-5/FIGURES/8.

Caffrey, Tara M, Emily Button, and Jerome Robert. 2021. “Toward Three-Dimensional in Vitro Models to Study Neurovascular Unit Functions in Health and Disease.” *Neural Regeneration Research*. https://doi.org/10.4103/1673-5374.310671.

Campisi, Marco, Yoojin Shin, Tatsuya Osaki, Cynthia Hajal, Valeria Chiono, and Roger D Kamm. 2018. “3D Self-Organized Microvascular Model of the Human Blood-Brain Barrier with Endothelial Cells, Pericytes and Astrocytes.” *Biomaterials* 180: 117–29. https://doi.org/10.1016/j.biomaterials.2018.07.014.

Chauhan, Ganesh, Corey R. Arnold, Audrey Y. Chu, Myriam Fornage, Azadeh Reyahi, Joshua C. Bis, Aki S. Havulinna, et al. 2016. “Identification of Additional Risk Loci for Stroke and Small Vessel Disease: A Meta-Analysis of Genome-Wide Association

Studies.” *The Lancet Neurology* 15 (7): 695–707. https://doi.org/10.1016/S1474-4422(16)00102-2.

Chistiakov, D. A., A. N. Orekhov, and Y. V. Bobryshev. 2017. “Effects of Shear Stress on Endothelial Cells: Go with the Flow.” *Acta Physiologica* 219 (2): 382–408. https://doi.org/10.1111/APHA.12725.

Concordet, Jean Paul, and Maximilian Haeussler. 2018. “CRISPOR: Intuitive Guide Selection for CRISPR/Cas9 Genome Editing Experiments and Screens.” *Nucleic Acids Research* 46 (W1): W242–45. https://doi.org/10.1093/NAR/GKY354.

Cucullo, Luca, Mohammed Hossain, Vikram Puvenna, Nicola Marchi, and Damir Janigro. 2011. “The Role of Shear Stress in Blood-Brain Barrier Endothelial Physiology.” *BMC Neuroscience* 12 (May): 40. https://doi.org/10.1186/1471-2202-12-40.

Daneman, Richard, Lu Zhou, Amanuel A. Kebede, and Ben A. Barres. 2010. “Pericytes Are Required for Blood–Brain Barrier Integrity during Embryogenesis.” *Nature 2010 468:7323* 468 (7323): 562–66. https://doi.org/10.1038/NATURE09513.

Delsing, Louise, Anna Herland, Anna Falk, Ryan Hicks, Jane Synnergren, and Henrik Zetterberg. 2020. “Models of the Blood-Brain Barrier Using IPSC-Derived Cells.” *Molecular and Cellular Neuroscience*. https://doi.org/10.1016/j.mcn.2020.103533.

Demichev, Vadim, Christoph B. Messner, Spyros I. Vernardis, Kathryn S. Lilley, and Markus Ralser. 2019. “DIA-NN: Neural Networks and Interference Correction Enable Deep Proteome Coverage in High Throughput.” *Nature Methods 2019 17:1* 17 (1): 41–44. https://doi.org/10.1038/S41592-019-0638-X.

Dijk, Christian G.M. van, Maarten M Brandt, Nikolaos Poulis, Jonas Anten, Matthijs van der Moolen, Liana Kramer, Erik F.G.A. Homburg, et al. 2020. “A New Microfluidic Model That Allows Monitoring of Complex Vascular Structures and Cell Interactions in a 3D Biological Matrix.” *Lab on a Chip* 20 (10): 1827–44. https://doi.org/10.1039/d0lc00059k.

Dimmeler, Stefanie, Judith Haendeler, Volker Rippmann, Michael Nehls, and Andreas M. Zeiher. 1996. “Shear Stress Inhibits Apoptosis of Human Endothelial Cells.” *FEBS Letters* 399 (1–2): 71–74. https://doi.org/10.1016/S0014-5793(96)01289-6.

Drake, Christopher J., Jill E. Hungerford, and Charles D. Little. 1998. “Morphogenesis of the First Blood Vessels.” *Annals of the New York Academy of Sciences* 857 (1): 155–79. https://doi.org/10.1111/J.1749-6632.1998.TB10115.X.

Duperron, Marie-Gabrielle, Maria J. Knol, Quentin Le Grand, Tavia E. Evans, Aniket Mishra, Ami Tsuchida, Gennady Roshchupkin, et al. 2023. “Genomics of Perivascular Space Burden Unravels Early Mechanisms of Cerebral Small Vessel Disease.” *Nature Medicine 2023 29:4* 29 (4): 950–62. https://doi.org/10.1038/s41591-023-02268-w.

Etchevers, H. C., C. Vincent, N. M. Le Douarin, and G. F. Couly. 2001. “The Cephalic Neural Crest Provides Pericytes and Smooth Muscle Cells to All Blood Vessels of the Face and

Forebrain." *Development* 128 (7): 1059–68. https://doi.org/10.1242/DEV.128.7.1059.

Faal, Tannaz, Duc T.T. Phan, Hayk Davtyan, Vanessa M. Scarfone, Erika Varady, Mathew Blurton-Jones, Christopher C.W. Hughes, and Matthew A. Inlay. 2019. "Induction of Mesoderm and Neural Crest-Derived Pericytes from Human Pluripotent Stem Cells to Study Blood-Brain Barrier Interactions." *Stem Cell Reports* 12 (3): 451–60. https://doi.org/10.1016/J.STEMCR.2019.01.005.

Hajal, Cynthia, Giovanni S. Offeddu, Yoojin Shin, Shun Zhang, Olga Morozova, Dean Hickman, Charles G. Knutson, and Roger D. Kamm. 2022. "Engineered Human Blood–Brain Barrier Microfluidic Model for Vascular Permeability Analyses." *Nature Protocols* 17 (1): 95–128. https://doi.org/10.1038/s41596-021-00635-w.

Hajal, Cynthia, Baptiste Le Roi, Roger D. Kamm, and Ben M. Maoz. 2021. "Biology and Models of the Blood–Brain Barrier." *Https://Doi.Org/10.1146/Annurev-Bioeng-082120-042814* 23 (July): 359–84. https://doi.org/10.1146/ANNUREV-BIOENG-082120-042814.

Hartmann, David A., Robert G. Underly, Roger I. Grant, Ashley N. Watson, Volkhard Lindner, and Andy Y. Shih. 2015. "Pericyte Structure and Distribution in the Cerebral Cortex Revealed by High-Resolution Imaging of Transgenic Mice." *Https://Doi.Org/10.1117/1.NPh.2.4.041402* 2 (4): 041402. https://doi.org/10.1117/1.NPH.2.4.041402.

He, Weihan, Yuanbo Kang, Wei Zhu, Bolun Zhou, Xingjun Jiang, Caiping Ren, and Weihua Guo. 2020. "FOXF2 Acts as a Crucial Molecule in Tumours and Embryonic Development." *Cell Death and Disease*. Nature Publishing Group. https://doi.org/10.1038/s41419-020-2604-z.

Hou, Xucheng, Tal Zaks, Robert Langer, and Yizhou Dong. 2021. "Lipid Nanoparticles for MRNA Delivery." *Nature Reviews. Materials* 6 (12): 1078. https://doi.org/10.1038/S41578-021-00358-0.

Huang, Da Wei, Brad T. Sherman, and Richard A. Lempicki. 2009. "Systematic and Integrative Analysis of Large Gene Lists Using DAVID Bioinformatics Resources." *Nature Protocols* 4 (1): 44–57. https://doi.org/10.1038/nprot.2008.211.

Hupe, Mike, Minerva Xueting Li, Susanne Kneitz, Daria Davydova, Chika Yokota, Julianna Kele-Olovsson, Belma Hot, Jan M. Stenman, and Manfred Gessler. 2017. "Gene Expression Profiles of Brain Endothelial Cells during Embryonic Development at Bulk and Single-Cell Levels." *Science Signaling* 10 (487): 1–13. https://doi.org/10.1126/scisignal.aag2476.

Iadecola, Costantino. 2017. "The Neurovascular Unit Coming of Age: A Journey through Neurovascular Coupling in Health and Disease." *Neuron*. https://doi.org/10.1016/j.neuron.2017.07.030.

Jamieson, John J., Raleigh M. Linville, Yuan Yuan Ding, Sharon Gerecht, and Peter C.

Searson. 2019. “Role of IPSC-Derived Pericytes on Barrier Function of IPSC-Derived Brain Microvascular Endothelial Cells in 2D and 3D.” *Fluids and Barriers of the CNS* 16 (1): 1–16. https://doi.org/10.1186/S12987-019-0136-7/FIGURES/7.

Kalucka, Joanna, Laura P.M.H. de Rooij, Jermaine Goveia, Katerina Rohlenova, Sébastien J. Dumas, Elda Meta, Nadine V. Conchinha, et al. 2020. “Single-Cell Transcriptome Atlas of Murine Endothelial Cells.” *Cell* 180 (4): 764-779.e20. https://doi.org/10.1016/j.cell.2020.01.015.

Kisler, Kassandra, Amy R Nelson, Axel Montagne, and Berislav V Zlokovic. 2017. “Cerebral Blood Flow Regulation and Neurovascular Dysfunction in Alzheimer Disease.” *Nature Reviews Neuroscience*. https://doi.org/10.1038/nrn.2017.48.

Kislinger, Georg, Helmut Gnägi, Martin Kerschensteiner, Mikael Simons, Thomas Misgeld, and Martina Schifferer. 2020. “ATUM-FIB Microscopy for Targeting and Multiscale Imaging of Rare Events in Mouse Cortex.” *STAR Protocols* 1 (3): 100232. https://doi.org/10.1016/J.XPRO.2020.100232.

Korn, Johannes, Bodo Christ, and Haymo Kurz. 2002. “Neuroectodermal Origin of Brain Pericytes and Vascular Smooth Muscle Cells.” *Journal of Comparative Neurology* 442 (1): 78–88. https://doi.org/10.1002/CNE.1423.

Kwart, Dylan, Dominik Paquet, Shaun Teo, and Marc Tessier-Lavigne. 2017. “Precise and Efficient Scarless Genome Editing in Stem Cells Using CORRECT.” *Nature Protocols* 12 (2): 329–34. https://doi.org/10.1038/nprot.2016.171.

Lippmann, Ethan S, Samira M Azarin, Jennifer E Kay, Randy A Nessler, Hannah K Wilson, Abraham Al-Ahmad, Sean P Palecek, and Eric V Shusta. 2012. “Derivation of Blood-Brain Barrier Endothelial Cells from Human Pluripotent Stem Cells.” *Nature Biotechnology*. https://doi.org/10.1038/nbt.2247.

Liu, Gary W., Edward B. Guzman, Nandita Menon, and Robert S. Langer. 2023. “Lipid Nanoparticles for Nucleic Acid Delivery to Endothelial Cells.” *Pharmaceutical Research 2023 40:1* 40 (1): 3–25. https://doi.org/10.1007/S11095-023-03471-7.

Lu, Tyler M., Sean Houghton, Tarig Magdeldin, José Gabriel Barcia Durán, Andrew P. Minotti, Amanda Snead, Andrew Sproul, et al. 2021. “Pluripotent Stem Cell-Derived Epithelium Misidentified as Brain Microvascular Endothelium Requires ETS Factors to Acquire Vascular Fate.” *Proceedings of the National Academy of Sciences* 118 (8): e2016950118. https://doi.org/10.1073/pnas.2016950118.

Malik, Rainer, Ganesh Chauhan, Matthew Traylor, Muralidharan Sargurupremraj, Yukinori Okada, Aniket Mishra, Loes Rutten-Jacobs, et al. 2018. “Multiancestry Genome-Wide Association Study of 520,000 Subjects Identifies 32 Loci Associated with Stroke and Stroke Subtypes.” *Nature Genetics* 50 (4): 524. https://doi.org/10.1038/S41588-018-0058-3.

Monet-Leprêtre, Marie, Iman Haddad, Céline Baron-Menguy, Maï Fouillot-Panchal, Meriem Riani, Valérie Domenga-Denier, Claire Dussaule, Emmanuel Cognat, Joelle Vinh, and Anne Joutel. 2013. “Abnormal Recruitment of Extracellular Matrix Proteins by Excess Notch3ECD: A New Pathomechanism in CADASIL.” *Brain* 136 (6): 1830. https://doi.org/10.1093/BRAIN/AWT092.

Myatt, Stephen S., and Eric W.F. Lam. 2007. “The Emerging Roles of Forkhead Box (Fox) Proteins in Cancer.” *Nature Reviews Cancer 2007 7:11* 7 (11): 847–59. https://doi.org/10.1038/NRC2223.

Obermeier, Birgit, Richard Daneman, and Richard M. Ransohoff. 2013. “Development, Maintenance and Disruption of the Blood-Brain Barrier.” *Nature Medicine 2013 19:12* 19 (12): 1584–96. https://doi.org/10.1038/nm.3407.

Oddo, Arianna, Bo Peng, Ziqiu Tong, Yingkai Wei, Wing Yin Tong, Helmut Thissen, and Nicolas Hans Voelcker. 2019. “Advances in Microfluidic Blood–Brain Barrier (BBB) Models.” *Trends in Biotechnology* 37 (12): 1295–1314. https://doi.org/10.1016/j.tibtech.2019.04.006.

Orlova, Valeria V., Francijna E. Van Den Hil, Sandra Petrus-Reurer, Yvette Drabsch, Peter Ten Dijke, and Christine L. Mummery. 2014. “Generation, Expansion and Functional Analysis of Endothelial Cells and Pericytes Derived from Human Pluripotent Stem Cells.” *Nature Protocols* 9 (6): 1514–31. https://doi.org/10.1038/nprot.2014.102.

Orlova, Valeria V, Dennis M Nahon, Amy Cochrane, Xu Cao, Christian Freund, Francijna van den Hil, Cornelius J J Westermann, et al. 2022. “Vascular Defects Associated with Hereditary Hemorrhagic Telangiectasia Revealed in Patient-Derived Isogenic IPSCs in 3D Vessels on Chip.” *Stem Cell Reports* 17 (7): 1536–45. https://doi.org/10.1016/j.stemcr.2022.05.022.

Paquet, Dominik, Dylan Kwart, Antonia Chen, Andrew Sproul, Samson Jacob, Shaun Teo, Kimberly Moore Olsen, Andrew Gregg, Scott Noggle, and Marc Tessier-Lavigne. 2016. “Efficient Introduction of Specific Homozygous and Heterozygous Mutations Using CRISPR/Cas9.” *Nature* 533 (7601): 125–29. https://doi.org/10.1038/nature17664.

Paunovska, Kalina, Carmen J Gil, Melissa P Lokugamage, Cory D Sago, Manaka Sato, Gwyn N Lando, Marielena Gamboa Castro, Anton V Bryksin, James E Dahlman, and Wallace H Coulter. 2018. “Analyzing 2000 in Vivo Drug Delivery Data Points Reveals Cholesterol Structure Impacts Nanoparticle Delivery.” https://doi.org/10.1021/acsnano.8b03640.

Perrin, Steve. 2014. “Preclinical Research: Make Mouse Studies Work.” *Nature 2014 507:7493* 507 (7493): 423–25. https://doi.org/10.1038/507423a.

Perriot, Sylvain, Amandine Mathias, Guillaume Perriard, Mathieu Canales, Nils Jonkmans, Nicolas Merienne, Cécile Meunier, et al. 2018. “Human Induced Pluripotent Stem Cell-

Derived Astrocytes Are Differentially Activated by Multiple Sclerosis-Associated Cytokines." *Stem Cell Reports* 11 (5): 1199–1210. https://doi.org/10.1016/j.stemcr.2018.09.015.

Potjewyd, Geoffrey, Samuel Moxon, Tao Wang, Marco Domingos, and Nigel M. Hooper. 2018. "Tissue Engineering 3D Neurovascular Units: A Biomaterials and Bioprinting Perspective." *Trends in Biotechnology*. Elsevier Ltd. https://doi.org/10.1016/j.tibtech.2018.01.003.

Reyahi, Azadeh, Ali M. Nik, Mozhgan Ghiami, Amel Gritli-Linde, Fredrik Pontén, Bengt R. Johansson, and Peter Carlsson. 2015. "Foxf2 Is Required for Brain Pericyte Differentiation and Development and Maintenance of the Blood-Brain Barrier." *Developmental Cell* 34 (1): 19–32. https://doi.org/10.1016/J.DEVCEL.2015.05.008.

Roudnicky, Filip, Bo Kyoung Kim, Yanjun Lan, Roland Schmucki, Verena Küppers, Klaus Christensen, Martin Graf, et al. 2020. "Identification of a Combination of Transcription Factors That Synergistically Increases Endothelial Cell Barrier Resistance." *Scientific Reports* 10 (1). https://doi.org/10.1038/s41598-020-60688-x.

Schindelin, Johannes, Ignacio Arganda-Carreras, Erwin Frise, Verena Kaynig, Mark Longair, Tobias Pietzsch, Stephan Preibisch, et al. 2012. "Fiji: An Open-Source Platform for Biological-Image Analysis." *Nature Methods 2012 9:7* 9 (7): 676–82. https://doi.org/10.1038/NMETH.2019.

Sherman, Brad T., Ming Hao, Ju Qiu, Xiaoli Jiao, Michael W. Baseler, H. Clifford Lane, Tomozumi Imamichi, and Weizhong Chang. 2022. "DAVID: A Web Server for Functional Enrichment Analysis and Functional Annotation of Gene Lists (2021 Update)." *Nucleic Acids Research* 50 (W1): W216–21. https://doi.org/10.1093/NAR/GKAC194.

Skarnes, William C., Enrica Pellegrino, and Justin A. McDonough. 2019. "Improving Homology-Directed Repair Efficiency in Human Stem Cells." *Methods* 164–165 (June 2019): 18–28. https://doi.org/10.1016/j.ymeth.2019.06.016.

Smyth, Leon C.D., Justin Rustenhoven, Emma L. Scotter, Patrick Schweder, Richard L.M. Faull, Thomas I.H. Park, and Mike Dragunow. 2018. "Markers for Human Brain Pericytes and Smooth Muscle Cells." *Journal of Chemical Neuroanatomy* 92 (October): 48–60. https://doi.org/10.1016/j.jchemneu.2018.06.001.

Sweeney, Melanie D., Zhen Zhao, Axel Montagne, Amy R. Nelson, and Berislav V. Zlokovic. 2019. "Blood-Brain Barrier: From Physiology to Disease and Back." *Physiological Reviews* 99 (1): 21–78. https://doi.org/10.1152/physrev.00050.2017.

Takahashi, Kazutoshi, and Shinya Yamanaka. 2006. "Induction of Pluripotent Stem Cells from Mouse Embryonic and Adult Fibroblast Cultures by Defined Factors." *Cell* 126 (4): 663–76. https://doi.org/10.1016/J.CELL.2006.07.024.

Todorov, Mihail Ivilinov, Johannes Christian Paetzold, Oliver Schoppe, Giles Tetteh,

Suprosanna Shit, Velizar Efremov, Katalin Todorov-Völgyi, et al. 2020. “Machine Learning Analysis of Whole Mouse Brain Vasculature.” *Nature Methods 2020 17:4* 17 (4): 442–49. https://doi.org/10.1038/s41592-020-0792-1.

Vanlandewijck, Michael, Liqun He, Maarja Andaloussi Mäe, Johanna Andrae, Koji Ando, Francesca Del Gaudio, Khayrun Nahar, et al. 2018. “A Molecular Atlas of Cell Types and Zonation in the Brain Vasculature.” *Nature* 554 (7693): 475–80. https://doi.org/10.1038/nature25739.

Vatine, Gad D., Riccardo Barrile, Michael J. Workman, Samuel Sances, Bianca K. Barriga, Matthew Rahnama, Sonalee Barthakur, et al. 2019. “Human IPSC-Derived Blood-Brain Barrier Chips Enable Disease Modeling and Personalized Medicine Applications.” *Cell Stem Cell* 24 (6): 995-1005.e6. https://doi.org/10.1016/j.stem.2019.05.011.

Vila Cuenca, Marc, Amy Cochrane, Francijna E. van den Hil, Antoine A.F. de Vries, Saskia A.J. Lesnik Oberstein, Christine L Mummery, and Valeria V Orlova. 2021. “Engineered 3D Vessel-on-Chip Using HiPSC-Derived Endothelial- and Vascular Smooth Muscle Cells.” *Stem Cell Reports* 16 (9): 2159–68. https://doi.org/10.1016/j.stemcr.2021.08.003.

Wardlaw, Joanna M, Colin Smith, and Martin Dichgans. 2019. “Small Vessel Disease: Mechanisms and Clinical Implications.” *Review Lancet Neurol* 18: 684–96. https://doi.org/10.1016/S1474-4422(19)30079-1.

Weisheit, Isabel, Joseph A. Kroeger, Rainer Malik, Julien Klimmt, Dennis Crusius, Angelika Dannert, Martin Dichgans, and Dominik Paquet. 2020. “Detection of Deleterious On-Target Effects after HDR-Mediated CRISPR Editing.” *Cell Reports* 31 (8): 107689. https://doi.org/10.1016/J.CELREP.2020.107689.

Weisheit, Isabel, Joseph A. Kroeger, Rainer Malik, Benedikt Wefers, Peter Lichtner, Wolfgang Wurst, Martin Dichgans, and Dominik Paquet. 2021. “Simple and Reliable Detection of CRISPR-Induced on-Target Effects by QgPCR and SNP Genotyping.” *Nature Protocols 2021 16:3* 16 (3): 1714–39. https://doi.org/10.1038/S41596-020-00481-2.

Winkler, Ethan A., Robert D. Bell, and Berislav V. Zlokovic. 2011. “Central Nervous System Pericytes in Health and Disease.” *Nature Neuroscience*. Nature Publishing Group. https://doi.org/10.1038/nn.2946.

Wu, Qiong, Wei Li, and Chongge You. 2021. “The Regulatory Roles and Mechanisms of the Transcription Factor FOXF2 in Human Diseases.” *PeerJ* 9 (March): e10845. https://doi.org/10.7717/peerj.10845.

Xiang, Dan-Ni, Yi-Fan Feng, Jing Wang, Xi Zhang, Jing-Jing Shen, Rong Zou, and Yuan-Zhi Yuan. 2019. “Platelet-Derived Growth Factor-BB Promotes Proliferation and Migration of Retinal Microvascular Pericytes by up-Regulating the Expression of C-X-C Chemokine Receptor Types 4.” *Experimental and Therapeutic Medicine* 18 (5): 4022.

https://doi.org/10.3892/ETM.2019.8016.

Yamazaki, Tomoko, Ani Nalbandian, Yutaka Uchida, Wenling Li, Thomas D. Arnold, Yoshiaki Kubota, Seiji Yamamoto, Masatsugu Ema, and Yoh suke Mukouyama. 2017. “Tissue Myeloid Progenitors Differentiate into Pericytes through TGF-β Signaling in Developing Skin Vasculature.” *Cell Reports* 18 (12): 2991–3004. https://doi.org/10.1016/j.celrep.2017.02.069.

Yang, Andrew C, Ryan T Vest, Fabian Kern, Davis P Lee, Christina A Maat, Patricia M Losada, Michelle B Chen, et al. 2021. “A Human Brain Vascular Atlas Reveals Diverse Cell Mediators of Alzheimer’s Disease Risk.” *BioRxiv*, 2021.04.26.441262. https://doi.org/10.1101/2021.04.26.441262.

Zellner, Andreas, Eva Scharrer, Thomas Arzberger, Chio Oka, Valérie Domenga-Denier, Anne Joutel, Stefan F. Lichtenthaler, Stephan A. Müller, Martin Dichgans, and Christof Haffner. 2018. “CADASIL Brain Vessels Show a HTRA1 Loss-of-Function Profile.” *Acta Neuropathologica* 136 (1): 111–25. https://doi.org/10.1007/S00401-018-1853-8/FIGURES/6.

Zhao, Zhen, Amy R Nelson, Christer Betsholtz, and Berislav V Zlokovic. 2015. “Establishment and Dysfunction of the Blood-Brain Barrier.” *Cell*. https://doi.org/10.1016/j.cell.2015.10.067.

Zlokovic, Berislav V. 2008. “The Blood-Brain Barrier in Health and Chronic Neurodegenerative Disorders.” *Neuron*. Elsevier. https://doi.org/10.1016/j.neuron.2008.01.003.

Zlokovic, Berislav V. 2011. “Neurovascular Pathways to Neurodegeneration in Alzheimer’s Disease and Other Disorders.” *Nature Reviews Neuroscience*. https://doi.org/10.1038/nrn3114.

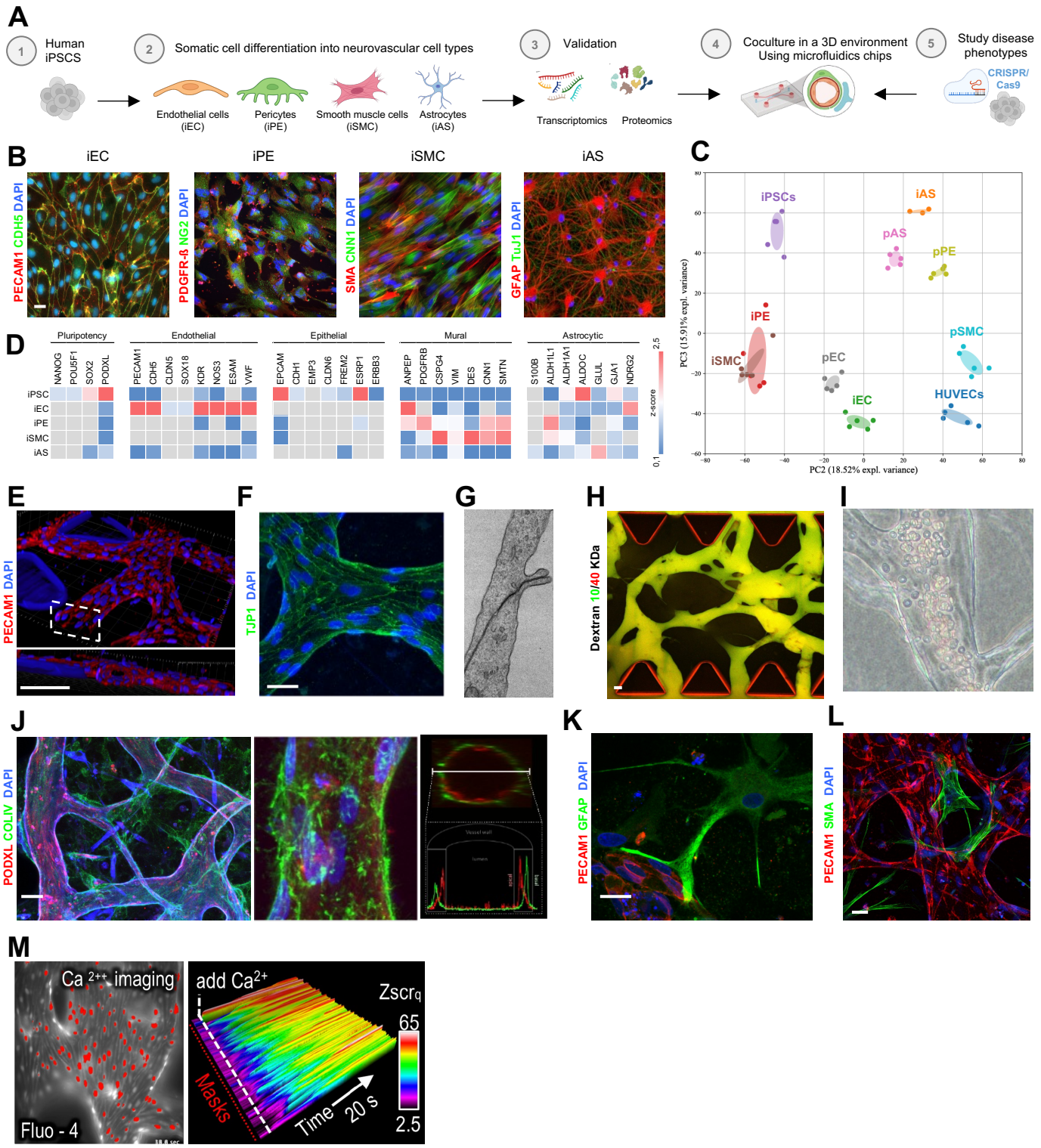

Figure 1. Generation and characterization of a fully human iPSC-derived 3D neurovascular unit model.

A. Experimental pipeline: iPSCs are differentiated into neurovascular cell types and validated via transcriptomics and proteomics (1-3). The 3D BBB model is generated by co-culturing differentiated cells in microfluid chips (4) and applied to study disease associated mutations inserted by CRISPR/Cas9 genome editing at the iPSCs level (5). **B**. Representative immunocytochemistry images of iPSC derived endothelial cells, pericytes, smooth muscle cells and astrocytes. Scale bar 20µm. **C**. Principal-component analysis (PCA) including all proteins detected in iPSC, iPSC-derived cells and human primary cells (n=3-5 samples/group). **D**. Abundance and individual changes of cell-specific markers for iPSC and iPSC-derived cells (n=3-5 samples/group) in proteomics analysis. **E**. Rendering of a representative immunocytochemistry image of vessel network formation in 3D BBB model stained for endothelial cell marker CD31. Scale bar 50µm. **F**. Representative immunocytochemistry image of endothelial cells in 3D BBB model expressing adherens and tight junctions using ZO1. Scale bar 25 µm. **G**. Representative scanning electron microscope (SEM) image of endothelial junction formation. **H**. Maximum image projections of 3D BBB model perfused with 10KDa (green) and 40KDa (red) dextran. Scale bar 50µm. **I**. Representative image of 3D BBB model perfused with human blood. **J**. Representative immunocytochemistry of the 3D BBB model stained for ECM proteins (left). Scale bar 50µm. Side view of vessel expressing markers (middle). Vessel topology analysis using intensity profile of COLIV and PDOXL staining in vessel cross-section (left). **K**. Immunocytochemistry of astrocyte localization in 3D BBB culture. Scale bar 25µm. **L**. Immunocytochemistry of smooth muscle cells localization in 3D BBB culture. Scale bar 25µm. **M**. Calcium waves in endothelial cells loaded with Fluo-4 in 3D BBB model after calcium addition. Imaged masks are indicated in red (left). Graphical representation of calcium signals at all masks over a time frame of 20 s. Singnal strength is indicated as $Zscr_q$ (right).

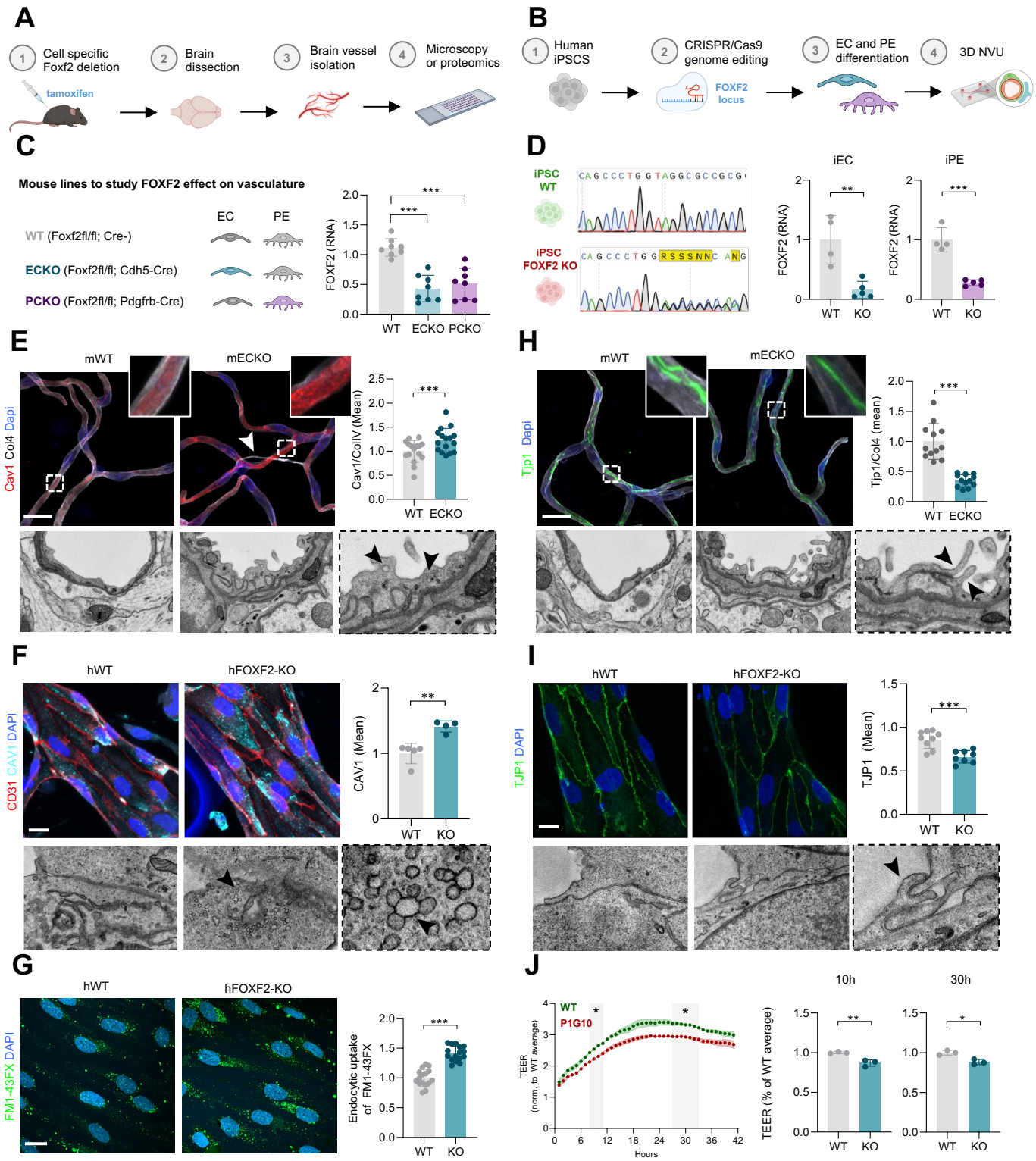

Figure 2. Human 3D BBB model phenocopies barrier dysfunction caused by Foxf2 deficiency *in vivo.*

A. Experimental overview for generating conditional cell-specific deletion of Foxf2 in mice and performing proteomics after vessel isolation. **B**. Experimental overview for generating human FOXF2-KO iPSCs via CRISPR/Cas9 genome editing and further characterization in endothelial cells and pericytes. **C**. Overview of Foxf2-deficient mouse lines and relative RNA levels of Foxf2 in each line (normalized to Actb and WT) (n=8 replicates/group, p-value <0,01). **D**. Sequencing traces of iPSC FOXF2 locus after genome editing and relative RNA levels of FOXF2 in iEC and iPE (normalized to EMC7 and WT respectively) (n=4-5 replicates/group, p-value <0,01). **E**. (**top**) Representative immunocytochemistry of mouse brain isolated vessels stained for Cav1 and ColIV with quantification of mean intensity of Cav1 normalized to ColIV (relative to WT) (n=5 replicates/sample). Scale bar 20µm. (**Bottom**) Representative TEM image of endothelium thickening and caveolae enrichment in EC-KO compared to WT vessel (n=1 replicate/sample). **F**. (**top**) Representative immunocytochemistry of 3D BBB model stained for CDH5 and CAV1 with quantification of CAV1 mean intensity (relative to WT) (n=4 replicates/group). Scale bar 25µm. (**bottom**) Representative transmission electron microscopy of caveolae enrichment in KO compared to WT (n=1 replicate/group). **G**. Increased uptake of FM1-43FX in FOXF2-KO iECs. Representative immunocytochemistry of iECs with quantification of mean intensity of FM1-43FX (relative to WT) (n=15 replicates/group). Scale bar 20µm. **H**. (**top**) Representative immunocytochemistry of mouse brain isolated vessels stained for Zo1 and ColIV with quantification of mean intensity of Zo1 normalized to ColIV (relative to WT) protein expression (n=5 replicates/sample). Scale bar 20µm. (bottom) Representative TEM image of endothelial tight junction protrusions in EC-KO compared to WT (n=1 replicate/group). (*continuation in the next page*)

Figure 2. Human 3D BBB model phenocopies barrier dysfunction caused by Foxf2 deficiency *in vivo*. (*continuation*)

I. (**top**) Representative immunocytochemistry of 3D BBB model stained for ZO1 with quantification of mean intensity (relative to WT) (n=8 replicates/sample). Scale bar 25μm (**bottom**) Representative TEM image of endothelial cell-cell adhesion and tight junction regions in KO compared to WT (n=1 replicate/group). **J**. Transendothelial electrical resistance (TEER) of FOXF2-KO iEC (relative to WT) over 42h and with quantification at 30h (relative to WT) (n=3 replicates/group).

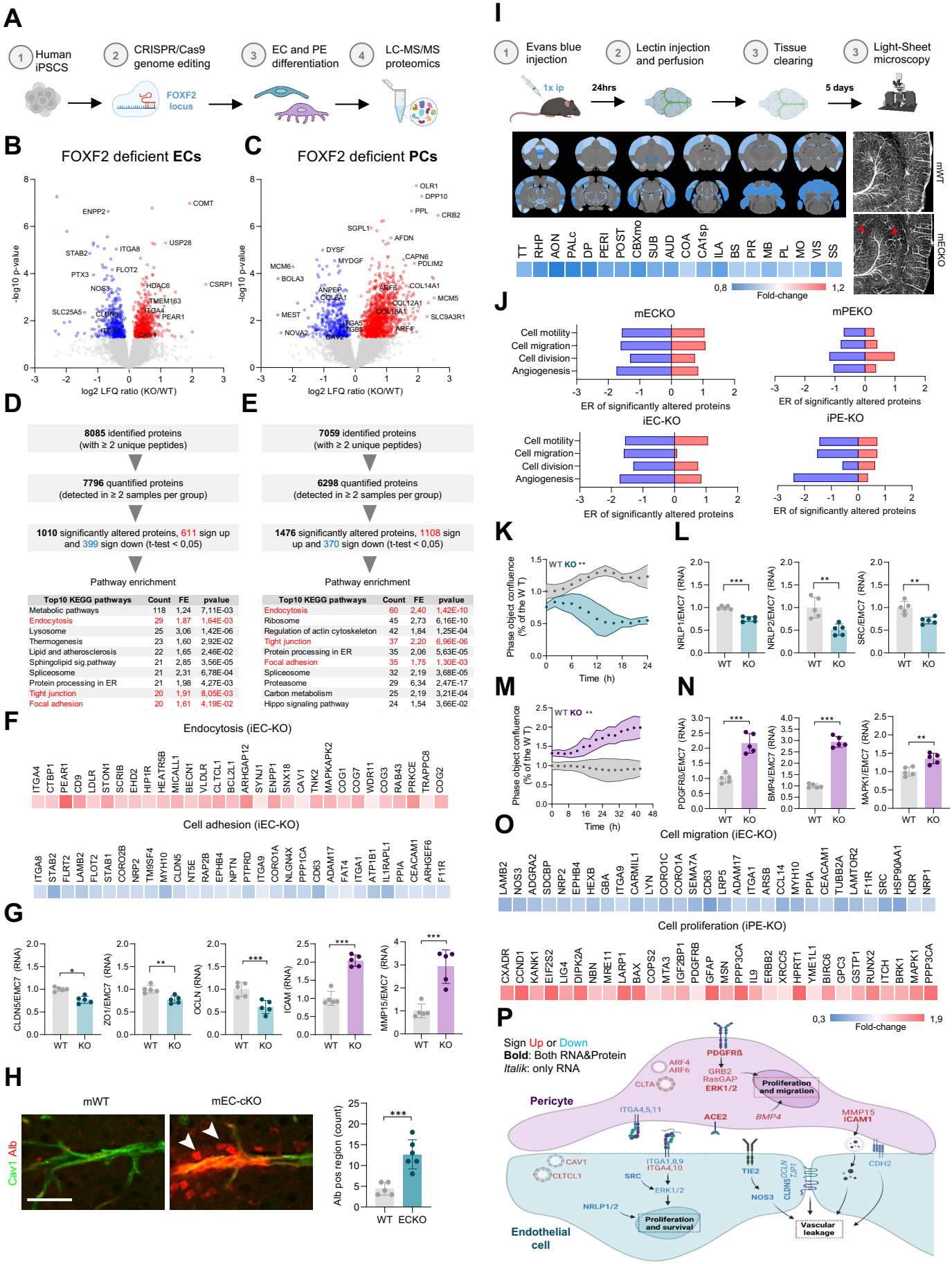

Figure 3. Cell-specific Foxf2 deficiency dysregulates proteins involved in vessel integrity and remodeling.

A. Experimental pipeline for studying endothelial and pericyte-specific FOXF2 deletion in human cells via proteomics. **B-C**. Volcano plots of log2 LFQ rations (KO vs WT) and -log10 p-values of all quantified proteins in iEC (**B**) and iPE (**C**). Red and blue circles indicate proteins that were significantly up- and downregulated respectively (n=5 replicates/group, t-test, p>0,05). Proteins related with vessel integrity and remodeling are marked with their gene name. **D-E**. Summary of the LC-MS/MS and LFQ results and enrichment analysis of top10 KEGG biological pathways for iEC (**D**) and iPE (**E**). (*continuation in the next page*)

Figure 3. Cell-specific Foxf2 deficiency dysregulates proteins involved in vessel integrity and remodeling (*continuation*)

F. Abundance of top 30 significantly upregulated proteins related to endocytosis and downregulated proteins related to cell adhesion (n=5 samples/group, t-test, p-value < 0,05). **G**. Relative RNA abundances of selected proteins related to vessel integrity in iEC and iPE normalized to EMC7 and WT (n=5 replicates/group). **H**. Confocal microscopy images and corresponding quantification of brain regions with focal albumin leakage (n=5 replicates/group). Scale bar 50µm. **I**. Experimental pipeline to study vessel morphology of whole adult mouse brain. Significant altered anatomic regions according to vessel density (n=4 samples/group, t-test, p-value<0,05). Representative images from one region

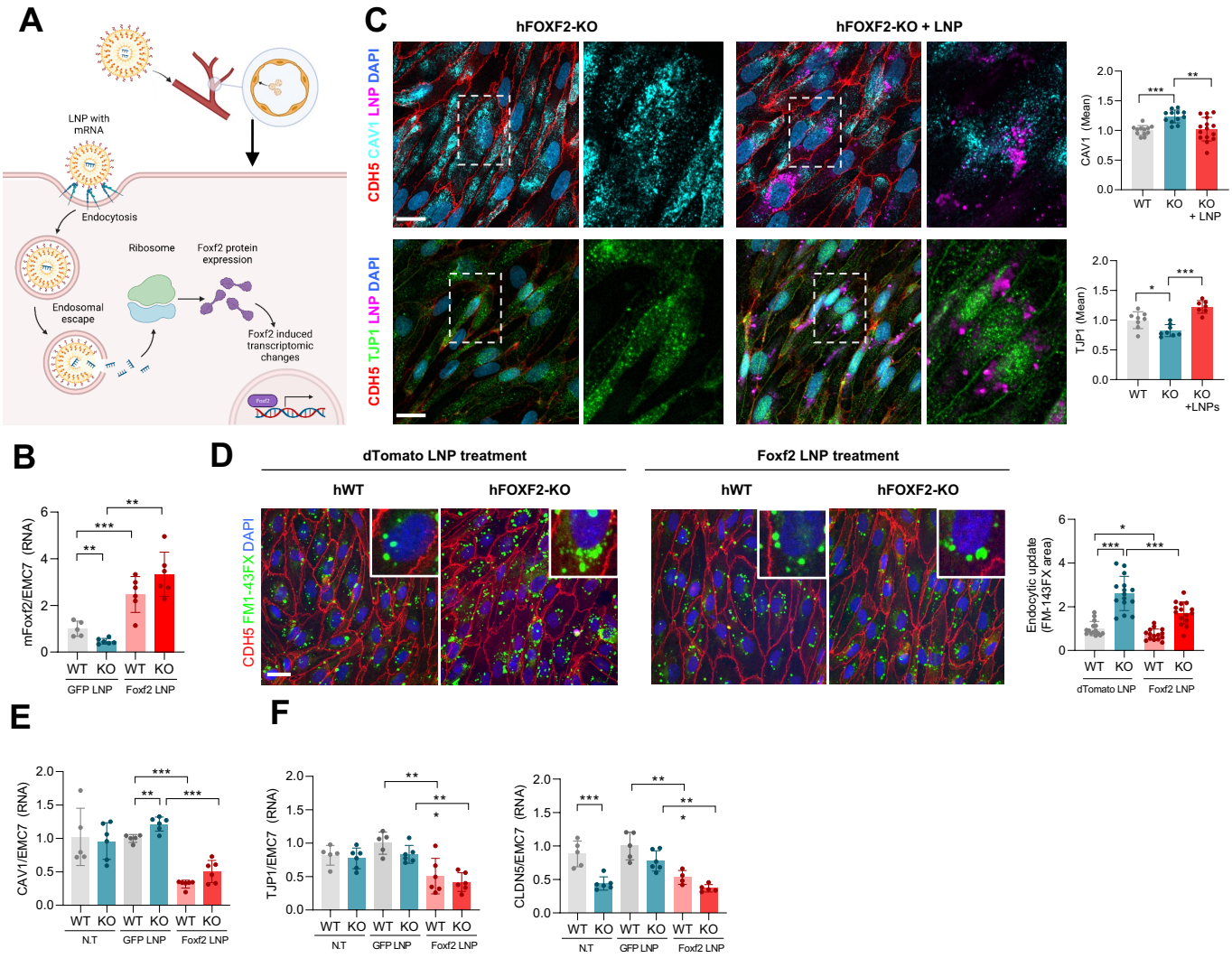

Figure 4. LNP delivery of Foxf2 restores barrier function in human 3D BBB model.

A. Overview of LNP mode of action: uptake by endothelial cells and Foxf2 mRNA translation into protein. **B**. Relative RNA abundance of mFoxf2 in iEC after LNP treatment, normalized to EMC7 and WT (GFP vs mFOXF2) (n=5 replicates/sample). **C**. (**top**) Representative immunocytochemistry of Foxf2 deficient endothelial cells treated with FOXF2 LNPs (in magenta) and stained for CDH5 and CAV1, with quantification of CAV1 mean intensity (relative to WT) (n=15 replicates/group). Scale bar 20µm. (**bottom**) Representative immunocytochemistry of Foxf2 deficient endothelial cells treated with FOXF2 LNPs (in magenta) and stained for CDH5 and ZO1, with quantification of ZO1 mean intensity (relative to WT) (n=15 replicates/group). Scale bar 20µm. **D**. Endocytic uptake of FM1-43FX in WT and FOXF2-KO iECs after LNP treatment (dTomato vs. mFoxf2). Representative immunocytochemistry of iEC with quantification of mean intensity of FM1-43FX (relative to WT) (n=15 replicates/group). Sale bar 20µm. **E**. Relative RNA abundance of CAV1 normalized to EMC7 and WT, in iEC not treated (N.T.) or treated with two LNP conditions (GFP vs mFoxf2) (n=5 replicates/sample). **F**. Relative RNA abundance of ZO1 and CLDN5 normalized to EMC7 and WT in iEC not treated (N.T.) or treated with two LNP conditions (GFP vs mFoxf2) (n=5 replicates/sample).

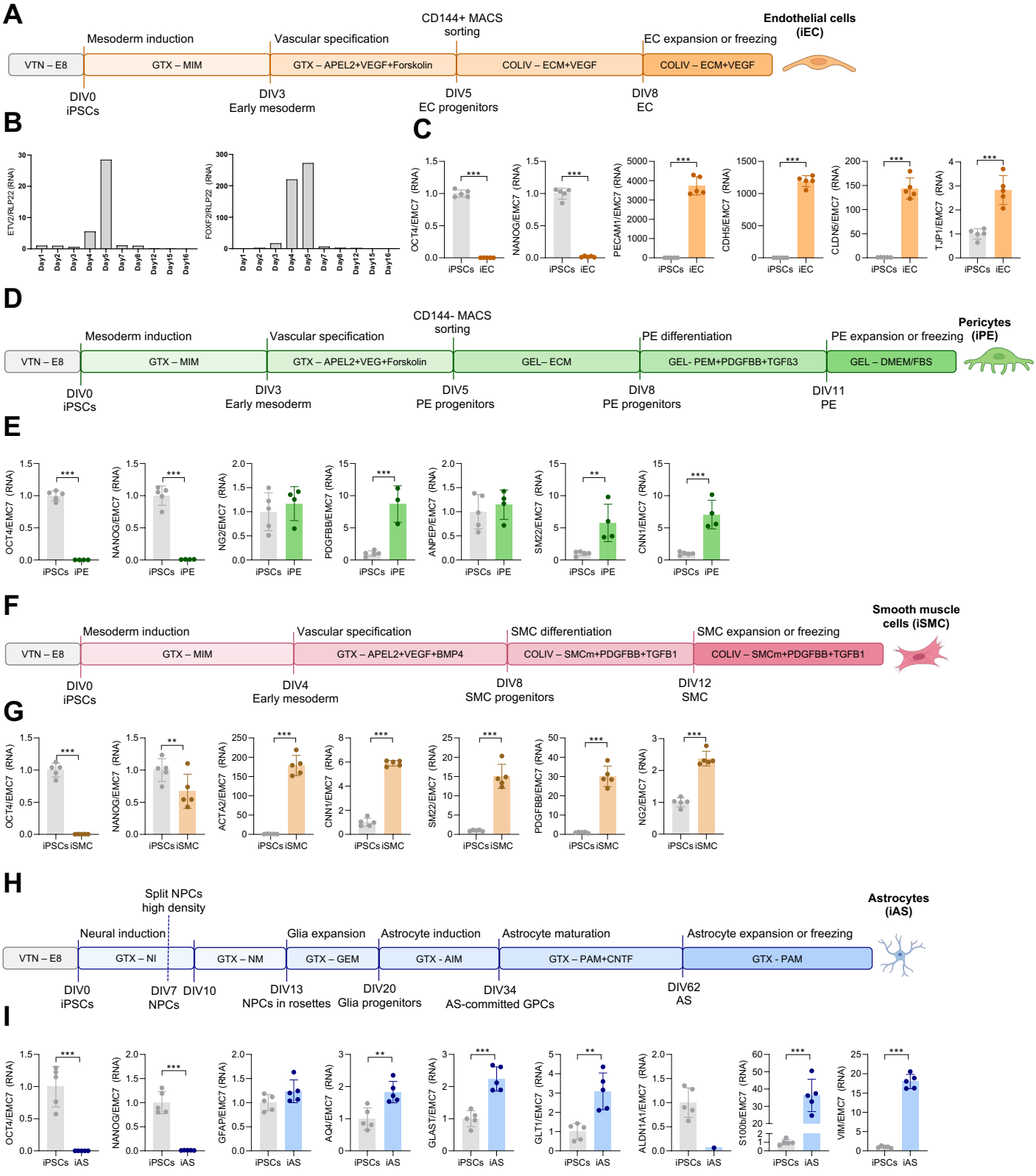

Supplementary Figure 1. Differentiation and characterization of iPSC-derived endothelial cells, pericytes, smooth muscle cells and astrocytes.

A. Overview of endothelial cell differentiation. **B**. Relative RNA abundance of ETV2 and FOXF2 during endothelial cell differentiation. **C**. Relative RNA abundance of pluripotency markers and endothelial-specific cell markers normalized to in iPSCs and iECs, normalized to iPSCs (n=5 replicates/group). **D**. Overview of pericyte differentiation protocol. **E**. Relative RNA abundance of pluripotency markers and mural cell-specific cell markers in iPSCs and iPE, normalized to iPSCs (n=5 replicates/group). **F**. Overview of smooth muscle cell differentiation protocol. **G**. Relative RNA abundance of pluripotency markers and mural cell-specific cell markers normalized to iPSCs in iPSCs and iPE (n=5replicates/group). **H**. Overview of astrocyte differentiation protocol. **I**. Relative RNA abundance of pluripotency markers and astrocytic-specific cell markers normalized to iPSCs in iPSCs and iAS (n=5replicates/group).

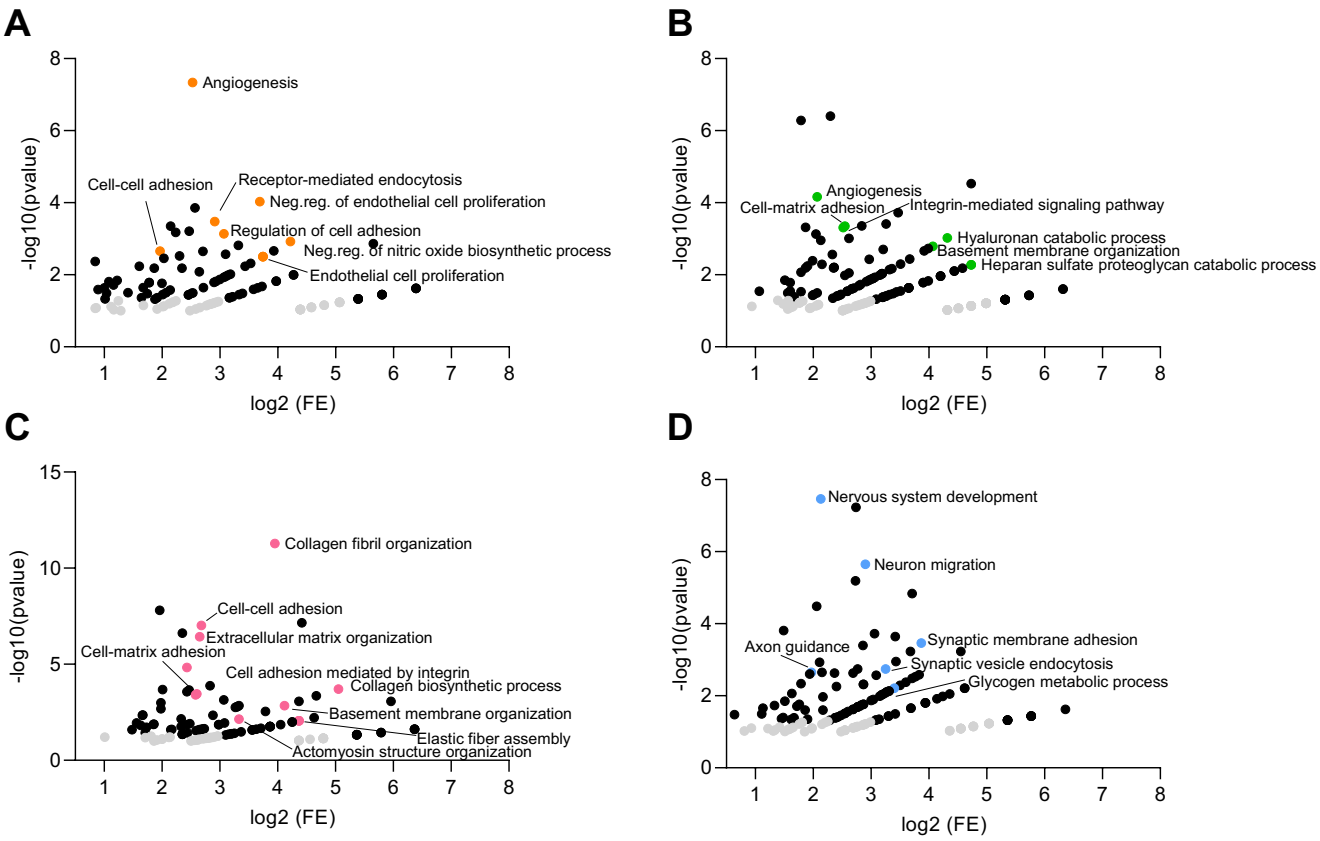

Supplementary Figure 2. Proteomics characterization of iPSC-derived endothelial cells, pericytes, smooth muscle cells and astrocytes.

A. Enrichment analysis results of biological processes using top 250 defined by PC1 when comparing iPSC vs. iEC. **B**. Enrichment analysis results of biological processes using top 250 defined by PC1 when comparing iPSC vs. iPE. **C**. Enrichment analysis results of biological processes using top 250 defined by PC1 when comparing iPSCs vs iSMC. **D**. Enrichment analysis results of biological processes using top250 defined by PC1 when comparing iPSC vs iAS.

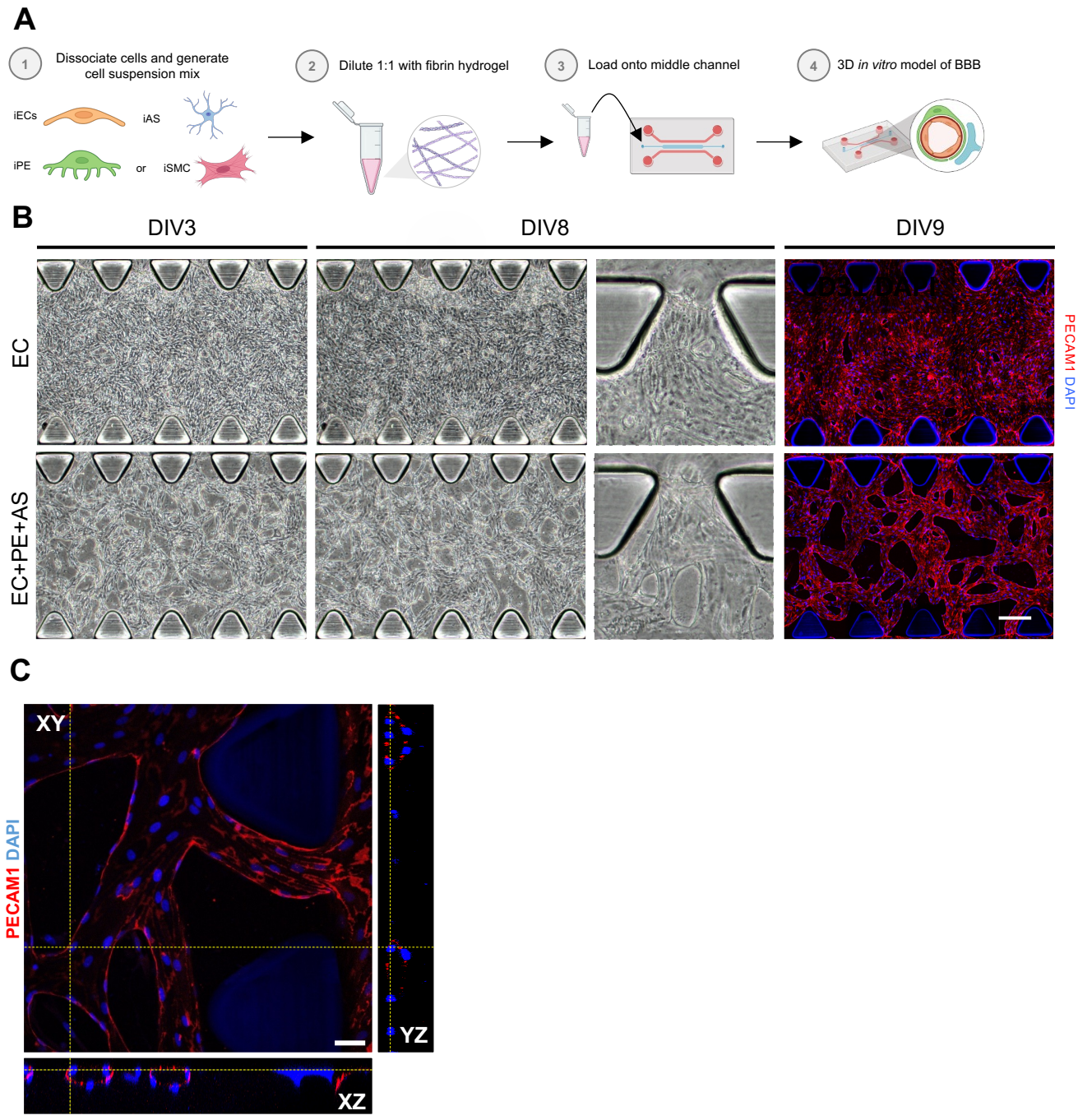

Supplementary Figure 3. Generation and characterization of 3D in vitro model of the BBB.

A. Experimental pipeline for 3D *in vitro* model assembling. **B**. Representative figures of in vitro modeling over time stained with PECAM1 and DAPI. Scale bar 250μm. **C**. Orthogonal projections of confocal imaging of tubular structures in 3D in vitro model. Scale bar 50μm.

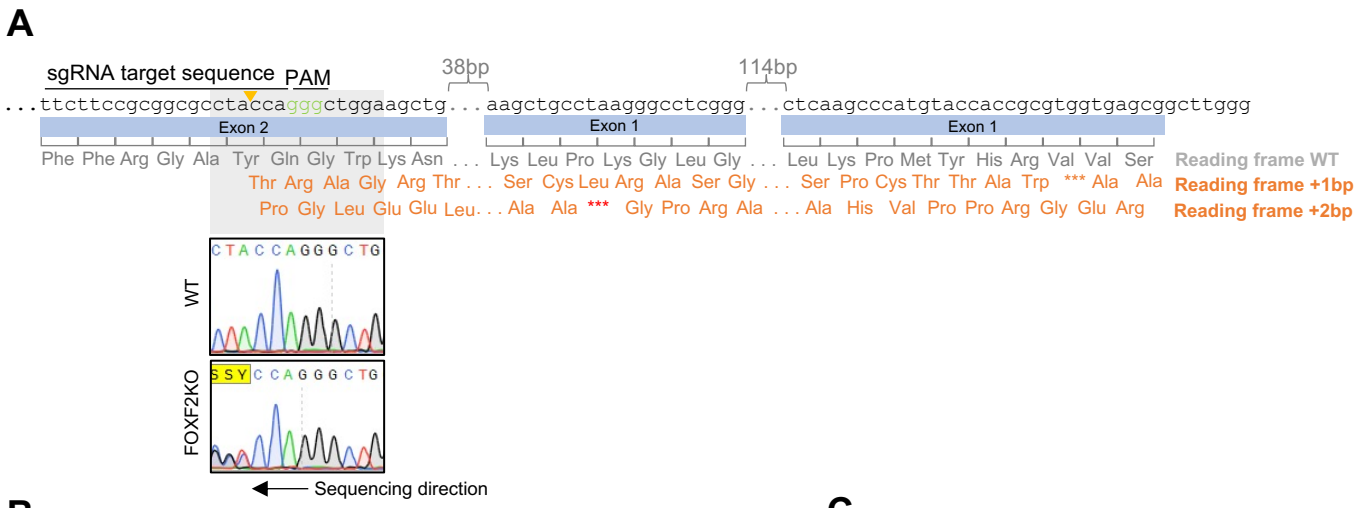

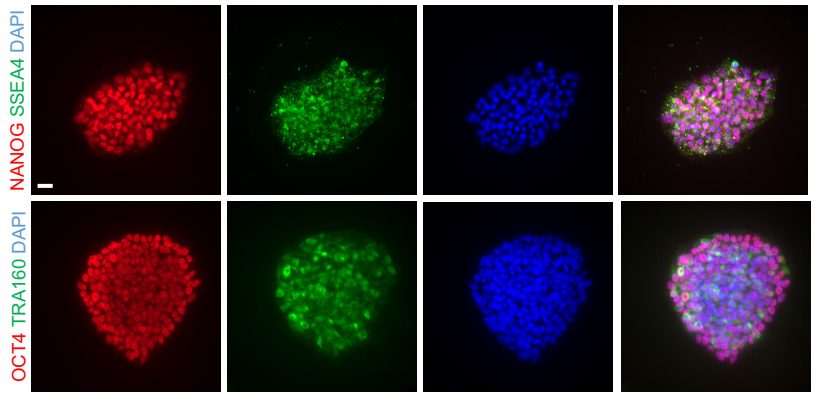

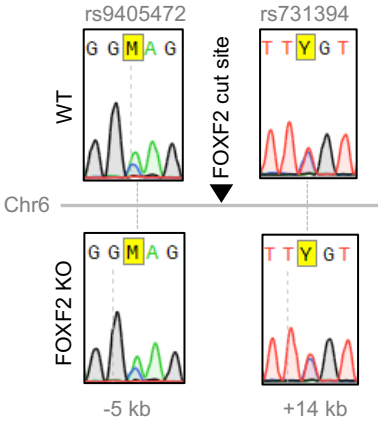

D

Gene	ID	Sequence	Mismatch position	MIT score	CFD score	Location	Location descrption	Indels detected
FOXF2	gRNA	TTCTTCCGCGGCGCCTACCAGGG	Target	-	-			
FOXF2	CFD OT 1	TTCTTTAGAGGCACCTACCAAGG	.....**.*...*.....	0,1334	0,551	6:7916970:7917492:-1	intergenic:TXNDC5-BLOC1S5/EEF1E1-BLOC1S5	None
FOXF2	CFD OT 2	TTCTACCAGGGCGCCTACCGCGG	....*..**.....*	0,4034	0,2367	20:38926550:38927072:1	exon:FAM83D	None
FOXF2	MIT OT 1	TTCTTCCGGGGCTCCTACCAGGG	.....*...*.....	1,4217	0,1857	16:86510569:86511091:1	exon:FOXF1/AC009108.2	None
FOXF2	MIT OT 2	ACCTTCAGCAGCGCCTACCAGGG	**....*..*.....	0,9	0,6	6:44272951:44273473:1	exon:TMEM151B/RP11-444E17.6	None
FOXF2	MIT OT 3	TCCCTCGGCAGCGCCTACCAGGG	.*.*..*..*.....	0,8586	0,2436	2:23667696:23668218:-1	intron:KLHL29	None
FOXF2	MIT OT 4	TTTTTCCTCAGTGCCTACCATGG	..*....*.*.....	0,6392	0,2159	19:12531341:12531863:-1	intron:CTD-2192J16.21	None
FOXF2	MIT OT 5	TCCTTCCACAGCCCCTACCATGG	.*.....*.*..*.....	0,5099	0,3368	9:122046793:122047315:-1	intron:TTLL11	None

Supplementary Figure 4. CRISPR/Cas9 mediated genome editing of human iPSCs to FOXF2 KO.

A. FOXF2 knockout strategy: Exon1 of FOXF2 was targeted by a sgRNA (target and PAM sequence shown), generating a 1 base pair insertion combined with a 5 base pair deletion on each allele. The resulting frameshift exposes a nearby stop codon in both cases. **B**. Immunofluorescence analysis of pluripotency markers: SSEA4, NANOG, TRA160 and OCT4 in iPSCs FOXF2-KO cells. Scale bar 25µm. **C**. Sanger sequences of unmodified SNPs near the edited locus in WT and FOXF2 KO iPSC lines showing maintenance of both alleles after editing. **D**. List of top five most similar off-target sites ranked by CFD and MIT prediction scores. Sites revealed by both algorithms (CFD OT3, 4 and 5) are only shown once.

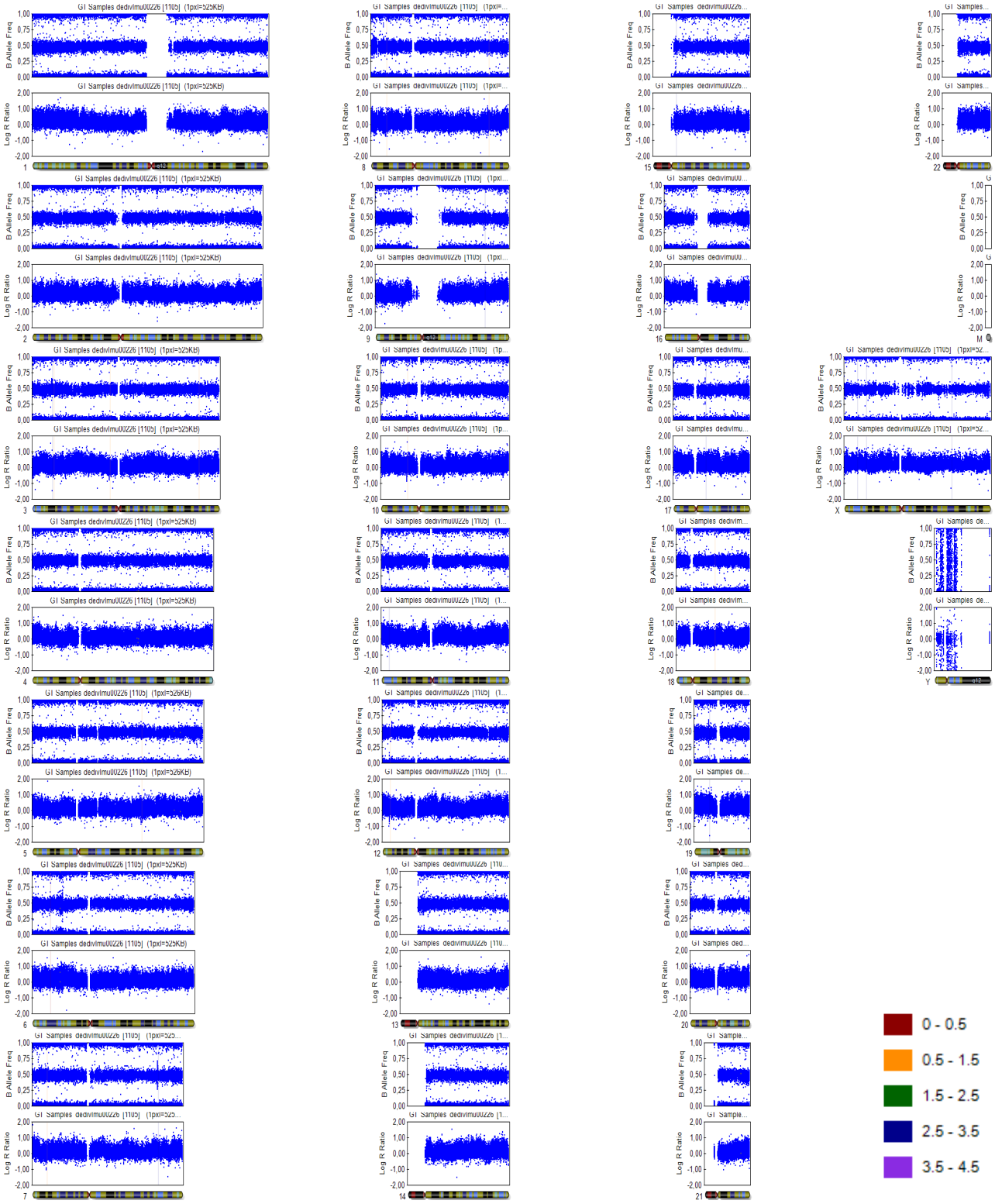

Supplementary Figure 5. Karyotyping of FOXF2-KO edited iPSC line.

B allele frequencies (BAF) and Log R ratios are shown for each chromosome in the FOXF2 KO iPSC line. All measured SNPs are indicated by blue dots. BAF values indicate normal zygosities on all chromosomes and Log R ratios show the absence of detectable insertions or deletions.

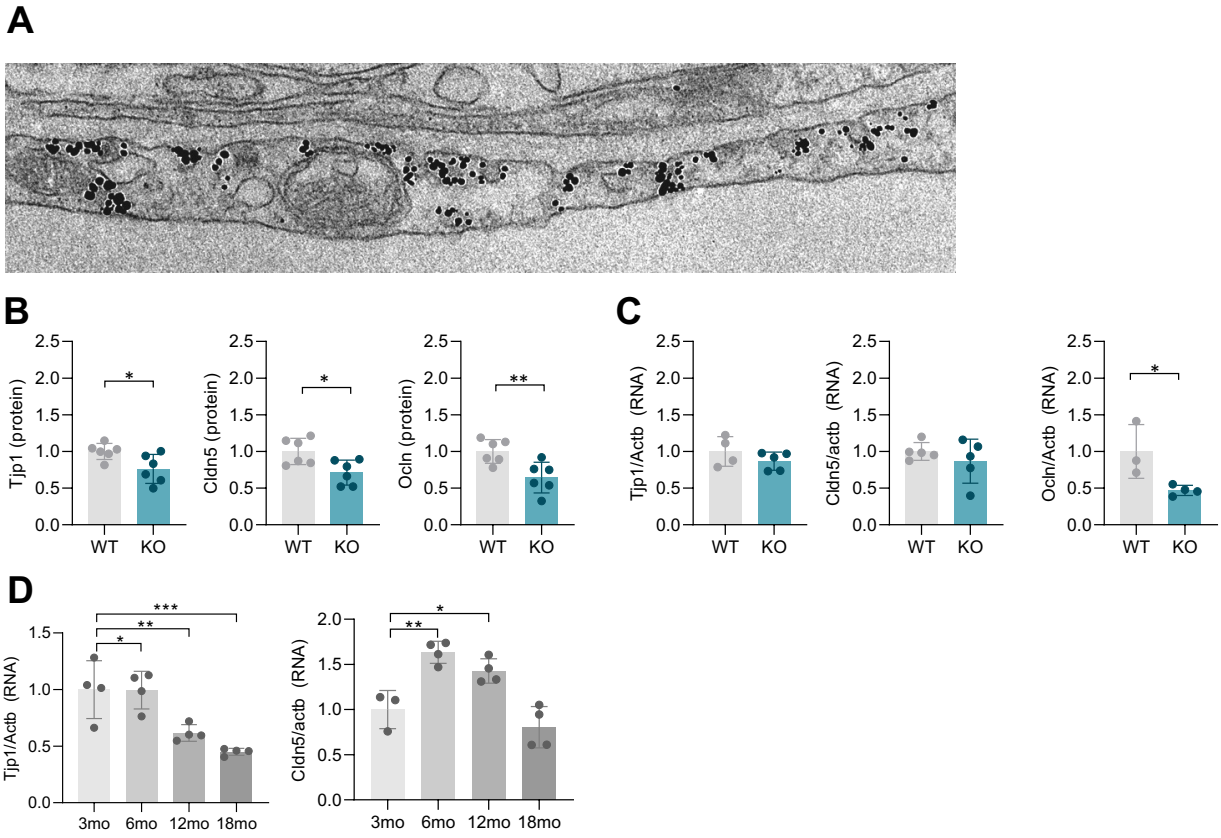

Supplementary Figure 6. Caveolae enrichment and cell junction reduction induced by endothelial Foxf2 deficiency in mouse.

A. Immunogold localization of Cav1 in ECKO endothelium using electron microscopy (n=1 replicate/sample). **B**. LFQ intensities of Tjp1, Cldn5 and Ocln in isolated BEC from EC-KO (n=6 replicates/group). **C**. Relative RNA abundances of Tjp1, Cldn5 and Ocln in full tissue of EC-KO normalized to Actb and WT (n=5 replicates/sample). **D**. Relative RNA abundances of Tjp1 and Cldn5 during healthy aging normalized to Actb and 3mo (n=4 replicate/group).

3.2. The stroke risk gene Foxf2 maintains brain endothelial cell function via Tie2-mediated Nos3 signaling

Authors:

Katalin Todorov-Völgyi*, **Judit González-Gallego***, Stephan A Müller, Burcu Fatma Seker, Mihail Ivilinov Todorov, Luise Schröger, Jiayu Cao, Ulrike Schillinger, Simon Frerich, Martina Fetting, Mikael Simons, Ali Ertürk, Arthur Liesz, Nikolaus Plesnila, Stefan Lichtenthaler, Dominik Paquet, Martin Dichgans

The stroke risk gene Foxf2 maintains brain endothelial cell function via Tie2-mediated Nos3 signaling

Katalin Todorov-Völgyi[1]*, Judit González-Gallego[1,2]*, Stephan A Müller[3], Burcu Fatma Seker[1], Mihail Ivilinov Todorov[1,4], Luise Schröger[1,2], Jiayu Cao[1,2], Ulrike Schillinger[1], Simon Frerich[1,2], Martina Fetting[3,5], Mikael Simons[3,5], Ali Ertürk[1,4,6], Arthur Liesz[1,5], Nikolaus Plesnila[1,5], Stefan Lichtenthaler[3,5], Dominik Paquet[1,2,5], Martin Dichgans[1,2,5,6]

1) Institute for Stroke and Dementia Research (ISD), University Hospital, LMU Munich, Munich, Germany;

2) Graduate School of Systemic Neuroscience (GSN), University Hospital, LMU Munich, Munich, Germany;

3) German Center for Neurodegenerative Diseases (DZNE) Munich, Munich, Germany;

4) Institute for Tissue Engineering and Regenerative Medicine (iTERM), Helmholtz Zentrum München, Neuherberg, Germany;

5) Munich Cluster for Systems Neurology (SyNergy), Munich, Germany.

6) German Center for Cardiovascular Diseases (DZHK) Munich, Munich, Germany;

* Contributed equally.

Electronic address:

Martin.Dichgans@med.uni-muenchen.de.

Abstract

Forkhead transcription factor f2 (Foxf2) has emerged as a key transcription factor in brain endothelial cells (BECs). FOXF2 further emerged as a major risk locus for stroke and chronic white matter lesions in humans. Global inactivation of Foxf2 in mice results in BBB leakage, endothelial thickening, and increased trans-endothelial vesicular transport but the underlying mechanisms remain largely undefined.

To explore the role of Foxf2 in maintaining BEC function we generated mice with EC-specific conditional inactivation of Foxf2 deficiency (eKO) we applied our recently developed BEC enrichment protocol compatible with mass spectrometry. Applying high-throughput proteomics to BECs and isolated brain microvessels from adult eKO mice we found prominent downregulation of proteins involved in Tie2-eNOS signaling, while expression of Foxo1, a negative regulator of eNOS was upregulated. eKO mice developed BBB leakage and parenchymal lesions and exhibited a compromise in functional hyperemia. They further showed larger infarct sizes upon experimental ischemia by middle cerebral artery occlusion (MCAO). Treatment with Razuprotafib (AKB9778), a small molecule activator of Tie2 receptor, restored the levels of multiple proteins implicated in Tie2 signaling, normalized the deficit in functional hyperemia and glial endfeet swelling, and limited infarct sizes upon MCAO.

To explore the transferability of these findings to human cells, we studied endothelial cells derived from CRISPR/Cas9 edited human induced pluripotent cells. Similar to the results in mice we found downregulation of TIE2-signaling at protein, RNA, and NO-production level which were restored by Razuprotafib.

Collectively, these findings identify Foxf2 as a key transcription factor required for the maintenance of BEC function Tie2 signaling and NO metabolism.

Introduction

Brain endothelial cells (BECs) have unique roles in controlling blood-brain barrier integrity (Abbott et al., 2006; Obermeier et al., 2013), maintaining brain homeostasis, and regulating cerebral blood flow and vascular growth (Terstappen et al., 2021). Endothelial cell (EC) specific functions are secured through dedicated signaling pathways such as Ang-Tie2 (Huang et al., 2010; Saharinen et al., 2017), Vegf-Vegfr2 (Gavard and Gutkind, 2006; Simons et al., 2016), and Notch (Andersson and Lendahl, 2014; Bray, 2016), which control vascular permeability, stability, and remodeling (Adams and Alitalo, 2007; London et al., 2009). Ang-Tie2 signaling further regulates vascular reactivity via nitric oxide (NO) mediated vasodilation (Alfieri et al., 2014; Xu et al., 2012).

Recent work has highlighted an outstanding role of the transcription factor Forkhead box protein f2 (Foxf2) in BECs: Both Foxf2 and Foxq1, another transcription factor in endothelial cells have been found to be highly enriched in brain endothelial cells (BECs) compared to endothelial cells from other organs during embryonic development (Hupe et al., 2017) and adulthood (Kalucka et al., 2020; Vanlandewijck et al., 2018). Foxf2 was further identified as a direct activator of Foxq1 transcription via binding to the enhancer region of Foxq1 thus potentially placing Foxf2 upstream of Foxq1 in the regulation of gene transcription (Ryu et al., 2022). Foxo1, another key transcription factor in endothelial cells, is highly expressed in mature ECs and has been shown to regulate endothelial cell migration and postnatal neovascularization via angiopoietin-2 (Ang2) activation and nitric oxide synthase 3 (Nos3 or eNos) repression (Potente et al., 2005). Like Foxq1, Foxo1 has been identified as a target gene of Foxf2 in a combined analysis of RNA-Seq and Chip-Seq data (Xu et al., 2020) thus underscoring the potential role of Foxf2 in orchestrating BEC specific functions. However, the precise role of Foxf2 in BECs and in maintaining brain health remains unexplored.

Interest into Foxf2 further comes from large-scale genetic studies that identified FOXF2 as a major risk locus for stroke and chronic white matter lesions in humans (Malik et al., 2018; Mishra et al., 2022; Neurology Working Group of the Cohorts for et al., 2016; Ryu et al., 2022; Traylor et al., 2020). Global inactivation of Foxf2 in mice results in defects of the BBB, endothelial thickening, and increased trans-endothelial transport (Reyahi et al., 2015). This phenotype has been attributed to Foxf2 being required for pericyte differentiation (Reyahi et al., 2015) but may also be due to a primary function of Foxf2 in brain endothelium given its role as a core transcription factor in BECs. Specifically, Foxf2 expression has been shown to induce the expression of BBB differentiation markers (Hupe et al., 2017) and increase the barrier resistance of endothelial cells (Roudnicky et al., 2020) in human umbilical vein ECs (HUVECs), and human induced pluripotent stem cell (iPSC)-derived endothelial cells, respectively. Nevertheless, targeted studies on the role of Foxf2 in BECs *in vivo* are lacking. Also, little is

known about the molecular and cellular pathways controlled by Foxf2 in ECs and the corresponding target genes beyond Foxq1 and Foxo1.

Here, we set out to investigate the role of Foxf2 in maintaining BEC function *in vivo* including its role in functional hyperemia. Considering the involvement of FOXF2 in human stroke we explored its involvement in the regulation of infarct size in experimental stroke. Applying high-throughput proteomics to isolated BECs and brain microvessels from adult EC-specific Foxf2-KO mice (eKO) we found marked downregulation of BEC proteins involved in Tie2 – endothelial nitric oxide synthase (eNos or Nos3) signaling, which was restored by activation of the Tie2 receptor with Razuprotafib (AKB9778), a small molecular inhibitor of vascular endothelial protein tyrosine phosphatase (Ptprb or VE-PTP). We further found a reduction in functional hyperemia in eKO mice which was also restored by Razuprotafib treatment. Deletion of FOXF2 in human iPSC-derived ECs reversibly attenuated TIE2-NOS3 signaling and NO production. Furthermore, EC-specific Foxf2-deficiency in adult mice resulted in increased infarct size in experimental ischemic stroke, which could be restored by Razuprotafib treatment. Collectively, these results demonstrate that Foxf2 maintains BEC function by regulating Tie2-Nos3 signaling, providing a perspective for therapeutic interventions in stroke and SVD.

Results

Endothelial Foxf2 deficiency causes BBB leakage and attenuates Tie2-signaling

Given the causal role of Foxf2 in stroke and the involvement of vascular, glial, and neuronal cells in regulating blood flow we first sought to obtain an overview of Foxf2 expression in different cell types in the adult mouse brain. Compiling the available scRNAseq data from mouse (Saunders et al., 2018; Tabula Muris et al., 2018; Vanlandewijck et al., 2018; Zeisel et al., 2018) and human brain (Winkler et al., 2022; Yang et al., 2022) we found that Foxf2 is predominantly expressed in BECs and pericytes but mostly absent in neurons, glia, and ependymal cells (**Fig 1A**). To investigate the function of Foxf2 in BECs and its role in maintaining vascular integrity, we generated mice with inducible deletion of Foxf2 specifically in endothelial cells (Cdh5-CreERT2;Foxf2fl/fl or 'eKO') (**Fig 1B**). Tamoxifen-induced inactivation of Foxf2 in ECs at 3 months followed by assessment at 6 months resulted in histological changes similar to those previously reported for mice with inducible global inactivation of Foxf2 (Reyahi et al., 2015). Specifically, correlative electron microscopy conducted on brain regions with focal albumin extravasation further revealed extravasation of erythrocytes, i.e. microhemorrhage, next to glial edema and neuronal lysis in eKO mice (**Fig 1C**, top). Using different size of fluorescent tracer injection (1-65kDa) and confocal microscopy screening to analyze BBB integrity we found significant leakage of different size of fluorescent tracers (between 1-40 kDa) (**Fig 1C**, bottom).

To identify the molecular and cellular pathways mediating the effects of Foxf2 in BECs, we applied our previously published BEC enrichment protocol combined with LC-MS/MS-based proteomics (Todorov-Völgyi & González-Gallego et al, *in revision*) to 6-months-old eKO and WT animals (**Fig. 1B**). Proteomic analysis of isolated BECs from 6-months-old animals captured a total 4929 proteins. Out of these, 225 and 391 proteins showed significant up-, and downregulation, respectively (t-test, p-value < 0.05, ≥ 3 samples per group) in eKO vs WT mice (**Fig. 1D-E, Suppl. Table 1**). Enrichment analysis of the significantly downregulated proteins revealed cell junction and endoplasmic reticulum among the most affected subcellular localizations (SL), while nitric oxide biosynthesis and endothelial cell development among the most affected biological processes (BP) in eKO mice (compared to age-matched WT). In case of significantly upregulated proteins mitochondria and cytoskeleton, as well as oxidative stress response and aging presented among the most enriched SL and BP categories, respectively (**Fig 1F-H,** p-value based on FDR of DAVID enrichment analysis). Intensity Based Absolute Quantification (iBAQ) and fold-change ranking of significantly altered proteins marked Tie2 as a low abundance and Nos3 as high abundance downregulated proteins (**Fig. 2H**). We further found several proteins involved in Tie2-regulated processes to be downregulated in eKO BECs (**Fig. 2I, Suppl. Fig. 1A**).

Razuprotafib rescues functional hyperemia and limits infarct size in mice with endothelial Foxf2 deficiency

To further explore the role of Tie2 signaling in mediating the effects of Foxf2 deficiency in endothelium, we treated eKO and WT mice with Razuprotafib (Raz) a selective small molecule inhibitor of vascular endothelial protein tyrosine phosphatase (Ptprb) shown to have a vascular stabilizing activity through Tie2 activation (Shen et al., 2014) (**Fig. 2A**). We initially focused on isolated brain vessels from Raz- and vehicle-treated eKO mice (eKO-Raz and eKO-Veh, respectively) and applied mass-spectrometry for proteomics analysis (**Fig. 2B**). Treatment with Raz for 48h restored the levels of multiple proteins involved in Tie2-Nos3 signaling (**Fig. 2B and C**). Specifically, Tie2, Nos3, and Nostrin (Nos-trafficking protein) were upregulated, while Nos-interacting protein (Nosip), a negative regulator of NO production was downregulated. Restoration of Nos3 was further confirmed by immunolabeling of isolated brain microvessels (**Fig. 3D**). Among the significantly dysregulated proteins in eKO-Veh mice, we found 27 proteins to be restored by Raz treatment (p-value < 0.05) (**Fig. 2C**). Given the effects on Nos3 expression, we next explored the physiological effect of Raz on functional hyperemia using laser spackle (LS) imaging and two-photon (2P) microscopy (**Fig. 2A and E**). Quantification of CBF in Barrel cortex in combination with whisker stimulation revealed an attenuation of functional hyperemia in eKO mice. This deficit was restored by Raz treatment as shown by the quantification of CBF in Razu treated compared with vehicle treated eKO mice (**Fig. 2E,** up). Using 2P microscopy we found compromised vessel dilation of capillaries and penetrating arterioles following whisker stimulation which was likewise restored by treatment with the Tie2-activator (**Fig. 2E**, down). In line with these data, Razuprotafib also rescued glial endfeet edema induced by endothelial Foxf2 deficiency (**Suppl. Fig2**).

To investigate the consequences of EC-specific loss of Foxf2 and Raz treatment on the susceptibility to cerebral ischemia we next subjected eKO-Veh, eKO-Raz and WT-Veh treated mice to experimental stroke using endovascular filament-mediated middle cerebral artery occlusion (fMCAo) for 60 min followed by reperfusion and assessment at 24 hours post occlusion (**Fig. 2F**). Quantification of infarct size and albumin leakage on consecutive coronal MRI and confocal images, respectively, revealed that eKO-Veh mice develop larger infarcts with more extensive BBB breakdown (t-test, $p < 0.05$) compared with WT-Veh. Moreover, the level of infarct size and BBB leakage were both attenuated upon Raz treatment compared with eKO-Veh (t-test, $p < 0.05$) (**Fig. 2F**). To check for a potential involvement of endothelial Foxf2 in vascular remodeling we next imaged the whole brain vasculature in 6-months-old mice using light-sheet microscopy and quantified key vascular metrics of the pial vasculature (**Suppl. Fig3**). Using unsupervised VesSAP-based (Todorov et al., 2020) quantification we found is that the metrics (vessel length, diameter, and number of bifurcations) of pial vasculature did

not differ between genotypes, suggesting that the larger infarct size in Foxf2 deficient mice is not explained by differences in MCA collaterization.

Collectively, these findings demonstrate a role of Foxf2 in functional hyperemia, in determining infarct size and BBB breakdown in adult mice, which were mediated by Tie2-Nos3 signaling pathway.

Razuprotafib rescues TIE2-signaling and NO production in human endothelial cells

To explore the transferability of results from mouse BECs and in mice to human endothelial cells, we next moved to human induced brain endothelial cells (iECs) derived from human pluripotent stem cells (iPSC). We used our previously generated CRISPR/Cas9 FOXF2-KO iPSC line and differentiated into iBECs (González-Gallego & Todorov-Völgyi et al, *in preparation*). We then treated differentiated FOXF2 KO and WT iBECs with Raz or Veh correspondingly to investigate the role of human FOXF2 in TIE2 signaling in human cells (**Fig. 3A**). Mass-spectrometry analysis of WT-Veh and FOXF2 KO-Veh iBECs revealed downregulation of multiple members of the TIE2-NOS3 signaling pathway similar to proteomic changes in mouse BECs (**Fig. 3B-C**). Comparison of the proteomes of Razu-treated FOXF2 KO iBECs and Veh-treated FOXF2 KO iBECs further showed that Razu treatment restored the levels of 28 Tie2-signaling related proteins (p-value < 0.05) (**Fig. 3C and Suppl. Fig4A)**. Restauration of TIE2 and NOS3 protein expression was confirmed by immunocytochemistry in iBEC cultures further recapitulating the results in mice (**Fig. 3D** and **Suppl. Fig4B**). We next checked the levels of phosphorylated-AKT (pAKT) normalized to the protein levels of AKT. Western blot analysis revealed a significant downregulation of pAKT in KO-Veh iBECs compared to WT-Veh iBECs consistent with the attenuation of TIE2-NOS3 signaling upon FOXF2 deletion. Moreover, pAKT levels were restored by RAZU treatment (**Fig. 3E**). Consistent with these data, immunocytochemical analysis of pTIE2 and pFOXO1 showed significant downregulation in KO-Veh compared to WT-Veh iBECs, which was also rescued by RAZU treatment (n=4 samples / group, t-test, p-value < 0.05) (**Fig. 3F-G**)

Finally, to investigate the functional effects of FOXF2 deficiency on NO metabolism and the possibility of pharmacological restoration of NO levels in iBECs, we quantified NO production in these cells. Consistent with the proteomics results, NO production was decreased in Veh-treated FOXF KO cells compared with Veh-treated WT cells and upregulated in Raz- compared with Veh-treated FOXF2 KO cells (**Fig. 3H**), suggesting an activating effect of Raz on NO metabolism.

Endothelial Foxf2 regulates Tie2-mediated Nos3 signaling via Foxo1 inhibition

To explore the regulatory effects by which Foxf2 regulates Tie2-Nos3 signaling, we next analyzed mRNA expression levels in the whole brain tissue of Foxf2 deficient and WT mice and human iBECs. While Tie2 and Nos3 are predominantly expressed in endothelial cells based on available scRNAseq data (**Suppl. Fig. 5A-B**), Foxo1 is expressed in multiple cell types beside endothelial cells in the brain (**Suppl. Fig. 5C**). qPCR analysis of Fox family members in whole brain tissue revealed a significant downregulation of Foxq1 and Foxc1 in eKO compared with WT mice, whereas Foxo1 showed an opposite directionality (**Fig. 4A**). Focusing on the Tie2-Nos3 signaling pathway we found that the mRNA expression levels of Tie2, Nos3, Gucy1b1, and Ang1 were decreased in eKO mice, suggesting a regulatory effect of Foxf2 on these genes.

Considering the decline of BEC function during aging (Ungvari et al., 2018) we further quantified the transcriptional levels of Foxf2, Tie2, Nos3, and Foxo1 in brains from 3, 6, 12, and 18 months old mice. The mRNA expression levels of Fox2, Tie2 and Nos3 all declined whereas those of Foxo1 increased with aging (**Fig. 4B**). Moreover, there was a strong correlation between the mRNA expression levels of Foxf2 and Foxo1 ($r=0.806$; $p=0.0002$) as well as Nos3 ($r=0.807$; $p=0.0002$) further supporting a regulatory effect of Foxf2 on these genes (**Fig. 4C**). Indeed, the transcriptional changes in eKO mice resembled those of an accelerated aging phenotype (**Fig. 4B**).

Next, we investigated the effects of Raz treatment on the transcription of Foxf2, Tie2 and Nos3 in eKO mice and iBECs. The relative mRNA abundance of Tie2, and Nos3 was lower in both mouse and human upon Foxf2 deficiency, which was restored upon Raz treatment. However, Raz treatment had no effect on the expression level of mouse or human Foxf2 (**Fig. 4D** and **E**). Using Foxf2 overexpression via lipid nanoparticle delivery we found the mRNA levels of TIE2 and NOS3 to be restored in FOXF2 deficient human ECs (**Fig. 4F**).

To summarize our data, we found that endothelial Foxf2 deficiency i) reduces the levels of multiple protein, phosphorylation, and mRNA of Tie2-mediated Nos3 signaling pathway, ii) compromises functional hyperaemia and NO production, that can be restored upon Raz treatment (**Fig. 4G**).

Discussion

Applying proteomics and pharmacological interventions to BECs from mice with EC-specific Foxf2 deficiency and genome-edited FOXF2 deficient human iPSC-derived ECs we found that i) endothelial Foxf2 deficiency causes BBB leakage and attenuates Tie2-signaling; ii) Razuprotafib rescues functional hyperemia, limits infarct size in mice with endothelial Foxf2 deficiency and further rescues TIE2-signaling and NO production in human ECs iii) endothelial Foxf2 regulates Tie2-mediated Nos3 signaling via Foxo1 inhibition. Collectively, these findings provide fundamental insights into BEC function and stroke mechanisms while also offering a perspective for therapeutic interventions.

Morphological characterization of the BBB integrity upon endothelial Foxf2 deficiency revealed similar histological changes to those previously reported in Foxf2 deficient mice at embryonic and adult phase (Reyahi et al., 2015) in particular microhemorrhages and glial edema. We further found extravasation of fluorescent tracers with different size (between 1 and 40 kDa).

Using our recently developed BEC enrichment protocol (Todorov-Völgyi & González-Gallego et al, *in revision*), we provided a proteome level characterization of mouse BECs. Enrichment analysis of significantly dysregulated proteins revealed NO metabolism among the most affected biological processes. Moreover, we found several members of Tie2-Nos3 signaling to be significantly downregulated such as Tie2, Nos3, Gucy1b1 (subunit of sGC), or Itgb1 (subunit of α1β1-Integrin receptor). The Ang-Tie2 signaling is essential for embryonic cardiovascular and lymphatic development, and further regulates vascular homeostasis, vessel permeability, inflammation and angiogenic responses during adulthood (David et al., 2013; Huang et al., 2010; Saharinen et al., 2017). In addition, Tie2 forms a stable interaction with α1β1-Integrin regulating endothelial cell response to Ang1 (Cascone et al., 2005). Signaling via the Tie2-Pi3k-Akt1 pathway contributes to Nos3 phosphorylation and NO production (Michell et al., 1999), which is implicated in vessel dilation and CBF regulation through a cGMP-mediated signal transduction pathway (Zhao et al., 2015). cGMP biosynthesis is catalyzed by sGC upon NO binding (Denninger and Marletta, 1999). Complementing our proteomics data on attenuated Tie2-Nos3 signaling, we further found that phosphorylation of AKT and FOXO1 is downregulated in human BECs upon FOXF2 deficiency, suggesting an inactivation of Tie2-Nos3 signaling. Overall, we described a remarkable alignment of Foxf2 deficient mouse and human models in the regulatory mechanisms of Tie2 signaling.

As a functional readout, we investigated cerebral blood flow *in vivo* and found attenuated functional hyperaemia in endothelial Foxf2 deficient mice. Interestingly, attenuated TIE2-NOS3 signaling and NO production were also found in human iBECs upon FOXF2 deficiency, validating the transferability of our results.

CBF is regulated by a variety of factors beyond NO production, such as arachidonic acid metabolism (Wang et al., 2021). Chemical or physical stimulation of vascular endothelium activates phospholipases and releases arachidonic acid, which is further metabolized by cyclooxygenases (Dubois et al., 1998), cytochrome P450s (Capdevila et al., 1982), and lipoxygenases (Zheng et al., 2020) to vasoactive products. Beside Tie2, the most prominently downregulated protein in eKO BECs was Alox12 lipoxygenase. We further found Ptgis (Cyp8), Cyp2d22, and Cyp20a1 members of the cytochrome p450 family to be significantly downregulated, reflecting their possible contribution to the functional hyperemia deficit induced by endothelial Foxf2 deficiency (**Suppl. Fig. 1B**).

Analysis of the mRNA expression levels of Fox family members in whole brain tissue revealed a significant downregulation of Foxq1 and Foxc1 and upregulation of Foxo1. Indeed, Foxf2 dependent regulation of Foxfq1 is further supported by Ryu and colleagues, who identified Foxf2 as a direct activator of Foxq1 transcription via binding to the enhancer region of Foxq1 (Ryu et al., 2022). Also, Foxo1 was reported as a target gene of Foxf2 in palate development (Xu et al., 2020). We also found the mRNA level of Tie2, Nos3, Gucy1b1, and Ang1 to be downregulated in eKO mouse and KO human iBECs. Expression of Nos3 is directly inhibited by Foxo1 via binding to the Nos3 promoter region (Potente et al., 2005). Hence, the transcriptional effects of Foxf2 on Nos3 might be mediated by the effects on Foxo1 expression. Interestingly, we found similar changes in the brain expression of Foxf2, Foxo1, and Nos3 during physiological aging as upon endothelial Foxf2 deficiency, suggesting an accelerating aging phenotype in the regulation of BEC transcription factors in the eKO mice. Moreover, we also found a strong correlation between the mRNA expression of Foxo1 and Foxf2, as well as Nos3 and Foxf2, further supporting the regulatory effect of Foxf2 on these genes.

The choice of Razuprotafib for pharmacological rescue was motivated by our BEC proteomic results, which identified Tie2 as one of the most prominently downregulated protein. Based on our BEC proteomics data the level of multiple proteins involved in Tie2-Nos3 signaling were restored in mouse and human Foxf2 deficient BECs upon Raz treatment. Notably, Nosip, a key inhibitor of Nos3 (Dedio et al., 2001) and ANG2, a potential inhibitory ligand of TIE2 receptor (Hansen et al., 2010), were the most prominently downregulated proteins upon Raz treatment in mouse and human, respectively, suggesting a disinhibition of Tie2 signaling via Nosip and ANG2 inhibition.

In addition to restoring the proteomic signature, treatment with the Tie2 activator further restored the deficit in functional hyperaemia upon endothelial Foxf2 deficiency. Interestingly, NO production was likewise restored in FOXF2-KO human iBECs.

Looking at the consequences of endothelial Foxf2 deficiency on the susceptibility of cerebral ischemia we found that eKO mice develop larger infarcts with more extensive BBB leakage,

both of which attenuated upon Raz treatment. In line with our data, Raz likewise rescued increased vessel permeability and infarct sizes in Ang2 GOF mice upon experimental stroke (Gurnik et al., 2016). Moreover, Ang2 GOF mice presented similar molecular changes as we found here in the BEC proteome of endothelial Foxf2 deficient mice, such as downregulated abundance of Cdh5 and Cldn5 cell junction proteins, while Cav1, an essential protein for caveolae formation was upregulated (Gurnik et al., 2016). Aside from the interaction with Tie2, Ptprb further associates with Cdh5 supporting its adhesive activity and endothelial junction integrity (Nawroth et al., 2002). However, Raz mediated inhibition of Ptprb stabilizes endothelial junctions in a Cdh5 independent way (Frye et al., 2015). In accordance with these data, the level of attenuated Cldn5 cell junction protein as well as the stroke related extensive albumin leakage were both significantly rescued by Raz treatment in eKO mice, while Cdh5 remained unchanged.

To further explore the possible anatomical factors that might contribute to the enlarged infarct phenotype in eKO mice, we analyzed the morphology of whole brain vasculature with light-sheet microscopy using our previously published VesSAP-based quantification and found no difference in the metrics of pial vasculature originated from MCA (Todorov et al., 2020), but we found significant reduction of parenchymal microvessel density in several anatomic regions, suggesting a role of endothelial Foxf2 in microvessel remodeling during adulthood (González-Gallego & Todorov-Völgyi, *in preparation*). Further supporting these data, endothelial cell development was identified among the top enriched biological process of the significantly downregulated BEC proteome of eKO mice. Moreover, key regulators of angiogenesis such as Tie2, Itgb1 or Cdh5 were likewise downregulated upon endothelial Foxf2 deficiency.

In summary, Foxf2 represents a major risk gene for stroke and SVD. Endothelial Foxf2 deficiency causes BBB leakage and attenuates Tie2-Nos3 signaling via Foxo1 inhibition. Razuprotafib, a small molecule inhibitor of Ptpbr, rescues functional hyperemia, limits infarct size in mice with endothelial Foxf2 deficiency, and further restores TIE2 signaling and NO production in FOXF2 deficient human ECs. Collectively, these findings identify Foxf2 as a key transcription factor required for the maintenance of BEC function via Tie2-mediated Nos3 signaling pathway.

Methods

Animals

Brain specimens were obtained from Foxf2fl/fl;Cdh5-Cre (eKO) and Foxf2fl/fl (WT) mice at 6 month of age. Tissues were harvested in parallel and during the same daytime. Both proteomic and immunohistochemical analyses were done on 6 mixed-gender mice per group (3 males and 3 females for each experiment). Animal experiments were performed in accordance with the German Animal Welfare Law and approved by the Government of Upper Bavaria (Vet_02-18-21).

Tissue harvesting

For BEC isolation, mice were deeply anesthetized using ketamine (100mg/kg, i.p) -xylazine (10mg/kg i.p), and transcardially perfused with ice-cold 20 ml 1X Hank's Balanced Salt Solution (HBSS) for brain dissection. Following perfusion, the brain was surgically removed and kept in HBSS at 4ºC for further analysis.

For vessel isolation, anesthetized animals were perfused with 1X HBSS and the dissected brains were immediately frozen on dry ice and stored at -80ºC until further use.

For immunohistochemical analysis, anesthetized animals were transcardially perfused with 1X HBSS and fixed with 4% paraformaldehyde (PFA). The dissected brain samples were incubated O/N in 4% PFA for vibratome sectioning.

BBB permeability assays

For the BBB permeability assays mice were used at 6 months of age. Evans blue (EB) (Sigma-Aldrich, Cat#E2129) was intraperitoneally-, whereas 40kDa TMR-conjugated dextran (Invitrogen, Cat# D1845) was tail vein injected 24 hrs before animal perfusion (3 mice per group). In a second cohort, A555-conjugated 1kDa Cadaverin (Invitrogen, Cat# A30677) and CB-conjugated 10kDa dextran (Invitrogen, Cat#D1976) were tail vein injected together 2 hrs before perfusion. Animals were transcardially perfused with 15ml HBSS and brains were dissected. Right hemispheres were further post-fixed with 4% PFA overnight for confocal analysis.

Brain endothelial cell isolation (BECs)

Brain endothelial cells were isolated from whole brain as described previously (Todorov-Völgyi & González-Gallego, *in revision*). In brief, the full brain was mechanical and enzymatically digested using a modified version of the Adult Brain Dissociation kit (Miltenyi Biotec, Cat# 130-107-677). Myelin was removed using 30% Percoll (GE Healthcare Cat#17-5445-02) and erythrocytes using the Red Blood Cell Removal Solution (Miltenyi Biotec, Cat# 130-094-183). BECs were enriched via magnetic activated cell sorting (MACS) using CD31 beads. Following

CD31 enrichment, the cell suspension was washed twice with PBS to remove residual MACS buffer and subsequently precipitated for further protein extraction.

Brain vessel isolation

Brain vessels were isolated from whole cerebrum as described previously (Monet-Lepretre et al., 2013; Zellner et al., 2018). In brief, tissue was homogenized in 15mL of cold minimum essential medium (ThermoFisher, Cat# 11095080) using a glass tissue grinder (Wheaton). Myelin was removed using a 15% Ficoll gradient. Isolated vessels were pelleted and resuspended in PBS with 1% BSA (BSA Fraction V, Sigma-Aldrich, Cat#10735096001), transferred onto a 40µm cell strainer (Corning, Cat#431750) and extensively washed with cold PBS (with 250ml). Isolated vessels were collected by washing the inverted cell strainer with PBS and centrifugation at 3000g for 5min.

Cell culture

iPSC experiments were performed in accordance with all relevant local guidelines and regulations. Work was done with the female iPSC line A18944 (ThermoFisher, Cat# A18945). iPSCs were cultured and maintained on vitronectin-coated plates in Essential 8 Flex Medium (E8F) (ThermoFisher, Cat# A2858501) at 37ºC with 5% CO2 until reaching 80-85% confluency. iPSCs were passaged using PBS + 500nM EDTA (ThermoFisher, Cat# 15575020) and replated using the same conditions as previously.

CRISPR/Cas9 Genome editing

We used the previously described and characterized genetic modified cell line of iPSCs with FOXF2 deletion (González-Gallego & Todorov-Völgyi, *in preparation*).

iPSC differentiation into brain endothelial cells huECs

iPSCs were differentiated into brain endothelial cells or huECs as previously described and characterized (González-Gallego & Todorov-Völgyi, *in preparation*). In brief, cells were seeded onto Gelatin-coated plates (ThermoFisher Cat# A1413302) at a density of 200k/cm2 and mesoderm was induced for the next 5 days using Mesoderm Induction Media (StemCell, Cat# 05220) for day1 and 2 and APEL2 media (StemCell, Cat# 05270) for day 3 and 4. On day5, endothelial cells were positively selected by Magnetic Activated Cell Sorting (MACS) using CDH magnetic beads (Milteny Biotec, Cat# 130-097-867) following manufacturer's instructions. Endothelial cells were further plated onto Collagen IV-coated plates (Sigma Aldrich, Cat# C5533-5MG) in endothelial cell media (PromoCell, Cat# C-22011) supplemented with 50ng/mL VEGF (Peprotech, Cat# 100-20). Cells were grown until reaching approximately 90% confluence and passaged with Trypsin-EDTA (ThermoFisher, Cat# 25200056) up to 5 passages in a ratio of 1:2-1:6.

NO measurements

NO production measurements were assessed using DAF-2DA compound (Enzo Life Sciences, Cat# ALX-620-056-M001). Cells were seeded onto Collagen IV-coated coverslips and cultured until reach confluency. Cells were treated with 10µM DAF-2DA diluted in the medium for 24h in phenol-free media. After incubation, cells were fixed with 4% PFA and mounted with Fluoromount for further imaging (Sigma-Aldrich, Cat# F4680-25ML).

Foxf2 overexpression via LNPs

FOXF2 was overexpressed in human differentiated endothelial cells via Lipid nanoparticles (LNP) mRNA delivery as previously reported (González-Gallego & Todorov-Völgyi, *in preparation*).

Protein extraction

Isolated mouse BECs and differentiated human ECs (iECs)

Protein was extracted from isolated mouse BECs and human iECs using RIPA buffer containing 150mM NaCl (Roth, Cat# 3957.1), 1M Tris-HCl pH 7.5 (Roth, Cat# 9090.3), 1% NP40 (Sigma Alrich Cat# 74385), 0.5% Deoxycholate (Roth, Cat# 3484.3), and 0.1% SDS (Serva, Cat# 20765.03) and protein inhibitors cocktail (Roche, Cat# 4693159001). Samples were resuspended in 50µL and 100µL respectively, incubated on ice for 30 minutes followed by centrifugation at 18000g for another 30min at 4ºC. Supernatants were collected in protein low binding tubes and kept at -20°C for further analysis.

Isolated vessels

Isolated vessels were lysed in a buffer containing 100mM Tris-Hcl pH 7.6 (Roth, Cat# 9090.3), 4% SDS (Serva, Cat# 20765.03) and 100mM DTT (Sigma, Cat# 3483-12-3) by homogenization with a dounce tissue grinder (Wheaton) followed by heating for 3min at 95ºC. After lysis, samples were sonicated (30s, amplitude 100%, duty cycle 50%) 5 times with intermediate cooling using VialTweeter sonicator (Hielscher). Samples were then centrifugated at 16000g for 15min at 4ºC. Supernatants were collected in protein low binding tubes and kept at -20°C for further analysis.

Mass spectrometry and data analysis

Sample preparation

The whole sample of acutely isolated BECs (~5 µg) and 20 µg of isolated brain vessel or full brain tissue lysates according to a BCA assay were subjected to proteolytical digestion using the single-pot solid-phase enhanced sample preparation (SP3) (Hughes et al., 2019). After 1:2 dilution with water, a benzonase digestion with 12.5 units was performed to remove remaining DNA/RNA. Proteins were reduced by addition of dithiothreitol (Biozol, Germany) in 50 mM

ammonium bicarbonate to a final concentration of 10 mM and incubation for 30 min at 37°C. Cysteine residues were alkylated by addition of iodoacetamide (Sigma Aldrich, US) to a final concentration of 40 mM and incubation for 30 min at room temperature in the dark. Afterwards, the reaction was quenched by adding dithiothreitol.

Proteins were bound to 40 µg of a 1:1 mixture of hydrophilic and hydrophobic magnetic Sera-Mag SpeedBeads (GE Healthcare, US) using a final concentration of 70% (v/v) acetonitrile for 30 min at room temperature. Beads were washed four times with 200 µL 80% (v/v) ethanol. For proteolytic digestion, LysC (Promega, Germany) was added in 20 µL 50 mM ammonium bicarbonate with a protease to protein ratio of 1:80. Samples were incubated on a Thermomixer (Eppendorf, Germany) for 30 min at 1000 rpm and 37°C. Afterwards, trypsin (Promega, Germany) was added in 20 µL 50 mM ammonium bicarbonate with a protease to protein ratio of 1:80 followed by an incubation for 16 h at room temperature. Beads were retained with a magnetic rack and the supernatants were collected. Next, 20 µL 0.1% formic acid were added to the magnetic beads followed by sonication for 30 s in a sonication bath (Hielscher Ultrasonics GmbH, Germany). The supernatants of each sample were combined, filtered with 0.22 µm spin filters (Costar Spin-x, Corning, USA) to remove remaining beads, and dried by vacuum centrifugation. Dried peptides were dissolved in 20 µL 0.1% formic. The peptide concentration after proteolytic digestion was estimated using the Qubit protein assay (Thermo Fisher Scientific, US).

Mass spectrometry

The isolated BEC, isolated vessel, and full tissue samples were analyzed on a nanoLC system (EASY-nLC 1200, Thermo Scientific, US) which was coupled online via a nanospray flex ion source (Proxeon – part of Thermo Scientific, US) equipped with a PRSO-V2 column oven (Sonation, Germany) to a Q-Exactive HF mass spectrometer (Thermo Scientific, US).

A peptide amount of 1 µg per sample was separated on a nanoLC system (EASY-nLC 1200, Thermo Scientific, US) using an in-house packed C18 column (30 cm x 75 µm ID, ReproSil-Pur 120 C18-AQ, 1.9 µm, Dr. Maisch GmbH, Germany) with a binary gradient of water (A) and acetonitrile (B) containing 0.1% formic acid at 50°C column temperature and a flow rate of 250 nl/min (gradient: 0 min, 2% B; 3:30 min, 5% B; 137:30 min, 25% B; 168:30 min, 35% B; 182:30 min, 60% B). Full MS spectra were acquired at a resolution of 120,000. The top 15 peptide ions were chosen for Higher-energy C-trap Dissociation (HCD) with a normalized collision energy of 26%. Fragment ion spectra were acquired at a resolution of 15,000. A dynamic exclusion of 120 s was used for peptide fragmentation.

The comparison of acutely isolated endothelial cells and brain homogenates as well as iPSC derived human endothelial cells were analyzed on a nanoElute nanoHPLC which was coupled to a TimsTOF pro mass spectrometer with a CaptiveSpray ion source (Bruker, Germany).

An amount of 350 ng of peptides were separated on a on an in-house packed C18 analytical column (15 cm × 75 µm ID, ReproSil-Pur 120 C18-AQ, 1.9 µm, Dr. Maisch GmbH) using a binary gradient of water and acetonitrile (B) containing 0.1% formic acid at flow rate of 250 nL/min (0 min, 2% B; 2 min, 5% B; 70 min, 24% B; 85 min, 35% B; 90 min, 60% B) and a column temperature of 50°C. A standard Data Dependent Acquisition Parallel Accumulation–Serial Fragmentation (DDA-PASEF) method with a cycle time of 1.1 s was used for spectrum acquisition. Briefly, ion accumulation and separation using Trapped Ion Mobility Spectrometry (TIMS) was set to a ramp time of 100 ms. One scan cycle included one TIMS full MS scan and 10 PASEF peptide fragmentation scans. The m/z scan range was set to 100-1700 for both, MS and MS/MS scans. The ion mobility scan range was set to 1/k0 0.75-1.40.

Data Analysis

The raw data was analyzed by the software Maxquant (maxquant.org, Max-Planck Institute Munich) version 1.6.3.4 (Cox et al., 2014; Sinitcyn et al., 2021). The MS data was searched against an one protein per gene canonical fasta databases of Mus musculus (downloads: September 09th 2020, 21997 entries or February the 10th 2021, 21998 entries) from UniProt. Trypsin was defined as protease. Two missed cleavages were allowed for the database search. The option first search was used to recalibrate the peptide masses within a window of 20 ppm. For the main search peptide mass tolerances were set to 4.5 and 10 ppm for the Orbitrap and TOF mass spectrometer, respectively. Peptide fragment mass tolerances were set to 20 and 40 ppm for the Orbitrap and TOF mass spectrometer, respectively. Carbamidomethylation of cysteine was defined as static modification. Acetylation of the protein N-term as well as oxidation of methionine were set as variable modifications. The false discovery rate for both peptides and proteins were adjusted to less than 1%. Label free quantification (LFQ) of proteins required at least two ratio counts of unique peptides. The option “match between runs” was enabled with a matching time of 1 min and an ion mobility window of 0.05 1/k0.

The protein LFQ intensities were log2 transformed and two-sided Student’s t-test was applied between the groups for statistical evaluation of differential protein abundance. If more than two groups were compared with each other, a one-way Anova test was additionally applied. To account for multiple hypotheses, a permutation-based FDR correction was applied separately for each comparison (Tusher et al., 2001). Only proteins with at least three valid values per group were considered for relative quantification.

Enrichment analysis

Enrichment analysis of biological processes (GOTERM_BP_DIRECT) of down- and upregulated proteins was performed using DAVID software (Huang da et al., 2009; Sherman et al., 2022) version 6.8 using Mus musculus as background dataset.

Razuprotafib AKB-9785 treatment

Razuprotafib treatment in vivo

Mice were intraperitoneally injected with 30mg/kg of AKB9785 or vehicle solution every 12h for a total of 4 times as previously reported (Gurnik et al., 2016).

Razuprotafib treatment of human iBECs

Cells were seeded onto Collagen IV-coated culture plates. Upon confluency, cells were treated with 1µM AKB-9785 (RAZ) or PBS (VEH) in endothelial cell medium (PromoCell, Cat# C-22011) for 24h. After 24h, cells were lysed on ice for protein and RNA analysis.

Transient ischemia-reperfusion stroke model

For experimental stroke induction in eKO and WT mice we applied a previously published protocol (Roth et al., 2021). Briefly, animals were anaesthetized with 2% isoflurane delivered in a mixture of 30% O2 and 70% N2O. The temporal bone was exposed by making an incision between the ear and the eye. In supine position, the mice were implanted with a laser Doppler probe that attached to the skull beyond the middle cerebral artery (MCA) territory. By performing a middle incision, the left common carotid artery (LCCA) and external carotid artery (ECA) were exposed and further isolated and ligated. A 2-mm silicon-coated filament (Doccol) was inserted into the internal carotid artery, advanced gently to the MCA until resistance was felt, and occlusion was confirmed by a corresponding decrease in blood flow as shown in the laser Doppler flow signal by > 80%. Following 60 minutes of occlusion, the animals were re-anesthetized, and the filament was removed. Once the mice awake, they were kept in their home cage with *ad libitum* access to water and food. In all mice, a feed-back-controlled heating pad maintained the body temperature of 37 °C during surgery. Exclusion criteria: 1. Insufficient MCA occlusion (a decrease in blood flow to > 20% of the baseline value). 2. Death during the surgery. 3. MRI scanning revealed no brain ischemia.

MRI

Aquisiton of the occlusion-induced infarct was done in a 3T NanoScan PET/MRI magnetic resonanse scanner equipped with a surface coil optimized for the mouse head (Mediso, Hungary), under Isoflurane anasetesia (isoflurane delivered in a mixture of 30% O2 and 70% N2O) and body temperature control set to 38°C. The acquisiton sequence used was T2 fast spin-echo (T2FSE) weighting: (AcqTime: 0:07:38, Slices: 22, NEX: 4, TR: 10911, TE: 66.3, averages: 4).

3D-stack MRI images were processed in Fiji and quantified as the sum of the infarct volume in 8 consecutive coronal slices (in the % of brain volume).

Immunohistochemistry

The dilution of primary and secondary antibodies during all experiments is specified in **Table 1**.

Brain slices

Brain samples were embedded in a 3% agarose block for further vibratome coronal sections of 100µm. Free-floating sections were incubated in 3%BSA/TritonX100 buffer for 1h at RT for permeabilization and blocking. Primary antibodies were diluted in the same blocking buffer and incubated at 4ºC overnight while secondary antibodies were diluted in PBS and incubated at RT for at least 2h. After carefully washing, DNA was stained using DAPI (Invitrogen Cat# D1306, 1:2000) at RT for 5min. Brain slices were mounted using Fluoromount medium (Sigma-Aldrich, Cat# F4680-25ML).

Isolated vessels

Directly after vessel isolation, vessels were transferred onto a microscope slide (ThermoFisher Cat# J1800AMNZ) and dried at RT. Vessels were fixed at -20ºC for 10min using ice-cold 100% acetone. After fixation and washing, vessels were permeabilized and blocked with 3%BSA/PBS buffer. Primary antibodies were diluted in the same blocking buffer and incubated at 4ºC overnight and secondary antibodies were diluted in PBS and incubated at RT for 2h. After washing, nucleus was stained using DAPI for 5min at RT. Isolated vessels when then mounted using Fluoromount medium.

Differentiated human endothelial cells

Human endothelial cells were seeded directly onto Collagen-IV coated coverslips and fixed using 4% PFA for 15min at RT upon confluency. Cells were blocked using 1%BSA/PBS buffer for 1h at RT. Primary antibodies were diluted in the same blocking buffer while secondary antibodies were diluted in PBS. Primary antibodies were incubated overnight at 4ºC and secondaries at RT for at least 1h. After washing, DNA was stained using DAPI and coverslips were mounted using Fluoromount medium.

Confocal microscopy and image analysis

Fluorescent images were using Zeiss Confocal microscope (LSM880 and LSM980) using 25X and 40X objectives and the ZEN black software. Images were processes and analyzed using ImageJ software.

Electron microscopy

Scaning electron microscopy of mouse tissue

For ultrastructural analysis of astrocyte endfeet, mice were perfused in 4% PFA, 2 mM calcium chloride in 1xPBS, pH 7.4 (Science Services). One hemisphere was dedicated to

ultrastructural analysis by immersion fixation in 4% PFA, 2.5% glutaraldehyde, 2 mM calcium chloride in 0.1 M cacodylate buffer for 24h. Coronal vibratome sections were incubated in the same fixative for another 24h and stored in 0.1 M cacodylate buffer at 4°C until the start of the postembedding.

For correlative analysis, mouse brain samples were perfusion fixed 4% PFA, 2 mM calcium chloride in 1xPBS, pH 7.4 (Science Services). Coronal, 100 µm thick vibratome sections were generated and every second section poststained for 24h in EM fixative (4% PFA, 2.5% glutaraldehyde, 2 mM calcium chloride in 0.1 M cacodylate buffer). The remaining sections were albumin stained and screened for BBB leakiness by confocal microscopy. Adjacent sections to the ones selected by fluorescence microscopy were subjected to EM processing.

For both, endfeet and correlative analysis we applied a rOTO en bloc staining protocol including postfixation in 2% osmium tetroxide (EMS), 1.5% potassium ferricyanide (Sigma) in 0.1 M sodium cacodylate (Science Services) buffer (pH 7.4) (Kislinger et al., 2020). Staining was enhanced by reaction with 1% thiocarbohydrazide (Sigma) for 45 min at 40°C. The tissue was washed in water and incubated in 2% aqueous osmium tetroxide, washed and further contrasted by overnight incubation in 1% aqueous uranyl acetate at 4°C and 2h at 50°C. Samples were dehydrated in an ascending ethanol series and infiltration with LX112 (LADD). Blocks were cured and trimmed (TRIM2, Leica).

Analysis

For endfeet analysis, 100 nm thick sections were taken with a 35° ultra-diamond knife (Diatome) on an ultramicrotome (UC7, Leica) and collected onto 1x0.5 cm carbon nanotube tape strips (Science Services) or onto TEM grids as described. The samples on tape were attached to adhesive carbon tape (Science Services) on 4-inch silicon wafers (Siegert Wafer) and grounded by adhesive carbon tape strips (Science Services). EM micrographs were acquired on a Crossbeam Gemini 340 SEM (Zeiss) with a four-quadrant backscatter detector at 8 kV using ATLAS5 Array Tomography (Fibics). Medium lateral resolution images (40-100 nm) allowed the identification of blood vessels that were in turn reimaged at 4 nm resolution. Higher resolution imaging of sections on grids was performed on a JEM 1400plus (JEOL) as described. Image analysis was performed in Fiji (Schindelin et al., 2012).

For correlative analysis, serial sections were taken with a 35° ultra-diamond knife (Diatome) on an ATUMtome (Powertome, RMC) at a nominal cutting thickness of 100 nm and collected onto freshly plasma-treated (custom-built, based on Pelco easiGlow, adopted from M. Terasaki, U. Connecticut, CT), carbon coated Kapton tape (kindly provided by Jeff Lichtman and Richard Schalek). Tape stripes were assembled onto adhesive carbon tape (Science Services) attached to 4-inch silicon wafers (Siegert Wafer) and grounded by adhesive carbon tape strips (Science Services). EM micrographs were acquired on a Crossbeam Gemini 340

SEM (Zeiss) as described. Hierarchical imaging of serial sections was performed by mapping the entire wafer at 2000 nm lateral resolution and acquisition of entire tissue sections at medium resolution (100-200 nm). The region of interest was correlated by anatomical landmarks including bleedings and vascular patterns and serial sections thereof acquired at 8x8x100 nm resolution. Serial section data were aligned by a sequence of automatic and manual processing steps in Fiji TrakEM2 (Kislinger et al., 2023).

Western blot and quantification

Protein amount was quantified using BCA analysis following manufacturer's instructions (ThermoFisher, Cat# 23227). Protein lysates were analyzed by sodium dodecyl sulfate–polyacrylamide gel electrophoresis (SDS-PAGE) and further transferred onto 0.2 µm nitrocellulose membranes using the Mini-Protean and Trans-Blot system. Prior to antibody incubation, membranes were blocked in 4% Milk in T-BST buffer for 1h at RT in a moderate shaking. Primary antibodies were diluted in the same blocking buffer and incubated overnight at 4ºC also shaking for proper distribution. Horseradish peroxidase (HRP)-conjugated secondary antibodies were incubated at RT for 1h. After further membrane washing, protein detection was done by chemiluminescence development using ECL detection agent (Merck Millipore, Cat# WBULS0100) in the Fusion FX7 (Vilber Lourmat) imager. Protein expression levels were quantified using Gel Analyzer from ImageJ.

RNA analysis

RNA extraction and cDNA synthesis

Total RNA from half cerebellum or cell pellet was extracted using Trizol (Qiagen, Cat# 79306) and purified using the RNeasy mini kit (Qiagen, Cat# 74106) as indicated in manufacture's instructions. RNA concentration was determined using a NanoDrop spectrophotometer. RNA was stored at -80ºC until use. cDNA was synthetized from 250ng - 1µg RNA using the Omniscript RT kit (Qiagen, Cat# 205113) following manufacturer's instructions and stored at -20ºC.

Quantitative real time qPCR (RT-qPCR)

SYBR Green Master Mix (Qiagen, Cat# 208056) was used to perform quantitative PCR (qPCR) and detection was done in the Roche thermocycler. Primer sequences are listed in **Table 2**.

Analysis of whole brain pial vasculature

For staining, imaging, and analyzing the whole brain pial vasculature of the optically cleared intact mouse brains of eKO and WT mice we followed the previously published VesSAP protocol (Todorov et al., 2020).

Vessel labeling and tissue preparation

For labeling the whole brain vasculature first we injected 150 µl (2% V/V% in saline) Evans blue dye (Sigma-Aldrich, E2129) intraperitoneally into 6 months old eKO and WT mice (n=4 per group). After 12 hrs of post-injection time, we injected 0.25 mg wheat germ agglutinin conjugated to Alexa Fluor 594 dye (ThermoFisher Scientific, W11262) in 150 µl PBS (pH 7.2) intravenously. Next, the fixed brains were optically cleared using the 3DISCO technique.

Imaging of the cleared whole brain samples with light-sheet microscopy

For imaging the cleared whole brain samples, we used a 4× objective lens (Olympus XLFLUOR 340) equipped with an immersion corrected dipping cap mounted on a LaVision UltraII microscope coupled to a white light laser module (NKT SuperK Extreme EXW-12).

Reconstruction of the datasets from the tiling volumes

For 3D data reconstruction from the tiling volumes, we used the TeraStitcher's automatic global optimization function (v1.10.10). To register our dataset to the reference atlas we used the average template, the annotation file and the latest ontology of the current Allen mouse brain atlas CCFv3 201710.

Light sheet data analysis

We used the vessel segmentation and analysis pipeline (VesSAP) to quantify the whole brain pial vasculature. Next, we ran the segmentation, preprocessing and feature extraction to obtain the total vessel length (sum of vessel centerline voxels), bifurcation density (sum of segmentation skeleton bifurcations), and average radius of vessels (distance of all centerline voxels to the nearest segmentation mask). All measures were then corrected by a constant to account for shrinkage due to fixation and clearing. Group comparison were done using student's t-test with equal variance assumed and followed by a Tukey's post-hoc test.

Functional hyperemia measurements

Laser Speckle Imaging (LSI) of local cerebral blood flow and two-photon microscopy (2-PM) microscopy analysis of vessel diameter changes in eKO and WT mice were performed based on previously published protocol (Seker et al., 2021).

Chronic Cranial Window Implantation

A chronic cranial window was implanted over the left somatosensory cortex. Mice received buprenorphine (0.1 mg/kg) 30 min before surgery for analgesia. Anesthesia was induced with 5% isoflurane and maintained with 2% isoflurane in 70% room air and 30% O2 during surgery. To maintain body temperature at 37°C a feedback-controlled heating pad was used. Animals were fixed in a stereotactic frame and the scalp was incised along the midline. As a local anesthetics lidocaine (2%) was applied topically onto the skull and a round craniotomy with a

diameter of 4 mm was performed above the somatosensory cortex and covered with a glass window. A plastic ring was glued on top of the cranial window (diameter: 1 cm; weight: 0.1 g). After surgery, mice were placed in a pre-heated box (32°C) until all vital functions recovered. All mice received buprenorphine and enrofloxacin (10 mg/kg s.c.) once daily for three days after surgery.

Whisker Stimulation

Three weeks after surgery, mice received medetomidine (0.05 mg/kg, sc) for light sedation. After 10 min animals were anesthetized with 2% isoflurane and placed in a stereotactic frame. Isoflurane was gradually reduced to 0.5–0.75% (in 70/30% Air/O2) and whisker stimulation was performed over one minute by manually with a brush at a frequency of 1–2 Hz. For 2-PM a custom-made motorized brush holder was used the same stimulation protocol as for the manual stimulation. The procedure was repeated three times with two min intervals.

Measurement and analysis of local cerebral blood flow by Laser Speckle Imaging

A laser speckle contrast imager (LSCI, Perimed, Järfälla, Sweden) was positioned 10.4 cm above the chronic cranial window and a 0.5 x 0.5 mm cortical field was imaged at 4.4 Hz. The data was recorded using the software supplied with the device (Pimsoft, Perimed, Järfälla, Sweden) and analyzed using a previously published Matlab script (MATLAB, R2016b, The MathWorks, Natick, MA) (Seker et al., 2021). Perfusion signal was averaged within 10 and 30 s after the automatically detected stimulation onset and normalized to the baseline perfusion signal, which was defined individually for each stimulation period as the average signal within 40 to 10 s before the automatically detected stimulation onset. The resulting normalized response of the perfusion signal to the stimulation was then averaged across stimulation periods. First individually for each animal and then across animals within each experimental group. To allow averaging across animals, the images, cropped around the spherical ROI, were resized to an image matrix of 120 x 120 pixels. For a better understanding of the individual responses, heat maps were also acquired for individual animals.

Measurement and analysis of vessel diameter by in vivo two-photon microscopy

Two-photon microscopy (2-PM) was performed after the LSCI imaging using the same anesthesia protocol as described above. For visualizing the cerebral vasculature 0.1 ml of fluorescein isothiocyanate (2,000 kDa) was injected through the tail vein. Then mice were transferred under the 2-PM. Pial and parenchymal vessels of the barrel cortex were visualized as time series videos (2 s per frame) at a depth of 50–100 µm with a 10x Zeiss EC Plan—NeoFluar objective using a Li: Ti laser tuned to 800 nm. A custom-made automated brush holder was used for whisker stimulation while imaging with 2-PM (Seker et al., 2021).

scRNA-seq data analysis of human and mouse brain cell datasets

Read processing was performed using 10X Genomics Cell Ranger (v6.0.0). After barcode assignment and UMI quantification, reads were aligned to the mouse reference genome mm10 (GENCODE vM23/Ensembl 98; 2020A from 10xGenomics). Further processing was performed using Scanpy (v1.9.1) (Wolf et al., 2018). Cells were excluded if they had ≤200 or ≥7000 unique genes, or ≥20 % mitochondrial gene counts. The count matrix was normalized (sc.pp.normalize_total) and log(x+1)-transformed (sc.pp.log1p), before proceeding with dimensionality reduction and clustering (sc.tl.pca, sc.pp.neighbors with n_pcs=50, sc.tl.umap, sc.tl.leiden with resolution=1.1). Cell types were annotated using known marker genes for endothelial cells (Cldn5, Pecam1), pericytes (Vtn, Pdgfrb), smooth muscle cells (SMCs; Acta2, Myocd), fibroblasts (Dcn, Col6a1, Col3a1), oligodendrocytes (Mbp, Enpp2), oligodendrocyte precursor cells (OPCs; Cspg4, Pdgfra), neurons (Rbfox3, Tubb3), astrocytes (Aqp4, Aldoc), microglia (Aif1, Tmem119), monocytes/macrophages (Cd14, Itgb2, Cd86, Adgre1, Ccr2), other immune cells (Cd19, Cd3e, Il2rb, Lat, Ifng, S100a9), ependymal cells (Pifo, Foxj1, Dynlrb2, Meig1). Cluster identities were manually verified using differential expression analysis based on Wilcoxon rank-sum tests (sc.tl.rank_genes_groups with method='wilcoxon'). The expression of marker genes and the full analysis pipeline is available at https://github.com/simonmfr/foxf2-per-celltype/blob/main/sc_pp_ISD_2022.ipynb.

We compared our scRNA-seq data to 8 independent single-cell/single-nucleus RNA-seq data sets from the mouse and human brain (Garcia et al., 2022; Saunders et al., 2018; Tabula Muris et al., 2018; Vanlandewijck et al., 2018; Winkler et al., 2022; Yang et al., 2022; Zeisel et al., 2018). Each dataset was processed separately in Scanpy (Wolf et al., 2018) by first normalizing (sc.pp.normalize_total) and log-scaling (sc.pp.log1p) raw count matrices. Available cell annotations were verified using known marker genes (as described above) and then harmonized into major cell types (astrocytes, microglia/macrophages, oligodendrocytes, oligodendrocyte precursor cells (OPCs), endothelial cells, pericytes, smooth muscle cells (SMCs), fibroblasts, neurons, neuroblasts/neural stem cells (NSCs), ependymal cells). Cell type clusters with < 50 cells were excluded from the analysis. Then, we extracted mean scaled expression levels and the fraction of cells expressing Foxf2 per cell type (sc.pl.dotplot). The expression of Foxo1, Nos3, and Tie2/Tek was examined accordingly. Overall, the analysis included 4,347,895 cells, out of which 86,588 cells were annotated as endothelial cells. Details of the analysis and the full code is available at https://github.com/simonmfr/foxf2-per-celltype.

Acknowledgements

We thank Peter Carlsson and Azadeh Reyahi for the Foxf2$^{fl/fl}$ mouse line, and Barbara Lindner, Melanie Schneider, Lea Peischer, and Alessia Nottebrock for the technical assistance. This study received funding from the European Union's Horizon 2020 research and innovation

programme No 666881, SVDs@target; the Deutsche Forschungsgemeinschaft (DFG) within the framework of the Munich Cluster for Systems Neurology (SyNergy; EXC 2145 SyNergy – ID 390857198) and individual project grants (DI 722/13-1; BE 6169/1-1), the Vascular Dementia Research Foundation, through the Federal Ministry for Education and Research (BMBF, CLINSPECT-M) and the LMUexcellent fund.

Author contributions

K.T.V., J.G.G. and M.D. designed the project; S.A.M. performed mass spectrometry; B.F.S. performed functional hyperemia measurements; J.G.G. performed cell culture experiments; K.T.V. and J.G.G. analyzed proteomics data; K.T.V., J.G.G., and L.S. performed biochemical experiments and confocal microscopy; M.I.T., K.T.V. and U.S. performed MRI; M.I.T. performed and analyzed light-sheet microscopy data; J.C. performed MCAo surgery, U.S. and K.T.V. performed BBB permeability assays, S.F. analyzed single cell RNA-seq data; M.F. and K.T.V. performed and analyzed electron microscopy; M.D., D.P., S.L., N.P., A.L., A.E., and M.S. supervised the experiments, K.T.V. and M.D. wrote the manuscript; all authors read and revised the manuscript. Graphics were created with Biorender.com

Competing interests

The authors declare no competing interests.

References

Abbott, N.J., Ronnback, L., and Hansson, E. (2006). Astrocyte-endothelial interactions at the blood-brain barrier. Nat Rev Neurosci *7*, 41-53.

Adams, R.H., and Alitalo, K. (2007). Molecular regulation of angiogenesis and lymphangiogenesis. Nat Rev Mol Cell Biol *8*, 464-478.

Alfieri, A., Ong, A.C., Kammerer, R.A., Solanky, T., Bate, S., Tasab, M., Brown, N.J., and Brookes, Z.L. (2014). Angiopoietin-1 regulates microvascular reactivity and protects the microcirculation during acute endothelial dysfunction: role of eNOS and VE-cadherin. Pharmacol Res *80*, 43-51.

Andersson, E.R., and Lendahl, U. (2014). Therapeutic modulation of Notch signalling--are we there yet? Nat Rev Drug Discov *13*, 357-378.

Bray, S.J. (2016). Notch signalling in context. Nat Rev Mol Cell Biol *17*, 722-735.

Capdevila, J., Marnett, L.J., Chacos, N., Prough, R.A., and Estabrook, R.W. (1982). Cytochrome P-450-dependent oxygenation of arachidonic acid to hydroxyicosatetraenoic acids. Proc Natl Acad Sci U S A *79*, 767-770.

Cascone, I., Napione, L., Maniero, F., Serini, G., and Bussolino, F. (2005). Stable interaction between alpha5beta1 integrin and Tie2 tyrosine kinase receptor regulates endothelial cell response to Ang-1. J Cell Biol *170*, 993-1004.

Cox, J., Hein, M.Y., Luber, C.A., Paron, I., Nagaraj, N., and Mann, M. (2014). Accurate proteome-wide label-free quantification by delayed normalization and maximal peptide ratio extraction, termed MaxLFQ. Mol Cell Proteomics *13*, 2513-2526.

David, S., Kumpers, P., van Slyke, P., and Parikh, S.M. (2013). Mending leaky blood vessels: the angiopoietin-Tie2 pathway in sepsis. J Pharmacol Exp Ther *345*, 2-6.

Dedio, J., Konig, P., Wohlfart, P., Schroeder, C., Kummer, W., and Muller-Esterl, W. (2001). NOSIP, a novel modulator of endothelial nitric oxide synthase activity. FASEB J *15*, 79-89.

Denninger, J.W., and Marletta, M.A. (1999). Guanylate cyclase and the .NO/cGMP signaling pathway. Biochim Biophys Acta *1411*, 334-350.

Dubois, R.N., Abramson, S.B., Crofford, L., Gupta, R.A., Simon, L.S., Van De Putte, L.B., and Lipsky, P.E. (1998). Cyclooxygenase in biology and disease. FASEB J *12*, 1063-1073.

Frye, M., Dierkes, M., Kuppers, V., Vockel, M., Tomm, J., Zeuschner, D., Rossaint, J., Zarbock, A., Koh, G.Y., Peters, K.*, et al.* (2015). Interfering with VE-PTP stabilizes endothelial junctions in vivo via Tie-2 in the absence of VE-cadherin. J Exp Med *212*, 2267-2287.

Garcia, F.J., Sun, N., Lee, H., Godlewski, B., Mathys, H., Galani, K., Zhou, B., Jiang, X., Ng, A.P., Mantero, J.*, et al.* (2022). Single-cell dissection of the human brain vasculature. Nature *603*, 893-899.

Gavard, J., and Gutkind, J.S. (2006). VEGF controls endothelial-cell permeability by promoting the beta-arrestin-dependent endocytosis of VE-cadherin. Nat Cell Biol *8*, 1223-1234.

Gurnik, S., Devraj, K., Macas, J., Yamaji, M., Starke, J., Scholz, A., Sommer, K., Di Tacchio, M., Vutukuri, R., Beck, H.*, et al.* (2016). Angiopoietin-2-induced blood-brain barrier compromise and increased stroke size are rescued by VE-PTP-dependent restoration of Tie2 signaling. Acta Neuropathol *131*, 753-773.

Hansen, T.M., Singh, H., Tahir, T.A., and Brindle, N.P. (2010). Effects of angiopoietins-1 and -2 on the receptor tyrosine kinase Tie2 are differentially regulated at the endothelial cell surface. Cell Signal *22*, 527-532.

Huang da, W., Sherman, B.T., and Lempicki, R.A. (2009). Systematic and integrative analysis of large gene lists using DAVID bioinformatics resources. Nat Protoc *4*, 44-57.

Huang, H., Bhat, A., Woodnutt, G., and Lappe, R. (2010). Targeting the ANGPT-TIE2 pathway in malignancy. Nat Rev Cancer *10*, 575-585.

Hughes, C.S., Moggridge, S., Muller, T., Sorensen, P.H., Morin, G.B., and Krijgsveld, J. (2019). Single-pot, solid-phase-enhanced sample preparation for proteomics experiments. Nat Protoc *14*, 68-85.

Hupe, M., Li, M.X., Kneitz, S., Davydova, D., Yokota, C., Kele, J., Hot, B., Stenman, J.M., and Gessler, M. (2017). Gene expression profiles of brain endothelial cells during embryonic development at bulk and single-cell levels. Sci Signal *10*.

Kalucka, J., de Rooij, L., Goveia, J., Rohlenova, K., Dumas, S.J., Meta, E., Conchinha, N.V., Taverna, F., Teuwen, L.A., Veys, K.*, et al.* (2020). Single-Cell Transcriptome Atlas of Murine Endothelial Cells. Cell *180*, 764-779 e720.

London, N.R., Whitehead, K.J., and Li, D.Y. (2009). Endogenous endothelial cell signaling systems maintain vascular stability. Angiogenesis *12*, 149-158.

Malik, R., Rannikmae, K., Traylor, M., Georgakis, M.K., Sargurupremraj, M., Markus, H.S., Hopewell, J.C., Debette, S., Sudlow, C.L.M., Dichgans, M.*, et al.* (2018). Genome-wide meta-analysis identifies 3 novel loci associated with stroke. Ann Neurol *84*, 934-939.

Michell, B.J., Griffiths, J.E., Mitchelhill, K.I., Rodriguez-Crespo, I., Tiganis, T., Bozinovski, S., de Montellano, P.R., Kemp, B.E., and Pearson, R.B. (1999). The Akt kinase signals directly to endothelial nitric oxide synthase. Curr Biol *9*, 845-848.

Mishra, A., Malik, R., Hachiya, T., Jurgenson, T., Namba, S., Posner, D.C., Kamanu, F.K., Koido, M., Le Grand, Q., Shi, M.*, et al.* (2022). Stroke genetics informs drug discovery and risk prediction across ancestries. Nature *611*, 115-123.

Monet-Lepretre, M., Haddad, I., Baron-Menguy, C., Fouillot-Panchal, M., Riani, M., Domenga-Denier, V., Dussaule, C., Cognat, E., Vinh, J., and Joutel, A. (2013). Abnormal recruitment of extracellular matrix proteins by excess Notch3 ECD: a new pathomechanism in CADASIL. Brain *136*, 1830-1845.

Nawroth, R., Poell, G., Ranft, A., Kloep, S., Samulowitz, U., Fachinger, G., Golding, M., Shima, D.T., Deutsch, U., and Vestweber, D. (2002). VE-PTP and VE-cadherin ectodomains interact to facilitate regulation of phosphorylation and cell contacts. EMBO J *21*, 4885-4895.

Neurology Working Group of the Cohorts for, H., Aging Research in Genomic Epidemiology Consortium, t.S.G.N., and the International Stroke Genetics, C. (2016). Identification of additional risk loci for stroke and small vessel disease: a meta-analysis of genome-wide association studies. Lancet Neurol *15*, 695-707.

Obermeier, B., Daneman, R., and Ransohoff, R.M. (2013). Development, maintenance and disruption of the blood-brain barrier. Nature medicine *19*, 1584-1596.

Potente, M., Urbich, C., Sasaki, K., Hofmann, W.K., Heeschen, C., Aicher, A., Kollipara, R., DePinho, R.A., Zeiher, A.M., and Dimmeler, S. (2005). Involvement of Foxo transcription factors in angiogenesis and postnatal neovascularization. J Clin Invest *115*, 2382-2392.

Reyahi, A., Nik, A.M., Ghiami, M., Gritli-Linde, A., Ponten, F., Johansson, B.R., and Carlsson, P. (2015). Foxf2 Is Required for Brain Pericyte Differentiation and Development and Maintenance of the Blood-Brain Barrier. Dev Cell *34*, 19-32.

Roth, S., Cao, J., Singh, V., Tiedt, S., Hundeshagen, G., Li, T., Boehme, J.D., Chauhan, D., Zhu, J., Ricci, A.*, et al.* (2021). Post-injury immunosuppression and secondary infections are caused by an AIM2 inflammasome-driven signaling cascade. Immunity *54*, 648-659 e648.

Roudnicky, F., Kim, B.K., Lan, Y., Schmucki, R., Kuppers, V., Christensen, K., Graf, M., Patsch, C., Burcin, M., Meyer, C.A.*, et al.* (2020). Identification of a combination of

transcription factors that synergistically increases endothelial cell barrier resistance. Sci Rep *10*, 3886.

Ryu, J.R., Ahuja, S., Arnold, C.R., Potts, K.G., Mishra, A., Yang, Q., Sargurupremraj, M., Mahoney, D.J., Seshadri, S., Debette, S.*, et al.* (2022). Stroke-associated intergenic variants modulate a human FOXF2 transcriptional enhancer. Proc Natl Acad Sci U S A *119*, e2121333119.

Saharinen, P., Eklund, L., and Alitalo, K. (2017). Therapeutic targeting of the angiopoietin-TIE pathway. Nat Rev Drug Discov *16*, 635-661.

Saunders, A., Macosko, E.Z., Wysoker, A., Goldman, M., Krienen, F.M., de Rivera, H., Bien, E., Baum, M., Bortolin, L., Wang, S.*, et al.* (2018). Molecular Diversity and Specializations among the Cells of the Adult Mouse Brain. Cell *174*, 1015-1030 e1016.

Seker, F.B., Fan, Z., Gesierich, B., Gaubert, M., Sienel, R.I., and Plesnila, N. (2021). Neurovascular Reactivity in the Aging Mouse Brain Assessed by Laser Speckle Contrast Imaging and 2-Photon Microscopy: Quantification by an Investigator-Independent Analysis Tool. Front Neurol *12*, 745770.

Shen, J., Frye, M., Lee, B.L., Reinardy, J.L., McClung, J.M., Ding, K., Kojima, M., Xia, H., Seidel, C., Lima e Silva, R.*, et al.* (2014). Targeting VE-PTP activates TIE2 and stabilizes the ocular vasculature. J Clin Invest *124*, 4564-4576.

Sherman, B.T., Hao, M., Qiu, J., Jiao, X., Baseler, M.W., Lane, H.C., Imamichi, T., and Chang, W. (2022). DAVID: a web server for functional enrichment analysis and functional annotation of gene lists (2021 update). Nucleic Acids Res *50*, W216-W221.

Simons, M., Gordon, E., and Claesson-Welsh, L. (2016). Mechanisms and regulation of endothelial VEGF receptor signalling. Nat Rev Mol Cell Biol *17*, 611-625.

Sinitcyn, P., Hamzeiy, H., Salinas Soto, F., Itzhak, D., McCarthy, F., Wichmann, C., Steger, M., Ohmayer, U., Distler, U., Kaspar-Schoenefeld, S.*, et al.* (2021). MaxDIA enables library-based and library-free data-independent acquisition proteomics. Nat Biotechnol.

Tabula Muris, C., Overall, c., Logistical, c., Organ, c., processing, Library, p., sequencing, Computational data, a., Cell type, a., Writing, g.*, et al.* (2018). Single-cell transcriptomics of 20 mouse organs creates a Tabula Muris. Nature *562*, 367-372.

Terstappen, G.C., Meyer, A.H., Bell, R.D., and Zhang, W. (2021). Strategies for delivering therapeutics across the blood-brain barrier. Nat Rev Drug Discov *20*, 362-383.

Todorov, M.I., Paetzold, J.C., Schoppe, O., Tetteh, G., Shit, S., Efremov, V., Todorov-Volgyi, K., During, M., Dichgans, M., Piraud, M.*, et al.* (2020). Machine learning analysis of whole mouse brain vasculature. Nat Methods *17*, 442-449.

Traylor, M., Amin Al Olama, A., Lyytikainen, L.P., Marini, S., Chung, J., Malik, R., Dichgans, M., Kahonen, M., Lehtimaki, T., Anderson, C.D.*, et al.* (2020). Influence of Genetic Variation in PDE3A on Endothelial Function and Stroke. Hypertension *75*, 365-371.

Tusher, V.G., Tibshirani, R., and Chu, G. (2001). Significance analysis of microarrays applied to the ionizing radiation response. Proc Natl Acad Sci U S A *98*, 5116-5121.

Ungvari, Z., Tarantini, S., Kiss, T., Wren, J.D., Giles, C.B., Griffin, C.T., Murfee, W.L., Pacher, P., and Csiszar, A. (2018). Endothelial dysfunction and angiogenesis impairment in the ageing vasculature. Nat Rev Cardiol *15*, 555-565.

Vanlandewijck, M., He, L., Mae, M.A., Andrae, J., Ando, K., Del Gaudio, F., Nahar, K., Lebouvier, T., Lavina, B., Gouveia, L.*, et al.* (2018). A molecular atlas of cell types and zonation in the brain vasculature. Nature *554*, 475-480.

Wang, B., Wu, L., Chen, J., Dong, L., Chen, C., Wen, Z., Hu, J., Fleming, I., and Wang, D.W. (2021). Metabolism pathways of arachidonic acids: mechanisms and potential therapeutic targets. Signal Transduct Target Ther *6*, 94.

Winkler, E.A., Kim, C.N., Ross, J.M., Garcia, J.H., Gil, E., Oh, I., Chen, L.Q., Wu, D., Catapano, J.S., Raygor, K.*, et al.* (2022). A single-cell atlas of the normal and malformed human brain vasculature. Science *375*, eabi7377.

Wolf, F.A., Angerer, P., and Theis, F.J. (2018). SCANPY: large-scale single-cell gene expression data analysis. Genome Biol *19*, 15.

Xu, J., Lan, D., Li, T., Yang, G., and Liu, L. (2012). Angiopoietins regulate vascular reactivity after haemorrhagic shock in rats through the Tie2-nitric oxide pathway. Cardiovasc Res *96*, 308-319.

Xu, J., Liu, H., Lan, Y., Park, J.S., and Jiang, R. (2020). Genome-wide Identification of Foxf2 Target Genes in Palate Development. J Dent Res *99*, 463-471.

Yang, A.C., Vest, R.T., Kern, F., Lee, D.P., Agam, M., Maat, C.A., Losada, P.M., Chen, M.B., Schaum, N., Khoury, N.*, et al.* (2022). A human brain vascular atlas reveals diverse mediators of Alzheimer's risk. Nature *603*, 885-892.

Zeisel, A., Hochgerner, H., Lonnerberg, P., Johnsson, A., Memic, F., van der Zwan, J., Haring, M., Braun, E., Borm, L.E., La Manno, G.*, et al.* (2018). Molecular Architecture of the Mouse Nervous System. Cell *174*, 999-1014 e1022.

Zellner, A., Scharrer, E., Arzberger, T., Oka, C., Domenga-Denier, V., Joutel, A., Lichtenthaler, S.F., Muller, S.A., Dichgans, M., and Haffner, C. (2018). CADASIL brain vessels show a HTRA1 loss-of-function profile. Acta Neuropathol *136*, 111-125.

Zhao, Y., Vanhoutte, P.M., and Leung, S.W. (2015). Vascular nitric oxide: Beyond eNOS. J Pharmacol Sci *129*, 83-94.

Zheng, Z., Li, Y., Jin, G., Huang, T., Zou, M., and Duan, S. (2020). The biological role of arachidonic acid 12-lipoxygenase (ALOX12) in various human diseases. Biomed Pharmacother *129*, 110354.

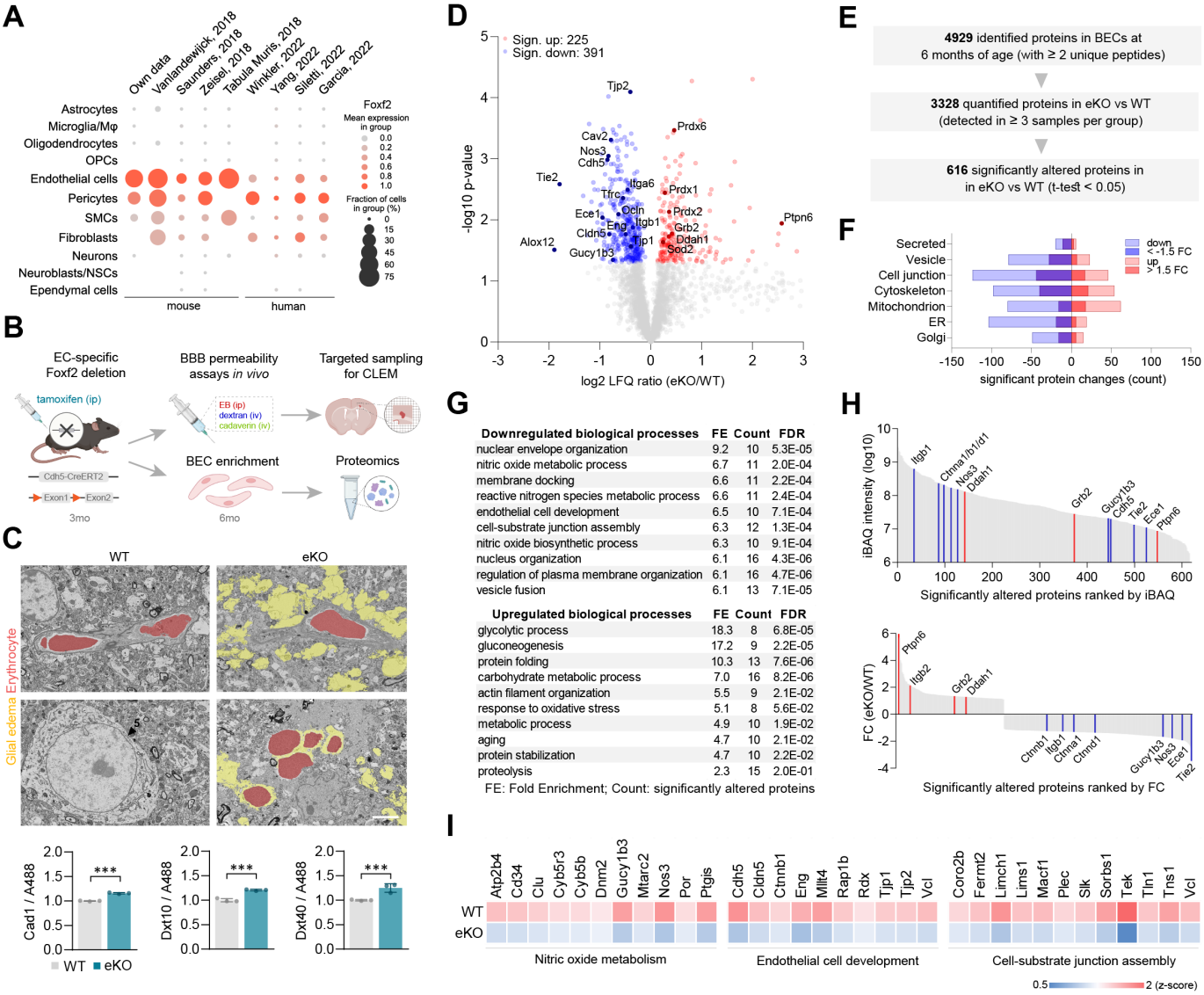

Figure 1. Endothelial Foxf2 deficiency causes BBB leakage and attenuates Tie2-signaling

A. Comparative analysis of Foxf2 expression in different brain cell types based on our own and already published single cell RNA sequencing data (References: #1 (Vanlandewijck et al., 2018), #2 (Saunders et al., 2018), #3 (Zeisel et al., 2018), #4 (Tabula Muris et al., 2018), #5 (Winkler et al., 2022), #6 (Yang et al., 2022)). **B.** Schematic of study design. Assessment of BBB permeability, histology, and BEC proteome in adult mice with EC-specific inactivation of Foxf2 (eKO) at 3 months. **C.** Correlative light- and electron microscopy (CLEM) on brain tissue with focal albumin extravasation in eKO and corresponding brain region from WT mouse (top) (scale bar: 5µm). Confocal microscopy images and quantification of extravasation of traces (cadaverin – 1kDa, dextran – 10 and 40 kDa) (bottom). **D.** Volcano plots of log2 LFQ ratios (eKO vs WT) and -log10 p values of all quantified proteins from 6 months old eKO and WT mice. Red and blue circles indicate proteins that were significantly up- and downregulated, respectively (n=6 mice / group, t-test, $p < 0.05$). Proteins related to Tie2-signaling are marked with their gene names. **E.** Summary of the LC–MS/MS and LFQ results. **F.** Subcellular localization of significantly dysregulated proteins. **G.** Enrichment analysis of biological processes of significantly dysregulated proteins in eKO vs WT mice based on Gene Ontology (GO) terms (FE: fold enrichment; count: number of significantly altered proteins; FDR: p-value of significantly enriched terms). **H.** iBAQ intensity and fold change ranking of the significantly altered proteins in eKO vs WT mice. Red and blue lines mark significantly up- and downregulated proteins, respectively, related to the Tie2-signaling pathway. **I.** Abundance of significantly downregulated proteins (n=6 mice / group, t-test, $p < 0.05$) according to the top enriched Tie2-regulated biological processes.

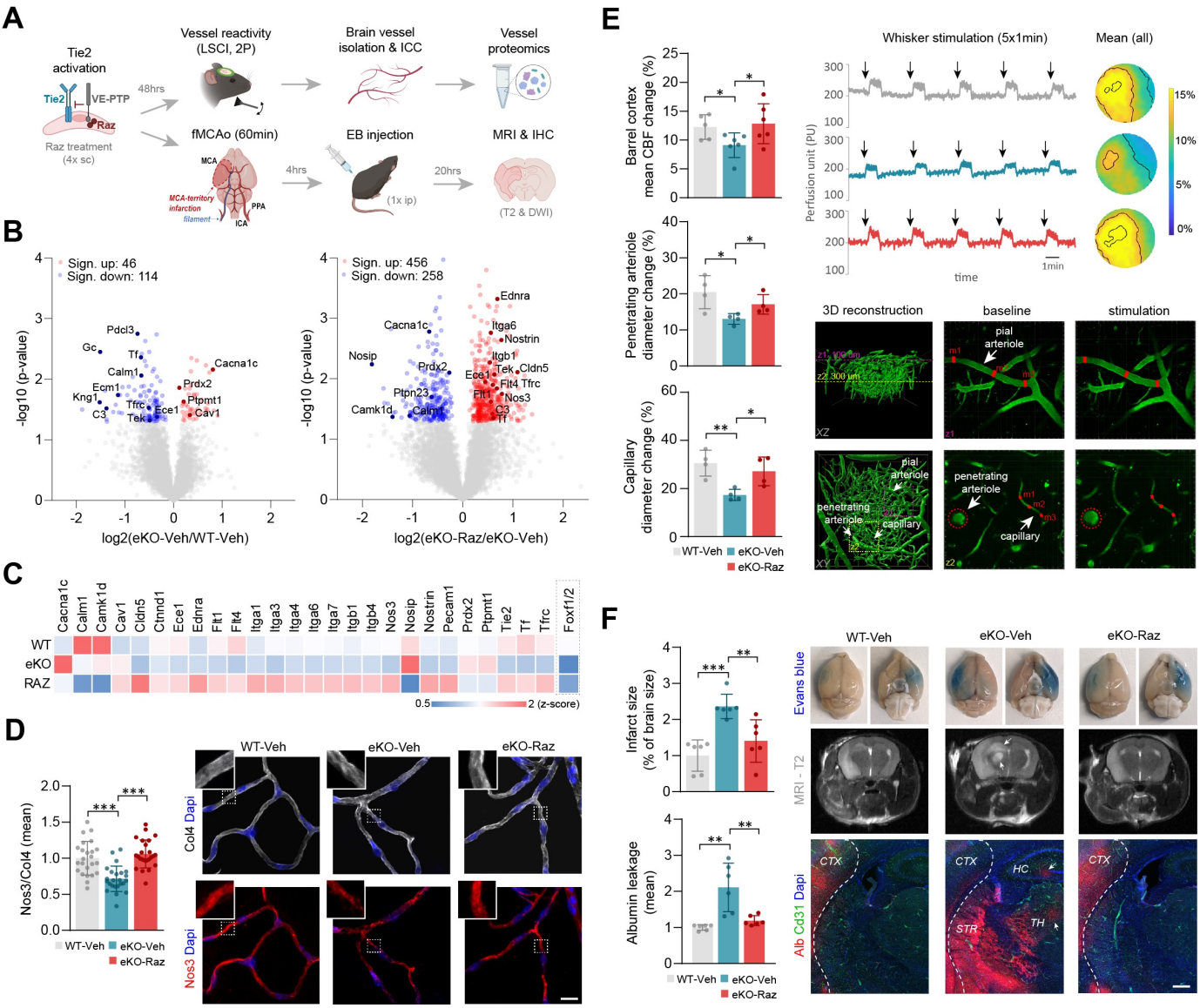

Figure 2. Razuprotafib rescues functional hyperemia and limits infarct size in mice with endothelial Foxf2 deficiency

A. Schematic of the interventional paradigm. Mice with EC-specific inactivation of Foxf2 at 3 months were treated subcutanously with the Tie2 activator Razuprotafib (AKB-9778) followed by CBF measurements and vessel proteomics. **B.** Volcano plots of log2 LFQ ratios and -log10 p values of all quantified proteins in isolated brain vessels from eKO mice and WT mice. Shown are the comparisons of vehicle treated animals (eKO-Veh vs WT-Veh) and of eKO mice treated with Razuprotafib vs vehicle (eKO-Raz vs eKO-Veh). Red and blue circles indicate proteins that were significantly (t-test, p-value < 0.05) up- and downregulated, respectively. Proteins related to Tie2-signaling are marked with their gene names. **C.** Abundance of Tie2-Nos3 signaling related proteins that were rescued by Razuprotafib treatment (eKO-Raz vs. eKO-Veh, t-test, $p < 0.05$). Foxf1 and 2 levels remained unaltered. **D.** Immunocytochemistry and quantification of Nos3 labeling in isolated brain microvessels (n=4 mice / group, t-test, $p < 0.05$) (Scale bar: 20µm). **E.** Upper panels: Quantification of mean CBF changes within Barrel cortex obtained by laser speckle imaging (LSCI) with individual registrations and averaged CBF heat maps following whisker stimulation. (n=6 mice / group, t-test, $p < 0.05$). Yellow color indicates a pronounced increase of cortical perfusion whereas blue color indicates no or small change. Lower panels: Representative images and quantification of vessel diameter changes of penetrating arterioles and capillaries following whisker stimulation. **F.** Quantification of infarct size and albumin leakage in mice treated with either vehicle or Razuprotafib prior to experimental stroke induction (n=6 mice / group, t-test, $p < 0.05$). Shown are exemplary images of whole brain, MRI, and confocal imaging (Scale bar: 500µm).

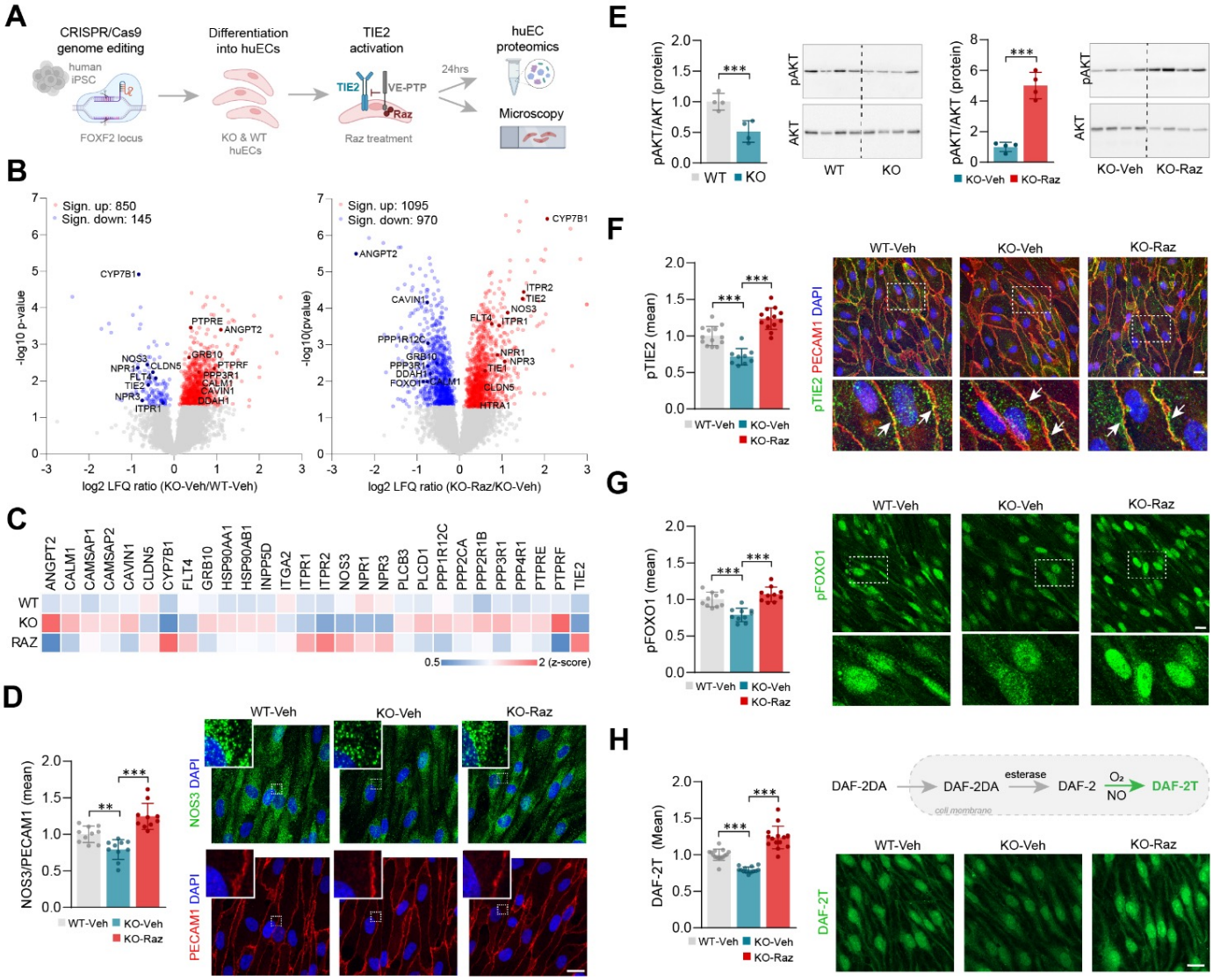

Figure 3. Razuprotafib rescues TIE2-signaling and NO production in FOXF2 deficient human endothelial cells

A. CRISPR/Cas9-mediated genome editing for FOXF2 deletion in human iPSCs, differentiation into brain endothelial cells (iBECs), and treatment strategy for proteomic and microscopic analysis. **B.** Volcano plots of log2 LFQ ratios (KO-Veh/WT-Veh and KO-Raz/KO-Veh) and -log10 p values of all quantified proteins. Red and blue circles indicate proteins that were significantly up- and downregulated respectively (n=5 samples / group, t-test, p-value < 0.05). Proteins related to TIE2-NOS3 signaling pathway are highlighted with their names in the volcano plot. **C.** Abundance of TIE2-NOS3 signaling related significantly altered (n=5 samples / group, KO-Veh vs WT-Veh, t-test, p-value < 0.05) and rescued proteins upon Razuprotafib treatment (n=5 samples / group, KO-Raz vs KO-Veh, p-value < 0.05). **D.** Immunocytochemistry and quantification of TIE2 in human WT and FOXF2 deficient (KO) iBECs (n=4 samples / group, t-test, p-value < 0.05) (scale bar: 20µm) after Veh/Raz treatment. **E.** Western blot quantification of pAKT/AKT in naive and Raz/Veh-treated iBECs (n=4 / group technical replicates, t-test, p-value < 0.05). **F.** Immunocytochemistry and quantification of NOS3 in human WT and KO iBECs (n=4 samples / group, t-test, p-value < 0.05) after Veh/Raz treatment (scale bar: 20µm). **G.** Immunocytochemistry and quantification of pFOXO1 in human WT and KO iBECs (n=4 samples / group, t-test, p-value < 0.05) after Veh/Raz treatment (scale bar: 20µm). **H.** Immunocytochemistry and quantification of NO production in FOXF2 deficient ECs by DAF fluorescence (n=4 samples / group, t-test, p-value < 0.05; scale bar: 20µm).

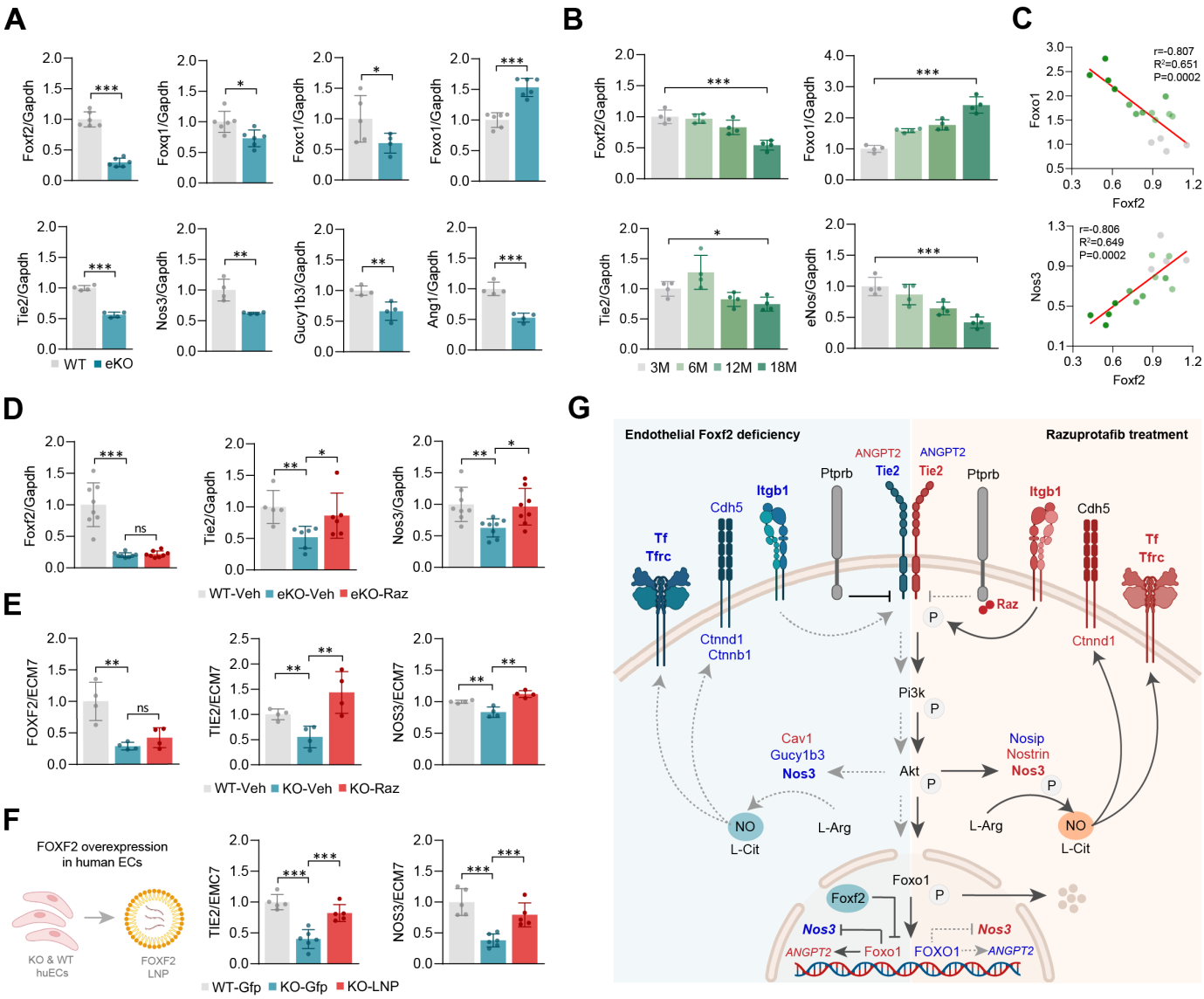

Figure 4. Endothelial Foxf2 regulates Tie2-mediated Nos3 signaling via Foxo1 inhibition

A. Relative RNA abundance of Foxf2, Foxq1, Foxc1, Foxo1, Tie2, Nos3, Gucy1b1, and Ang1 in brain tissue of eKO and WT mice (normalized to Gapdh and WT) (n=4-6 samples / group, t-test, p-value < 0.05). **B.** Relative RNA abundance of Foxf2, Foxo1, Tie2, and Nos3 during physiological aging. **C.** Significant negative and positive correlation between Foxf2-Foxo1, and Foxf2-Nos3, respectively (n=16 samples, red line marks simple linear regression). **D.** Relative RNA abundance of Foxf2, Tie2, and Nos3 in eKO and WT mice upon Veh/Raz treatment (normalized to Gapdh and WT) (n=6 samples / group, t-test, p-value < 0.05). **E.** Relative RNA abundance of FOXF2, TIE2, and NOS3 in eKO and WT iBECs upon Veh/Raz treatment (normalized to ECM7 and WT) (n=6 samples / group, t-test, p-value < 0.05). **F.** Relative RNA abundance of TIE2, and NOS3 in eKO and WT iBECs upon LNP treatment (normalized to ECM7 and WT) (n=4 samples / group, t-test, p-value < 0.05). **G.** EC-specific Foxf2-deficiency induced downregulation of Tie2-mediated Nos3 signaling. Red and blue colors indicate proteins that were significantly (t-test, p-value < 0.05) up- and downregulated in EC-specific Foxf2 deficient mice and FOXF2 KO human ECs (capital letters) compared to WT, respectively. Bold/italic letters indicate proteins that were changes in both mouse and human, and at RNA level, respectively.

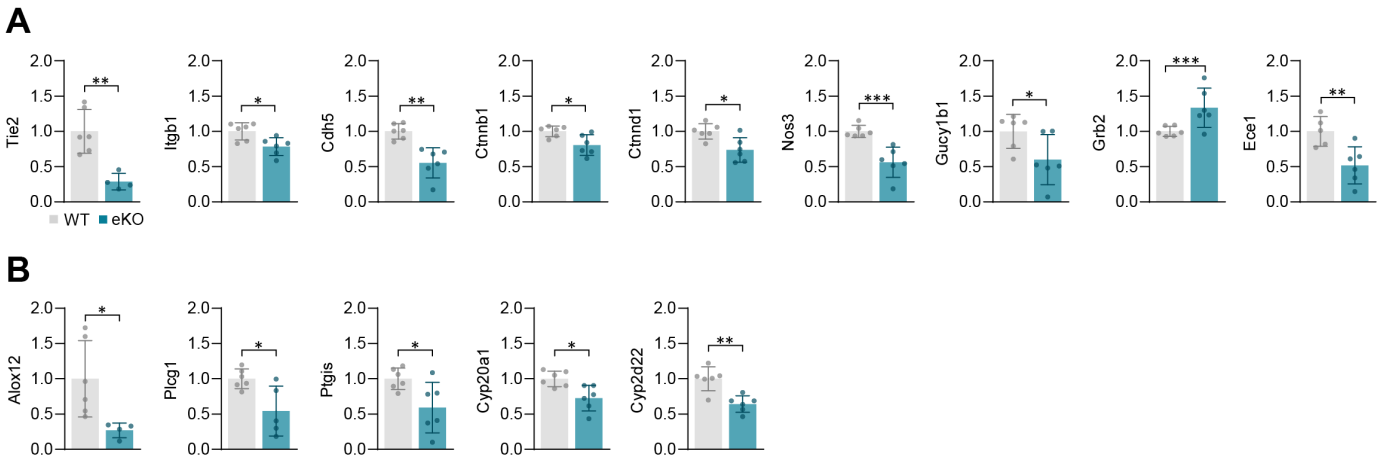

Suppl. Figure 1. Tie2-signaling and arachidonic acid metabolism related BEC protein changes induced by endothelial Foxf2 deficiency

LFQ values of Tie2 signaling (**A**) and arachidonic acid metabolism (**B**) related BEC protein changes in eKO mice normalized to WT (datapoints represent individual mice, n=6 mice / group, t-test, $p < 0.05$).

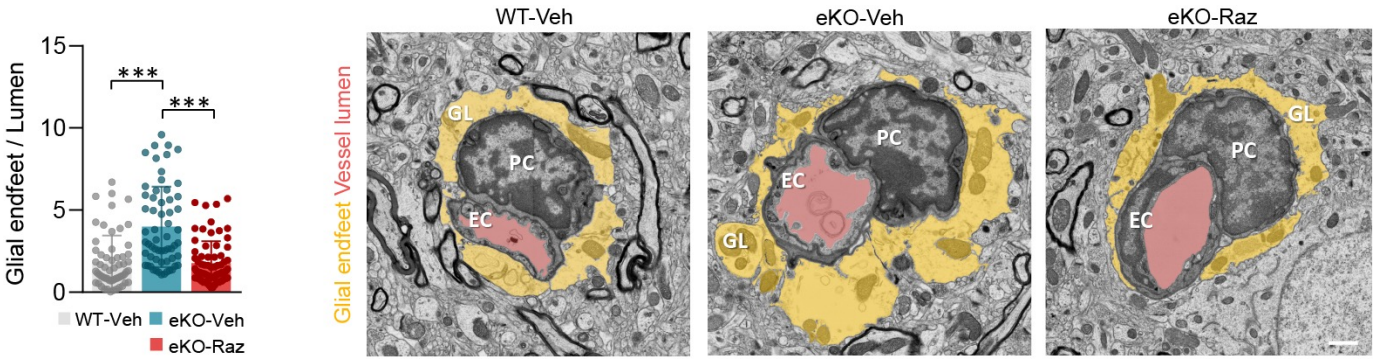

Suppl. Figure 2. Razuprotafib rescues glial edema endfeet induced by endothelial Foxf2 deficiency

Scanning electron microscopy (SEM) imaging with quantification of glial endfeet edema of eKO compared to WT mice (n=4 mice / group, t-test, $p < 0.05$) (Scale bar: 1µm).

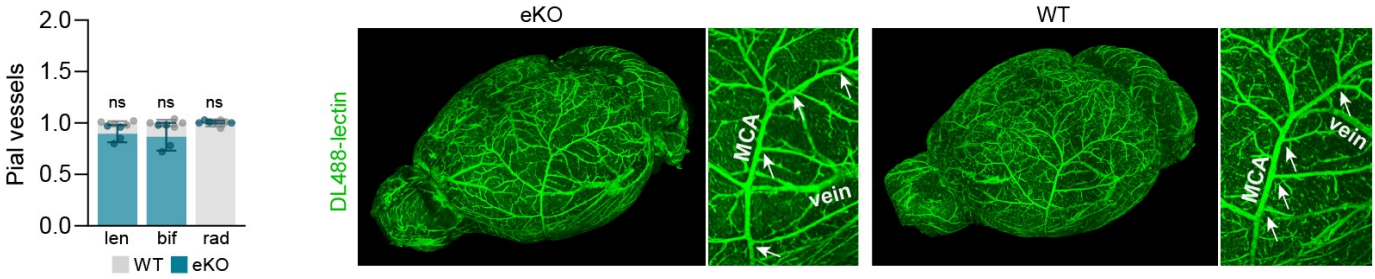

Suppl. Figure 3. Endothelial Foxf2 deficiency has no effect on the anatomy of whole brain pial vasculature

Light-sheet microscopy imaging with quantification of key vascular metrics of whole brain pial vasculature in eKO compared to WT mice (n=4 mice / group, t-test, $p < 0.05$).

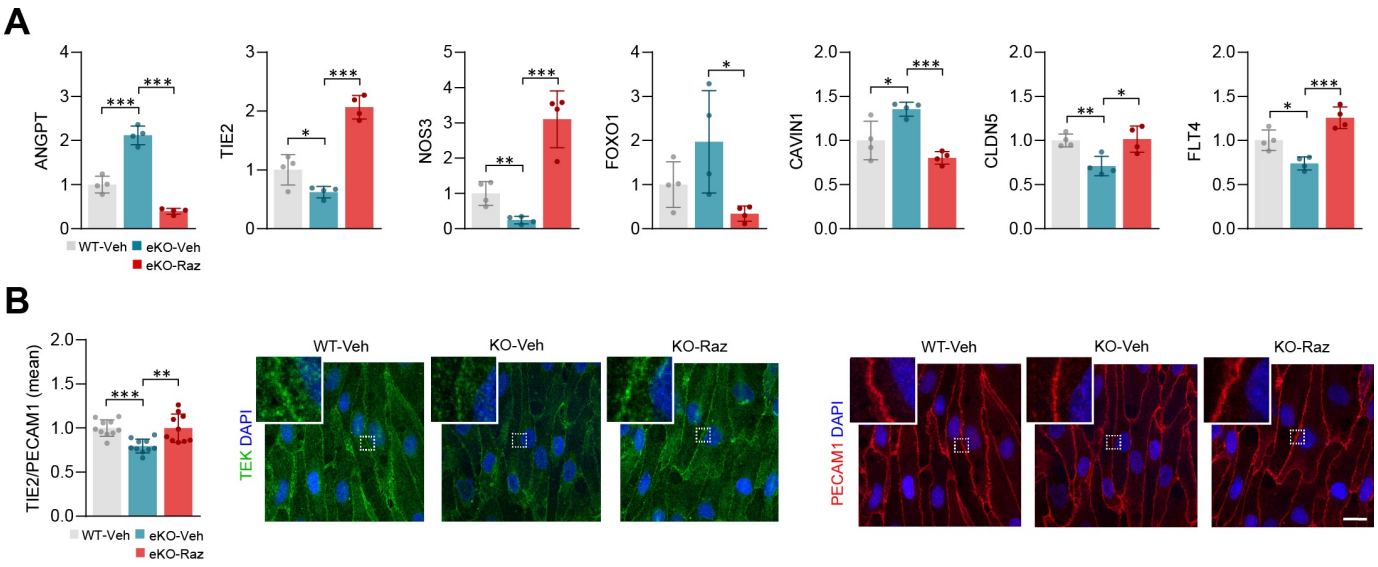

Suppl. Figure 4. Razuprotafib rescues Tie2-signaling related protein changes in FOXF2 deficient human ECs

A. LFQ values of Tie2 signaling related human EC protein changes in KO cells normalized to WT (datapoints represent individual samples, n=4 samples / group, t-test, $p < 0.05$). **B.** Immunocytochemistry and quantification of TIE2 in human KO and WT ECs (n=4 samples / group, t-test, p-value < 0.05) after Veh/Raz treatment (scale bar: 20µm).

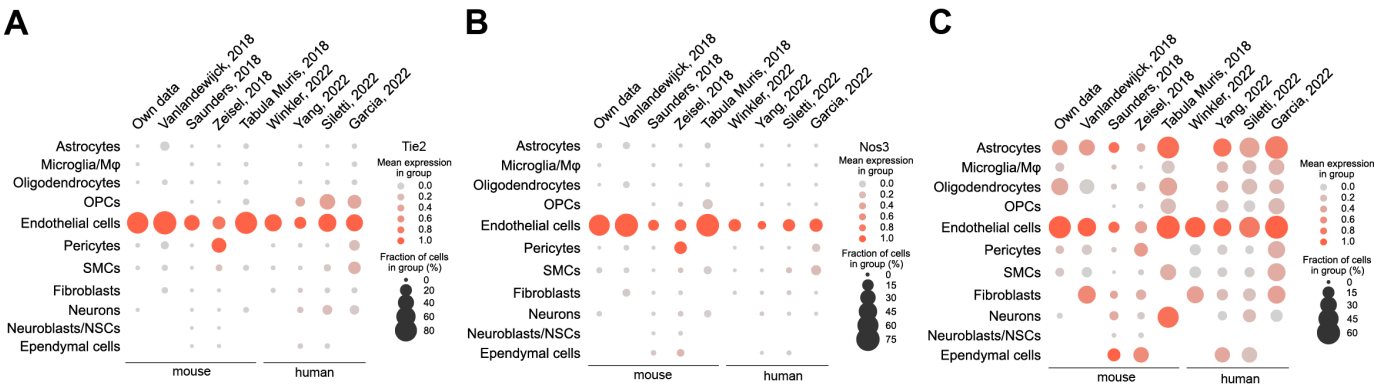

Suppl. Figure 5. Comparative analysis of Tie2, Nos3, and Foxo1 expression in different brain cell types

Comparative analysis of Tie2 (**A**), Nos3 (**B**), and Foxo1 (**C**) expression was performed based on our own and already published single cell RNA sequencing data (References: #1 (Vanlandewijck et al., 2018), #2 (Saunders et al., 2018), #3 (Zeisel et al., 2018), #4 (Tabula Muris et al., 2018), #5 (Winkler et al., 2022), #6 (Yang et al., 2022)).

4. Discussion

Cerebral small vessel diseases contribute to a large portion of dementias and increases the risk for stroke, posing a major burden on our society. Causes and phatomechanisims of cSVD are not fully understood and therefore, the availability of treatments remains limited. Most of BBB research, including drug delivery approaches have been based on animal models, which have been shown to have limited transferability to humans and the clinic. Therefore, developing reliable *in vivo* and *in vitro* models that can be used parallel to animal models is essential to better understand mechanisms leading to BBB breakdown.

This thesis deals with the generation of a human *in vitro* model of the BBB in parallel with *in vivo* models of FOXF2 deficient vascular cell types to better understand the cell autonomous effect of FOXF2 in endothelial cells and pericytes.

4.1. Generation and characterization of iPSC-derived cells for *in vitro* modelling

Advances in the generation of iPSCs (Takahashi and Yamanaka 2006) and differentiation protocols into somatic cells including the components of the NVU (Aday et al. 2016; Delsing et al. 2020) have provided unique tools for the generation of human derived *in vitro* models. However, the lack of standardization and deep characterization as well as difficulties in generating specific cell types have led the field to use differentiation protocols which do not fully recapitulate the cells present in the adult human brain. For example, a widely used protocol for the differentiation of brain endothelial cells (Lippmann et al. 2012) has been shown to yield cells with epithelial rather than endothelial identities (Lu et al. 2021). Moreover, most of astrocytes differentiation protocols (Lundin et al. 2018; TCW et al. 2017) use serum in their media, which has been shown to activate them (Zamanian et al. 2012; Y. Zhang et al. 2016), leading to non-physiological morphology and activity. These drawbacks resulted in the development of new protocols using serum-free media (Perriot et al. 2018). This illustrates the importance of a wide and deep characterization of iPSC-derived somatic cells before *in vitro* modelling.

To overcome this problem, we, after adopting and optimizing protocols for the differentiation of endothelial cells (iEC), smooth muscle cells (iSMC), pericytes (iPE) and astrocytes (iAS), characterized these cells by transcriptomics, proteomics and immunohistochemistry. To better understand how they approximate human brain cells, we directly compared them to human primary capillary endothelial cells (pEC), umbilical vein endothelial cells (HUVECs), vascular smooth muscle cells (pSMC), vascular pericytes (pPE) and mid brain astrocytes (pAS) by proteomic analysis. Unsupervised principal component analysis (PCA) of the proteomics results revealed a clear separation between iPSCs, differentiated cells and primary cells. When focusing on the endothelial cells, we found that iECs differentiated by us by our protocol, cluster closer to pEC than to HUVEC, a widely used cell type for *in*

vitro modelling. Furthermore, they do not express any of the key epithelial markers and upregulate key processes such as endothelial cell migration, angiogenesis and cell adhesion when compared to iPSCs, suggesting that iECs more closely resemble brain endothelium rather than epithelium. Similar results were obtained when comparing our iAS to pAS, which cluster together and quite distant from the mesoderm-derived cells. Moreover, when compared to iPSCs they upregulate key biological processes like neuron migration, synaptic vesicle endocytosis or axon guidance, overlapping processes between neurons and astrocytes. The characterization of derived mural cells, iSMC and iPE, was more difficult due to the lack of specific markers for each cell type (Armulik, Genové, and Betsholtz 2011b; Obermeier, Daneman, and Ransohoff 2013) and their heterogeneous distribution in the brain (Hartmann et al. 2015; Kisler et al. 2017). While they clustered based on their origin rather than cell type, marker expression revealed an upregulation of MCAM, CPSG4 and ACTA2 in iSMCs and downregulation of DES in iPE, as would be expected (Armulik, Genové, and Betsholtz 2011b; Smyth et al. 2018a), suggesting a proper cell differentiation.

We further evaluated relative RNA expression by quantitative polymerase chain reaction (qPCR) of the differentiated cells compared to iPSCs. In all cases, we found an upregulation of cell specific key markers and a downregulation of pluripotency markers, again demonstrating the differentiation into somatic cells. Moreover, immunohistochemistry validated the presence of the most common markers at protein level and typical morphology of the derived cells.

It is important to mention that in our differentiation protocols, both iSMC and iPE have a mesoderm lineage. However, the origin of SMCs and pericytes during development has been questioned and debated over the last years. Early studies suggested a mesoderm lineage for mural cells (Drake, Hungerford, and Little 1998) whereas recent quail-chick chimeras and lineage-tracing studies have prooved that forebrain mural cells arise from the neural crest, and therefore are derived from the ectoderm rather than mesoderm (Etchevers et al. 2001; Korn, Christ, and Kurz 2002; Armulik, Genové, and Betsholtz 2011b). Still, some other studies have shown that hematopoietic cells, which are derived from the mesoderm, can also generate brain pericytes (Yamazaki et al. 2017), suggesting the possibility of two distinct populations of mural cells in the brain which differ in their origin, mesoderm or ectoderm. One of the limitations of our iPSC-derived cells is the restriction of mesoderm derived mural cells and it would be interesting to include ectoderm derived cells with recently available protocols (A. Wang et al. 2011; Stebbins et al. 2019; Faal et al. 2019) and compare them with our current derived cells.

Another important topic in the context of differentiation of endothelial cells is overexpression of key endothelial transcription factors such as ETV2, SOX18, ERG, and FLI1 (Roudnicky et al. 2020; Lu et al. 2021; H. Zhang et al. 2022), which can improve their BBB phenotype. In our study we do not compare our protocol with overexpression of key transcription factors, which of course could improve the cell characteristics and functionality.

4.2. Generation and characterization of a human iPSC-derived 3D *in vitro* model of the BBB

Most of the widely used *in vitro* models of the BBB are based on a 2D transwell culture. Despite providing a better representation than monoculture and induction of greater endothelial cell barrier (Hatherell et al. 2011b; Lippmann et al. 2012) they do not recapitulate the typical 3D conformation, the establishment of direct cell-cell contacts and aspects of shear stress, key features of the BBB in vivo (Gastfriend, Palecek, and Shusta 2018). Advances in microfluidic systems, which allow these characteristics to be present, have provided a better alternative for BBB modelling (Aday et al. 2016; Oddo et al. 2019). Recent studies combining human primary cells with iPSC-derived cells have shown that co-culture of endothelial cells, mural cells and astrocytes generates a self-organized vascular network with perfusable lumens (Campisi et al. 2018; Vila Cuenca et al. 2021; Orlova et al. 2022).

To study genetic neurovascular disorders *in vitro* it would be necessary to develop a fully iPSC-derived model, where mutations can be introduced and studied in an isogenic manner in the different cell types. However, few iPSC-models have been developed and none of them have included endothelial cells, mural cells and astrocytes and rather focus only on a set of cells like endothelial cells, pericytes or neuronal progenitors (Jamieson et al. 2019; Vatine et al. 2019b). To overcome this problem we decided to use our fully characterized differentiated cells and co-culture them in 3D conformation using microfluidic chips.

Similarly to previous reports, our BBB *in vitro* model self-organized into vascular networks with perfusable lumens and secreted extracellular matrix (ECM) proteins (Belair et al. 2015; Campisi et al. 2018; Vila Cuenca et al. 2021). Moreover, our endothelial cells showed presence of adherens and tight junctions not only confirmed by the expression of PECAM1 and TJP1 but also by ultrastructural analysis via electron microscopy. Furthermore, endothelial cells also showed a typical vessel topology, secreting Collagen-IV towards the outside of the vessel and Podocalyxin towards the lumen. Due to the 3D conformation of the microfluidic chip we could also observe cell-cell interactions, where smooth muscle cells and astrocytic end feet are in close contact with the endothelial cells.

To explore and assess the applicability of the BBB model for therapeutic screening we developed a rescue paradigm using lipid nanoparticles (LNPs). In the past years, LNPs carrying mRNA have been used to treat infectious disease and cancer (Hou et al. 2021). Since BEC form the inner layer of the vasculature, there has been an emerging interest over the past years in optimizing LNP selectivity for ECs (Paunovska et al. 2018; G. W. Liu et al. 2023). To see if we can target our endothelial cells in 3D, we treated FOXF2 deficient cultures with LNPs containing mouse Foxf2 mRNA. LNP treatment not only efficiently targeted the endothelium but also rescued FOXF2-related phenotypes, such as the TJP1 downregulation, CAV1 upregulation and upregulated endocytic uptake. These results demonstrate that our model can be used to screen and test endothelium targeted therapeutics. Nevertheless, it would also be interesting to test other therapeutics which can cross the BBB and therefore target other cell types. Recent studies have shown that therapeutics connected to transferrin-binding 'brain-shuttles' can effectively cross the BBB (Logan et al. 2021; van Lengerich et al. 2023), which would be interesting also to test in our *in vitro* model.

Taken together, we developed a human *in vitro* BBB model which presents several advantages compared to the currently available models. First, our model is composed of fully iPSCs derived somatic cells, which have been thoroughly characterized. Second, combination of our iPSCs model with CRISPR/Cas-based genome editing enables studying disease phenotypes in an isogenic manner. Nevertheless, several improvements and characterizations could still be added. First, it has been shown that shear stress increases endothelial BBB phenotype (Chistiakov, Orekhov, and Bobryshev 2017; Cucullo et al. 2011), and therefore the addition of physiological flow would resemble more in vivo conditions. Second, the NVU has a complex cellular composition, and addition of other cell types like neurons, microglia and monocytes could improve recapitulation of the NVU *in vitro* and study cell crosstalk and inflammatory responses. Third, it has been shown that coculture of endothelial cells with pericytes and astrocytes upregulates several markers improving similarity to in vivo phenotypes (Campisi et al. 2018), but we did not assess that aspect in our co-culture model. Therefore, further characterization with proteomics and single cell sequencing would provide a confirmation of the co-culture benefits and at the same time allow the study of cell-cell communication *in vitro*, which can be essential to elucidate important mechanisms involved in formation of a healthy or diseased BBB. Lastly, it would also be informative to perform some electrophysiological measurements to see if the cell types have a synchronized activity.

4.3 A broad approach to investigate the role of FOXF2 in mouse and human, *in vivo* and *in vitro*

FOXF2 encodes a transcription factor which is mainly expressed in endothelial cells and pericytes in human and mouse (Vanlandewijck et al. 2018; Kalucka et al. 2020; A. C. Yang et al. 2021). It has been shown that Foxf2 induces the expression of BBB specific markers (He et al. 2020) and regulates the interaction between endothelial cells and pericytes (Wu, Li, and You 2021). Furthermore, common genetic variants which induce a reduction of FOXF2 are associated with stroke and cSVD (Chauhan et al. 2016a; Malik et al. 2018; J. R. Ryu et al. 2022) and global inactivation in mice leads to BBB impairment (Reyahi et al. 2015).

To uncover the cell-autonomous effects of FOXF2 in endothelial cells and pericytes and understand how it might be implicated in BBB impairment, we had to develop different models. For the *in vivo* study, we generated cell-specific deletion of Foxf2 in endothelial cells and pericytes. For that, we crossed our conditional Foxf2 fl/fl mice with Cre-specific promoters, for the endothelial cells Cdh5-creERT and for the pericytes Pdgfrb-CreERT2, which allowed cell specific deletion at a defined time point. For the *in vitro* study, we generated a FOXF2-KO in human iPSCs, which could be further differentiated into endothelial cells or pericytes.

4.4 The need of cell-specific proteomics and transcriptomics for *in vivo* studies

To better understand the role of Foxf2 in endothelial cells and pericytes we need to study them separately. While *in vitro* studies allow that relatively easily, they might lack phenotypes provided by the *in viv*o environment. Therefore, there is a need for developing isolation protocols which allow visualization and characterization of specific cell types. Recent developments in transcriptomics have enabled the study of different cell types at single cell resolution, including endothelial cells and pericytes from mouse brain (Aldridge and Teichmann 2020; Kalucka et al. 2020; Bjørnholm et al. 2023). However, proteomic profiles from individual cell types, including endothelial cells and pericytes are still missing.

Analysis of the cell-specific proteomics, together with transcriptomic analysis, is necessary for understanding the molecular pathways implicated in pathological dysfunction for several reasons. First, protein abundance levels may poorly correlate with mRNA levels due to intermediate processes like protein synthesis and degradation that are not captured during transcriptomic analysis (Maier, Güell, and Serrano 2009; Vogel and Marcotte 2012; Carlyle et al. 2017; D. Wang et al. 2019). Second, proteins are closer to cellular functions and biosynthetic output compared to mRNA (Bludau and Aebersold 2020). Third, transcriptomics analysis cannot capture internalized molecules or those bound to the cell surface.

Since Foxf2 is mainly expressed in endothelial cells and pericytes to study their cell-autonomous effect in each cell type we would need to combine the available transcriptomic protocols with the development of new specific protocols for proteomic analysis. Due to a lack of specific markers for pericytes (Armulik, Genové, and Betsholtz 2011b) and the limited protein amount, we could not develop a protocol which would allow the isolation of pericytes for proteomic analysis. However, we managed to develop a brain endothelial cell (BEC) enrichment protocol compatible with mass spectrometry. The multilevel characterization and validation of our MS-compatible mouse BEC enrichment protocol and a study to understand BEC proteome changes during aging do not form part of this thesis (Todorov-Völgyi & González-Gallego, *in revision*) but allowed us to apply the same protocol to study the effects of FOXF2 deletion in endothelial cells.

4.5 The BBB *in vitro* model phenocopies *in vivo* Foxf2 phenotypes

To demonstrate the applicability of iPSC-derived cells cultured in 2D and our newly developed 3D *in vitro* model of the BBB to study genetic vascular diseases we decided to focus on FOXF2 deletion. For that, we performed correlative in vivo and in vitro experiments comparing FOXF2 deficient endothelial cells (iEC) with endothelial-specific Foxf2 deficient mice.

Similar to global Foxf2 inactivation (Reyahi et al. 2015), endothelial-specific Foxf2 inactivation during adulthood induced endothelial thickening, elongated tight junctions, downregulation of Tjp1 and increased caveolae. The 3D in vitro model phenocopies the downregulation of TJP1, malformation of tight junctions with the formation of protrusions and the upregulation of CAV1. Additionally, *in vitro* disease modelling allowed us to assess endocytic uptake and transendothelial electrical resistance (TEER), which are challenging in vivo. FOXF2-KO cultures presented with a downregulation of TEER and an upregulation of endocytic uptake, in line with the down- and upregulation of TJP1 and CAV1 correspondingly.

Taken together, this demonstrates not only an alignment of Foxf2 deficient mouse and human models in the regulatory mechanisms but also proves that *in vitro* models can be used to study genetic neurovascular diseases.

4.6 Endothelial Foxf2 deficiency impairs BBB integrity

Morphological characterization of BBB integrity using fluorescent tracers of different size *in vivo* revealed barrier leakage upon Foxf2 deletion in endothelial cells for tracers between 1-40KDa. Furthermore, Evans blue injection and albumin staining showed an increase of focal albumin leakage areas in endothelial Foxf2 deficient mice when compared to wild type. Correlative electron microscopy of those positive areas revealed microhemorrhages with extravasation of erythrocytes in the parenchyma, glial edema and neuronal lysis. This phenotype is comparable to the phenotype

previously reported for mice in which Foxf2 is globally inactivated during adulthood (Reyahi et al. 2015). Using our *in vitro* system, FOXF2 deficient endothelial cells also showed a reduced transendothelial electrical resistance, which would be consistent with a BBB leakage *in vivo*. However, we did not test fluorescent tracers of different size in or 3D *in vitro* model parallel to the *in vivo* studies, which could be interesting and provide insights on BBB impairment as well as provide further characterization of the *in vitro* model.

To investigate the susceptibility of endothelial Foxf2 loss to cerebral ischemia we subjected our mice to experimental stroke using endovascular filament-mediated middle cerebral artery occlusion (fMCAo). Endothelial Foxf2 deficient mice presented larger infarct size and albumin leakage, suggesting a role of Foxf2 in BBB breakdown.

Enrichment analysis of significantly dysregulated proteins in human deficient FOXF2 endothelial cells revealed endocytosis and cell adhesion among the most affected biological processes. Among the enriched endocytosis proteins we found several members of the caveolin and clathrin-coated vesicles as well as proteins involved in the intracellular protein, specifically in the Golgi vesicle transport. This could explain the upregulation of endocytic uptake in FOXF2-KO cultures as well as the vascular defects *in vivo* (Andreone et al. 2017; Zhou et al. 2021). Among the enriched cell adhesion proteins we found proteins involved in the formation of tight junctions, cell-cell junctions, cell-matrix adhesion and cytoskeleton reorganization, which could suggest a cell structure reorganization in FOXF2 deficient endothelial cells. Moreover, the reduction in cell adhesion proteins could explain the reduced TEER in human deficient FOXF2 cells and correlate with the *in vivo* BBB impairment (Zlokovic 2011; Abdullahi, Tripathi, and Ronaldson 2018). Similarly, isolated BEC from endothelial Foxf2 deficient mice also showed a downregulation of tight junctions and upregulation of endocytosis proteins, giving one more time a correlation between human and mouse findings and supporting the idea of Foxf2 being involved in the maintenance of the BBB.

4.7 Endothelial Foxf2 deficiency dysregulates vessel remodeling

To further investigate whether the cytoskeleton reorganization, downregulation of cell-adhesion, or increased BBB leakage relate to anatomical differences we analyzed the whole brain vasculature using light-sheet microscopy. VesSAP-based quantification (Todorov et al. 2020) revealed a significant reduction of parenchymal microvessel density in several anatomic regions in endothelial specific deficient Foxf2 mice, suggesting a role of endothelial Foxf2 in microvessel remodeling during adulthood.

Further supporting this data, enrichment analysis of significantly downregulated proteins in Foxf2 deficient BECs revealed endothelial cell development among the most affected biological processes. Furthermore, key regulators of angiogenesis like Itgb1, Cdh5 and Tie2 were likewise downregulated, In addition, proteomic analysis of human FOXF2 deficient ECs revealed several angiogenesis, cell migration and vessel sprouting related proteins to be downregulated, further suggesting the importance of FOXF2 in the regulation of these processes. In line with these data, *in vitro* proliferation assays showed a downregulation in EC proliferation in FOXF2 deficient human ECs. Taken together, molecular and *in vitro* data identify Foxf2 as a key regulator of vessel remodeling, however some further *in vitro* experiments, like angiogenic sprouting (Tetzlaff and Fischer 2018; Kannan, Schain, and Lane 2022) or angiogenic tube formation measurements (Arnaoutova and Kleinman 2010; DeCicco-Skinner et al. 2014), would be necessary to understand better the underlying mechanism.

4.8 Endothelial Foxf2 deficiency attenuates Tie2-mediated Nos3 signaling via Foxo1 inhibition

To better understand the molecular changes induced by Foxf2 deletion in endothelial cells we run our optimized BEC enrichment protocol (Todorov-Völgyi & González-Gallego, *in revision*) in endothelial Foxf2 deficient mice. Enrichment analysis of significant dysregulated proteins revealed NO metabolism among the most affected biological processes. The Tie2-Pi3k-Akt1 signaling pathway contributes to the phosphorylation of Nos3 and further NO production (Michell et al. 1999). Among our dysregulated proteins we found Tie2, Nos3 to be significant downregulated in endothelial Foxf2 deficient mice both at protein and mRNA level. In line with those results, we found a downregulation of TIE2, NOS3 and AKT phosphorylation in human FOXF2 deficient endothelial cells, showing one more time an alignment between mouse and human Foxf2 regulatory mechanisms.

NO production is involved in cerebral blood flow (CBF) regulation and vessel dilation through a cGMP-mediated signal transduction pathway (Y. Zhao, Vanhoutte, and Leung 2015). *In vivo* analysis of cerebral blood flow revealed that endothelial Foxf2 deficient mice present with attenuated functional

hyperemia. Complementing these results, human FOXF2 deficient cells showed a downregulation in NO production.

Foxo1 is a target gene of the Tie2-Pi3k-Akt phosphorylation signaling pathway (Leligdowicz et al. 2018). As would be expected from the downregulation of Tie2 signaling in FOXF2 deficient human endothelial cells, we also found a downregulation of FOXO1 phosphorylation in these cells, which is in lie with an attenuated signaling pathway upon FOXF2 deficiency. Recent studies have identified Foxo1 as a target gene of Foxf2 in palate development (Xu et al. 2020) and further found Nos3 to be inhibited by Foxo1 (Potente et al. 2005). In line with those reports, we found Foxo1 to be upregulated and Nos3 to be downregulated in our endothelial specific Foxf2 deficient mice. Furthermore, we found a strong correlation between Foxf2 and Foxo1 mRNA expression as well as Foxf2 and Nos3, suggesting a regulatory effect of Foxf2 on the Tie2-mediated Nos3 signaling pathway via Foxo1 inhibition.

Despite the fact, that we established a link between Foxf2 and Foxo1 based on mRNA and protein levels a direct interaction between the two transcription factors is still missing. Therefore, experiments on ChipSeq to determine the binding partners of Foxf2 would be essential to further understand how Foxf2 regulates the Tie2-Nos3 signaling pathway.

4.9 Tie2-Nos3 signaling rescue using Razuprotafib

To better understand the role of Foxf2 in the Tie2-Nos3 signaling pathway and the effects on endothelial cells we decided to use a pharmacological intervention. We choose Razuprotafib (Raz), a small inhibitor of the vascular endothelial protein tyrosine phosphatase (Ptprb) that has been shown to stabilize the endothelium through Tie2 activation (Shen et al. 2014). Raz treatment of endothelial Foxf2 deficient mice and endothelial FOXF2 deficient human endothelial cells restored several proteins involved in the Tie2-Nos3 signaling, suggesting a restoration of the signaling pathway. As an example, not only Tie2 and Nos3 were upregulated upon treatment but also Nosip, an inhibitor of Nos3 was downregulated in mouse endothelial cells. In the same line, ANG2, an inhibitory ligand of TIE2 was downregulated in human endothelial cells, suggesting disinhibition of Tie2 signaling and therefore activation upon treatment.

Moreover, Raz treatment restored not only the deficit in functional hyperemia in adult mice but also NO production in human endothelial cells. Furthermore, Raz treatment limited infarct size and downregulated BBB leakage upon experimental stroke. Importantly, Raz treatment had no significant effect on FOXF2 expression in human cells while TIE2 and NOS3 were upregulated in human and mouse endothelial cells following Raz treatment. Taken together we could show that Raz treatment in both, adult mice and human endothelial cells, rescues Foxf2-induced deficits of the Tie2-Nos3 signaling.

4.10 Human FOXF2 deficient pericytes have increased proliferation rate

Despite FOXF2 being expressed in endothelial cells and pericytes to similar levels the main focus of this thesis has been in great part on the effects in the endothelium. However, the thesis also includes some experiments in FOXF2 deficient pericytes which helps better understanding the role of FOXF2 in this cell type.

We performed proteomic analysis of human FOXF2 deficient pericytes and enrichment analysis revealed cell adhesions and endocytosis among the most affected biological processes. Both processes are highly regulated and crucial for the maintenance of the BBB and already suggest the importance of FOXF2 in pericytes for a functional BBB. Moreover, several proteins related to cell proliferation and cell division were upregulated, suggesting a more proliferative state of pericytes upon FOXF2 deletion. Furthermore, we could see a higher proliferative rate of human FOXF2 deficient pericytes *in vitro*, in line with previous reports when Foxf2 is globally inactivated in adult mice (Reyahi et al. 2015).

Despite having some data on FOXF2 deficient pericytes and Foxf2 deficient mice we do not have an overall picture of the cell specific role of FOXF2 into this cell type. Further analysis of the proteomics data in human pericytes as well as proteomic analysis of isolated vessels would be expected to provide new insights into the role of Foxf2 in this cell type. *in vivo* studies on leakage, pericyte coverage, cerebral blood flow, and vessel anatomy would be required to understand the role of Foxf2 pericytes in BBB maintenance. Furthermore, since FOXF2 is mainly expressed in endothelial cells and pericytes it would be interesting to study the crosstalk between both cell types in the presence and absence of FOXF2 in each cell type, which could reveal key mechanisms by which FOXF2 regulates BBB maintenance.

5. Summary and outlook

In summary during this thesis we developed:

- Optimization and characterization of differentiation protocols for endothelial cells, pericytes, smooth muscle cells and astrocytes
- A fully iPSC-derived 3D BBB *in vitro* model, in which endothelial cells express adherens and tight junctions, are polarized and form perfusable lumens
- A mouse BEC enrichment protocol compatible with mass spectrometry
- An iPSCs line with FOXF2 deletion
- Cell-specific deletion of Foxf2 for endothelial cells and pericytes in adult brain

Using these methods we found that:

- The 3D *in vitro* model phenocopies SVD phenotypes induced by FOXF2 deficiency in endothelial cells such as a downregulation of tight junctions, caveolae upregulation and barrier dysfunction, illustrating the suitability of our human *in vitro* model for the investigation of genetic neurovascular disorders.
- The 3D *in vitro* model can be used to test therapeutic interventions in the endothelium since LNP delivery of mouse Foxf2 rescued the vesicle and barrier deficits induced by FOXF deletion
- Endothelial Foxf2 deficiency impairs BBB integrity in mouse and human. Specifically, we see a downregulation of cell adhesion and upregulation of endocytosis proteins in Foxf2 deficient mice. These mice further show an increase of focal leakage areas. Experimental stroke resulted in larger infarct size. In human iPSCs, we likewise see a downregulation of cell adhesion and upregulation of endocytosis proteins. Moreover, FOXF2 deficient endothelial cells have reduced TEER when compared to WT.
- Foxf2 deficiency in endothelial cells dysregulates vessel remodeling processes in mouse and human. In mouse, whole brain vasculature analysis shows a significant reduction of microvessel density in several regions. Furthermore, several regulators of angiogenesis are downregulated at protein level. In human cells, proteomic analysis shows a downregulation of proteins involved in angiogenesis, vessel sprouting and cell migration. Moreover, FOXF2 deficient endothelial cells have lower proliferation rates when compared to WT.
- Foxf2 deficient endothelial cells present with attenuated Tie2-mediated Nos3 signaling in mouse and human. Proteomic analysis of Foxf2 deficient BEC and human FOXF2 deficient endothelial cells shows key proteins involved in the Tie2-mediated Nos3 signaling to be dysregulated. Furthermore, Foxf2 deficient mice presents with attenuated functional hyperemia and human cells with NO production downregulation.

- Endothelial Foxf2 regulates Tie2-Nos3 pathway by Foxo1 inhibition. Foxf2 deletion in BEC upregulates Foxo1 and downregulates Nos3 mRNA levels. Moreover, Foxf2 and Foxo1 mRNA level strongly correlate in mouse.
- Razuprotafib rescues Tie2-mediated Nos3 signaling. Treatment with Raz restores several proteins involved in the Tie2-Nos3 pathway isolated vessels from mice and human endothelial cells. Furthermore, treatment with Razuprotafib rescues functional hyperemia and limits infarct size in endothelial Foxf2 deficient mice and NO production in FOXF2 deficient endothelial cells.
- Human FOXF2 deficient pericytes have increased proliferation rate in *in vitro* studies. Moreover, proteomic analysis shows several proteins involved in cell proliferation and division to be upregulated.

There are some points that we did not address in this thesis that would need to be further investigated to understand the cell-autonomous effect of Foxf2 in endothelial cells and pericytes.

Endothelial cells and pericytes are key components of the BBB and their crosstalk as well as coordinate activity secures BBB maintenance during development and adulthood. Since Foxf2 is mainly expressed in those cell types in the vasculature it would be interesting to further understand its implication in crosstalk and functionality of both cell types. Therefore, single cell experiments with global, endothelial-specific and pericyte-specific Foxf2 deletion would provide a better understanding if and how Foxf2 regulates pericyte-endothelial communication. Using such an experimental design we could also elucidate how pericytes change upon Foxf2 deletion in endothelial cells and vice versa. This type of experiment could be done not only in mice but also in our *in vitro* model of the BBB, since incorporation of different genotypes would be even more feasible here.

Since Foxf2 is a transcription factor it would be necessary to elucidate the target genes in endothelial cells and pericytes. Such experiment would give us a better overview of which mechanisms is Foxf2 regulating *in vivo* during adulthood. Furthermore, since recent reports suggest that FOXF2 may promote differentiation of iPSCs into brain endothelial cells, knowing its target genes might provide insights to better understand endothelial cell differentiation and how to modulate it *in vitro*.

6. References

Abbott, N. Joan. 2002. “Astrocyte-Endothelial Interactions and Blood-Brain Barrier Permeability.” *Journal of Anatomy*. https://doi.org/10.1046/j.1469-7580.2002.00064.x.

Abbott, N. Joan. 2004. “Prediction of Blood-Brain Barrier Permeation in Drug Discovery from in Vivo, in Vitro and in Silico Models.” *Drug Discovery Today: Technologies* 1 (4): 407–16. https://doi.org/10.1016/j.ddtec.2004.11.014.

Abbott, N. Joan, Adjanie A.K. Patabendige, Diana E.M. Dolman, Siti R. Yusof, and David J. Begley. 2010. “Structure and Function of the Blood-Brain Barrier.” *Neurobiology of Disease* 37 (1): 13–25. https://doi.org/10.1016/j.nbd.2009.07.030.

Abbott, N. Joan, Lars Rönnbäck, and Elisabeth Hansson. 2006. “Astrocyte-Endothelial Interactions at the Blood-Brain Barrier.” *Nature Reviews Neuroscience* 7 (1): 41–53. https://doi.org/10.1038/nrn1824.

Abdullahi, Wazir, Dinesh Tripathi, and Patrick T. Ronaldson. 2018. “Blood-Brain Barrier Dysfunction in Ischemic Stroke: Targeting Tight Junctions and Transporters for Vascular Protection.” *American Journal of Physiology - Cell Physiology* 315 (3): C343–56. https://doi.org/10.1152/ajpcell.00095.2018.

Aday, S, R Cecchelli, D Hallier-Vanuxeem, M P Dehouck, and L Ferreira. 2016. “Stem Cell-Based Human Blood-Brain Barrier Models for Drug Discovery and Delivery.” *Trends in Biotechnology*. https://doi.org/10.1016/j.tibtech.2016.01.001.

Ahn, Song Ih, Yoshitaka J. Sei, Hyun Ji Park, Jinhwan Kim, Yujung Ryu, Jeongmoon J. Choi, Hak Joon Sung, Tobey J. MacDonald, Allan I. Levey, and Yong Tae Kim. 2020. “Microengineered Human Blood–Brain Barrier Platform for Understanding Nanoparticle Transport Mechanisms.” *Nature Communications 2020 11:1* 11 (1): 1–12. https://doi.org/10.1038/s41467-019-13896-7.

Aitola, Marjo, Peter Carlsson, Margit Mahlapuu, Sven Enerbäck, and Markku Pelto-Huikko. 2000. “Forkhead Transcription Factor FoxF2 Is Expressed in Mesodermal Tissues Involved in Epithelio-Mesenchymal.” *Developmental Dynamics* 218 (1): 136–49. https://doi.org/10.1002/(SICI)1097-0177(200005)218:1<136::AID-DVDY12>3.0.CO;2-U.

Âla Kis, Be, Ca A Ma Âria Deli, Hideyuki Kobayashi, Csongor S A Â braha Âm, Toshihiko Yanagita, Hiroyuki Kaiya, Toyohi Isse, et al. n.d. “Adrenomedullin Regulates Blood±brain Barrier Functions in Vitro.” Vol. 12.

Alahmari, Abeer. 2021. “Blood-Brain Barrier Overview: Structural and Functional Correlation.” *Neural Plasticity*. Hindawi Limited. https://doi.org/10.1155/2021/6564585.

Aldridge, Sarah, and Sarah A. Teichmann. 2020. “Single Cell Transcriptomics Comes of Age.” *Nature Communications 2020 11:1* 11 (1): 1–4. https://doi.org/10.1038/S41467-020-18158-5.

Ambasudhan, Rajesh, Scott D. Ryan, Nima Dolatabadi, Shing Fai Chan, Xiaofei Zhang, Mohd Waseem Akhtar, James Parker, et al. 2013. “Isogenic Human IPSC Parkinson’s Model Shows Nitrosative Stress-Induced Dysfunction in MEF2-PGC1α Transcription.” *Cell* 155 (6): 1351–64. https://doi.org/10.1016/J.CELL.2013.11.009.

Andreone, Benjamin J., Brian Wai Chow, Aleksandra Tata, Baptiste Lacoste, Ayal Ben-Zvi, Kevin Bullock, Amy A. Deik, David D. Ginty, Clary B. Clish, and Chenghua Gu. 2017. “Blood-Brain Barrier Permeability Is Regulated by Lipid Transport-Dependent Suppression of Caveolae-Mediated Transcytosis.” *Neuron* 94 (3): 581-594.e5. https://doi.org/10.1016/j.neuron.2017.03.043.

Appelt-Menzel, Antje, Alevtina Cubukova, Katharina Günther, Frank Edenhofer, Jörg Piontek, Gerd

Krause, Tanja Stüber, Heike Walles, Winfried Neuhaus, and Marco Metzger. 2017. “Establishment of a Human Blood-Brain Barrier Co-Culture Model Mimicking the Neurovascular Unit Using Induced Pluri- and Multipotent Stem Cells.” *Stem Cell Reports* 8 (4): 894–906. https://doi.org/10.1016/j.stemcr.2017.02.021.

Armulik, Annika, Guillem Genové, and Christer Betsholtz. 2011a. “Pericytes: Developmental, Physiological, and Pathological Perspectives, Problems, and Promises.” *Developmental Cell*. https://doi.org/10.1016/j.devcel.2011.07.001.

Armulik, Annika, Guillem Genové, Maarja Mäe, Maya H. Nisancioglu, Elisabet Wallgard, Colin Niaudet, Liqun He, et al. 2010. “Pericytes Regulate the Blood-Brain Barrier.” *Nature* 468 (7323): 557–61. https://doi.org/10.1038/nature09522.

Arnaoutova, Irina, and Hynda K. Kleinman. 2010. “In Vitro Angiogenesis: Endothelial Cell Tube Formation on Gelled Basement Membrane Extract.” *Nature Protocols 2010 5:4* 5 (4): 628–35. https://doi.org/10.1038/nprot.2010.6.

Attwell, David, Alastair M. Buchan, Serge Charpak, Martin Lauritzen, Brian A. MacVicar, and Eric A. Newman. 2010. “Glial and Neuronal Control of Brain Blood Flow.” *Nature 2010 468:7321* 468 (7321): 232–43. https://doi.org/10.1038/NATURE09613.

Bandopadhyay, R., C. Orte, J. G. Lawrenson, A. R. Reid, S. De Silva, and G. Allt. 2001. “Contractile Proteins in Pericytes at the Blood-Brain and Blood-Retinal Barriers.” *Journal of Neurocytology* 30 (1): 35–44. https://doi.org/10.1023/A:1011965307612.

Barrangou, Rodolphe. 2007. “CRISPR Provides Acquired Resistance against Viruses in Prokaryotes.” *Science*, September. https://doi.org/10.1029/2004GL019460.

Belair, David G., Jordan A. Whisler, Jorge Valdez, Jeremy Velazquez, James A. Molenda, Vernella Vickerman, Rachel Lewis, et al. 2015. “Human Vascular Tissue Models Formed from Human Induced Pluripotent Stem Cell Derived Endothelial Cells.” *Stem Cell Reviews and Reports* 11 (3): 511–25. https://doi.org/10.1007/S12015-014-9549-5/FIGURES/8.

Bell, Robert D., Ethan A. Winkler, Abhay P. Sagare, Itender Singh, Barb LaRue, Rashid Deane, and Berislav V. Zlokovic. 2010. “Pericytes Control Key Neurovascular Functions and Neuronal Phenotype in the Adult Brain and during Brain Aging.” *Neuron* 68 (3): 409–27. https://doi.org/10.1016/J.NEURON.2010.09.043.

Bergmann, Sonja, Sean E. Lawler, Yuan Qu, Colin M. Fadzen, Justin M. Wolfe, Michael S. Regan, Bradley L. Pentelute, Nathalie Y.R. Agar, and Choi Fong Cho. 2018. “Blood–Brain-Barrier Organoids for Investigating the Permeability of CNS Therapeutics.” *Nature Protocols* 13 (12): 2827–43. https://doi.org/10.1038/s41596-018-0066-x.

Bjørnholm, Katrine Dahl, Francesca Del Gaudio, Hao Li, Weihan Li, Elisa Vazquez-Liebanas, Maarja Andaloussi Mäe, Urban Lendahl, et al. 2023. “A Robust and Efficient Microvascular Isolation Method for Multimodal Characterization of the Mouse Brain Vasculature.” *Cell Reports Methods* 3 (3). https://doi.org/10.1016/j.crmeth.2023.100431.

Blasi, Paolo, Stefano Giovagnoli, Aurélie Schoubben, Maurizio Ricci, and Carlo Rossi. 2007. “Solid Lipid Nanoparticles for Targeted Brain Drug Delivery.” *Advanced Drug Delivery Reviews*. https://doi.org/10.1016/j.addr.2007.04.011.

Bludau, Isabell, and Ruedi Aebersold. 2020. “Proteomic and Interactomic Insights into the Molecular Basis of Cell Functional Diversity.” *Nature Reviews Molecular Cell Biology 2020 21:6* 21 (6): 327–40. https://doi.org/10.1038/S41580-020-0231-2.

Bonni, Azad, Yi Sun, Mireya Nadal-Vicens, Ami Bhatt, David A Frank, Lrina Rozovsky, Neil Stahl, George D Yancopoulos, and Michael E Greenberg. n.d. “Regulation of Gliogenesis in the Central Nervous

System by the JAK-STAT Signaling Pathway." www.sciencemag.org.

Busija, David W, Ferenc Bari, Ferenc Domoki, and Thomas Louis. 2007. "Mechanisms Involved in the Cerebrovascular Dilator Effects of N-Methyl-D-Aspartate in Cerebral Cortex." https://doi.org/10.1016/j.brainresrev.2007.05.011.

Caffrey, Tara M, Emily Button, and Jerome Robert. 2021. "Toward Three-Dimensional in Vitro Models to Study Neurovascular Unit Functions in Health and Disease." *Neural Regeneration Research*. https://doi.org/10.4103/1673-5374.310671.

Cakir, Bilal, Yangfei Xiang, Yoshiaki Tanaka, Mehmet H Kural, Maxime Parent, Young Jin Kang, Kayley Chapeton, et al. 2019. "Engineering of Human Brain Organoids with a Functional Vascular-like System." *Nature Methods* 16 (11): 1169–75. https://doi.org/10.1038/s41592-019-0586-5.

Campisi, Marco, Yoojin Shin, Tatsuya Osaki, Cynthia Hajal, Valeria Chiono, and Roger D Kamm. 2018. "3D Self-Organized Microvascular Model of the Human Blood-Brain Barrier with Endothelial Cells, Pericytes and Astrocytes." *Biomaterials* 180: 117–29. https://doi.org/10.1016/j.biomaterials.2018.07.014.

Canfield, Scott G., Matthew J. Stebbins, Bethsymarie Soto Morales, Shusaku W. Asai, Gad D. Vatine, Clive N. Svendsen, Sean P. Palecek, and Eric V. Shusta. 2017. "An Isogenic Blood–Brain Barrier Model Comprising Brain Endothelial Cells, Astrocytes, and Neurons Derived from Human Induced Pluripotent Stem Cells." *Journal of Neurochemistry* 140 (6): 874–88. https://doi.org/10.1111/jnc.13923.

Carlyle, Becky C., Robert R. Kitchen, Jean E. Kanyo, Edward Z. Voss, Mihovil Pletikos, André M.M. Sousa, Tu Kiet T. Lam, Mark B. Gerstein, Nenad Sestan, and Angus C. Nairn. 2017. "A Multiregional Proteomic Survey of the Postnatal Human Brain." *Nature Neuroscience 2017 20:12* 20 (12): 1787–95. https://doi.org/10.1038/S41593-017-0011-2.

Chaigneau, Emmanuelle, Martin Oheim, Etienne Audinat, and Serge Charpak. 2003. "Two-Photon Imaging of Capillary Blood Flow in Olfactory Bulb Glomeruli." *Proceedings of the National Academy of Sciences of the United States of America* 100 (22): 13081–86. https://doi.org/10.1073/PNAS.2133652100/ASSET/4A980DB8-86E1-4A04-92BC-67D5E3FA154B/ASSETS/GRAPHIC/PQ2133652005.JPEG.

Chambers, Stuart M., Christopher A. Fasano, Eirini P. Papapetrou, Mark Tomishima, Michel Sadelain, and Lorenz Studer. 2009. "Highly Efficient Neural Conversion of Human ES and IPS Cells by Dual Inhibition of SMAD Signaling." *Nature Biotechnology 2009 27:3* 27 (3): 275–80. https://doi.org/10.1038/NBT.1529.

Chauhan, Ganesh, Corey R. Arnold, Audrey Y. Chu, Myriam Fornage, Azadeh Reyahi, Joshua C. Bis, Aki S. Havulinna, et al. 2016a. "Identification of Additional Risk Loci for Stroke and Small Vessel Disease: A Meta-Analysis of Genome-Wide Association Studies." *The Lancet Neurology* 15 (7): 695–707. https://doi.org/10.1016/S1474-4422(16)00102-2.

Chen, Yan, and Lihong Liu. 2012. "Modern Methods for Delivery of Drugs across the Blood–Brain Barrier." *Advanced Drug Delivery Reviews* 64 (7): 640–65. https://doi.org/10.1016/J.ADDR.2011.11.010.

Cheung, Christine, Andreia S. Bernardo, Roger A. Pedersen, and Sanjay Sinha. 2014. "Directed Differentiation of Embryonic Origin–Specific Vascular Smooth Muscle Subtypes from Human Pluripotent Stem Cells." *Nature Protocols 2014 9:4* 9 (4): 929–38. https://doi.org/10.1038/nprot.2014.059.

Chiaradia, Ilaria, and Madeline A. Lancaster. 2020. "Brain Organoids for the Study of Human Neurobiology at the Interface of in Vitro and in Vivo." *Nature Neuroscience 2020 23:12* 23 (12):

1496–1508. https://doi.org/10.1038/s41593-020-00730-3.

Chistiakov, D. A., A. N. Orekhov, and Y. V. Bobryshev. 2017. “Effects of Shear Stress on Endothelial Cells: Go with the Flow.” *Acta Physiologica* 219 (2): 382–408. https://doi.org/10.1111/APHA.12725.

Cho, Choi Fong, Justin M. Wolfe, Colin M. Fadzen, David Calligaris, Kalvis Hornburg, E. Antonio Chiocca, Nathalie Y.R. Agar, Bradley L. Pentelute, and Sean E. Lawler. 2017. “Blood-Brain-Barrier Spheroids as an in Vitro Screening Platform for Brain-Penetrating Agents.” *Nature Communications* 8 (June). https://doi.org/10.1038/ncomms15623.

Chojdak-Łukasiewicz, Justyna, Edyta Dziadkowiak, Anna Zimny, and Bogusław Paradowski. 2021. “Cerebral Small Vessel Disease: A Review.” *Advances in Clinical and Experimental Medicine* 30 (3): 349–56. https://doi.org/10.17219/acem/131216.

Cipolla, Marilyn J. 2009. “The Cerebral Circulation.” *The Cerebral Circulation.*, 185–87. https://www.ncbi.nlm.nih.gov/books/NBK53081/.

Cong, Le, F. Ann Ran, David Cox, Shuailiang Lin, Robert Barretto, Naomi Habib, Patrick D. Hsu, et al. 2013. “Multiplex Genome Engineering Using CRISPR/Cas Systems.” *Science* 339 (6121): 819–23. https://doi.org/10.1126/science.1231143.

Cox, Stephanie B., Thomas A. Woolsey, and Carl M. Rovainen. 2016. “Localized Dynamic Changes in Cortical Blood Flow with Whisker Stimulation Corresponds to Matched Vascular and Neuronal Architecture of Rat Barrels.” *Http://Dx.Doi.Org.Emedien.Ub.Uni-Muenchen.de/10.1038/Jcbfm.1993.113* 13 (6): 899–913. https://doi.org/10.1038/JCBFM.1993.113.

Cucullo, Luca, Mohammed Hossain, Vikram Puvenna, Nicola Marchi, and Damir Janigro. 2011. “The Role of Shear Stress in Blood-Brain Barrier Endothelial Physiology.” *BMC Neuroscience* 12 (1): 1–15. https://doi.org/10.1186/1471-2202-12-40/FIGURES/7.

Cudmore, Robert H., Sarah E. Dougherty, and David J. Linden. 2017. “Cerebral Vascular Structure in the Motor Cortex of Adult Mice Is Stable and Is Not Altered by Voluntary Exercise.” *Journal of Cerebral Blood Flow and Metabolism* 37 (12): 3725–43. https://doi.org/10.1177/0271678X16682508/ASSET/IMAGES/LARGE/10.1177_0271678X16682508-FIG1.JPEG.

Daneman, Richard. 2012. “The Blood-Brain Barrier in Health and Disease.” *Annals of Neurology* 72 (5): 648–72. https://doi.org/10.1002/ana.23648.

Daneman, Richard, and Alexandre Prat. 2015. “The Blood–Brain Barrier.” *Cold Spring Harbor Perspectives in Biology* 7 (1). https://doi.org/10.1101/cshperspect.a020412.

Daneman, Richard, Lu Zhou, Amanuel A. Kebede, and Ben A. Barres. 2010. “Pericytes Are Required for Blood–Brain Barrier Integrity during Embryogenesis.” *Nature 2010 468:7323* 468 (7323): 562–66. https://doi.org/10.1038/NATURE09513.

Davalos, Dimitrios, Jae Kyu Ryu, Mario Merlini, Kim M. Baeten, Natacha Le Moan, Mark A. Petersen, Thomas J. Deerinck, et al. 2012. “Fibrinogen-Induced Perivascular Microglial Clustering Is Required for the Development of Axonal Damage in Neuroinflammation.” *Nature Communications 2012 3:1* 3 (1): 1–15. https://doi.org/10.1038/NCOMMS2230.

Debette, Stéphanie, Sabrina Schilling, Marie Gabrielle Duperron, Susanna C. Larsson, and Hugh S. Markus. 2019. “Clinical Significance of Magnetic Resonance Imaging Markers of Vascular Brain Injury: A Systematic Review and Meta-Analysis.” *JAMA Neurology* 76 (1): 81. https://doi.org/10.1001/JAMANEUROL.2018.3122.

DeCicco-Skinner, Katie L., Gervaise H. Henry, Christophe Cataisson, Tracy Tabib, J. Curtis Gwilliam,

Nicholas J. Watson, Erica M. Bullwinkle, et al. 2014. “Endothelial Cell Tube Formation Assay for the In Vitro Study of Angiogenesis.” *Journal of Visualized Experiments : JoVE*, no. 91 (January): 51312. https://doi.org/10.3791/51312.

Dehouck, Marie-Pierre -P, Stéphane Méresse, Pierre Delorme, Jean-Charles -C Fruchart, and Roméo Cecchelli. 1990. “An Easier, Reproducible, and Mass-Production Method to Study the Blood–Brain Barrier In Vitro.” *Journal of Neurochemistry* 54 (5): 1798–1801. https://doi.org/10.1111/J.1471-4159.1990.TB01236.X.

Delsing, Louise, Pierre Dönnes, José Sánchez, Maryam Clausen, Dimitrios Voulgaris, Anna Falk, Anna Herland, et al. 2018. “Barrier Properties and Transcriptome Expression in Human IPSC-Derived Models of the Blood-Brain Barrier.” *Stem Cells (Dayton, Ohio)* 36 (12): 1816–27. https://doi.org/10.1002/STEM.2908.

Delsing, Louise, Anna Herland, Anna Falk, Ryan Hicks, Jane Synnergren, and Henrik Zetterberg. 2020. “Models of the Blood-Brain Barrier Using IPSC-Derived Cells.” *Molecular and Cellular Neuroscience*. https://doi.org/10.1016/j.mcn.2020.103533.

Demolli, Shemsi, Anuradha Doddaballapur, Kavi Devraj, Konstantin Stark, Yosif Manavski, Annekathrin Eckart, Christoph M. Zehendner, et al. 2017. “Shear Stress-Regulated MiR-27b Controls Pericyte Recruitment by Repressing SEMA6A and SEMA6D.” *Cardiovascular Research* 113 (6): 681–91. https://doi.org/10.1093/CVR/CVX032.

Ding, Shichao, Aminul Islam Khan, Xiaoli Cai, Yang Song, Zhaoyuan Lyu, Dan Du, Prashanta Dutta, and Yuehe Lin. 2020. “Overcoming Blood–Brain Barrier Transport: Advances in Nanoparticle-Based Drug Delivery Strategies.” *Materials Today*. https://doi.org/10.1016/j.mattod.2020.02.001.

Drake, Christopher J., Jill E. Hungerford, and Charles D. Little. 1998. “Morphogenesis of the First Blood Vessels.” *Annals of the New York Academy of Sciences* 857 (1): 155–79. https://doi.org/10.1111/J.1749-6632.1998.TB10115.X.

Eigenmann, Daniela E., Gongda Xue, Kwang S. Kim, Ashlee V. Moses, Matthias Hamburger, and Mouhssin Oufir. 2013. “Comparative Study of Four Immortalized Human Brain Capillary Endothelial Cell Lines, HCMEC/D3, HBMEC, TY10, and BB19, and Optimization of Culture Conditions, for an in Vitro Blood-Brain Barrier Model for Drug Permeability Studies.” *Fluids and Barriers of the CNS* 10 (1): 1–17. https://doi.org/10.1186/2045-8118-10-33/FIGURES/8.

Etchevers, H. C., C. Vincent, N. M. Le Douarin, and G. F. Couly. 2001. “The Cephalic Neural Crest Provides Pericytes and Smooth Muscle Cells to All Blood Vessels of the Face and Forebrain.” *Development* 128 (7): 1059–68. https://doi.org/10.1242/DEV.128.7.1059.

Faal, Tannaz, Duc T.T. Phan, Hayk Davtyan, Vanessa M. Scarfone, Erika Varady, Mathew Blurton-Jones, Christopher C.W. Hughes, and Matthew A. Inlay. 2019. “Induction of Mesoderm and Neural Crest-Derived Pericytes from Human Pluripotent Stem Cells to Study Blood-Brain Barrier Interactions.” *Stem Cell Reports* 12 (3): 451–60. https://doi.org/10.1016/J.STEMCR.2019.01.005.

Falk, Sven, and Magdalena Götz. 2017. “Glial Control of Neurogenesis.” *Current Opinion in Neurobiology* 47 (December): 188–95. https://doi.org/10.1016/J.CONB.2017.10.025.

Fernandes, Diogo C., Rui L. Reis, and J. Miguel Oliveira. 2021. “Advances in 3D Neural, Vascular and Neurovascular Models for Drug Testing and Regenerative Medicine.” *Drug Discovery Today*. Elsevier Ltd. https://doi.org/10.1016/j.drudis.2020.11.009.

Filosa, Jessica A., Adrian D. Bonev, Stephen V. Straub, Andrea L. Meredith, M. Keith Wilkerson, Richard W. Aldrich, and Mark T. Nelson. 2006. “Local Potassium Signaling Couples Neuronal Activity to Vasodilation in the Brain.” *Nature Neuroscience 2006 9:11* 9 (11): 1397–1403. https://doi.org/10.1038/NN1779.

Fish, Jason E., and Joshua D. Wythe. 2015. “The Molecular Regulation of Arteriovenous Specification and Maintenance.” *Developmental Dynamics* 244 (3): 391–409. https://doi.org/10.1002/DVDY.24252.

French, Curtis R., Sudha Seshadri, Anita L. Destefano, Myriam Fornage, Corey R. Arnold, Philip J. Gage, Jonathan M. Skarie, et al. 2014. “Mutation of FOXC1 and PITX2 Induces Cerebral Small-Vessel Disease.” *The Journal of Clinical Investigation* 124 (11): 4877–81. https://doi.org/10.1172/JCI75109.

Garberg, P., M. Ball, N. Borg, R. Cecchelli, L. Fenart, R. D. Hurst, T. Lindmark, et al. 2005. “In Vitro Models for the Blood-Brain Barrier.” *Toxicology in Vitro* 19 (3): 299–334. https://doi.org/10.1016/j.tiv.2004.06.011.

Garneau, Josiane E., Marie Ève Dupuis, Manuela Villion, Dennis A. Romero, Rodolphe Barrangou, Patrick Boyaval, Christophe Fremaux, Philippe Horvath, Alfonso H. Magadán, and Sylvain Moineau. 2010. “The CRISPR/Cas Bacterial Immune System Cleaves Bacteriophage and Plasmid DNA.” *Nature 2010 468:7320* 468 (7320): 67–71. https://doi.org/10.1038/NATURE09523.

Gastfriend, Benjamin D., Sean P. Palecek, and Eric V. Shusta. 2018. “Modeling the Blood-Brain Barrier: Beyond the Endothelial Cells.” *Current Opinion in Biomedical Engineering* 5 (March): 6. https://doi.org/10.1016/J.COBME.2017.11.002.

Gastfriend, Benjamin D., Matthew J. Stebbins, Feifan Du, Eric V. Shusta, and Sean P. Palecek. 2021. “Differentiation of Brain Pericyte-Like Cells from Human Pluripotent Stem Cell−Derived Neural Crest.” *Current Protocols* 1 (1): e21. https://doi.org/10.1002/cpz1.21.

Georgakis, Marios K., Marco Duering, Joanna M. Wardlaw, and Martin Dichgans. 2019. “WMH and Long-Term Outcomes in Ischemic Stroke.” *Neurology* 92 (12): e1298–1308. https://doi.org/10.1212/WNL.0000000000007142.

Gerhardt, Holger, Hartwig Wolburg, and Christoph Redies. 2000. “N-Cadherin Mediates Pericytic-Endothelial Interaction during Brain Angiogenesis in the Chicken.” *Developmental Dynamics* 218 (3): 472–79. https://doi.org/10.1002/1097-0177(200007)218:3<472::aid-dvdy1008>3.0.co;2-%23.

Girouard, Hélène, Adrian D. Bonev, Rachael M. Hannah, Andrea Meredith, Richard W. Aldrich, and Mark T. Nelson. 2010. “Astrocytic Endfoot Ca2+ and BK Channels Determine Both Arteriolar Dilation and Constriction.” *Proceedings of the National Academy of Sciences of the United States of America* 107 (8): 3811–16. https://doi.org/10.1073/PNAS.0914722107/SUPPL_FILE/SM02.MPG.

Gordon, Grant R.J., Hyun B. Choi, Ravi L. Rungta, Graham C.R. Ellis-Davies, and Brian A. MacVicar. 2008. “Brain Metabolism Dictates the Polarity of Astrocyte Control over Arterioles.” *Nature 2008 456:7223* 456 (7223): 745–49. https://doi.org/10.1038/NATURE07525.

Hall, Catherine N, Clare Reynell, Bodil Gesslein, Nicola B Hamilton, Anusha Mishra, Brad A Sutherland, Fergus M. Oâ Farrell, Alastair M Buchan, Martin Lauritzen, and David Attwell. 2014. “Capillary Pericytes Regulate Cerebral Blood Flow in Health and Disease.” *Nature* 508 (1): 55–60. https://doi.org/10.1038/nature13165.

Ham, Onju, Yeung Bae Jin, Janghwan Kim, and Mi Ok Lee. 2020. “Blood Vessel Formation in Cerebral Organoids Formed from Human Embryonic Stem Cells.” *Biochemical and Biophysical Research Communications* 521 (1): 84–90. https://doi.org/10.1016/j.bbrc.2019.10.079.

Hartmann, David A., Robert G. Underly, Roger I. Grant, Ashley N. Watson, Volkhard Lindner, and Andy Y. Shih. 2015. “Pericyte Structure and Distribution in the Cerebral Cortex Revealed by High-Resolution Imaging of Transgenic Mice.” *Https://Doi.Org/10.1117/1.NPh.2.4.041402* 2 (4):

041402. https://doi.org/10.1117/1.NPH.2.4.041402.

Hatherell, Kathryn, Pierre Olivier Couraud, Ignacio A. Romero, Babette Weksler, and Geoffrey J. Pilkington. 2011a. "Development of a Three-Dimensional, All-Human in Vitro Model of the Blood-Brain Barrier Using Mono-, Co-, and Tri-Cultivation Transwell Models." *Journal of Neuroscience Methods* 199 (2): 223–29. https://doi.org/10.1016/j.jneumeth.2011.05.012.

Hatherell, Kathryn, Pierre Olivier Couraud, Ignacio A Romero, Babette Weksler, and Geoffrey J Pilkington. 2011b. "Development of a Three-Dimensional, All-Human in Vitro Model of the Blood-Brain Barrier Using Mono-, Co-, and Tri-Cultivation Transwell Models." *Journal of Neuroscience Methods* 199 (2): 223–29. https://doi.org/10.1016/j.jneumeth.2011.05.012.

He, Weihan, Yuanbo Kang, Wei Zhu, Bolun Zhou, Xingjun Jiang, Caiping Ren, and Weihua Guo. 2020. "FOXF2 Acts as a Crucial Molecule in Tumours and Embryonic Development." *Cell Death and Disease*. Nature Publishing Group. https://doi.org/10.1038/s41419-020-2604-z.

Heidenreich, Matthias, and Feng Zhang. 2015. "Applications of CRISPR-Cas Systems in Neuroscience." *Nature Publishing Group* 17. https://doi.org/10.1038/nrn.2015.2.

Helms, Hans C., N. Joan Abbott, Malgorzata Burek, Romeo Cecchelli, Pierre Olivier Couraud, Maria A. Deli, Carola Förster, et al. 2016. "In Vitro Models of the Blood–Brain Barrier: An Overview of Commonly Used Brain Endothelial Cell Culture Models and Guidelines for Their Use." *Journal of Cerebral Blood Flow & Metabolism* 36 (5): 862. https://doi.org/10.1177/0271678X16630991.

Higashimori, Akira, Yujuan Dong, Yanquan Zhang, Wei Kang, Geicho Nakatsu, Simon S.M. Ng, Tetsuo Arakawa, Joseph J.Y. Sung, Francis K.L. Chan, and Jun Yu. 2018. "Forkhead Box F2 Suppresses Gastric Cancer through a Novel FOXF2–IRF2BPL–b-Catenin Signaling Axis." *Cancer Research* 78 (7): 1643–56. https://doi.org/10.1158/0008-5472.CAN-17-2403.

Hille, Frank, Hagen Richter, Shi Pey Wong, Majda Bratovič, Sarah Ressel, and Emmanuelle Charpentier. 2018. "The Biology of CRISPR-Cas: Backward and Forward." *Cell* 172 (6): 1239–59. https://doi.org/10.1016/J.CELL.2017.11.032.

Hong, Hee Kyung, Janice K. Noveroske, Denis J. Headon, Tong Liu, Man Sun Sy, Monica J. Justice, and Aravinda Chakravarti. 2001. "The Winged Helix/Forkhead Transcription Factor Foxq1 Regulates Differentiation of Hair in Satin Mice." *Genesis* 29 (4): 163–71. https://doi.org/10.1002/GENE.1020.

Hou, Xucheng, Tal Zaks, Robert Langer, and Yizhou Dong. 2021. "Lipid Nanoparticles for MRNA Delivery." *Nature Reviews. Materials* 6 (12): 1078. https://doi.org/10.1038/S41578-021-00358-0.

Hupe, Mike, Minerva Xueting Li, Susanne Kneitz, Daria Davydova, Chika Yokota, Julianna Kele-Olovsson, Belma Hot, Jan M. Stenman, and Manfred Gessler. 2017. "Gene Expression Profiles of Brain Endothelial Cells during Embryonic Development at Bulk and Single-Cell Levels." *Science Signaling* 10 (487): 1–13. https://doi.org/10.1126/scisignal.aag2476.

Iadecola, Costantino. 2017. "The Neurovascular Unit Coming of Age: A Journey through Neurovascular Coupling in Health and Disease." *Neuron*. https://doi.org/10.1016/j.neuron.2017.07.030.

Jamieson, John J., Raleigh M. Linville, Yuan Yuan Ding, Sharon Gerecht, and Peter C. Searson. 2019. "Role of IPSC-Derived Pericytes on Barrier Function of IPSC-Derived Brain Microvascular Endothelial Cells in 2D and 3D." *Fluids and Barriers of the CNS* 16 (1): 1–16. https://doi.org/10.1186/S12987-019-0136-7/FIGURES/7.

Jeon, Iksoo, Nayeon Lee, Jia Yi Li, In Hyun Park, Kyoung Sun Park, Jisook Moon, Sung Han Shim, et al. 2012. "Neuronal Properties, in Vivo Effects, and Pathology of a Huntington's Disease Patient-Derived Induced Pluripotent Stem Cells." *Stem Cells (Dayton, Ohio)* 30 (9): 2054–62.

https://doi.org/10.1002/STEM.1135.

Johnsen, Kasper Bendix, Annette Burkhart, Louiza Bohn Thomsen, Thomas Lars Andresen, and Torben Moos. 2019. “Targeting the Transferrin Receptor for Brain Drug Delivery.” *Progress in Neurobiology*. Pergamon. https://doi.org/10.1016/j.pneurobio.2019.101665.

Kalucka, Joanna, Laura P.M.H. de Rooij, Jermaine Goveia, Katerina Rohlenova, Sébastien J. Dumas, Elda Meta, Nadine V. Conchinha, et al. 2020. “Single-Cell Transcriptome Atlas of Murine Endothelial Cells.” *Cell* 180 (4): 764-779.e20. https://doi.org/10.1016/j.cell.2020.01.015.

Kannan, Pavitra, Martin Schain, and David P. Lane. 2022. “An Automated Quantification Tool for Angiogenic Sprouting From Endothelial Spheroids.” *Frontiers in Pharmacology* 13 (April). https://doi.org/10.3389/FPHAR.2022.883083/FULL.

Kaplan, Luke, Brian W. Chow, and Chenghua Gu. 2020. “Neuronal Regulation of the Blood–Brain Barrier and Neurovascular Coupling.” *Nature Reviews Neuroscience 2020 21:8* 21 (8): 416–32. https://doi.org/10.1038/s41583-020-0322-2.

Katt, Moriah E., Lakyn N. Mayo, Shannon E. Ellis, Vasiliki Mahairaki, Jeffrey D. Rothstein, Linzhao Cheng, and Peter C. Searson. 2019. “The Role of Mutations Associated with Familial Neurodegenerative Disorders on Blood-Brain Barrier Function in an IPSC Model.” *Fluids and Barriers of the CNS* 16 (1): 1–13. https://doi.org/10.1186/S12987-019-0139-4/FIGURES/6.

Katt, Moriah E., and Eric V. Shusta. 2020. “In Vitro Models of the Blood-Brain Barrier: Building in Physiological Complexity.” *Current Opinion in Chemical Engineering* 30 (December): 42. https://doi.org/10.1016/J.COCHE.2020.07.002.

Keaney, James, and Matthew Campbell. 2015. “The Dynamic Blood-Brain Barrier.” *FEBS Journal* 282 (21): 4067–79. https://doi.org/10.1111/febs.13412.

Kisler, Kassandra, Amy R Nelson, Axel Montagne, and Berislav V Zlokovic. 2017. “Cerebral Blood Flow Regulation and Neurovascular Dysfunction in Alzheimer Disease.” *Nature Reviews Neuroscience*. https://doi.org/10.1038/nrn.2017.48.

Korn, Johannes, Bodo Christ, and Haymo Kurz. 2002. “Neuroectodermal Origin of Brain Pericytes and Vascular Smooth Muscle Cells.” *Journal of Comparative Neurology* 442 (1): 78–88. https://doi.org/10.1002/CNE.1423.

Kugler, Elisabeth C., John Greenwood, and Ryan B. MacDonald. 2021. “The ‘Neuro-Glial-Vascular’ Unit: The Role of Glia in Neurovascular Unit Formation and Dysfunction.” *Frontiers in Cell and Developmental Biology* 9 (September): 2641. https://doi.org/10.3389/FCELL.2021.732820/BIBTEX.

Kumar, Akhilesh, Saritha Sandra D’Souza, Oleg V Moskvin, Huishi Toh, Bowen Wang, Jue Zhang, Scott Swanson, Lian Wang Guo, James A Thomson, and Igor I Slukvin. 2017. “Specification and Diversification of Pericytes and Smooth Muscle Cells from Mesenchymoangioblasts.” *Cell Reports* 19 (9): 1902–16. https://doi.org/10.1016/j.celrep.2017.05.019.

Kutuzov, Nikolay, Henrik Flyvbjerg, and Martin Lauritzen. 2018. “Contributions of the Glycocalyx, Endothelium, and Extravascular Compartment to the Blood–Brain Barrier.” *Proceedings of the National Academy of Sciences of the United States of America* 115 (40): E9429–38. https://doi.org/10.1073/PNAS.1802155115/SUPPL_FILE/PNAS.1802155115.SAPP.PDF.

Lacoste, Baptiste, Cesar H. Comin, Ayal Ben-Zvi, Pascal S. Kaeser, Xiaoyin Xu, Lucianoda F. Costa, and Chenghua Gu. 2014. “Sensory-Related Neural Activity Regulates the Structure of Vascular Networks in the Cerebral Cortex.” *Neuron* 83 (5): 1117–30. https://doi.org/10.1016/J.NEURON.2014.07.034.

Lancaster, Madeline A., Magdalena Renner, Carol Anne Martin, Daniel Wenzel, Louise S. Bicknell, Matthew E. Hurles, Tessa Homfray, Josef M. Penninger, Andrew P. Jackson, and Juergen A. Knoblich. 2013. "Cerebral Organoids Model Human Brain Development and Microcephaly." *Nature 2013 501:7467* 501 (7467): 373–79. https://doi.org/10.1038/nature12517.

Lee, Sae Won, Woo Jean Kim, Yoon Kyung Choi, Hyun Seok Song, Myung Jin Son, Irwin H. Gelman, Yung Jin Kim, and Kyu Won Kim. 2003. "SSeCKS Regulates Angiogenesis and Tight Junction Formation in Blood-Brain Barrier." *Nature Medicine 2003 9:7* 9 (7): 900–906. https://doi.org/10.1038/nm889.

Lee, Somin, Minhwan Chung, Seung Ryeol Lee, and Noo Li Jeon. 2020. "3D Brain Angiogenesis Model to Reconstitute Functional Human Blood–Brain Barrier in Vitro." *Biotechnology and Bioengineering* 117 (3): 748–62. https://doi.org/10.1002/BIT.27224.

Leligdowicz, Aleksandra, Melissa Richard-Greenblatt, Julie Wright, Valerie M. Crowley, and Kevin C. Kain. 2018. "Endothelial Activation: The Ang/Tie Axis in Sepsis." *Frontiers in Immunology* 9 (APR): 838. https://doi.org/10.3389/FIMMU.2018.00838/BIBTEX.

Lengerich, Bettina van, Lihong Zhan, Dan Xia, Darren Chan, David Joy, Joshua I. Park, David Tatarakis, et al. 2023. "A TREM2-Activating Antibody with a Blood–Brain Barrier Transport Vehicle Enhances Microglial Metabolism in Alzheimer's Disease Models." *Nature Neuroscience 2023 26:3* 26 (3): 416–29. https://doi.org/10.1038/s41593-022-01240-0.

Li, Xiang, Yezheng Tao, Robert Bradley, Zhongwei Du, Yunlong Tao, Linghai Kong, Yi Dong, et al. 2018. "Fast Generation of Functional Subtype Astrocytes from Human Pluripotent Stem Cells." *Stem Cell Reports* 11 (4): 998–1008. https://doi.org/10.1016/j.stemcr.2018.08.019.

Linville, Raleigh M., Renée F. Nerenberg, Gabrielle Grifno, Diego Arevalo, Zhaobin Guo, and Peter C. Searson. 2022. "Brain Microvascular Endothelial Cell Dysfunction in an Isogenic Juvenile IPSC Model of Huntington's Disease." *Fluids and Barriers of the CNS* 19 (1): 1–16. https://doi.org/10.1186/S12987-022-00347-7/FIGURES/5.

Lippmann, Ethan S., Samira M. Azarin, Jennifer E. Kay, Randy A. Nessler, Hannah K. Wilson, Abraham Al-Ahmad, Sean P. Palecek, and Eric V. Shusta. 2012. "Derivation of Blood-Brain Barrier Endothelial Cells from Human Pluripotent Stem Cells." *Nature Biotechnology 2012 30:8* 30 (8): 783–91. https://doi.org/10.1038/NBT.2247.

Lippmann, Ethan S, Abraham Al-Ahmad, Samira M Azarin, Sean P Palecek, and Eric V Shusta. 2014. "A Retinoic Acid-Enhanced, Multicellular Human Blood-Brain Barrier Model Derived from Stem Cell Sources." *Scientific Reports* 4. https://doi.org/10.1038/srep04160.

Liu, Chun, Angelos Oikonomopoulos, Nazish Sayed, and Joseph C. Wu. 2018. "Modeling Human Diseases with Induced Pluripotent Stem Cells: From 2D to 3D and Beyond." *Development (Cambridge)* 145 (5). https://doi.org/10.1242/DEV.156166/48659.

Liu, Gary W., Edward B. Guzman, Nandita Menon, and Robert S. Langer. 2023. "Lipid Nanoparticles for Nucleic Acid Delivery to Endothelial Cells." *Pharmaceutical Research 2023 40:1* 40 (1): 3–25. https://doi.org/10.1007/S11095-023-03471-7.

Logan, Todd, Matthew J. Simon, Anil Rana, Gerald M. Cherf, Ankita Srivastava, Sonnet S. Davis, Ray Lieh Yoon Low, et al. 2021. "Rescue of a Lysosomal Storage Disorder Caused by Grn Loss of Function with a Brain Penetrant Progranulin Biologic." *Cell* 184 (18): 4651-4668.e25. https://doi.org/10.1016/j.cell.2021.08.002.

Longden, Thomas A., Fabrice Dabertrand, Masayo Koide, Albert L. Gonzales, Nathan R. Tykocki, Joseph E. Brayden, David Hill-Eubanks, and Mark T. Nelson. 2017. "Capillary K+-Sensing Initiates Retrograde Hyperpolarization to Increase Local Cerebral Blood Flow." *Nature Neuroscience 2017*

20:5 20 (5): 717–26. https://doi.org/10.1038/nn.4533.

Longden, Thomas A., David C. Hill-Eubanks, and Mark T. Nelson. 2016. "Ion Channel Networks in the Control of Cerebral Blood Flow." *Journal of Cerebral Blood Flow and Metabolism* 36 (3): 492–512. https://doi.org/10.1177/0271678X15616138/ASSET/IMAGES/LARGE/10.1177_0271678X15616138-FIG2.JPEG.

Lu, Tyler M., Sean Houghton, Tarig Magdeldin, José Gabriel Barcia Durán, Andrew P. Minotti, Amanda Snead, Andrew Sproul, et al. 2021. "Pluripotent Stem Cell-Derived Epithelium Misidentified as Brain Microvascular Endothelium Requires ETS Factors to Acquire Vascular Fate." *Proceedings of the National Academy of Sciences* 118 (8): e2016950118. https://doi.org/10.1073/pnas.2016950118.

Lundin, Anders, Louise Delsing, Maryam Clausen, Piero Ricchiuto, José Sanchez, Alan Sabirsh, Mei Ding, et al. 2018. "Human IPS-Derived Astroglia from a Stable Neural Precursor State Show Improved Functionality Compared with Conventional Astrocytic Models." *Stem Cell Reports* 10 (3): 1030–45. https://doi.org/10.1016/J.STEMCR.2018.01.021.

Maier, Tobias, Marc Güell, and Luis Serrano. 2009. "Correlation of MRNA and Protein in Complex Biological Samples." *FEBS Letters* 583 (24): 3966–73. https://doi.org/10.1016/j.febslet.2009.10.036.

Majumder, Anirban, Sujoy K. Dhara, Raymond Swetenburg, Miloni Mithani, Kaixiang Cao, Magdalena Medrzycki, Yuhong Fan, and Steven L. Stice. 2013. "Inhibition of DNA Methyltransferases and Histone Deacetylases Induces Astrocytic Differentiation of Neural Progenitors." *Stem Cell Research* 11 (1): 574–86. https://doi.org/10.1016/J.SCR.2013.03.003.

Mali, Prashant, Luhan Yang, Kevin M. Esvelt, John Aach, Marc Guell, James E. DiCarlo, Julie E. Norville, and George M. Church. 2013. "RNA-Guided Human Genome Engineering via Cas9." *Science* 339 (6121): 823–26. https://doi.org/10.1126/science.1232033.

Malik, Rainer, Ganesh Chauhan, Matthew Traylor, Muralidharan Sargurupremraj, Yukinori Okada, Aniket Mishra, Loes Rutten-Jacobs, et al. 2018. "Multiancestry Genome-Wide Association Study of 520,000 Subjects Identifies 32 Loci Associated with Stroke and Stroke Subtypes." *Nature Genetics* 50 (4): 524. https://doi.org/10.1038/S41588-018-0058-3.

Mansour, Abed Alfatah, J. Tiago Gonçalves, Cooper W. Bloyd, Hao Li, Sarah Fernandes, Daphne Quang, Stephen Johnston, Sarah L. Parylak, Xin Jin, and Fred H. Gage. 2018. "An in Vivo Model of Functional and Vascularized Human Brain Organoids." *Nature Biotechnology 2018 36:5* 36 (5): 432–41. https://doi.org/10.1038/nbt.4127.

Mcallister, Mark S, Ljiljana Krizanac-Bengez, Francesco Macchia, Richard J Naftalin, Kevin C Pedley, Marc R Mayberg, Matteo Marroni, Susan Leaman, Kathe A Stanness, and Damir Janigro. 2001. "Mechanisms of Glucose Transport at the Blood-Brain Barrier: An in Vitro Study a a a C." *Brain Research* 409: 20–30. www.elsevier.com/locate/bres.

McCarty, Joseph H. 2009. "Cell Adhesion and Signaling Networks in Brain Neurovascular Units." *Current Opinion in Hematology*. https://doi.org/10.1097/MOH.0b013e32832a07eb.

Mcconnell, Heather L, Cymon N Kersch, Randall L Woltjer, Edward A Neuwelt, and Paul E Fraser. 2016. "The Translational Significance of the Neurovascular Unit *." https://doi.org/10.1074/jbc.R116.760215.

Michell, B J, J E Griffiths, K I Mitchelhill, I Rodriguez-Crespo, T Tiganis, S Bozinovski, P R Ortiz De Montellano, B E Kemp, and R B Pearson. 1999. "The Akt Kinase Signals Directly to Endothelial Nitric Oxide Synthase." *Current Biology* 9: 845–48. http://biomednet.com/elecref/0960982200900845.

Mishra, Anusha, James P. Reynolds, Yang Chen, Alexander V. Gourine, Dmitri A. Rusakov, and David Attwell. 2016. “Astrocytes Mediate Neurovascular Signaling to Capillary Pericytes but Not to Arterioles.” *Nature Neuroscience 2016 19:12* 19 (12): 1619–27. https://doi.org/10.1038/nn.4428.

Mojica, F. J.M., C. Díez-Villaseñor, J. García-Martínez, and C. Almendros. 2009. “Short Motif Sequences Determine the Targets of the Prokaryotic CRISPR Defence System.” *Microbiology* 155 (3): 733–40. https://doi.org/10.1099/mic.0.023960-0.

Munji, Roeben Nocon, Allison Luen Soung, Geoffrey Aaron Weiner, Fabien Sohet, Bridgette Deanne Semple, Alpa Trivedi, Kayleen Gimlin, et al. 2019. “Profiling the Mouse Brain Endothelial Transcriptome in Health and Disease Models Reveals a Core Blood–Brain Barrier Dysfunction Module.” *Nature Neuroscience*. https://doi.org/10.1038/s41593-019-0497-x.

Myatt, Stephen S., and Eric W.F. Lam. 2007. “The Emerging Roles of Forkhead Box (Fox) Proteins in Cancer.” *Nature Reviews Cancer 2007 7:11* 7 (11): 847–59. https://doi.org/10.1038/NRC2223.

Nag, Sukriti. 2011. “Morphology and Properties of Brain Endothelial Cells.” *Methods in Molecular Biology (Clifton, N.J.)*. https://doi.org/10.1007/978-1-60761-938-3_1.

Nagasawa, Kunihiko, Hideki Chiba, Hiroki Fujita, Takashi Kojima, Tsuyoshi Saito, Toshiaki Endo, and Norimasa Sawada. 2006. “Possible Involvement of Gap Junctions in the Barrier Function of Tight Junctions of Brain and Lung Endothelial Cells.” *Journal of Cellular Physiology* 208 (1): 123–32. https://doi.org/10.1002/JCP.20647.

Naik, Pooja, and Luca Cucullo. 2012. “In Vitro Blood-Brain Barrier Models: Current and Perspective Technologies.” *Journal of Pharmaceutical Sciences*. John Wiley and Sons Inc. https://doi.org/10.1002/jps.23022.

Ngai, Al C, Kathryn R Ko, Seiji Morii, H Richard Winn, and H Rich-ard Winn. 1988. “Effect of Sciatic Nerve Stimulation on Pial Arterioles in Rats.” www.physiology.org/journal/ajpheart.

Nitta, Takehiro, Masaki Hata, Shimpei Gotoh, Yoshiteru Seo, Hiroyuki Sasaki, Nobuo Hashimoto, Mikio Furuse, and Shoichiro Tsukita. 2003. “Size-Selective Loosening of the Blood-Brain Barrier in Claudin-5-Deficient Mice.” *The Journal of Cell Biology* 161 (3): 653–60. https://doi.org/10.1083/jcb.200302070.

Norden, Anouk G.W. van, Karlijn F. de Laat, Rob A.R. Gons, Inge W.M. van Uden, Ewoud J. van Dijk, Lucas J.B. van Oudheusden, Rianne A.J. Esselink, et al. 2011. “Causes and Consequences of Cerebral Small Vessel Disease. The RUN DMC Study: A Prospective Cohort Study. Study Rationale and Protocol.” *BMC Neurology* 11 (1): 1–8. https://doi.org/10.1186/1471-2377-11-29/PEER-REVIEW.

Obermeier, Birgit, Richard Daneman, and Richard M. Ransohoff. 2013. “Development, Maintenance and Disruption of the Blood-Brain Barrier.” *Nature Medicine 2013 19:12* 19 (12): 1584–96. https://doi.org/10.1038/nm.3407.

Oddo, Arianna, Bo Peng, Ziqiu Tong, Yingkai Wei, Wing Yin Tong, Helmut Thissen, and Nicolas Hans Voelcker. 2019. “Advances in Microfluidic Blood–Brain Barrier (BBB) Models.” *Trends in Biotechnology* 37 (12): 1295–1314. https://doi.org/10.1016/j.tibtech.2019.04.006.

Omidi, Yadollah, Lee Campbell, Jaleh Barar, David Connell, Saeed Akhtar, and Mark Gumbleton. 2003. “Evaluation of the Immortalised Mouse Brain Capillary Endothelial Cell Line, b.End3, as an in Vitro Blood-Brain Barrier Model for Drug Uptake and Transport Studies.” *Brain Research* 990 (1–2): 95–112. https://doi.org/10.1016/S0006-8993(03)03443-7.

Orlova, Valeria V., Yvette Drabsch, Christian Freund, Sandra Petrus-Reurer, Francijna E. Van Den Hil, Suchitra Muenthaisong, Peter Ten Dijke, and Christine L. Mummery. 2014. “Functionality of Endothelial Cells and Pericytes from Human Pluripotent Stem Cells Demonstrated in Cultured

Vascular Plexus and Zebrafish Xenografts." *Arteriosclerosis, Thrombosis, and Vascular Biology* 34 (1): 177–86. https://doi.org/10.1161/ATVBAHA.113.302598/FORMAT/EPUB.

Orlova, Valeria V., Francijna E. Van Den Hil, Sandra Petrus-Reurer, Yvette Drabsch, Peter Ten Dijke, and Christine L. Mummery. 2014. "Generation, Expansion and Functional Analysis of Endothelial Cells and Pericytes Derived from Human Pluripotent Stem Cells." *Nature Protocols* 9 (6): 1514–31. https://doi.org/10.1038/nprot.2014.102.

Orlova, Valeria V, Dennis M Nahon, Amy Cochrane, Xu Cao, Christian Freund, Francijna van den Hil, Cornelius J J Westermann, et al. 2022. "Vascular Defects Associated with Hereditary Hemorrhagic Telangiectasia Revealed in Patient-Derived Isogenic IPSCs in 3D Vessels on Chip." *Stem Cell Reports* 17 (7): 1536–45. https://doi.org/10.1016/j.stemcr.2022.05.022.

Pacitti, Dario, Riccardo Privolizzi, and Bridget E. Bax. 2019. "Organs to Cells and Cells to Organoids: The Evolution of In Vitro Central Nervous System Modelling." *Frontiers in Cellular Neuroscience* 13 (January): 129. https://doi.org/10.3389/FNCEL.2019.00129/BIBTEX.

Page, Shyanne, Snehal Raut, and Abraham Al-Ahmad. 2019. "Oxygen-Glucose Deprivation/Reoxygenation-Induced Barrier Disruption at the Human Blood–Brain Barrier Is Partially Mediated Through the HIF-1 Pathway." *NeuroMolecular Medicine 2019 21:4* 21 (4): 414–31. https://doi.org/10.1007/S12017-019-08531-Z.

Paquet, Dominik, Dylan Kwart, Antonia Chen, Andrew Sproul, Samson Jacob, Shaun Teo, Kimberly Moore Olsen, Andrew Gregg, Scott Noggle, and Marc Tessier-Lavigne. 2016. "Efficient Introduction of Specific Homozygous and Heterozygous Mutations Using CRISPR/Cas9." *Nature* 533 (7601): 125–29. https://doi.org/10.1038/nature17664.

Park, Sang Wook, Young Jun Koh, Jongwook Jeon, Yun Hee Cho, Mi Jin Jang, Yujung Kang, Min Jeong Kim, et al. 2010. "Efficient Differentiation of Human Pluripotent Stem Cells into Functional CD34+ Progenitor Cells by Combined Modulation of the MEK/ERK and BMP4 Signaling Pathways." *Blood* 116 (25): 5762–72. https://doi.org/10.1182/BLOOD-2010-04-280719.

Park, Tae-Eun, Nur Mustafaoglu, Anna Herland, Ryan Hasselkus, Robert Mannix, Edward A. FitzGerald, Rachelle Prantil-Baun, et al. 2019. "Hypoxia-Enhanced Blood-Brain Barrier Chip Recapitulates Human Barrier Function and Shuttling of Drugs and Antibodies." *Nature Communications* 10 (1): 2621. https://doi.org/10.1038/s41467-019-10588-0.

Patsch, Christoph, Ludivine Challet-Meylan, Eva C Thoma, Eduard Urich, Tobias Heckel, John F. O'Sullivan, Stephanie J Grainger, et al. 2015. "Generation of Vascular Endothelial and Smooth Muscle Cells from Human Pluripotent Stem Cells." *Nature Cell Biology* 17 (8): 994–1003. https://doi.org/10.1038/ncb3205.

Paunovska, Kalina, Carmen J Gil, Melissa P Lokugamage, Cory D Sago, Manaka Sato, Gwyn N Lando, Marielena Gamboa Castro, Anton V Bryksin, James E Dahlman, and Wallace H Coulter. 2018. "Analyzing 2000 in Vivo Drug Delivery Data Points Reveals Cholesterol Structure Impacts Nanoparticle Delivery." https://doi.org/10.1021/acsnano.8b03640.

Peppiatt, Claire M., Clare Howarth, Peter Mobbs, and David Attwell. 2006. "Bidirectional Control of CNS Capillary Diameter by Pericytes." *Nature* 443 (7112): 700–704. https://doi.org/10.1038/NATURE05193.

Perrin, Steve. 2014. "Preclinical Research: Make Mouse Studies Work." *Nature 2014 507:7493* 507 (7493): 423–25. https://doi.org/10.1038/507423a.

Perriot, Sylvain, Amandine Mathias, Guillaume Perriard, Mathieu Canales, Nils Jonkmans, Nicolas Merienne, Cécile Meunier, et al. 2018. "Human Induced Pluripotent Stem Cell-Derived Astrocytes Are Differentially Activated by Multiple Sclerosis-Associated Cytokines." *Stem Cell Reports* 11 (5):

1199–1210. https://doi.org/10.1016/j.stemcr.2018.09.015.

Pham, Missy T., Kari M. Pollock, Melanie D. Rose, Whitney A. Cary, Heather R. Stewart, Ping Zhou, Jan A. Nolta, and Ben Waldau. 2018. “Generation of Human Vascularized Brain Organoids.” *NeuroReport* 29 (7): 588–93. https://doi.org/10.1097/WNR.0000000000001014.

Pieper, Christian, Jasmin Jacqueline Marek, Marlies Unterberg, Tanja Schwerdtle, and Hans-Joachim Galla. 2014. “Brain Capillary Pericytes Contribute to the Immune Defense in Response to Cytokines or LPS in Vitro.” https://doi.org/10.1016/j.brainres.2014.01.004.

Potente, Michael, Carmen Urbich, Ken Ichiro Sasaki, Wolf K. Hofmann, Christopher Heeschen, Alexandra Aicher, Ramya Kollipara, Ronald A. DePinho, Andreas M. Zeiher, and Stefanie Dimmeler. 2005. “Involvement of Foxo Transcription Factors in Angiogenesis and Postnatal Neovascularization.” *The Journal of Clinical Investigation* 115 (9): 2382–92. https://doi.org/10.1172/JCI23126.

Potjewyd, Geoffrey, Katherine A.B. Kellett, and Nigel M. Hooper. 2021. “3D Hydrogel Models of the Neurovascular Unit to Investigate Blood–Brain Barrier Dysfunction.” *Neuronal Signaling* 5 (4): 1–24. https://doi.org/10.1042/ns20210027.

Praça, Catarina, Susana C. Rosa, Emmanuel Sevin, Romeo Cecchelli, Marie Pierre Dehouck, and Lino S. Ferreira. 2019. “Derivation of Brain Capillary-like Endothelial Cells from Human Pluripotent Stem Cell-Derived Endothelial Progenitor Cells.” *Stem Cell Reports* 13 (4): 599–611. https://doi.org/10.1016/J.STEMCR.2019.08.002.

Raichle, Marcus E., and Mark A. Mintun. 2006. “BRAIN WORK AND BRAIN IMAGING.” *Https://Doi-Org.Emedien.Ub.Uni-Muenchen.de/10.1146/Annurev.Neuro.29.051605.112819* 29 (October): 449–76. https://doi.org/10.1146/ANNUREV.NEURO.29.051605.112819.

Reyahi, Azadeh, Ali M. Nik, Mozhgan Ghiami, Amel Gritli-Linde, Fredrik Pontén, Bengt R. Johansson, and Peter Carlsson. 2015. “Foxf2 Is Required for Brain Pericyte Differentiation and Development and Maintenance of the Blood-Brain Barrier.” *Developmental Cell* 34 (1): 19–32. https://doi.org/10.1016/J.DEVCEL.2015.05.008.

Richter, Corinna, James T. Chang, and Peter C. Fineran. 2012. “Function and Regulation of Clustered Regularly Interspaced Short Palindromic Repeats (CRISPR) / CRISPR Associated (Cas) Systems.” *Viruses* 4 (10): 2291. https://doi.org/10.3390/V4102291.

Roudnicky, Filip, Bo Kyoung Kim, Yanjun Lan, Roland Schmucki, Verena Küppers, Klaus Christensen, Martin Graf, et al. 2020. “Identification of a Combination of Transcription Factors That Synergistically Increases Endothelial Cell Barrier Resistance.” *Scientific Reports* 10 (1). https://doi.org/10.1038/s41598-020-60688-x.

Rubin, L. L., D. E. Hall, S. Porter, K. Barbu, C. Cannon, H. C. Horner, M. Janatpour, et al. 1991. “A Cell Culture Model of the Blood-Brain Barrier.” *Journal of Cell Biology* 115 (6): 1725–35. https://doi.org/10.1083/JCB.115.6.1725.

Ryu, Jae Kyu, Mark A. Petersen, Sara G. Murray, Kim M. Baeten, Anke Meyer-Franke, Justin P. Chan, Eirini Vagena, et al. 2015. “Blood Coagulation Protein Fibrinogen Promotes Autoimmunity and Demyelination via Chemokine Release and Antigen Presentation.” *Nature Communications 2015 6:1* 6 (1): 1–15. https://doi.org/10.1038/ncomms9164.

Ryu, Jae Ryeon, Suchit Ahuja, Corey R. Arnold, Kyle G. Potts, Aniket Mishra, Qiong Yang, Muralidharan Sargurupremraj, et al. 2022. “Stroke-Associated Intergenic Variants Modulate a Human FOXF2 Transcriptional Enhancer.” *Proceedings of the National Academy of Sciences of the United States of America* 119 (35). https://doi.org/10.1073/pnas.2121333119.

Sagare, Abhay P., Robert D. Bell, Zhen Zhao, Qingyi Ma, Ethan A. Winkler, Anita Ramanathan, and

Berislav V. Zlokovic. 2013a. “Pericyte Loss Influences Alzheimer-like Neurodegeneration in Mice.” *Nature Communications 2013 4:1* 4 (1): 1–14. https://doi.org/10.1038/ncomms3932.

Saitou, M., M. Furuse, H. Sasaki, J. D. Schulzke, M. Fromm, H. Takano, T. Noda, and S. Tsukita. 2000. “Complex Phenotype of Mice Lacking Occludin, a Component of Tight Junction Strands.” *Molecular Biology of the Cell* 11 (12): 4131–42. https://doi.org/10.1091/MBC.11.12.4131/ASSET/IMAGES/LARGE/MK1201372007.JPEG.

Sander, Jeffry D., and J. Keith Joung. 2014. “CRISPR-Cas Systems for Editing, Regulating and Targeting Genomes.” *Nature Biotechnology 2014 32:4* 32 (4): 347–55. https://doi.org/10.1038/nbt.2842.

Scully, Ralph, Arvind Panday, Rajula Elango, and Nicholas A. Willis. 2019. “DNA Double-Strand Break Repair-Pathway Choice in Somatic Mammalian Cells.” *Nature Reviews Molecular Cell Biology 2019 20:11* 20 (11): 698–714. https://doi.org/10.1038/s41580-019-0152-0.

Segal, Steven S. 2015. “Integration and Modulation of Intercellular Signaling Underlying Blood Flow Control.” *Journal of Vascular Research* 52 (2): 136–57. https://doi.org/10.1159/000439112.

Sen, Tirthankar, and Rajkumar P. Thummer. 2022. “CRISPR and IPSCs: Recent Developments and Future Perspectives in Neurodegenerative Disease Modelling, Research, and Therapeutics.” *Neurotoxicity Research 2022 40:5* 40 (5): 1597–1623. https://doi.org/10.1007/S12640-022-00564-W.

Sharma, Kushal, Yunpei Zhang, Keshav Raj Paudel, Allan Kachelmeier, Philip M. Hansbro, and Xiaorui Shi. 2022. “The Emerging Role of Pericyte-Derived Extracellular Vesicles in Vascular and Neurological Health.” *Cells*. Multidisciplinary Digital Publishing Institute. https://doi.org/10.3390/cells11193108.

Shen, Jikui, Maike Frye, Bonnie L. Lee, Jessica L. Reinardy, Joseph M. McClung, Kun Ding, Masashi Kojima, et al. 2014. “Targeting VE-PTP Activates TIE2 and Stabilizes the Ocular Vasculature.” *The Journal of Clinical Investigation* 124 (10): 4564–76. https://doi.org/10.1172/JCI74527.

Shi, Chang-He, Mi-Bo Tang, Shao-Hua Li, Zhi-Jie Wang, Xin-Jing Liu, Lu Zhao, Yuan Gao, et al. 2017. “Association of FOXF2 Gene Polymorphisms with Ischemic Stroke in Chinese Han Population.” *Oncotarget* 8 (52): 89867–75. https://doi.org/10.18632/ONCOTARGET.21263.

Siegenthaler, Julie A., Youngshik Choe, Katelin P. Patterson, Ivy Hsieh, Dan Li, Shou Ching Jaminet, Richard Daneman, Tsutomu Kume, Eric J. Huang, and Samuel J. Pleasure. 2013. “Foxc1 Is Required by Pericytes during Fetal Brain Angiogenesis.” *Biology Open* 2 (7): 647–59. https://doi.org/10.1242/BIO.20135009.

Smyth, Leon C.D., Justin Rustenhoven, Emma L. Scotter, Patrick Schweder, Richard L.M. Faull, Thomas I.H. Park, and Mike Dragunow. 2018a. “Markers for Human Brain Pericytes and Smooth Muscle Cells.” *Journal of Chemical Neuroanatomy* 92 (October): 48–60. https://doi.org/10.1016/j.jchemneu.2018.06.001.

Smyth, Leon C.D., Justin Rustenhoven, Emma L Scotter, Patrick Schweder, Richard L.M. Faull, Thomas I.H. Park, and Mike Dragunow. 2018b. “Markers for Human Brain Pericytes and Smooth Muscle Cells.” *Journal of Chemical Neuroanatomy* 92: 48–60. https://doi.org/10.1016/j.jchemneu.2018.06.001.

Soldner, Frank, Josée Laganière, Albert W. Cheng, Dirk Hockemeyer, Qing Gao, Raaji Alagappan, Vikram Khurana, et al. 2011. “Generation of Isogenic Pluripotent Stem Cells Differing Exclusively at Two Early Onset Parkinson Point Mutations.” *Cell* 146 (2): 318–31. https://doi.org/10.1016/J.CELL.2011.06.019.

Song, Liqing, Xuegang Yuan, Zachary Jones, Kyle Griffin, Yi Zhou, Teng Ma, and Yan Li. 2019. “Assembly of Human Stem Cell-Derived Cortical Spheroids and Vascular Spheroids to Model 3-D Brain-like

Tissues." *Scientific Reports* 9 (1): 1–16. https://doi.org/10.1038/s41598-019-42439-9.

Stebbins, Matthew J., Benjamin D. Gastfriend, Scott G. Canfield, Ming Song Lee, Drew Richards, Madeline G. Faubion, Wan Ju Li, Richard Daneman, Sean P. Palecek, and Eric V. Shusta. 2019. "Human Pluripotent Stem Cell-Derived Brain Pericyte-like Cells Induce Blood-Brain Barrier Properties." *Science Advances* 5 (3). https://doi.org/10.1126/SCIADV.AAU7375.

Sweeney, Mark, and Gabor Foldes. 2018. "It Takes Two: Endothelial-Perivascular Cell Cross-Talk in Vascular Development and Disease." *Frontiers in Cardiovascular Medicine* 5 (October): 154. https://doi.org/10.3389/FCVM.2018.00154/BIBTEX.

Sweeney, Melanie D., Shiva Ayyadurai, and Berislav V. Zlokovic. 2016. "Pericytes of the Neurovascular Unit: Key Functions and Signaling Pathways." *Nature Neuroscience 2016 19:6* 19 (6): 771–83. https://doi.org/10.1038/nn.4288.

Sweeney, Melanie D., Zhen Zhao, Axel Montagne, Amy R. Nelson, and Berislav V. Zlokovic. 2019. "Blood-Brain Barrier: From Physiology to Disease and Back." *Physiological Reviews* 99 (1): 21–78. https://doi.org/10.1152/physrev.00050.2017.

Syvänen, Stina, Örjan Lindhe, Mikael Palner, Birgitte R. Kornum, Obaidur Rahman, Bengt Långström, Gitte M. Knudsen, and Margareta Hammarlund-Udenaes. 2009. "Species Differences in Blood-Brain Barrier Transport of Three Positron Emission Tomography Radioligands with Emphasis on P-Glycoprotein Transport." *Drug Metabolism and Disposition* 37 (3): 635–43. https://doi.org/10.1124/dmd.108.024745.

Takahashi, Kazutoshi, Koji Tanabe, Mari Ohnuki, Megumi Narita, Tomoko Ichisaka, Kiichiro Tomoda, and Shinya Yamanaka. 2007. "Induction of Pluripotent Stem Cells from Adult Human Fibroblasts by Defined Factors." *Cell* 131 (5): 861–72. https://doi.org/10.1016/J.CELL.2007.11.019.

Takahashi, Kazutoshi, and Shinya Yamanaka. 2006. "Induction of Pluripotent Stem Cells from Mouse Embryonic and Adult Fibroblast Cultures by Defined Factors." *Cell* 126 (4): 663–76. https://doi.org/10.1016/J.CELL.2006.07.024.

Tallini, Yvonne N., Johan Fredrik Brekke, Bo Shui, Robert Doran, Seong Min Hwang, Junichi Nakai, Guy Salama, Steven S. Segal, and Michael I. Kotlikoff. 2007. "Propagated Endothelial Ca2+ Waves and Arteriolar Dilation In Vivo." *Circulation Research* 101 (12): 1300–1309. https://doi.org/10.1161/CIRCRESAHA.107.149484.

Tapia, Natalia, and Hans R. Schöler. 2016. "Molecular Obstacles to Clinical Translation of IPSCs." *Cell Stem Cell* 19 (3): 298–309. https://doi.org/10.1016/J.STEM.2016.06.017.

TCW, Julia, Minghui Wang, Anna A. Pimenova, Kathryn R. Bowles, Brigham J. Hartley, Emre Lacin, Saima I. Machlovi, et al. 2017. "An Efficient Platform for Astrocyte Differentiation from Human Induced Pluripotent Stem Cells." *Stem Cell Reports* 9 (2): 600–614. https://doi.org/10.1016/J.STEMCR.2017.06.018.

Terstappen, Georg C., Axel H. Meyer, Robert D. Bell, and Wandong Zhang. 2021. "Strategies for Delivering Therapeutics across the Blood–Brain Barrier." *Nature Reviews Drug Discovery* 20 (5): 362–83. https://doi.org/10.1038/s41573-021-00139-y.

Tetzlaff, Fabian, and Andreas Fischer. 2018. "Human Endothelial Cell Spheroid-Based Sprouting Angiogenesis Assay in Collagen." *Bio-Protocol* 8 (17). https://doi.org/10.21769/BIOPROTOC.2995.

Todorov, Mihail Ivilinov, Johannes Christian Paetzold, Oliver Schoppe, Giles Tetteh, Suprosanna Shit, Velizar Efremov, Katalin Todorov-Völgyi, et al. 2020. "Machine Learning Analysis of Whole Mouse Brain Vasculature." *Nature Methods 2020 17:4* 17 (4): 442–49. https://doi.org/10.1038/s41592-020-0792-1.

Tong, Lei, Robert A. Hill, Eyiyemisi C. Damisah, Katie N. Murray, Peng Yuan, Angelique Bordey, and Jaime Grutzendler. 2020. “Imaging and Optogenetic Modulation of Vascular Mural Cells in the Live Brain.” *Nature Protocols 2020 16:1* 16 (1): 472–96. https://doi.org/10.1038/S41596-020-00425-W.

Trillhaase, Anja, Marlon Maertens, Zouhair Aherrahrou, and Jeanette Erdmann. 2015. “Induced Pluripotent Stem Cells (IPSCs) in Vascular Research: From Two- to Three-Dimensional Organoids.” https://doi.org/10.1007/s12015-021-10149-3.

Tsai, Hui Hsin, Huiliang Li, Luis C. Fuentealba, Anna V. Molofsky, Raquel Taveira-Marques, Helin Zhuang, April Tenney, et al. 2012. “Regional Astrocyte Allocation Regulates CNS Synaptogenesis and Repair.” *Science* 337 (6092): 358–62. https://doi.org/10.1126/SCIENCE.1222381/SUPPL_FILE/TSAI.SM.PDF.

Tsukita, Shoichiro, Mikio Furuse, and Masahiko Itoh. 2001. “Multifunctional Strands in Tight Junctions.” *Nature Reviews Molecular Cell Biology 2001 2:4* 2 (4): 285–93. https://doi.org/10.1038/35067088.

Uchida, Yasuo, Sumio Ohtsuki, Yuki Katsukura, Chiemi Ikeda, Takashi Suzuki, Junichi Kamiie, and Tetsuya Terasaki. 2011. “Quantitative Targeted Absolute Proteomics of Human Blood-Brain Barrier Transporters and Receptors.” *Journal of Neurochemistry* 117 (2): 333–45. https://doi.org/10.1111/j.1471-4159.2011.07208.x.

Umeda, Kazuaki, Junichi Ikenouchi, Sayaka Katahira-Tayama, Kyoko Furuse, Hiroyuki Sasaki, Mayumi Nakayama, Takeshi Matsui, Sachiko Tsukita, Mikio Furuse, and Shoichiro Tsukita. 2006. “ZO-1 and ZO-2 Independently Determine Where Claudins Are Polymerized in Tight-Junction Strand Formation.” *Cell* 126 (4): 741–54. https://doi.org/10.1016/j.cell.2006.06.043.

Vanlandewijck, Michael, Liqun He, Maarja Andaloussi Mäe, Johanna Andrae, Koji Ando, Francesca Del Gaudio, Khayrun Nahar, et al. 2018. “A Molecular Atlas of Cell Types and Zonation in the Brain Vasculature.” *Nature* 554 (7693): 475–80. https://doi.org/10.1038/nature25739.

Vargas-Valderrama, Alejandra, Antonietta Messina, Maria Teresa Mitjavila-Garcia, and Hind Guenou. 2020. “The Endothelium, a Key Actor in Organ Development and HPSC-Derived Organoid Vascularization.” *Journal of Biomedical Science* 27 (1): 1–13. https://doi.org/10.1186/S12929-020-00661-Y/FIGURES/1.

Vatine, Gad D., Riccardo Barrile, Michael J. Workman, Samuel Sances, Bianca K. Barriga, Matthew Rahnama, Sonalee Barthakur, et al. 2019a. “Human IPSC-Derived Blood-Brain Barrier Chips Enable Disease Modeling and Personalized Medicine Applications.” *Cell Stem Cell* 24 (6): 995-1005.e6. https://doi.org/10.1016/j.stem.2019.05.011.

Verzi, Michael P., Abdul H. Khan, Susumu Ito, and Ramesh A. Shivdasani. 2008. “Transcription Factor Foxq1 Controls Mucin Gene Expression and Granule Content in Mouse Stomach Surface Mucous Cells.” *Gastroenterology* 135 (2): 591–600. https://doi.org/10.1053/j.gastro.2008.04.019.

Vila Cuenca, Marc, Amy Cochrane, Francijna E. van den Hil, Antoine A.F. de Vries, Saskia A.J. Lesnik Oberstein, Christine L Mummery, and Valeria V Orlova. 2021. “Engineered 3D Vessel-on-Chip Using HiPSC-Derived Endothelial- and Vascular Smooth Muscle Cells.” *Stem Cell Reports* 16 (9): 2159–68. https://doi.org/10.1016/j.stemcr.2021.08.003.

Vogel, Christine, and Edward M. Marcotte. 2012. “Insights into the Regulation of Protein Abundance from Proteomic and Transcriptomic Analyses.” *Nature Reviews Genetics 2012 13:4* 13 (4): 227–32. https://doi.org/10.1038/nrg3185.

Wang, Aijun, Zhenyu Tang, Xian Li, Yisu Jiang, Danielle A. Tsou, and Song Li. 2011. “Derivation of Smooth Muscle Cells with Neural Crest Origin from Human Induced Pluripotent Stem Cells.” *Cells,*

Tissues, Organs 195 (1–2): 5. https://doi.org/10.1159/000331412.

Wang, Dongxue, Basak Eraslan, Thomas Wieland, Björn Hallström, Thomas Hopf, Daniel Paul Zolg, Jana Zecha, et al. 2019. "A Deep Proteome and Transcriptome Abundance Atlas of 29 Healthy Human Tissues." *Molecular Systems Biology* 15 (2): e8503. https://doi.org/10.15252/MSB.20188503.

Wang, Kai, Ruei-Zeng Lin, Xuechong Hong, Alex H. Ng, Chin Nien Lee, Joseph Neumeyer, Gang Wang, et al. 2020. "Robust Differentiation of Human Pluripotent Stem Cells into Endothelial Cells via Temporal Modulation of ETV2 with Modified MRNA." *Science Advances* 6 (30): eaba7606. https://doi.org/10.1126/sciadv.aba7606.

Wardlaw, Joanna M., Eric E. Smith, Geert J. Biessels, Charlotte Cordonnier, Franz Fazekas, Richard Frayne, Richard I. Lindley, et al. 2013. "Neuroimaging Standards for Research into Small Vessel Disease and Its Contribution to Ageing and Neurodegeneration." *The Lancet Neurology* 12 (8): 822–38. https://doi.org/10.1016/S1474-4422(13)70124-8.

Wardlaw, Joanna M, Colin Smith, and Martin Dichgans. 2019. "Small Vessel Disease: Mechanisms and Clinical Implications." *Review Lancet Neurol* 18: 684–96. https://doi.org/10.1016/S1474-4422(19)30079-1.

Wei, Helen Shinru, Hongyi Kang, Izad Yar Daniel Rasheed, Sitong Zhou, Nanhong Lou, Anna Gershteyn, Evan Daniel McConnell, et al. 2016. "Erythrocytes Are Oxygen-Sensing Regulators of the Cerebral Microcirculation." *Neuron* 91 (4): 851–62. https://doi.org/10.1016/j.neuron.2016.07.016.

Weksler, Babette, Ignacio A. Romero, and Pierre Olivier Couraud. 2013. "The HCMEC/D3 Cell Line as a Model of the Human Blood Brain Barrier." *Fluids and Barriers of the CNS* 10 (1): 1–10. https://doi.org/10.1186/2045-8118-10-16/TABLES/1.

Whiteus, Christina, Catarina Freitas, and Jaime Grutzendler. 2013. "Perturbed Neural Activity Disrupts Cerebral Angiogenesis during a Postnatal Critical Period." *Nature 2013 505:7483* 505 (7483): 407–11. https://doi.org/10.1038/NATURE12821.

Williams, Ian M., and Joseph C. Wu. 2019. "Generation of Endothelial Cells from Human Pluripotent Stem Cells: Methods, Considerations, and Applications." *Arteriosclerosis, Thrombosis, and Vascular Biology* 39 (7): 1317. https://doi.org/10.1161/ATVBAHA.119.312265.

Wilson, Hannah K., Scott G. Canfield, Michael K. Hjortness, Sean P. Palecek, and Eric V. Shusta. 2015. "Exploring the Effects of Cell Seeding Density on the Differentiation of Human Pluripotent Stem Cells to Brain Microvascular Endothelial Cells." *Fluids and Barriers of the CNS* 12 (1): 1–12. https://doi.org/10.1186/S12987-015-0007-9/FIGURES/4.

Wimmer, Reiner A., Alexandra Leopoldi, Martin Aichinger, Nikolaus Wick, Brigitte Hantusch, Maria Novatchkova, Jasmin Taubenschmid, et al. 2019. "Human Blood Vessel Organoids as a Model of Diabetic Vasculopathy." *Nature* 565 (7740): 505–10. https://doi.org/10.1038/s41586-018-0858-8.

Winkler, Ethan A., Robert D. Bell, and Berislav V. Zlokovic. 2011. "Central Nervous System Pericytes in Health and Disease." *Nature Neuroscience*. Nature Publishing Group. https://doi.org/10.1038/nn.2946.

Wolff, Anette, Maria Antfolk, Birger Brodin, and Maria Tenje. 2015. "In Vitro Blood-Brain Barrier Models - An Overview of Established Models and New Microfluidic Approaches." *Journal of Pharmaceutical Sciences*. John Wiley and Sons Inc. https://doi.org/10.1002/jps.24329.

Wu, Qiong, Wei Li, and Chongge You. 2021. "The Regulatory Roles and Mechanisms of the Transcription Factor FOXF2 in Human Diseases." *PeerJ* 9 (March): e10845. https://doi.org/10.7717/peerj.10845.

Xu, J., H. Liu, Y. Lan, J. S. Park, and R. Jiang. 2020. “Genome-Wide Identification of Foxf2 Target Genes in Palate Development.” *Journal of Dental Research* 99 (4): 463–71. https://doi.org/10.1177/0022034520904018.

Yagi, Takuya, Daisuke Ito, Yohei Okada, Wado Akamatsu, Yoshihiro Nihei, Takahito Yoshizaki, Shinya Yamanaka, Hideyuki Okano, and Norihiro Suzuki. 2011. “Modeling Familial Alzheimer’s Disease with Induced Pluripotent Stem Cells.” *Human Molecular Genetics* 20 (23): 4530–39. https://doi.org/10.1093/HMG/DDR394.

Yamazaki, Tomoko, Ani Nalbandian, Yutaka Uchida, Wenling Li, Thomas D. Arnold, Yoshiaki Kubota, Seiji Yamamoto, Masatsugu Ema, and Yoh suke Mukouyama. 2017. “Tissue Myeloid Progenitors Differentiate into Pericytes through TGF-β Signaling in Developing Skin Vasculature.” *Cell Reports* 18 (12): 2991–3004. https://doi.org/10.1016/j.celrep.2017.02.069.

Yang, Andrew C., Ryan T. Vest, Fabian Kern, Davis P. Lee, Maayan Agam, Christina A. Maat, Patricia M. Losada, et al. 2022. “A Human Brain Vascular Atlas Reveals Diverse Mediators of Alzheimer’s Risk.” *Nature 2022 603:7903* 603 (7903): 885–92. https://doi.org/10.1038/S41586-021-04369-3.

Yang, Andrew C, Ryan T Vest, Fabian Kern, Davis P Lee, Christina A Maat, Patricia M Losada, Michelle B Chen, et al. 2021. “A Human Brain Vascular Atlas Reveals Diverse Cell Mediators of Alzheimer’s Disease Risk.” *BioRxiv*, 2021.04.26.441262. https://doi.org/10.1101/2021.04.26.441262.

Yang, Libang, Zhaohui Geng, Thomas Nickel, Caitlin Johnson, Lin Gao, James Dutton, Cody Hou, and Jianyi Zhang. 2016. “Differentiation of Human Induced-Pluripotent Stem Cells into Smooth-Muscle Cells: Two Novel Protocols.” *PLOS ONE* 11 (1): e0147155. https://doi.org/10.1371/JOURNAL.PONE.0147155.

Yuan, Xiaochen, Qingbin Wu, Peng Wang, Yingli Jing, Haijiang Yao, Yinshan Tang, Zhigang Li, Honggang Zhang, and Ruijuan Xiu. 2019. “Exosomes Derived From Pericytes Improve Microcirculation and Protect Blood–Spinal Cord Barrier After Spinal Cord Injury in Mice.” *Frontiers in Neuroscience* 13 (April): 319. https://doi.org/10.3389/FNINS.2019.00319/BIBTEX.

Zamanian, Jennifer L., Liun Xu, Lynette C. Foo, Navid Nouri, Lu Zhou, Rona G. Giffard, and Ben A. Barres. 2012. “Genomic Analysis of Reactive Astrogliosis.” *Journal of Neuroscience* 32 (18): 6391–6410. https://doi.org/10.1523/JNEUROSCI.6221-11.2012.

Zeisel, Amit, Ana B Muñoz Manchado, Simone Codeluppi, Peter Lönnerberg, Gioele La Manno, Anna Juréus, and Sueli Marques. 2015. “Cell Types in the Mouse Cortex and Hippocampus Revealed by Single-Cell RNA-Seq.” *Science* 347 (February): 1138–1142. 10.1126/science.aaa1934.

Zhang, Hongyan, Tomoko Yamaguchi, Yasuhiro Kokubu, and Kenji Kawabata. 2022. “Transient ETV2 Expression Promotes the Generation of Mature Endothelial Cells from Human Pluripotent Stem Cells.” *Biological and Pharmaceutical Bulletin* 45 (4): 483–90. https://doi.org/10.1248/BPB.B21-00929.

Zhang, Ye, Steven A. Sloan, Laura E. Clarke, Christine Caneda, Colton A. Plaza, Paul D. Blumenthal, Hannes Vogel, et al. 2016. “Purification and Characterization of Progenitor and Mature Human Astrocytes Reveals Transcriptional and Functional Differences with Mouse.” *Neuron* 89 (1): 37–53. https://doi.org/10.1016/J.NEURON.2015.11.013.

Zhao, Yingzi, Paul M. Vanhoutte, and Susan W.S. Leung. 2015. “Vascular Nitric Oxide: Beyond ENOS.” *Journal of Pharmacological Sciences* 129 (2): 83–94. https://doi.org/10.1016/J.JPHS.2015.09.002.

Zhao, Zhen, Amy R Nelson, Christer Betsholtz, and Berislav V Zlokovic. 2015. “Establishment and Dysfunction of the Blood-Brain Barrier.” *Cell*. https://doi.org/10.1016/j.cell.2015.10.067.

Zhou, Min, Samuel X. Shi, Ning Liu, Yinghua Jiang, Mardeen S. Karim, Samuel J. Vodovoz, Xiaoying Wang, Boli Zhang, and Aaron S. Dumont. 2021. “Caveolae-Mediated Endothelial Transcytosis

across the Blood-Brain Barrier in Acute Ischemic Stroke." *Journal of Clinical Medicine 2021, Vol. 10, Page 3795* 10 (17): 3795. https://doi.org/10.3390/JCM10173795.

Zidarič, Tanja, Lidija Gradišnik, and Tomaž Velnar. 2022. "Astrocytes and Human Artificial Blood-Brain Barrier Models." *Bosnian Journal of Basic Medical Sciences*, April. https://doi.org/10.17305/bjbms.2021.6943.

Zlokovic, Berislav V. 2011. "Neurovascular Pathways to Neurodegeneration in Alzheimer's Disease and Other Disorders." *Nature Reviews Neuroscience*. https://doi.org/10.1038/nrn3114.

Zonta, Micaela, María Cecilia Angulo, Sara Gobbo, Bernhard Rosengarten, Konstantin A. Hossmann, Tullio Pozzan, and Giorgio Carmignoto. 2002. "Neuron-to-Astrocyte Signaling Is Central to the Dynamic Control of Brain Microcirculation." *Nature Neuroscience 2002 6:1* 6 (1): 43–50. https://doi.org/10.1038/NN980.

Zuris, John A., David B. Thompson, Yilai Shu, John P. Guilinger, Jeffrey L. Bessen, Johnny H. Hu, Morgan L. Maeder, J. Keith Joung, Zheng Yi Chen, and David R. Liu. 2014. "Cationic Lipid-Mediated Delivery of Proteins Enables Efficient Protein-Based Genome Editing in Vitro and in Vivo." *Nature Biotechnology 2014 33:1* 33 (1): 73–80. https://doi.org/10.1038/NBT.3081.

7. Copyright information

Figure in the thesis	Figure 1
License number	5547041348240
License date	May 13, 2023
Licensed content publisher	Springer Nature
Licensed content publication	Nature Reviews Neuroscience
Licensed content title	Cerebral blood flow regulation and neurovascular dysfunction in Alzheimer disease
Licensed content author	Kassandra Kisler et al

Figure in the thesis	Figure 2
License number	5547050376403
License date	May 13, 2023
Licensed content publisher	Springer Nature
Licensed content publication	Nature Reviews Neuroscience
Licensed content title	Neuronal regulation of the blood–brain barrier and neurovascular coupling
Licensed content author	Luke Kaplan et al

Figure in the thesis	Figure 3
License number	5547050608229
License date	May 13, 2023
Licensed content publisher	Springer Nature
Licensed content publication	Nature Reviews Neuroscience
Licensed content title	Astrocyte–endothelial interactions at the blood–brain barrier
Licensed content author	N. Joan Abbott et al

Figure in the thesis	Figure 4
License number	5547051024064
License date	May 13, 2023
Licensed content publisher	Springer Nature
Licensed content publication	Nature Reviews Neuroscience
Licensed content title	Cerebral blood flow regulation and neurovascular dysfunction in Alzheimer disease
Licensed content author	Kassandra Kisler et al

Figure in the thesis	Figure 7
License number	5547150071746
License date	May 13, 2023
Licensed content publisher	Springer Nature
Licensed content publication	Nature Neuroscience
Licensed content title	Pericytes of the neurovascular unit: key functions and signaling pathways
Licensed content author	Melanie D Sweeney et al

Figure in the thesis	Figure 8 (left)
License number	5547150754055
License date	May 13, 2023
Licensed content publisher	Elsevier
Licensed content publication	Cell
Licensed content title	Single-Cell Transcriptome Atlas of Murine Endothelial Cells
Licensed content author	Joanna Kalucka,Laura P.M.H. de Rooij,Jermaine Goveia,Katerina Rohlenova,Sébastien J. Dumas,Elda Meta,Nadine V. Conchinha,Federico Taverna,Laure-Anne Teuwen,Koen Veys,Melissa García-Caballero,Shawez Khan,Vincent Geldhof,Liliana Sokol,Rongyuan Chen et al.

Figure in the thesis	Figure 8 (right)
License number	5547151135276
License date	May 13, 2023
Licensed content publisher	Elsevier
Licensed content publication	The Lancet Neurology
Licensed content title	Stroke genetics: discovery, biology, and clinical applications
Licensed content author	Martin Dichgans,Sara L Pulit,Jonathan Rosand

Figure in the thesis	Figure 9
License number	5547151434551
License date	May 13, 2023
Licensed content publisher	Elsevier
Licensed content publication	The Lancet Neurology
Licensed content title	Identification of additional risk loci for stroke and small vessel disease: a meta-analysis of genome-wide association studies
Licensed content author	Ganesh Chauhan,Corey R Arnold,Audrey Y Chu,Myriam Fornage,Azadeh Reyahi,Joshua C Bis,Aki S Havulinna,Muralidharan Sargurupremraj,Albert Vernon Smith,Hieab H H Adams,Seung Hoan Choi,Sara L Pulit,Stella Trompet,Melissa E Garcia,Ani Manichaikul et al.

Figure in the thesis	Figure 10
License number	5547160132169
License date	May 13, 2023
Licensed content publisher	Elsevier
Licensed content publication	Developmental Cell
Licensed content title	Foxf2 Is Required for Brain Pericyte Differentiation and Development and Maintenance of the Blood-Brain Barrier
Licensed content author	Azadeh Reyahi,Ali M. Nik,Mozhgan Ghiami,Amel Gritli-Linde,Fredrik Pontén,Bengt R. Johansson,Peter Carlsson

Figure in the thesis	Figure 13
License number	5547160610923
License date	May 13, 2023
Licensed content publisher	Springer Nature
Licensed content publication	Nature Reviews Neuroscience
Licensed content title	Applications of CRISPR–Cas systems in neuroscience
Licensed content author	Matthias Heidenreich et al

8. Curriculum Vitae

JUDIT GONZÁLEZ GALLEGO

EDUCATION

2018 - Now	**Graduate school of System Neurosciences (GSN, LMU) - Munich** Fast-track PhD student in Neuroscience
2012 – 2016	**Universitat Autónoma de Barcelona (UAB) - Barcelona** Bachelor in biochemistry **Technische Universität Hamburg – Harburg (TUHH) - Hamburg** Exchange year during the bachelor
2010 – 2012	**Escola Sant Gervasi – Barcelona** High School Diploma

PROFESSIONAL EXPERIENCE

2018 – Now	**Institute for Stroke and Dementia Research (ISD) - Munich** PhD student with Prof. Dr. Martin Dichgans a Prof. Dr. Dominik Paquet "Cell autonomous effects of Foxf2 in endothelial cells and pericytes using mouse and human models"
2016 – 2017	**Zentrum für Molekulare Biologie in Hamburg (ZMNH) – Hamburg** Internship with Prof. Dr. Marina Mikhaylova "Role of Synaptopod in the spine apparatus formation and relation of this structure with motor proteins"
2015	**Hospital Sant Pau – Barcelona** Internship with Dr. Olivia Belbin "Study of genetic correlations and biomarkers of Alzheimer Disease"

9. List of publications

Anja Konietzny, **Judit González-Gallego**, Julia Bär, Alberto Perez-Alvarer, Alexander Drakew, Jeroen A A Demmers, Dick H W Dekkers, John A Hammer, Michael Frotscher, Thomas G Oertner, Wolfgang Wagner, Matthias Kneussel, Marina Mikhaylova: Myosin V regulates synaptopodin clustering and localization in the dendrites of hippocampal neurons. **Journal of Cell science, 2019**. PMID: 31371487

10. Affidavit

Eidesstattliche Versicherung/Affidavit

Judit González Gallego (Studierende / Student)

Hiermit versichere ich an Eides statt, dass ich die vorliegende Dissertation “Cell autonomous effects of Foxf2 in endotelial cells and pericytes” selbstständig angefertigt habe, mich außer der angegebenen keiner weiteren Hilfsmittel bedient und alle Erkenntnisse, die aus dem Schrifttum ganz oder annähernd übernommen sind, als solche kenntlich gemacht und nach ihrer Herkunft unter Bezeichnung der Fundstelle einzeln nachgewiesen habe.

I hereby confirm that the dissertation “Cell autonomous effects of Foxf2 in endotelial cells and pericytes” is the result of my own work and that I have only used sources or materials listed and specified in the dissertation.

München, Munich, 17.05.2023 Judit González Gallego

11. Declaration of Author contributions

11.1 Manuscript I

A human iPSC-derived 3D blood-brain-barrier in vitro model recapitulates mouse cerebrovascular phenotypes induced by FOXF2 deficiency

Manuscript in preparation

Authors and contributions:

Judit González-Gallego*, Katalin Todorov-Völgyi*, Stephan A Müller, Martina Schifferer, Isabel Weisheit, Mihail Ivilinov Todorov, Barbara Lindner[1], Dennis Crusius, Joseph Kroeger, Mark Nelson, Tom R. Webb, Ali Ertürk, Mika Simons, Stefan Lichtenthaler, Martin Dichgans*, Dominik Paquet*

J.G.G., K.T.V., D.P. and M.D designed the project; J.G.G. performed cell culture experiments and established *in vitro* model; I.W., T.W. helped during differentiation protocols; J.K. and D.C. differentiated astrocytes; J.G.G and J.K. performed TEER and calcium experiments; M.N. analyzed calcium experiments; S.A.M performed mass spectrometry; J.G.G. and K.T.V. analyzed proteomics experiments; M.I.T performed PCA analysis and light-sheet microscopy; K.T.V performed experiments on isolated mouse brain vasculature and BBB permeability; J.G.G. and K.T.V performed and analyzed biochemical and immunocytochemistry experiments; M.S. performed electron microscopy; D.P., M.D., S.L., M.S. M.S. and A.E. supervised the experiments; J.G.G., K.T.V., M.D. and D.P wrote the manuscript; all the authors read and revised the manuscript.

My contribution to this publication in detail:

For this publication, I optimized and adapted the protocols for the differentiation of endothelial cells, pericytes and smooth muscle cells. I optimized and characterized the 3D culture of all the cell types to generate an *in vitro* BBB model. I further generated the gene editing for FOXF2-KO in iPSCs and the corresponding validations. Furthermore, I prepared the human samples for proteomics and confocal imaging and perform the corresponding analysis. Lastly, I optimized and performed the functional assays like endocytic uptake and LNP treatment in human endothelial cells.

11.2 Manuscript II

The stroke risk gene Foxf2 maintains brain endothelial cell function via Tie2-mediated Nos3 signaling

Manuscript in preparation

Authors and contributions:

Katalin Todorov-Völgyi*, **Judit González-Gallego***, Stephan A Müller, Burcu Fatma Seker, Mihail Ivilinov Todorov, Luise Schröger, Jiayu Cao, Ulrike Schillinger, Simon Frerich, Martina Fetting, Mikael Simons, Ali Ertürk, Arthur Liesz, Nikolaus Plesnila, Stefan Lichtenthaler, Dominik Paquet, Martin Dichgans

K.T.V., J.G.G. and M.D. designed the project; S.A.M. performed mass spectrometry; B.F.S. performed functional hyperemia measurements; J.G.G. performed cell culture experiments; K.T.V. and J.G.G. analyzed proteomics data; K.T.V., J.G.G., and L.S. performed biochemical experiments and confocal microscopy; M.I.T., K.T.V. and U.S. performed MRI; M.I.T. performed and analyzed light-sheet microscopy data; J.C. performed MCAo surgery, U.S. and K.T.V. performed BBB permeability assays, S.F. analyzed single cell RNA-seq data; M.F. and K.T.V. performed and analyzed electron microscopy; M.D., D.P., S.L., N.P., A.L., A.E., and M.S. supervised the experiments, K.T.V. and M.D. wrote the manuscript; all authors read and revised the manuscript.

My contribution to this publication in detail:

For this publication, I contributed in the optimization of endothelial cell isolation from mouse brain and performed the mouse brain endothelial cell isolation from the Foxf2-deficient mice for proteomic analysis. I further participated in the treatment of the animals with Razuprotafib for physiological and proteomic measurements and participated in the animal perfusion and brain dissection methods. I generated the human FOXF2-deficient endothelial cells for proteomics and performed immunolabeling for confocal microscopy analysis.

12. Acknowledgements

First, I would like to thank my mentors and supervisors, Martin and Dominik. Thank you for giving me the opportunity of doing my PhD in your labs. I am very grateful for all the resources and time spend in my project as well as the amazing collaborations along the way. Thank you for all the guidance, knowledge and scientific discussions. I learned a lot from you but mostly motivation, perseverance and patient. I would also like to thank you for all the encouragement after failed experiments, without it my project would not be where it is. But most importantly, I would like to thank you for providing me with an environment where I could not only develop as a scientist but also as a person.

A special thanks goes to Katalin, for the great supervision and guidance during the whole project. Thank you for all the scientific (and not scientific) discussions, the late meetings, the lastminute corrections and all the input that made me become a better scientist. I really enjoyed brainstorming and building up the project together and I could not ask for a better tandem scientist. Thank you for giving me the space when I was overwhelmed and encouragement when I needed it the most. But most importantly, thank you for becoming a friend rather than a colleague.

I would also like to thank my other thesis advisory committee members Dr. Sabina Tahirovic, Dr. Sabine Steffens and Dr. Archana Misrha. Thank you for making time not only to come to my yearly reports but also to give me valuable input during the project. Also, thank you for being such amazing inspiring women in science and encourage me after each meeting to continue with science.

I am also very grateful to all our collaborators that made science fun and interesting while pushed the projects and made them better. Thank you to Stephan Muller, Bucu Seker, Mihail Todorov and Martina Fetting. Also I would like to thank the entire CSD community for providing a great collaborative environment. I would also like to express my gratitude to the Graduate School of Neurosciences. It was an honor to be a Fast-track student in such a prestigious program. Thank you for exposing me to beautiful minds and scientist and providing me an outside institute scientific networking.

I cannot help the Paquet group enough. Thank you for being family far from home, for all the lunches and events outside the lab. I could not be happier to have belong to this group during my PhD. I feel privileged to have share with you this amazing road full of good scientific discussion, advice and support. A special thanks to Sophie, for being a great scientist and a better friend. You are a beautiful surprised and a present through this journey. I would also like to thank Julien, Isabel and Dennis to take me in the group when it was only you, for the supervision, answering all the question and the patience. To Carolina for always have a hand to help a kind words. Also a huge thank goes to Dennis, Lili, Angelika, Merle, Joey and Jenny for making a great working atmosphere.

I would also like to thank the Dichgans group. Thank you for all the great support along the way. A special thanks goes to Barbara Linder, thank you not only for all the scientific help but also for being such a kind and inspiring woman that always cared about me. Thank you to Andi, for helping me during the beginning of the PhD and teach me patience. Thanks also to Katalin and Nathalie for every single group meeting where you gave me your feedback and helped me to become more independent. Also a huge thanks to Federica, Arailym, Simon, Luise, Melanie, Nathalie, Rainer, Matthias, Christoff, Yaw, Gabi and Yan to make a great working environment.

I would also like to thank all the colleagues outside my labs which helped me through this journey. A special thanks to Berni, for the incredible support and philosophical conversations. You are a beautiful soul and friend. Thanks to also to Christina, for being considerate and always listen to me. Also thank you to Mike, Igor, Alba and Gemma for the nice breaks and interesting conversations.

I would also like to thank also to all the students I supervised along the way that gave me the chance to become better as a teacher. Also, the Neurocamp team, for being inspirational and give the best to all your friends and collages.

I am also very grateful to everyone I meet in Hamburg and encourage me to move to Munich for my PhD. A special thanks to Prof. Dr. Marina Mikhaylova, to believe me as a bachelor student and made me fall in love with Neuroscience. Thank you for all your guidance and support, I learned a lot not only from your scientific skills but also as a team leader. Thank you to Etienne, for being there when I started my PhD and never doubted that I will make it. I would also like to thank Maru for teaching me early that science is about love and patience, I missed you during my PhD.

I would also like to thank my friends from back home, to make me feel like nothing changed since I left Barcelona 7 years ago. Especialment vull agrair a l'Albert, per motivar-me cada cop que no veia el final y confiar en mi (més del que jo he confiat a vegades). Gràcies per ser des de fa temps, soc una afortunada d'haver crescut al teu costat. Gràcies a les "nenes" per fer qualsevol lloc del món casa, per no jutjar i sempre confiar que tornaré a casa. Gràcies Maria, Ainhoa, Mar, Anna, Carmina, Carme i Sara. En especial, gracias Maria, por siempre preocuparte de mi, aunque este lejos y hacer un hueco para verme. También gracias, Pablo y Miguel, mi gran familia del Eramus. Por reíros de mí, por preguntar, por mantener el contacto, pero sobre todo por estar siempre. Ahora, por fin, aspiro a un título más que vosotros. Finalmente, gracias a Wendy, Alba, Carla y Xavi, por demostrar interés por lo que hago y buscar tiempo para verme cuando visito. Gracias a todos de corazón por seguir estando a mi lado pese a no estar cerca. También me gustaría agradecer a Anna por enseñarme a confiar y a demostrarme que en el balance está la victoria.

Special thanks to Dennis, for understanding and encourage me in every way I needed during my PhD. Thank you for supporting me during the hard days, the kind words and especially for always believing in me. Thank you for all the love when I was exhausted and all the motivation when I thought I could not more. You are vitamin person and a beautiful soul, and I could not be luckier to share my live with you.

But most importantly, I would like to thank my family. Muchas gracias mama y papa, nunca os podré agradecer lo suficiente todo lo que habéis hecho por mí. Gracias por darme todo lo que tenéis y buscar la mejor educación para mí. Gracias por nunca exigirme nada, por confiar y por dejarme elegir mi futuro. Pero, sobre todo, muchas gracias por apoyarme en cada decisión que he tomado, por estar a mi lado y por hacerme ser mejor persona cada día. Sé que ha sido difícil tenerme tan lejos, y creedme para mí tampoco ha sido fácil, pero siempre os he sentido cerca de mí. Gracias por confiar en que algún día seré doctora. Y perdón por deciros que volvería en 6 meses aquel septiembre del 2016… creo que se me ha liado un poco la cosa, os prometo que vuelvo pronto. También gracias a toda mi familia, mis abuelos, tíos y primos, por estar y preocuparos de mí siempre. En especial gracias a Wendy, por crecer juntas y mantenernos cerca, por ser la hermana que nunca he tenido. Me encanta verte crecer y ver en la mujer que te has convertido, espero poder compartir más tiempo juntas. Gracias a ti también Silvia, por el tiempo compartido en Hamburgo y por darme la oportunidad de estar rodeada de familia tan lejos de casa. A todos, muchas gracias, os quiero de corazón.